Experimental Study on Steel-Concrete Composite NPS System Beam Column Joints Under Reversed Cyclic Earthquake Loading

Ann Albright

A thesis
submitted in partial fulfillment of the
requirements for the degree of

Master of Science in Civil Engineering

University of Washington

2022

Committee:
Professor Paolo M. Calvi
Professor Marc Eberhard
Professor Michael Motley

Program Authorized to Offer Degree:
Civil Engineering

University of Washington

Abstract

Experimental Study on Steel-Concrete Composite NPS® System Beam Column Joints
Under Reversed Cyclic Earthquake Loading

Ann Albright

Chair of the Supervisory Committee:

Professor Paolo M. Calvi

Department of Civil Engineering

> Reinforced concrete (RC) moment resisting frames (MRF) have traditionally been one of the most common structural systems used to resist lateral loads induced by seismic activities. Earthquake ground-shaking seismic loads cause displacement of the building, also known as “sway” or “drift”, over multiple displacement cycles. The RC MRF, which consists of beams, columns, and beam-column joints, is designed to achieve a ductile response through optimized detailing and proportioning to resist flexural, axial, and shear forces transferred into the structure during building sway. The current accepted design procedure for seismically active locations is to provide capacity protected members. This theory states that the columns of the beam-column system should be stronger than the beams, such that during ultimate design loads the beams will fail prior to the columns, which is a ductile failure mechanism.

> There is an abundant desire to improve reliability, safety, economic costs, efficiency, and performance of MRFs. To that end, many innovative MRF solutions have been proposed over the years, including precast or partially precast systems, steel braced RC joints, and concrete-steel composite systems. Among the many

novel suggestions, the NPS® system represents a recent and promising solution which aims to be unique, advanced, and technologically efficient to attain ductile MRFs capable of high seismic performance.

> The NPS® system is a steel concrete composite system, consisting of a steel HSS square, circular, or rectangular cross sectional column with self-supporting beams made of a flexural steel plate bottom chord with a welded truss (to act as the beam shear reinforcement) and undeformed top rebar steel. The system is completed with concrete cast in-situ. Use of partially prefabricated elements as well as in-place elements represents a delicate challenge of providing adequate moment continuity of the beam-column joint while ensuring the integrity of the joint region. To attempt to solve this challenge and achieve moment continuity, integrative steel elements are inserted through the joint after the beam trusses have been set in position but before the concrete is cast. Prior to this project, no experimental evidence was available to support the dependability of this moment continuity configuration.

> This thesis presents and discusses the results of an experimental program of nine (five interior and four exterior) full-scale 2D concrete-steel composite NPS® beam column joints, and two traditionally Eurocode compliant reinforced concrete beam-column joints (one interior and one exterior). This program was developed to investigate and ultimately assess the seismic performance of the NPS® system with specific consideration to the integrative steel elements providing moment continuity. The different moment continuity solutions adopted included the use of integrated truss elements (i.e., continuity trusses) and straight or hooked deformed bars (i.e., continuity bars). Additional variables considered included the level of shear protection of the joint "panel" region and the presence/absence of additional shear reinforcement in the beam end-regions (i.e., the "critical" or "plastic hinge" length).

> This thesis provides a detailed discussion of the experimental outcomes and a careful analysis of the observed response mechanisms and any subsequent design implications. The results of the experimental investigation were extrapolated to assess the performance of the specimen in terms of shear stress and shear strain in the joint, sub-component contribution to the total drift, energy dissipation, peak and residual

strength, initial and residual stiffness, and ductility. The response of the NPS® specimens was compared against a tangible target performance from the traditionally Eurocode compliant RC specimens.

> The experimental results demonstrated that, in at least one configuration, the NPS® system can effectively achieve modern proficient seismic performance objectives. This can be seen through equivalent or superior performance criteria comparison to their traditional RC counterparts.

ACKNOWLEDGEMENTS

> I would like to first and foremost profusely thank my advisor, Professor Paolo M. Calvi, for his endless support and patience. His expertise was invaluable in formulating research questions, analytical methods, and the entirety of the experimental program. Without him this report would not be possible. Mille grazie Paolo!

> I would also like to thank NPS® Systems, for their financial support, without which this project could not have been conceived or completed.

> Thanks go to the technicians at the Tecnostrutture srl in Noventa di Piave Italy, who built and tested the construction materials utilized in the specimens. Additionally, thank you to the technicians at the Shake Lab in Eucentre, Italy who tested and monitored all the specimens noted in this program.

> I'd also like to thank M.S. Ashtiani who provided integral support in determining the sub-components of specimen drift.

> Thank you to my colleagues who let me collaborate and talk through issues of both technical and philosophical nature.

> Finally, my wonderful parents who have supported me throughout this endeavor, as well as in life, deserve a massive endorsement. Thanks Mom and Dad!

TABLE OF CONTENTS

TABLE OF CONTENTS v

LIST OF FIGURES ix

LIST OF TABLES xii

Chapter 1 INTRODUCTION 1

1.1 Scope of the Document and Outline 1

1.2 Background and Research Motivation 2

Chapter 2 LITERATURE REVIEW 7

2.1 Previous Modeing of Beam-Column Joints 8

2.2 Previous Tests on Composite Systems 12

2.3 Code Compliance 13

Chapter 3 EXPERIMENTAL PROGRAM 15

3.1 Experimental Specimen Summary 15

3.2 Seismic Demand 18

3.3 Design of MDI-Series Specimen 19

3.3.1 Reference Specimen (REFi) Design 19

3.3.2 NPS® Specimen Design (MDI series) 21

3.4 Design of MDE-Series Specimens 26

3.5 Design of HD-Series Specimens 29

3.6 Design Summary 31

3.7 Specimen Fabrication and Material Testing [42] [43] 35

3.8 Testing and Analysis 37

3.8.1 Experimental Setup and Loading Protocol 37

3.8.2 Instrumentation and Measurements 42
3.8.3 Linear Potentiometers 42
3.8.4 Load Cells 45
3.8.5 Strain Gauges 45
3.8.6 Crack Mapping and Crack Width Measurements 47
3.8.7 Photos and Videos 47
Chapter 4 CALCULATIONS 48
4.1 Moment and Shear in the System 48
4.2 Sub-Components of Drift 52
4.3 Stiffness, Energy, and Ductility 54
Chapter 5 EXPERIMENTAL RESULTS 57
5.1 MDI Test series 57
5.1.1 REFi Specimen 59
5.1.2 NPS1i Specimen 63
5.1.3 NPS2Ai Specimen 67
5.1.4 NPS2Bi Specimen 71
5.1.5 NPS4i Specimen 75
5.2 MDE Test Series 79
5.2.1 REFe Specimen 80
5.2.2 NPS1e Specimen 85
5.2.3 NPS2Ae Specimen 89
5.2.4 NPS4e Specimen 93

5.3 HD Test Series 97
5.3.1 NPS3i Specimen 98
5.3.2 NPS3e Specimen 102
5.3.3 HD Experimental Analysis 106
5.4 Experimental Results Summary 109
5.4.1 MDI Test Series: 109
5.4.2 MDE Test Series: 109
5.4.3 HD Test Series: 110
Chapter 6 EXPERIMENTAL ANALYSIS 111
6.1 MDI (Internal) Effects of Studied Design Variables 112
6.1.1 NPSi - Effect of Different Continuity Solutions 116
6.1.2 NPSi - Influence of Joint Shear Reinforcement and Confinement 121
6.1.3 NPSi - Influence of Additional Beam Stirrups 124
6.2 MDI Response Classification 127
6.2.1 MDI Stiffness and Strength Degradation 127
6.2.2 MDI Energy Dissipation 128
6.2.3 MDI Ductility 129
6.2.4 MDI ACI Comparison 130
6.2.5 MDI Comparison Between NPS® and Ref 132
6.2.6 MDI Shear Stress vs. Shear Strain 136
6.3 MDE (External) Effects of Studied Design Variables 138
6.3.1 NPSe - Effect of Different Continuity Solutions 143

6.3.2 NPSe - Influence of Joint Shear Reinforcement and Confinement 146
6.4 MDE Response Classification 149
6.4.1 MDE Stiffness and Strength Degradation 149
6.4.2 MDE Energy Dissipation 150
6.4.3 MDE Ductility 151
6.4.4 MDE ACI Comparison 152
6.4.5 MDE Comparison Between NPS® and Ref 153
6.5 MD Performance Summary 155
Chapter 7 CONCLUSIONS 157
7.1 MD Specimens 157
7.1.1 With Respect to the Design Variables Studied 157
7.1.2 With Respect to the NPS® Joint Performance 158
7.1.3 With Respect to Design Implications 158
7.2 HD Specimens 159
7.3 Future Work 159
REFERENCES 162

LIST OF FIGURES

Figure 1.1: Examples of Continuity Elements in NPS® Beam-Column Joints....4
Figure 2.1: Simple Joint Model, Loading Condition and Free Body Diagram at Mid-height of the Joint....8
Figure 2.2: From Paulay [12]: Fig 2: "Strut" and "Truss" Mechanisms....9
Figure 2.3: From Leon [13]: "Truss" and "Strut" Development....9
Figure 2.4: From Shiohara [19]: Comparing Proposed Model to Existing Strut/Truss Models....11
Figure 2.5: Lowes [8]: Proposed Joint Panel Model....11
Figure 3.1:Internal vs External Specimen Examples....16
Figure 3.2: Hypothetical Reference Building Structure....19
Figure 3.3: Specimen REFi Reinforcement Layout Details....21
Figure 3.4: Qualitative View of Beam and Panel Zone Reinforcement Layout for MDI NPS® Specimens....24
Figure 3.5: MDI NPS® Specimens Reinforcement Layout Details....25
Figure 3.6: REFe Specimen Reinforcement Details....27
Figure 3.7: MDE NPS® Specimens Reinforcement Layout Details....28
Figure 3.8: Qualitative View of Beam and Panel Zone Reinforcement Layout for HD NPS® Specimens....30
Figure 3.9: HD NPS® Specimens Reinforcement Layout Details....31
Figure 3.10: Specimen Fabrication and Delivery....35
Figure 3.11: View of Eucentre Laboratory....37
Figure 3.12: Schematic Representation of Experimental Setup....38
Figure 3.13: Photographic View of Experimental Setup....39
Figure 3.14: View of Loading Configuration....40
Figure 3.15: Loading Protocol....41
Figure 3.16: Surface Instrumentation/Potentiometer Arrangement for Interior Specimens....44
Figure 3.17: Surface Instrumentation/Potentiometer Arrangement for Exterior Specimens....44
Figure 3.18: Typical Joint Panel Potentiometer Layout....44
Figure 3.19: View of Strain Gauge Locations....46
Figure 3.20: Photographic View of Installed Strain Gauges....47
Figure 4.1: Shear and Moment in Beam-Column Joints....48
Figure 4.2: Force Transfer in the System (Image Adapted from ACI352 R-02 [45])....49
Figure 4.3: Simplified Representation of Joint-Region Deformations....50
Figure 4.4: Example Rosette Configurations for Joint Shear Calculations....51
Figure 4.5: Simplified Specimen Setup....52
Figure 4.6: Fixed End Rotation....53
Figure 4.7: Specimen Performance Parameter Calculation....55
Figure 5.1: Reference Specimen Initial (Before Loading) and Final (After Loading) Conditions....59
Figure 5.2: Force-Displacement Response of REFi Specimen....60

Figure 5.3: Internal Strain Data 61
Figure 5.4: REFi – View of Joint Region at Various Drift Ratios 62
Figure 5.5: REFi Drift Subcomponents 62
Figure 5.6: View of Specimen NPS1i Before (Left) and After (Right) Testing 63
Figure 5.7: Force-Displacement Response of Specimen NPS1i 64
Figure 5.8: View of Joint Region at Various Drift Ratios 65
Figure 5.9: NPS1i Drift Subcomponents 66
Figure 5.10: View of Specimen NPS2Ai Before (Left) and After (Right) 67
Figure 5.11: Force-Displacement Response of Specimen NPS2Ai 68
Figure 5.12: NPS2Ai – View of Joint Region at Various Drift Ratios 69
Figure 5.13: NPS2Ai Drift Subcomponents 70
Figure 5.14: View of Specimen NPS2Bi Before (Left) and After (Right) Testing 71
Figure 5.15: Force-Displacement Response of Specimen NPS2Bi 72
Figure 5.16: NPS2Bi – View of Joint Region at Various Drift Ratios 73
Figure 5.17: NPS2Bi Drift Subcomponents 74
Figure 5.18: View of Specimen NPS4i Before (Left) and After (Right) Testing 75
Figure 5.19: Force-Displacement Response of Specimen NPS4i 76
Figure 5.20: NPS4i - View of Joint Region at Various Drift Ratios 77
Figure 5.21: NPS4i Drift Subcomponents 78
Figure 5.22: View of Specimen REFe Before (Left) and After (Right) Testing 81
Figure 5.23: Force-Displacement Response of Specimen REFe 81
Figure 5.24: Base of the Column After Out-of-Plane Failure Occurred 82
Figure 5.25: REFe Panel Zone at 3% 83
Figure 5.26: REFe - Beam Cracking Propagation 83
Figure 5.27: REFe Drift Subcomponents 84
Figure 5.28: View of Specimen REFe Before (Left) and After (Right) Testing 85
Figure 5.29: Force-Displacement Response of Specimen NPS1e 86
Figure 5.30: NPS1e – Beam Cracking Propagation 87
Figure 5.31: NPS1e - View of Joint Region and Main Flexural Crack 87
Figure 5.32: NPS1e Drift Subcomponents 88
Figure 5.33: View of Specimen NPS2Ae Before (Left) and After (Right) Testing 89
Figure 5.34: Force-Displacement Response of Specimen NPS2Ae 90
Figure 5.35: NPS2Ae - Beam Cracking Propagation 91
Figure 5.36: NPS2Ae – View of Joint Region and Main Flexural Crack 91
Figure 5.37: NPS2Ae Drift Subcomponents 92
Figure 5.38: View of Specimen NPS4e Before (Left) and After (Right) Testing 93
Figure 5.39: Force-Displacement Response of Specimen NPS4e 94

Figure 5.40: NPS4e - Beam Cracking Propagation 95
Figure 5.41: NPS4e - View of Joint Region and Main Flexural Crack 95
Figure 5.42: NPS4e Drift Subcomponents 96
Figure 5.43: View of Specimen NPS3i Before (Left) and After (Right) Testing 98
Figure 5.44: Force-Displacement Response of Specimen NPS3i 99
Figure 5.45: NPS3i - Beam-end and Joint Region Damage Propagation 101
Figure 5.46: NPS3i Drift Subcomponents 102
Figure 5.47: View of Specimen NPS3e Before (Left) and After (Right) Testing 103
Figure 5.48: Force-Displacement Response of Specimen NPS3e 104
Figure 5.49: NPS3e - Beam-end Region Damage Propagation 105
Figure 5.50: NPS3e Drift Subcomponents 106
Figure 6.1: MDI Backbone Force-Displacement Comparison 114
Figure 6.2: MDI Drift Subcomponent Comparison 115
Figure 6.3: View of Joint Region of MDI Specimens at Failure 116
Figure 6.4: Force-Displacement Response of Specimens NPS1i and NPS2Bi 118
Figure 6.5: View of Beam and Joint Region of Specimens NPS1i and NPS2Bi at Failure 120
Figure 6.6: Force-Displacement Response of Specimens NPS2Ai and NPS4i 122
Figure 6.7: View of Beam and Joint Region of Specimens NPS2Ai and NPS4i at Failure 123
Figure 6.8: Force-Displacement Response of Specimens NPS2Ai and NPS2Bi 125
Figure 6.9: View of Beam and Joint Region of Specimens NPS2Ai and NPS2Bi at Failure 126
Figure 6.10: MDI Stiffness Degradation 128
Figure 6.11: MDI Energy Dissipation 129
Figure 6.12: Force-Displacement Response of Specimens NPS2Ai and REFi 133
Figure 6.13: View of Beam and Joint Region of Specimens NPS2Ai and REFi at Failure 135
Figure 6.14: MDI Shear Strain vs. Shear Stress 137
Figure 6.15: MDE Backbone Force-Displacement Comparison 140
Figure 6.16: MDE Drift Subcomponent Comparison 141
Figure 6.17: View of Joint Region of MDE Specimens at Failure 142
Figure 6.18: Force-Displacement Response of Specimens NPS1e and NPS2Ae 144
Figure 6.19: View of Beam and Joint Region of Specimens NPS1e and NPS2Ae at Failure 145
Figure 6.20: Force-Displacement Response of Specimens NPS2Ae and NPS4e 147
Figure 6.21: View of Beam and Joint Region of Specimens NPS2Ae and NPS4e at Failure 148
Figure 6.22: MDE Stiffness Degradation 150
Figure 6.23: MDE Energy Dissipation 151
Figure 6.24: Force-Displacement Response of Specimens NPS2Ae and REFe 154

LIST OF TABLES

Table 2.1: Summary of International Code Requirements 13
Table 3.1: Test Matrix 17
Table 3.2: Seismic Demand on Beam and Column - Analysis 19
Table 3.3: Summary of Reinforcement Properties for all Specimens 32
Table 3.4: Specimens' Nominal Strength (Eurocode) 34
Table 3.5: Reinforcing Steel Properties 36
Table 3.6: Concrete Properties 36
Table 3.7: Reaction System Characteristics 38
Table 3.8: Loading Protocol 41
Table 4.1: Summary of Drift Sub-Component Equations 54
Table 5.1: Summary of Test Results - MDI Test Series 59
Table 5.2: Summary of Test Results - MDE Test Series 80
Table 5.3: Summary of Test Results - HD Test Series 98
Table 5.4: Summary of Test Results - HD Test Series 107
Table 5.5: HD Performance Assessment Results 107
Table 6.1: Summary of Test Results – MDI Test Series 113
Table 6.2: MDI Performance Assessment Results 127
Table 6.3: MDI ACI Acceptance Criteria 131
Table 6.4: Summary of Test Results – MDE Test Series 139
Table 6.5: MDE Performance Assessment Results 149
Table 6.6: MDE ACI Acceptance Criteria 152

CHAPTER 1 INTRODUCTION

1.1 SCOPE OF THE DOCUMENT AND OUTLINE

> The scope of this document is to present the results of an experimental program performed on a series of eleven (11) 2D full-scale beam-column joints intended to represent components of a moderately-ductile moment resisting frame (MRF). There were six (6) interior and (5) exterior joints. The specimens were manufactured with NPS® technology and were tested in the Shake Lab at Eucentre, Italy, under a combination of constant axial load and reversed cyclic horizontal load.

> The primary objective of this experimental program was to provide comprehensive experimental evidence in support of the implementation and further development of the NPS® frame as a stand-alone lateral load resisting system. To achieve this status, the NPS® frame system needed to meet several quantitative performance objectives including, but not limited to, adequate strength, stiffness, ductility, energy dissipation, and the ability to sustain loads over multiple loading cycles. In reinforced concrete frame systems, the structural response is typically a function of the behavior of the beam column joints.

> The experimental evidence was analyzed by the University of Washington team from the data collected in Italy. The data was able to provide insight of the NPS® beam-column joints, along with photographic and video evidence, to assess the effects of a series of variables often considered in seismic performance. The findings in this report have several important design implications for the NPS® systems that are discussed in more detail in CHAPTER 6 MD Experimental Analysis.

> This report is organized in chapters, as follows:

- 0provides a brief introduction, background, and motivations for undertaking the project.
- CHAPTER 2 provides an overview of the literature studied for this report, both to consider previous research to ensure unique findings as well as to provide comparisons and further expansion of proposed analytical methodology.

- CHAPTER 3 presents the specimen details and testing methodologies used in the experimental program. The instrumentation and data measurement techniques employed are also summarized here.
- CHAPTER 4 presents the calculations and technical procedures used for the remainder of the document.
- CHAPTER 5 presents the test results from the experimental program, delving in detail into the response of each specimen, individually.
- CHAPTER 6 examines the experimental results of the MD specimens in the context of assessing the observed results with further analytical explanation. It provides a preliminary assessment of the specimens relative to one another and a preliminary classification with respect to selected ACI acceptance criteria.
- CHAPTER 7 presents the conclusions from the experimental program and the analysis of the results. It provides recommendations for implementation of design guidelines.

1.2 BACKGROUND AND RESEARCH MOTIVATION

> Earthquakes are one of the most devastating natural disasters providing unpredictable and intense ground motion, responsible for thousands of casualties and billions of dollars in financial loss every year. The mitigation of the negative effects of earthquakes on the built environment requires innovative design development of resilient structural systems capable of providing high seismic performance, while also providing cost effective designs.

> This research is therefore dedicated to the implementation and improvement of a steel-concrete composite system (referred to as the NPS® system) takes advantage of the speed at which traditional steel and precast structures are built with the durability of reinforced concrete systems. Composite members also offer more advantageous compressive or shear behavior than either steel or RC members individually [1].

> The NPS® system aims at providing an advanced and efficient technological solution to attain ductile moment resisting frames capable of high seismic performance. The NPS® frame consists of a self-

supporting system made of hollow square, rectangular or circular steel columns (referred to as PDTI® columns and concrete filled steel tubes (CFST)) with traditional deformed steel rebar and shear stirrups, and steel truss beams with steel plate bottom cord and top plain rebar, completed with concrete cast in situ (also referred to as composite steel truss and concrete (CSTC) beams).

> To ensure performance-based design objectives, the NPS® system is designed as a capacity protected system, which ensures the column and joint have higher capacities than the beam, forcing beam flexural yielding to occur first, and subsequently preventing undesirable failure mechanisms. The beams are designed to form flexural plastic hinges, which evidently can form at the beam ends if the joint region and the adjacent columns are sufficiently reinforced. If this is the case, the joint absorbs the local action from the yielding of the longitudinal beam reinforcement. The level of ductility and the extent of the energy dissipation that the structure achieves is, for the most part, dictated by the characteristics of the beam plastic hinge.

> Moment continuity across the beam joint region represents the trickiest aspect to be addressed in the NPS® system; it was the principal variable considered in this research and was addressed experimentally. Since part of the beam-column joint were prefabricated, the continuity elements (which span between the prefabricated elements) needed to fit within the allowable space. Providing adequate integrity of the joint was a delicate challenge which was addressed during the design phase.

> The continuity connections adopted for the NPS® system consisted of three main options: 1) an integrative truss made of plain steel, 2) plain hooked bars, and 3) straight deformed bars. These continuity examples can be seen in Figure 1.1, noted as the “bending reinforcement”.

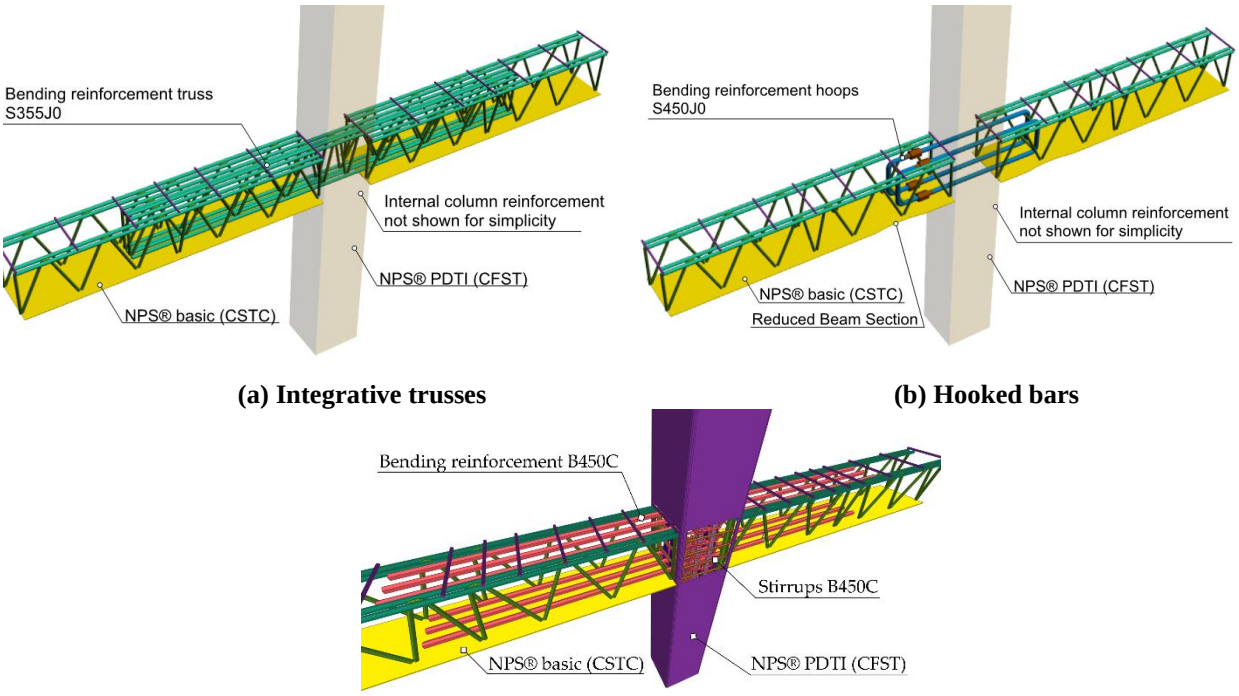

(a) Integrative trusses **(b) Hooked bars**

(c) Straight deformed bars

Figure 1.1: Examples of Continuity Elements in NPS® Beam-Column Joints

> Per design, the NPS® system is weaker in flexure at the beam-column interface, where strength is provided solely by the continuity reinforcement. Namely, in the beams the top plain steel and the bottom steel plate chord provide additional capacity to the continuity element, whereas in the joint the continuity element is the only flexural steel bridging the joint and providing flexural strength. The parallel action of the steel in the beam-end regions suggests it would be unlikely for significant plastic deformation to occur in this region. Therefore, under seismic loads, flexural yielding is expected to first occur at the beam-column interface. In addition, assuming the joint is adequately protected against the high shear loads arising in the panel zone following the yielding of the continuity elements, a localized flexural plastic hinge is expected to occur in the form of a single major crack at the beam-column interface. This is expected to serve as an efficient flexural fuse, limiting the demand on all other structural elements and allowing the prevention of undesired failure modes (e.g. shear failures). Note that to properly work, the following attributes need to be assured in the system:

- Adequate anchorage of the continuity elements. Upon yielding, the continuity elements are subject to severe bond demand, particularly in interior joints. If those elements are not adequately anchored within the joint, excessive bond-slip deterioration may occur, jeopardizing the overall system response.
- Adequate strength and integrity of the joint panel zone. The joint panel zone needs to possess enough strength to allow the activation of the plastic mechanisms at the beam-column interfaces. Additionally, it needs to be able to absorb multiple loading cycles without experiencing excessive strength drop.
- Furthermore, the localized plastic hinge needs to have sufficient rotation capacity. In over-reinforced joints, the full displacement demand on the system must be absorbed in the form of localized rotation at the beam ends. In under-reinforced joints, the displacement demand is mostly absorbed as a combination of localized rotation at the beam ends and of shear deformation of the panel zone.

> These are key features (more extensively discussed in the technical report by Calvi [2]) that need to be fully understood to establish the type of performance that can be expected out of the NPS® system and, ultimately to achieve its classification in the context of seismic lateral load resisting systems. From a design standpoint, the performance of the beam-column joints determines what "ductility class" the NPS® system should belong to, and what "behavior factors" should be adopted in design.

> The experimental program presented in this thesis was undertaken with the objectives of addressing the aspects discussed in this section. The specimens tested were designed considering variables that included the solution adopted to provide moment continuity across the beam-column interface (trusses versus bars) and the level of shear protection provided at the joint "panel" region. A third variable was also considered: the presence/absence of additional shear reinforcement in the beam end regions (a.k.a. the "critical" or "plastic hinge" length). This variable was included in the test matrix to investigate its effects on the overall responses and was expected to be negligible.

> Two traditional Eurocode compliant reinforced concrete joint specimens were designed and tested to provide a tangible target performance that was considered in the assessment and classification of the NPS® specimen response.

CHAPTER 2 LITERATURE REVIEW

> Reinforced concrete beam-column joints have been extensively studied and there are a myriad of experimental programs available in the literature. In the 1970s, excessive damage to the joint region prompted investigation into the mechanical properties and specific influence parameters of the panel zone. Consequently, “pre” and “post 1970’s era structures” are typical designations used in literature. However, despite the extensive research and the resulting advancements, beam-column joints continue to be critical elements of moment resisting frames (MRF). Earthquakes, such as the ones in Italy (May 20, 2012; M_L 5.9) and New Zealand (September 4,2010; M_w 7.1), have demonstrated that one of the main failure modes of reinforced concrete (RC) MRF buildings continues to be related to failures in the beam-column joints [3, 4]. The difficulty in accurately assigning joint capacity is what sustains research interest in this area.

> The joint region is still not universally understood. There are many models to describe the panel zone, which utilize different assumptions as a basis for the behavior in the region. Some of the more relevant or widely accepted models are described herein. They provide context for a better understanding of the conclusions drawn in this paper.

> Some pertinent experiments are also noted below, to provide a small basis of understanding of the variables seeking to be tested in this experimental program. This is not a comprehensive list; however, it is all relevant and relatively recent.

> Finally, the irregular requirements imposed through different international code systems offers some insight into this critical region. As determined by bodies of panels (which ultimately write the design codes for structural integrity), it is clear which components MRF systems are considered important and how components provide capacity per each international entity. It is interesting to note the differences among them and consider how additional research might shape the development of design guidelines.

2.1 PREVIOUS MODEING OF BEAM-COLUMN JOINTS

Many experimental programs have been undertaken to define the exact mechanics occurring within a reinforced concrete beam-column joint. These tests are typically motivated by an intent to create models which might empirically estimate the shear strength of the joint, thereby determining the ultimate capacity and ensuring a safer design [5, 6, 7, 8, 9]

Simplified models to calculate the shear strength of a joint region tend to isolate the contribution of the shear and concrete independently, and then sum them together. The joint shear, V_j, is taken at the mid-height of the joint region and is considered a sum of both the tensile forces, T and T', due to the reinforcement passing through the joint region, and the shear in the column, V_c. The overall joint shear can be seen in Figure 2.1 as V_j and noted by Hanson and Connor in 1967 is $V_j = T + T' - V_c$. It should be noted that the American Concrete Institute (ACI) currently utilizes the mid-height of the joint region for analysis of joint shear as well.

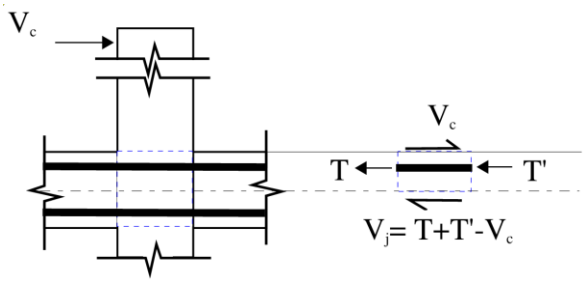

Figure 2.1: Simple Joint Model, Loading Condition and Free Body Diagram at Mid-height of the Joint

The strut and tie method (STM) has been widely used in analyzing joint regions, typically because it falls within a "disturbed" region of concrete which does not follow Bernoulli's governing assumption that plane sections remain plane. It assumes that the concrete forms a compression "strut" while the reinforcement acts as tension "ties", intersecting at specified "nodes"; the entire method relies on force equilibrium. The components act together to represent a basic truss. The forces acting on each member and resulting stresses can then be calculated and checked against material limit states. One of the drawbacks to this method is the iterative nature, which requires engineering judgement and assumptions to create the strut dimensions and to place the locations of the nodes [10].

> A highly cited method of analysis, specifically for the joint region of reinforced concrete beam column joints, comes from Paulay and Priestly, which postulates two main mechanisms of shear resistance: truss (sometimes referred to as “arch”) action and strut action [11, 12]. The strut mechanism comes about from the compression due to flexure of the external members on the joint core, and the reinforcement which carries these longitudinal forces into and out of the joint. These actions cause compression at opposite corners of the joint region, thereby developing a “strut” in the concrete. The truss mechanism assumes that all forces enter the joint through bond, and it is therefore dependent on the transverse joint reinforcement and longitudinal column bars. Through this bond the shear from the bar is transferred to the surrounding concrete, creating many small instances of inclined compression struts, with damage resulting from dilation of the concrete. The strut and truss mechanisms are both the extreme cases, and it is more likely that the true behavior of the joint falls somewhere between them [13]. The strut mechanism or the truss mechanism employed by Paulay assumes that failure of the joint is reached when either yielding of the transverse reinforcement or crushing of the diagonal concrete compression strut occurs and can be seen in Figure 2.2 and Figure 2.3 [12].

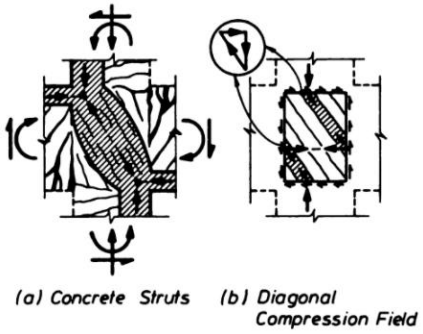

Figure 2.2: From Paulay [12]: Fig 2: "Strut" and "Truss" Mechanisms

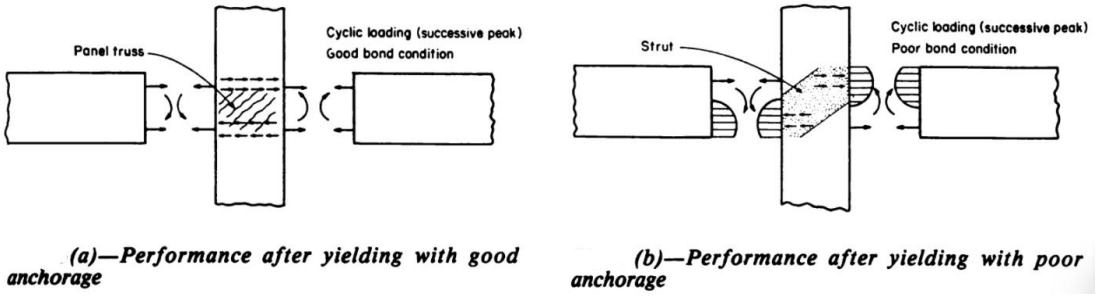

Figure 2.3: From Leon [13]: "Truss" and "Strut" Development

> Models and tests have also been developed to correlate the deterioration and general response of the beam-column joint panel regions to the expected strength [5, 9, 14, 15, 16]. One such model has been proposed by Wang, Dai, and Tang assuming a homogenous material for the joint and considering both vertical and horizontal steel in the joint region [15]. The model utilizes an average plane stress approach through the application of the three fundamental principles of mechanics. It also utilizes the Kupfer-Gerstle biaxial failure envelope of shear failure which allows it to be applicable for concrete crushing failures and diagonal tension failures. This proposed model was compared against 106 tests for both interior and exterior beam column joints, with favorable results.

> Studies have also been done on the amount of shear in the joint region, and the effect it plays on the beam-column joint. Studies have shown that the ratio of shear steel present in a joint region does increase the general strength of the system, up to a certain threshold, beyond which the addition of shear steel does not correlate to an increase in strength [17]. It has been suggested that the increase in shear steel beyond 0.4% does not significantly enhance the joint shear strength [18].

> Kusuhara and Shiohara proposed a model to account for the shear expansion of joints, which the strut method or truss mechanism does not account for [11, 19]. This model assumes the joint region can be broken into four independently moving triangles which can rotate separately, but which are connected by springs. The springs allow the moment of the beams and columns to be transferred in the joint region, along with shear forces. Shiohara and Kusuhara claim this allows the joint region to continue resisting shear mechanisms despite the ever-increasing joint shear deformation. The model was found to simulate interior and exterior seismic beam-column joints successfully. A view of the joint model can be seen in Figure 2.4.

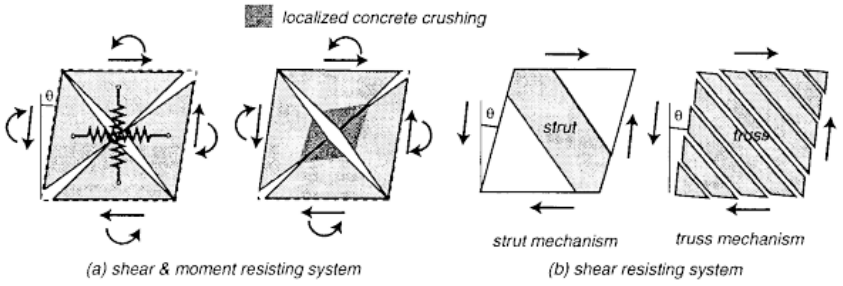

FIG. 15. Comparison of Mechanisms for New Model and Existing Models

Figure 2.4: From Shiohara [19]: Comparing Proposed Model to Existing Strut/Truss Models

> Lowes, Mitra, and Altoontash have proposed a widely cited model which assumes spring elements in place of rebar and at the faces of the shear panel, shown in Figure 2.5 [8]. There are four interface-shear springs and eight bar-slip springs. This model is particularly useful for older non-ductile frames without joint reinforcement. It also showed the importance of bond-slip response and joint-core response to the overall specimen performance.

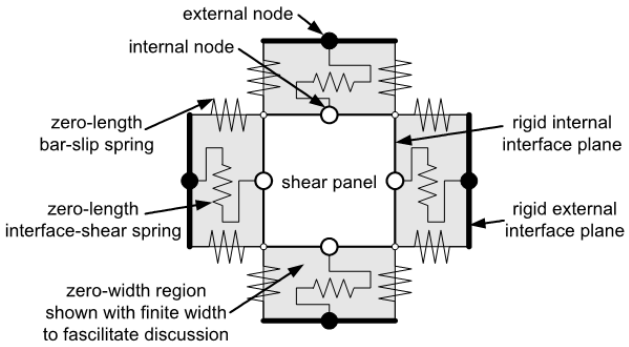

Fig. 4. Components of the Beam-Column Joint Model

Figure 2.5: Lowes [8]: Proposed Joint Panel Model

> In general, it has been shown that under cyclic loading, when the beam flexural steel yields and then forces penetrate the joint region, the joint panel exhibits diagonal cracking, bond slip, and loss of shear strength [5, 7, 11, 14, 20, 21].

> There are many more models noted in the literature. For the sake of brevity, only a few have been detailed here, including the relevant ones used for noting structural components and understanding of the joint region (more details in CHAPTER 4).

2.2 PREVIOUS TESTS ON COMPOSITE SYSTEMS

> Experimental studies on the behavior of composite beam-column joints have been conducted in the past, and they have led to guidelines for the design of beam-column moment connections in composite reinforced concrete steel (RCS) frames [22, 23, 24, 25, 26, 27]. Composite systems tend to have advantages such as speed of construction, additional confinement of concrete, and limited buckling of the steel.

> Sheikh and Gregory in 1989 considered the overall effects of beam-column moment connections for composite frames, instead of strictly steel-only or concrete-only frames and found that they produced compatible if not superior results, especially in regard to the joint region [26]. Modern composite research seeks to implement the benefits of the composite system in efficient and cost effective solutions. Parra-Montesinos in 2005 considered the implementation of prefabricated composite systems which reduced the cumbersome requirement of placing steel cages exactly on site [24]. Their model also utilized exterior steel rods with bolted connections, and overall it was found to be successful at capacities beyond 4% drift.

> Additional tests focusing on the improvement of composite systems have been carried out by research-focused groups including ASCE Task Committee on Design Criteria for Composite Structures in Steel and Concrete [28, 29, 30]. This is an ongoing effort to improve composite design. Results show that performance of modern composite beam column joints are as expected per code designs.

> The effect of plain vs deformed bars was also a variable of note for this project. The truss within the NPS® beams of this experimental program (more details are provided in CHAPTER 3 as well as the continuity truss of NPS1 and the hooked bars of NPS3, are all made of plain steel rather than deformed. This typically is worse for bond slip, as deformed bars have ridges which allow for better grip of the concrete to the steel and without those ridges the concrete has a harder time holding onto the rebar. There have been investigations into the usefulness of plain versus deformed bars in RC joints, namely Cosgun and Turk, as well as Fernandes, found that inadequate reinforcing in the joint region resulted in adverse performance of the joints [31, 32]. General bond slip models have been extensively researched by Eligehausen in 1983 and Soroushian in 1991 [33, 34].

> Previous studies have been inconclusive, if not contradictory, on the influence of an axial column load to increase or decrease the shear strength of the beam column joints [35]. This project did not consider this variable; the 300 kN axial load was applied as constant throughout the experiment and was meant to simulate the weight of another floor acting vertically on the system.

2.3 CODE COMPLIANCE

> Despite the agreement that the joint is a critical part of the frame, and despite the coordinated international effort undertaken by Japan, New Zealand and the United States since the 1970's, there is not one internationally accepted method for designing and analyzing beam-column joints for earthquake loading [15, 17, 36, 37, 38, 39]. International codes described herein will be limited to some of the more well-known codes, namely the American code (American Concrete Institute 352-R02 (ACI) 2003), the European code (Eurocode (EN) 1998), and the New Zealand code (New Zealand Standard (NZS) 2006) and can be seen in Table 2.1.

Table 2.1: Summary of International Code Requirements

	ACI 318M-02	**EN 1998-1:2003**	**NZS 2006**
Development Length [39]	$\frac{d_b}{h_c} > 0.05$	$\frac{d_b}{h_c} > 0.0345$	$\frac{d_b}{h_c} > 0.0322$
Strong Column Weak Beam [39]	$\sum M_{n,c} \geq 1.2 \sum M_{n,b}$	$\sum M_{Rc} \geq 1.3 \sum M_{Rb}$	$\sum_c M_n \geq 1.4 \sum_b \phi_O M_n$
Horizontal Shear Reinforcement A_{sh} [39]	$0.3 \frac{sh_c'' f_c'}{f_{yh}} \left[\frac{A_g}{A_{ch}} - 1\right]$	$\frac{b_j h_{jw}}{f_{yhd}} \left[\left(\frac{V_{jh}}{b_j h_{jc}}\right)^2 \frac{1}{f_{ctd} + v_d f_{cd}} - f_{ctd}\right]$	$\frac{6v_{jh}}{f_c'} \frac{f_y}{f_{yh}} \left(1.4 - 1.6 \frac{C_j N^*}{f_c' A_g}\right) A_s^*$
Joint Shear Strength V_j [16, 40]	$\lambda \phi \sqrt{f_c'} A_j$	$\eta f_{cd} \sqrt{1 - \frac{v_d}{\eta}} A_j$	$0.2 f_c A_j$

> ACI 352-R02 separates joints into two categories: Type 1 for structures in a non-seismically hazardous area and Type 2 in a seismically hazardous area. Type 2 is the relevant type for this research work. Energy dissipation capacity in type 2 joints is important. The shear stress in the joint is described by "arch action" per ACI and the AJI code books of America and Japan, respectively [16]. The current ACI code requires a minimum depth-to-bar diameter ratio (h_c/d_b) as greater than 20, to provide adequate development length. The nominal moment of the incoming columns should be at least 1.2 times the nominal moment strength of the beams – strong column weak beam theory. The shear steel required in the joint region is merely a function of the hoop spacing and the strength of the concrete and the steel yield stress – it does not consider the shear stress in the joint region or the axial load on the column as other codes do.

> The EU code acknowledges axial load as providing additional confinement on the joint core and considers it to improve the overall bond condition and therefore sets the h_c/d_b as greater than 29. The nominal flexural moment of the columns should be 1.3 times greater than the adjacent columns. The EU code prescribes the shear reinforcement in the joint to be limited by the tensile stress in the concrete, and to maintain a certain level of performance post diagonal cracking [39]. This code considers forces on the beam reinforcement, which results in more stringent requirements at lower concrete strengths [39].

> The New Zealand Standards describe the arch as well as truss action of the joint region. The axial load on the column contributes to confinement of the concrete and improves bond, so this code requires an h_c/d_b of greater than 31. The flexural strength of the column should be 1.4 times higher than the sum of the adjacent beams [39]. The shear steel required in joint core for interior specimens is a function of the nominal shear stress and considers the effects of axial loads on the column by reducing the amount of shear steel. Conclusively, the higher the strength of the concrete, the lower the amount of shear reinforcement needed in the joint [39]. However, there are upper bounds in this code, so the strength of a joint is always limited even if the concrete strength increases.

CHAPTER 3 EXPERIMENTAL PROGRAM

> The experimental program for this project consisted of eleven (11) full-scale beam-column specimens. Two (2) specimens were traditional reinforced concrete, while nine (9) were steel-concrete composite (NPS® system) full-scale beam-column joint specimens. All specimens were subject to identical loading protocols. The motivations for this program were provided in 0additionally, more information can be found in the technical report by Calvi which studied the theoretical response of NPS® frames subjected to seismic loads [2]. This chapter provides a detailed description of the main aspects of the experimental program and gives an overview of the specimens tested, experimental setup, loading apparatus, instrumentation, and testing protocols.

3.1 EXPERIMENTAL SPECIMEN SUMMARY

> The primary goal of this study was to investigate the seismic performance of NPS® beam-column joint specimens subjected to earthquake-induced reversed cyclic loading and assess whether the NPS® system can be used as a standalone moderately ductile moment resisting frame.

> This program tested eleven full size specimens: two (2) traditionally reinforced concrete and nine (9) made of the NPS® system. Six (6) of the specimens represented internal joints and five (5) represented external joints. Note that the external joint specimens were identical to the internal joint specimens, minus one beam as can be seen in Figure 3.1.

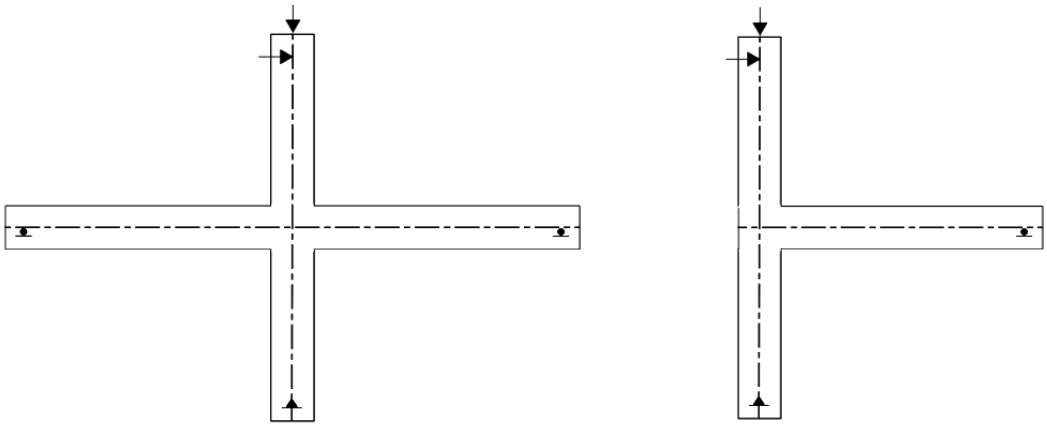

(a) Internal Specimen **(b) External Specimen**

Figure 3.1:Internal vs External Specimen Examples

A total of eleven full-scale beam-column joint specimens were tested in the Eucentre Laboratory (Pavia, Italy). All specimens were made of a 3.5 m long column and a 5 m long beam, both with 400 x 400 mm cross section. The NPS® specimens were composed of three main components: the columns, the beams, and the beam-column joints. The columns consisted of square steel HSS columns with traditional longitudinal deformed rebar and shear stirrups and will be referred to as columns. The beams were comprised of a steel plate bottom chord with welded steel trusses and top plain rebar, which will be referred to as NPS® beams or simply beams. Finally, the beam-to-column joints (or joints) typically had shear stirrups, but the continuous steel used to provide moment continuity differed between the specimens and was one of the main variables in this experimental program; it is discussed in detail in Section 3.3.2 and Section 3.5.

The specimens have been given the designations shown in Table 3.1 and may be grouped into three different Test Series, namely MDI (moderately ductile interior), MDE (moderately ductile exterior) and HD (highly ductile). Moderately ductile joints (MD) were designed using a behavior factor of 3.9 as per Eurocode recommendations. The two specimens intended to represent highly ductile systems (HD) were designed considering a behavior factor of 5.85.

Within each MD Test Series a traditional reinforced concrete specimen, intended to serve as a baseline reference, was designed and tested. The main variables considered within each series (internal and external) were the type of moment continuity across the beam-column interface (trusses vs bars), the level of

reinforcement provided within the joint region (i.e., the panel zone), and the presence of a wrapped steel joint core. Additionally, the internal specimens also considered the presence/absence of additional shear reinforcement in the beam end-regions, also known as the "critical" or "plastic hinge" length. This is summarized in Table 3.1.

Table 3.1: Test Matrix

Test Series	Specimen ID	Moment continuity	Joint shear reinforcement	Beam-end shear reinforcement	Wrapped Joint
MDI	REFi	Beam reinforcement continuous through joint	Yes	Yes	No
	NPS1i	Added trusses	No	Yes	No
	NPS2Ai	Loose deformed bars	Yes	No	No
	NPS2Bi	Loose deformed bars	Yes	Yes	No
	NPS4i	Loose deformed bars	Yes (greater spacing than NPS2)	No	Yes
MDE	REF	Beam reinforcement continuous through joint	Yes	Yes	No
	NPS1e	Added trusses	No	Yes	No
	NPS2Ae	Loose deformed bars	Yes	No	No
	NPS4e	Loose deformed bars	Yes (greater spacing than NPS2)	No	Yes
HD	NPS3i	Short plain bars anchored mechanically – force plastic hinge relocation	Yes	Yes	No
	NPS3e	Short plain bars anchored mechanically – force plastic hinge relocation	Yes	Yes	No

> A thorough investigation of the NPS® as a highly ductile moment resisting frame (MRF) is beyond the scope of this work. However, the two HD Test Series specimens are intended to explore an interesting alternative solution that may be used to achieve highly ductile systems without the need of providing heavy shear reinforcement within the joint region. The solution investigated in this pilot series attempts to protect the joint region by forcing plastic hinge relocation within the beams, some distance away from the beam-column interface.

> More details pertaining to specimen design, experimental setup, loading protocols, data acquisition etc. are provided in the following sections. It should be noted that the design of the specimens is discussed in a

general sense and that some explicit calculations are shown only for specimen REFi. For reference, the design of all specimens was carried out according to Eurocode provisions, following the recommendations summarized in the recent technical papers by Calvi [2, 40, 41].

3.2 SEISMIC DEMAND

- The specimens were designed to represent an interior beam-column joint located at the third floor of a three-bay four-story moderately ductile MRF (q = 3.9). A schematic representation of the hypothetical reference structure is outlined in Figure 3.2. In designing the reference joint, earthquake action acting in the horizontal direction was considered, with the seismic force resisting system consisting of the two outer frames.
- The structure was assumed to be located in a seismically active region, characterized by a PGA of 0.4g. The seismic demand at the site was estimated according to the Type 1 Eurocode Spectrum, soil class A (i.e., S = 1.0) [38]. The column height, beam length and floor seismic weight (constant for all floors) were 3.5 m, 5.0 m and w = 12 kN/m^2, respectively. It was further assumed that the gravity load acting at each floor was coincident to the seismic weight.
- The design demand on the structural elements was estimated using the equivalent lateral force (ELF) approach and the simplified structural analysis of the structure was performed using the portal method, assuming no gravity load acting on the beams, consistently with the slab orientation indicated in Figure 3.2.

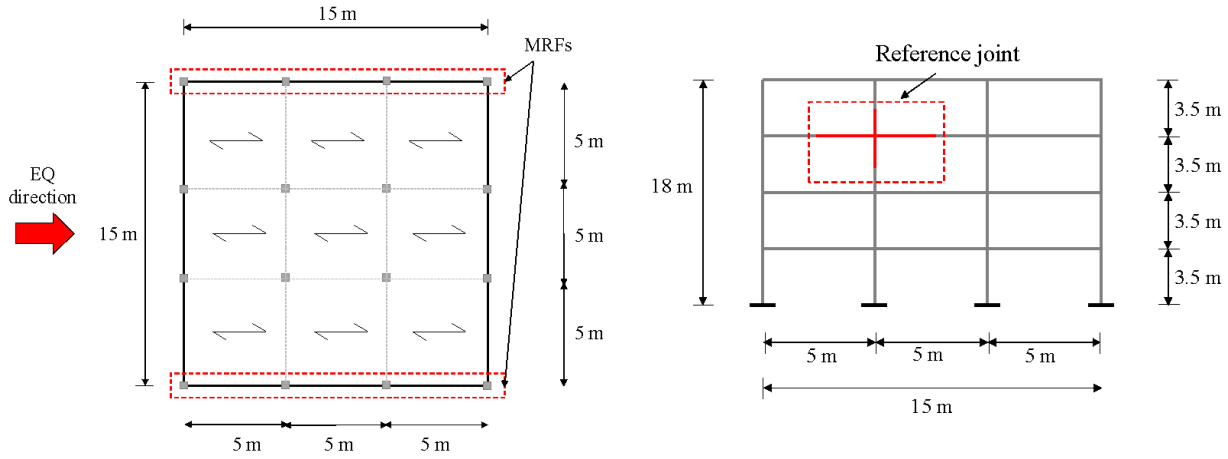

Figure 3.2: Hypothetical Reference Building Structure

The resulting design demand in terms of shear forces, moments and axial loads in the column and beam of the third floor of the building are summarized in Table 3.2.

Table 3.2: Seismic Demand on Beam and Column - Analysis

Element	Moment, M (kNm)	Shear, V (kN)	Axial load, N (kN)
Column	350	200	-300
Beam	275	120	0

3.3 DESIGN OF MDI-SERIES SPECIMEN

3.3.1 Reference Specimen (REFi) Design

Specimen REFi, a traditional moderately ductile RC beam-column joint, was designed assuming the following material properties: f'_c = 40 MPa, f_y = 410 MPa and f_u = 560 MPa (which represent the concrete compressive strength, the reinforcing steel yield strength, and the reinforcing steel ultimate strength, respectively). The column and the beam cross sections were 400 x 400 mm and 400 x 400 mm, respectively. The system was designed in line with Eurocode recommendations, following capacity design principles [38].

The beam was designed to meet the flexural demand obtained from the analysis (i.e., $M_b = 275\ kNm$). Adequate strength for yielding and ultimate demand (M_{bRy} = 278 kNm and M_{bRu} = 347 kNm, respectively) can be achieved with 8-18 mm diameter reinforcement bars at the top and bottom of the cross section (with a 40 mm cover, measured with respect to the center of the bars).

> To ensure adequate protection against shear failures, the shear demand on the beam was computed from the assigned flexural strength as:

$$V_{bd} = \frac{2 \cdot M_{bRu}}{L_{bcl}} \cong 156\ kN$$

> According to the Eurocode formulation (key equations reported below), conservatively setting the strut angle equal to 45 degrees (and with the angles α and β both equal to 1.0), sufficient strength can be achieved using 4 leg-10 mm diameter stirrups spaced at 200 mm [38]. Within the critical region of the beam (conservatively set equal to 650 mm), this spacing was reduced to 100 mm. The estimated shear strengths within the two beam regions were found with (Eq. 3-1):

$$\begin{gathered} V_{Rd} = \min\left(V_{Rd,s}, V_{Rd,c}\right) \\ V_{Rd,s} = \frac{0.9 d A_{sd} f_{yd}}{s}(cot\alpha + cot\theta) sin\alpha sin\beta \\ V_{Rd,c} = z b_w \nu_1 f_{cd}(cot\alpha + cot\theta)/(1 + cot^2\theta) \\ V_{bR,200} = 208\ kN\ and\ V_{bR,100} = 417\ kN \end{gathered} \qquad \textbf{Eq. 3-1}$$

> The column was designed to achieve a flexural strength approximately 30% higher than the strength of the beam (i.e., $M_c = 1.3 \cdot 347 = 452\ kNm$). To this end, a total of 12-28 mm diameter reinforcement bars equally distributed with 40 mm of cover from the cross-section edge provides adequate strength and cover. The theoretical yielding and ultimate flexural strength were M_{cRy} = 432 kNm and M_{cRu} = 522 kNm, respectively.

> To ensure that a premature shear failure of the column would not occur, the shear demand was estimated as a function of the column peak flexural strength. This is somewhat over conservative given that the maximum moment that can be experienced by the column is limited by the strength of the beam, but it was done in the interest of addressing any unaccounted beam over-strength or other phenomena that may lead to higher than expected demands. Thus, the estimated shear demand in the column was estimated using (Eq. 3-2):

$$V_{cd} = \frac{2 \cdot M_{cRu}}{L_{ccl}} = \frac{2 \cdot 522}{3.15} \cong 331\ kN \qquad \textbf{Eq. 3-2}$$

> Sufficient shear strength was achieved using 4 leg-12 mm diameter stirrups, spaced at 150 mm over the entire length of the column, excepting the joint region where the stirrup spacing was reduced to 100 mm. This results in a theoretical nominal shear strength $V_{cR} = 342\ kN$.

> The final design of specimen REFi is summarized in Figure 3.3.

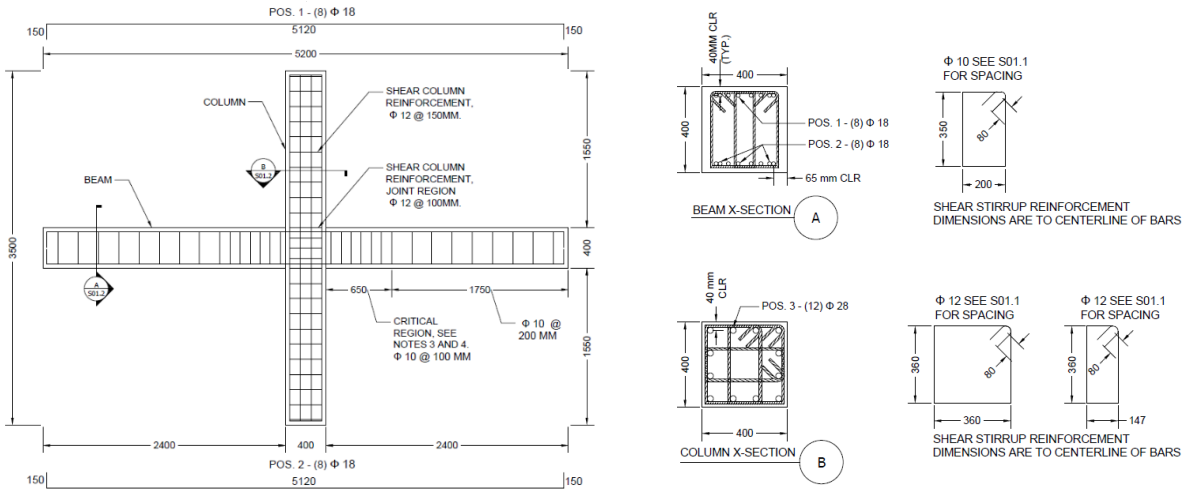

(a) View of reinforcement layout **(b) Joint details**

Figure 3.3: Specimen REFi Reinforcement Layout Details

3.3.2 NPS® Specimen Design (MDI series)

> The experimental program presented in this thesis is intended to assess the seismic performance of the NPS® moment resisting frame system, and gauge whether the NPS® system can achieve analogous to better performance than a moderately ductile RC MRF. The following parameters were selected criteria for addressing this concern:

- The solution adopted to provide moment continuity at the joint. Two approaches were considered:
  - added trusses
  - added deformed loose reinforcement
- The presence/absence of additional shear reinforcement in the beam end-regions
- The presence/absence of additional shear reinforcement in the joint region
- The presence/absence of a wrapped steel joint, where beams were not present.

> These aspects were discussed in Section 3.1 and a Test Matrix with details pertaining to each specimen was provided in Table 3.1.

> The design of the NPS® elements was performed following the Eurocode guidelines summarized in the technical report by Calvi [2] (considering the seismic demand estimated earlier in Section 3.3.1). It was further assumed that the "continuity elements" would have the same material properties as the reference specimen (REFi) beam reinforcement, namely f'_c = 40 MPa, f_y = 410 MPa and f_u = 560 MPa. The properties of the NPS® beam truss were assumed to be f_y = 360 MPa and f_u = 510 MPa. Evidently, the key objective targeted in this phase was to design capacity protected NPS® specimens that could approximately achieve the same strength and overall performance as the reference specimen, REFi.

> A "standard" NPS® beam was designed with the following properties: (i) bottom longitudinal reinforcement consisting of a 5 mm thick (400 mm wide) steel plate; (ii) top longitudinal reinforcement consisting of 4-26 mm diameter plain bars located 360 mm from the bottom fiber of the cross section; (iii) shear reinforcement consisting of two sets of 20 mm diameter diagonal bars spaced at 400 mm, welded to the bottom plate and to the top longitudinal reinforcement. The top longitudinal steel was welded to the top of the truss to provide stability. Also stabilizing the truss were 14 mm diameter bars at 400 mm spacing.

> The internal reinforcement layout of the NPS® column was identical to that of the reference column, with longitudinal reinforcement consisting of 12-28 mm deformed steel bars, and 4 leg-12 mm diameter shear reinforcement spaced at 150 mm. This spacing was reduced to 100 mm within the panel zone for specimens NPS2Ai and NPS2Bi. In contrast, specimen NPS1i was designed with no shear reinforcement within the joint region. All specimens except NPS4i were designed to have "windows" opened in the steel HSS in the joint panel region, on the sides without beams connected. This was done to gauge the contribution of the steel HSS column encasement to the integrity of the system.

> Different moment continuity, steel surrounding the joint, and beam-end confinement solutions were adopted for the different specimens. Details are as follows:

- Specimen NPS1i: The continuity elements were made of two 3.2 m long, 325 mm deep (top-to-bottom chord) truss elements. The top and bottom chords of each truss were made of pairs of 26 mm diameter smooth bars. Welded 20 mm diameter diagonal smooth bars spaced at 400 mm formed the web of each truss. Additional shear reinforcement consisting of 2 leg-14 mm diameter deformed bars was adopted within the beam critical region (i.e., from the beam-column interface to 650 mm into the beam), also called the beam end-regions.
- Specimen NPS2Ai, NPS2Bi and NPS4i: A total of six (equally split between top and bottom) 3.2 m long 30 mm diameter deformed bars provided moment continuity for these three specimens. Identical continuity elements lead, at least theoretically, to identical nominal strength (assuming the flexural response of the beam end-regions is the component that dictates the overall system response). The joint shear reinforcement for NPS2Ai consisted of 4 leg-12 mm diameter joint stirrups spaced at 100 mm.
- NPS2Bi: This was identical to specimen NPS2Ai but had additional shear steel, namely 2 leg- 14 mm diameter stirrups spaced at 100 mm within the beam critical region (650 mm).
- NPS4i: This was identical to NPS2Ai with respect to beam reinforcement configuration (i.e., no added stirrups in the over the critical beam length) but presented a different reinforcement solution pertaining to the joint region. NPS4i used a spacing of 150 mm rather than 100 mm for the join shear reinforcement, which involved 4 leg-12 mm diameter joint stirrups. NPS4i also utilized an intact steel HSS tube (i.e., with no "windows" cut out for phantom future beams of the HSS steel tube, as in NPS2Ai).

The differences between the continuity solutions adopted and the different shear reinforcement arrangements within the joint and beam end-regions are summarized in Figure 3.4, which provides a qualitative representation of the beam and panel zone reinforcement layout for all four specimens described in this section.

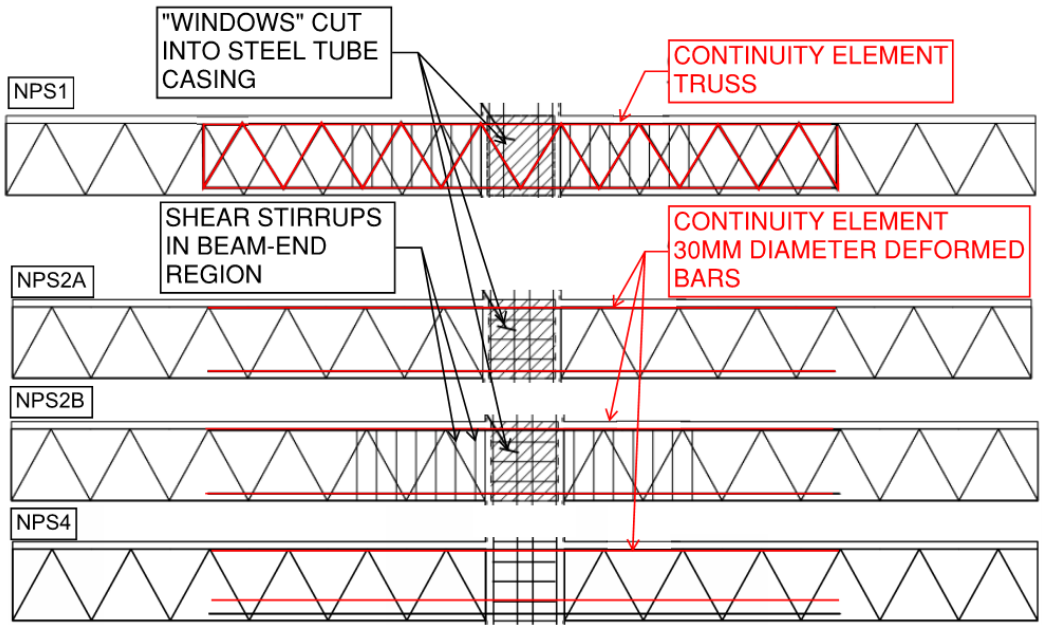

Figure 3.4: Qualitative View of Beam and Panel Zone Reinforcement Layout for MDI NPS® Specimens

The final design of all NPS® specimens apart of the MDI Test Series is summarized in Figure 3.5.

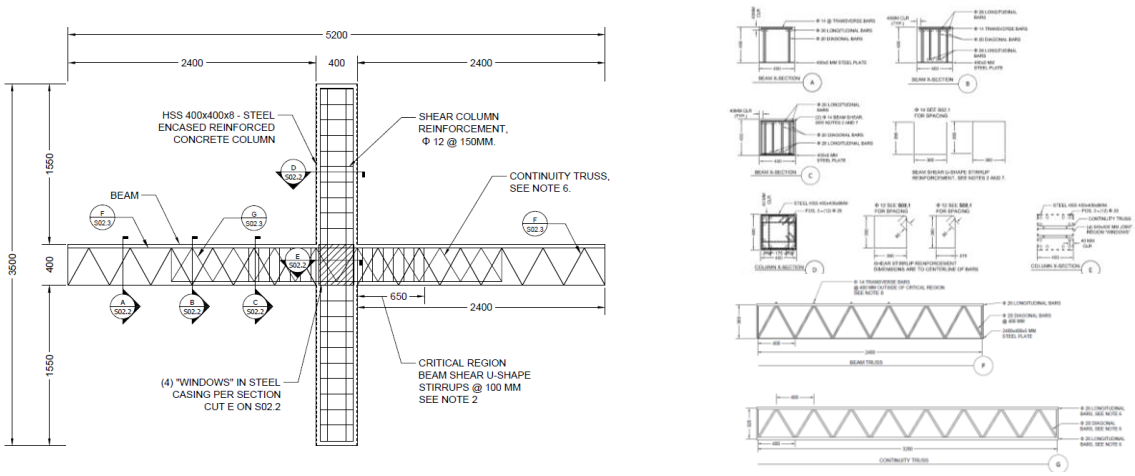

(a) NPS1i – View of reinforcement layout (left); Joint and beam details (right)

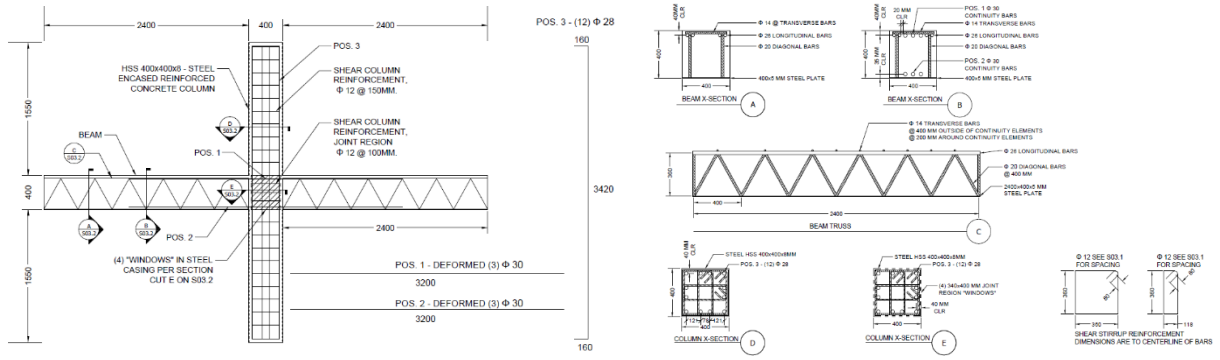

(b) NPS2Ai – View of reinforcement layout (left); Joint and beam details (right)

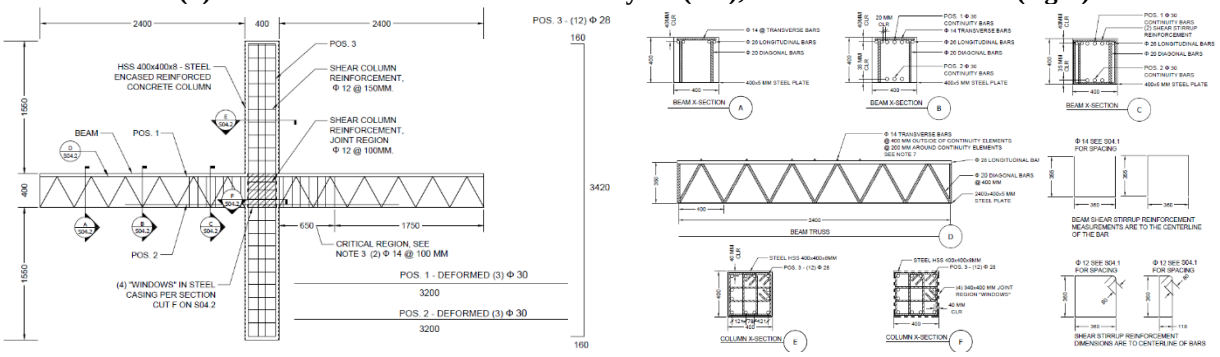

(c) NPS2Bi – View of reinforcement layout (left); Joint and beam details (right)

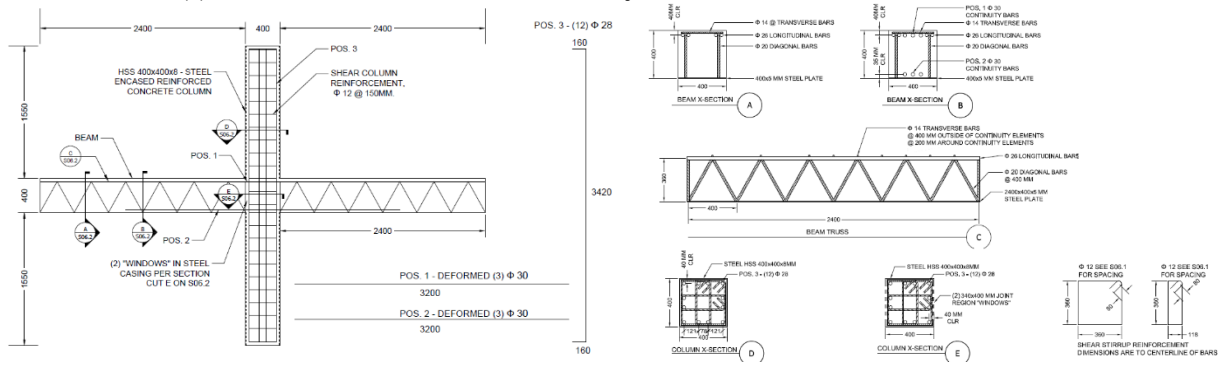

(d) NPS4i – View of reinforcement layout (left); Joint and beam details (right)

Figure 3.5: MDI NPS® Specimens Reinforcement Layout Details

3.4 DESIGN OF MDE-SERIES SPECIMENS

A second series of specimens, referred to as MDE Test Series, moderately ductile external specimens, was designed as part of this experimental program. This series of specimens was intended to represent an exterior beam-column joint of the same hypothetical structure described in Section 3.2. Both internal and external beam column joint subassemblies were assumed to be located at the same floor of the same theoretical building. Therefore, design solutions adopted for MDE Test Series were identical to the MDI Test Series but adjusted for the reduced development length available across the joint region. The beam reinforcement layout remained unchanged, given that the flexural seismic demand on the specimen did not change between the MDE Test Series and the MDI Test Series. In contrast, the demand on the column and the joint region was lower for an exterior joint than for its interior companion. This could lead to a reduction in the amount of shear reinforcement in the joint region. However, the design solution adopted for interior joints was maintained for this second Test Series, which was a conservative condition. This also allowed for simplicity during the construction process and provided the opportunity for a more direct comparison between the overall specimen performances.

The reinforcement detailing was modified to meet the necessary reinforcement anchorage requirements. This design decision resulted in a capacity protected system. A capacity protected system is one in which the beam possesses adequate flexural strength (capacity protected against shear mechanisms), but where columns and joints will be overdesigned, in the context of a moderately ductile frame. While this may be undesirable from an optimization standpoint, it is perfectly acceptable given the objectives of this study. In fact, adopting the design solution described herein allows this study to explore the response of the beam in a case where the joint has the benefits of a higher level of protection. In other words, where the beam is expected to play a somewhat more predominant role with respect to the overall performance of the system.

It is also interesting to point out that, despite being overdesigned, the joint does not meet the Eurocode high-ductility requirements. Hence, it still classified as a moderately ductile beam-column joint.

The final design of all NPS® MDE Test Series specimens is summarized in Figure 3.6 and Figure 3.7.

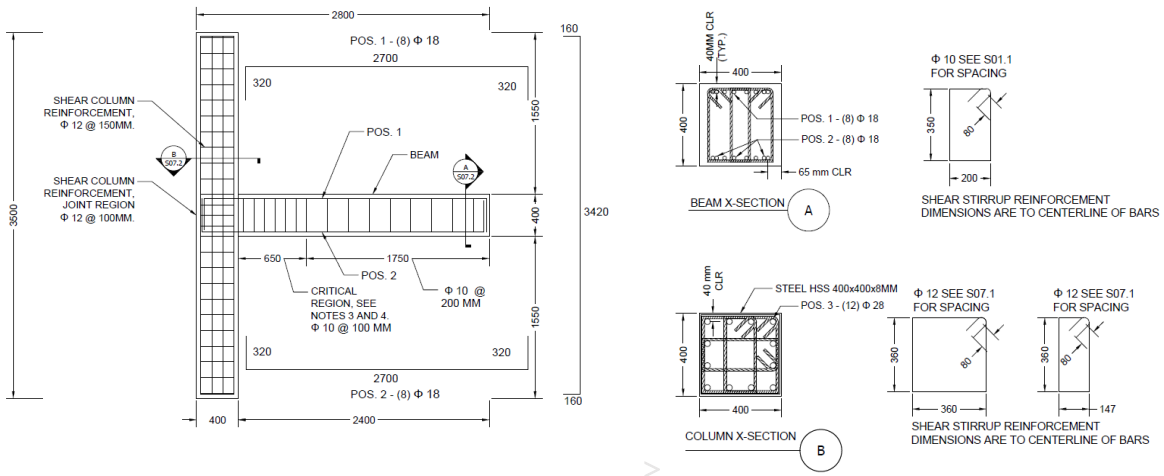

REFe – View of reinforcement layout (left); Joint details (right)

Figure 3.6: REFe Specimen Reinforcement Details

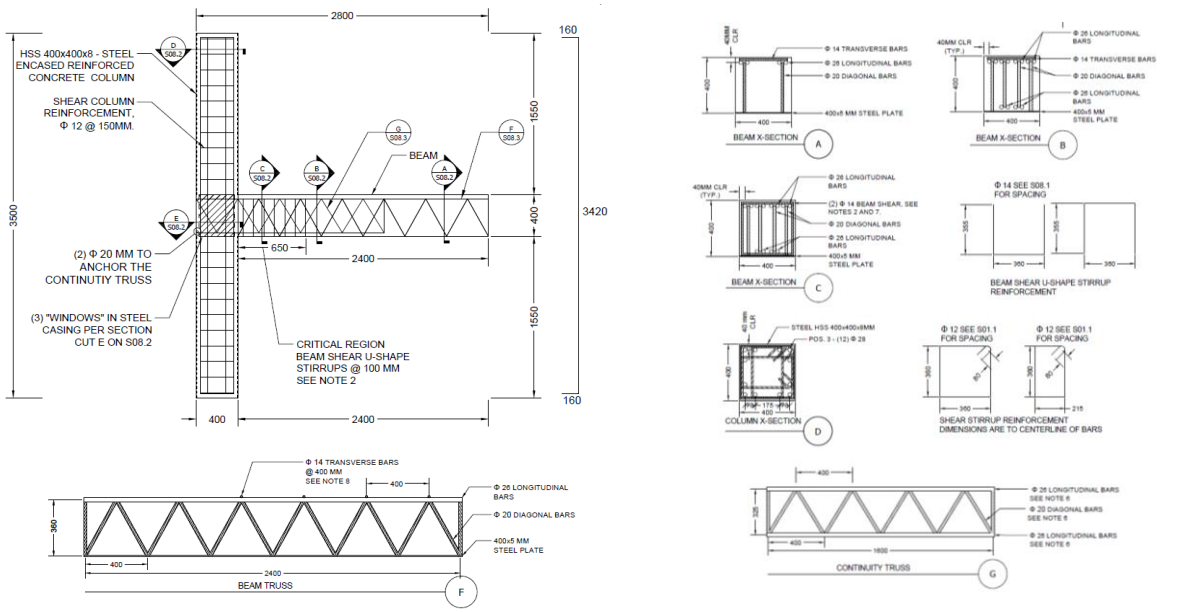

(a) NPS1e – View of reinforcement layout (left); Joint and beam details (right)

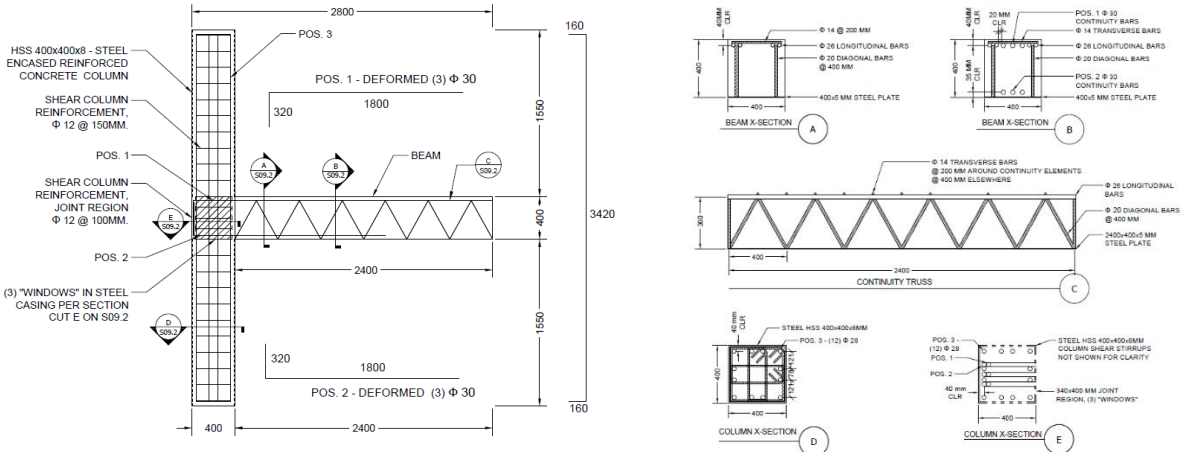

(b) NPS2Ae – View of reinforcement layout (left); Joint and beam details (right)

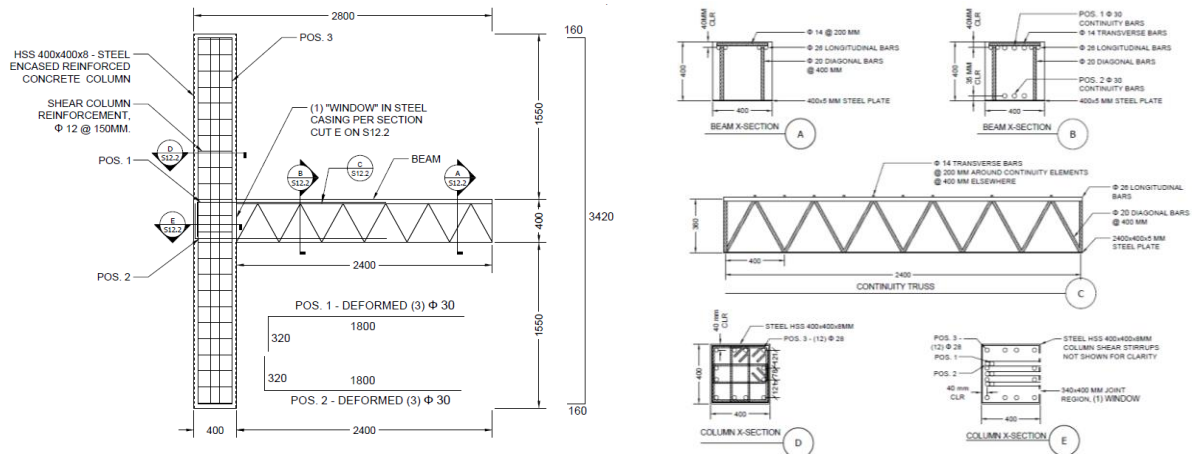

(c) NPS24e – View of reinforcement layout (left); Joint and beam details (right)

Figure 3.7: MDE NPS® Specimens Reinforcement Layout Details

3.5 DESIGN OF HD-SERIES SPECIMENS

> While this research project focused on moderately ductile frame system, a preliminary explorative effort was made into viable ways of achieving systems potentially capable of achieving higher ductility and energy dissipation by fully developing flexural mechanisms in the form of plastic hinges. It is well known that moderately ductile RC frames may not exploit the full ductility potentially available in the beams because of the inability of the joint to sustain multiple post-yielding loading cycles. Evidently, a highly ductile system could be achieved with adequate shear reinforcement in the joint region. However, this is not always possible, particularly in the NPS® system, because of reinforcement congestion and constructability concerns. Thus, this pilot HD Test Series was dedicated to exploring whether high ductility systems can be achieved by protecting the joint region through plastic hinge relocation. This concept has been used in the past to achieve this objective in RC frames. A detailed discussion on plastic hinge relocation strategies can be found in Paulay and Priestley [11].

> Adapting RC plastic hinge relocation concepts, two NPS® beam-column joints (one interior and one exterior) intended to form traditional plastic hinges in the beams, 500 mm from the beam-column interface, were designed. The seismic demand on the system was computed as described in Section 3.2 for all other specimens, using a response factor q = 5.85 (instead of 3.9) to address the potential higher ductile nature of the specimens.

> The notable outcomes of the series design include (i) an NPS® top truss beam chord of 4-24 mm diameter bars (instead of the 26 mm diameter bars used for all other NPS® specimens due to space concerns), (ii) a 400 x 5 mm plate bottom cord (with a reduced beam section (RBS), width reduced to 360 mm in the intended plastic hinge region) and (iii) continuity bars made of 2-36 mm diameter smooth hoop bars, arranged as shown in Figure 3.8 and Figure 3.9. Mechanically anchored plain bars were selected because they tend to be more effective at driving part of the demand away from the joint region. They also induce transfer of shear forces through the joint via strut action rather than bond, thus protecting the joint from cracking and deterioration under cycles. In this context, the plastic hinge region of the beam needed to be

adequately reinforced in shear, hence integrative hoops consisting of 2-leg 14 mm stirrups spaced at 100 mm were used within the beam critical length (850 mm in this case) and seen in Figure 3.10.

> The columns were identical to those used for all others NPS® specimens, while the joint region was reinforced in shear using 4-leg 14 mm diameter bars, spaced at 100 mm.

> A qualitative representation of the beam and panel zone reinforcement layout for the two HD specimens designed in this section is provided in Figure 3.8, while the final design outcome is summarized in Figure 3.9.

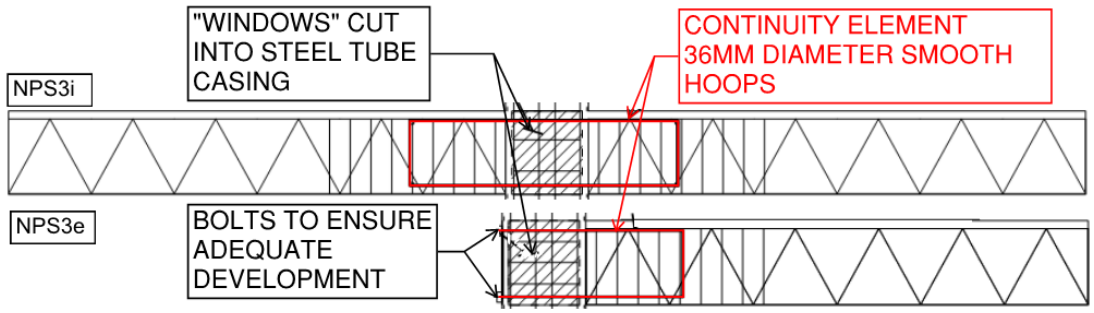

Figure 3.8: Qualitative View of Beam and Panel Zone Reinforcement Layout for HD NPS® Specimens

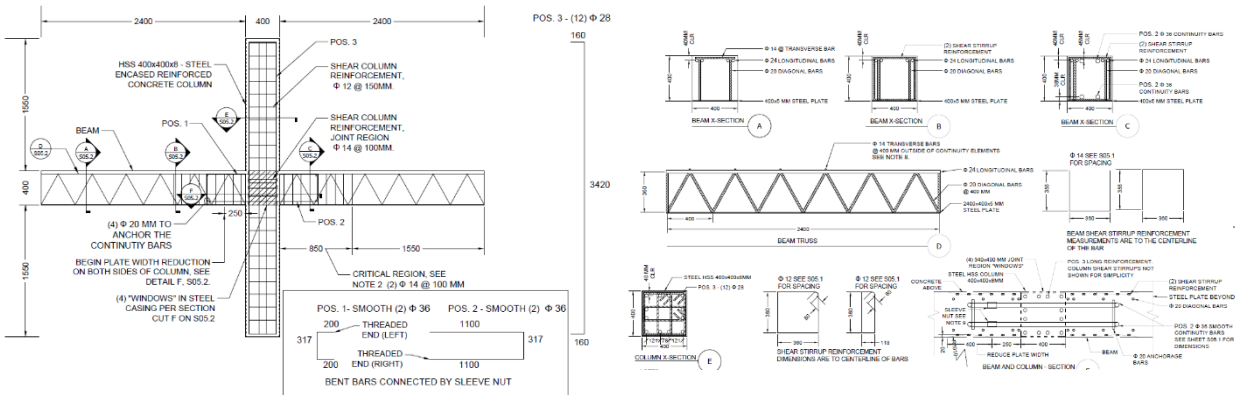

(a) NPS3i – View of reinforcement layout (left); Joint and beam details (right)

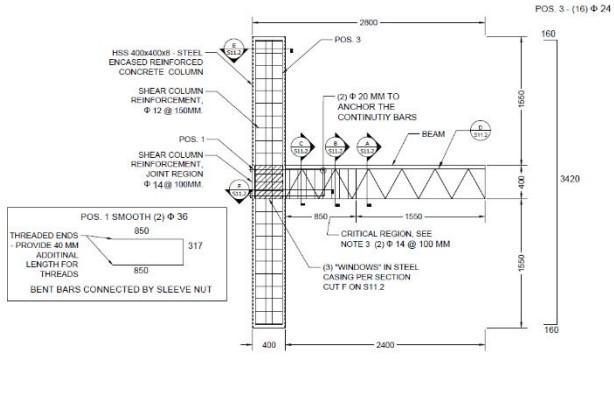

(b) NPS3e – View of reinforcement layout

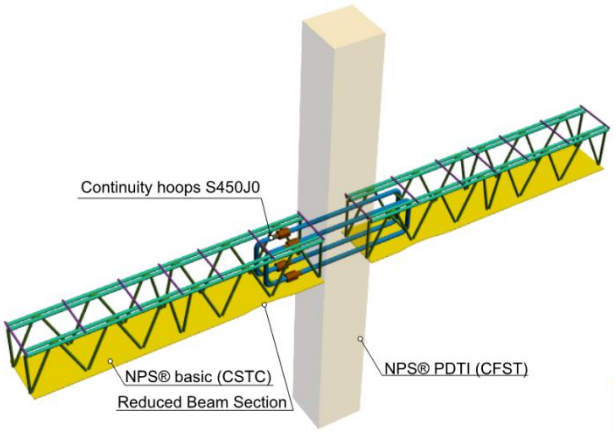

(c) NPS3i – 3D view of continuity reinforcement

Figure 3.9: HD NPS® Specimens Reinforcement Layout Details

3.6 DESIGN SUMMARY

> A total of 11 moderately ductile beam-column joint specimens were designed and tested in this experimental program. External specimens were identical to internal specimens except for the number of beams (i.e., one instead of two). All specimens had identical overall dimensions. The main structural components included 5 m long beams and 3.5 m long columns. Both these elements had 400 x 400 mm cross sections. The design of all specimens was carried out in line with Eurocode recommendations, following capacity design principles (strong column-weak beam) and assuming a concrete compressive strength of 40 MPa.

> The key design outcomes (i.e., reinforcement layouts and steel type) are summarized in Table 3.3.

Table 3.3: Summary of Reinforcement Properties for all Specimens

	Beam		Column		Continuity elements	
Specimen -Series-	**Steel type**	**Top long. bars Bot. long. bars Trans. bars Trans. bars end-region**	**Steel type**	**HSS Long. Bars Trans. bars Trans. bars panel zone Panel zone HSS**	**Steel type**	**Top long. Bars Bot long. bars Trans. bars**
REFi -MDI-	B450C B450C B450C B450C	8-ϕ18 (cover 40 mm) 8-ϕ18 (cover 40 mm) 4-leg ϕ10 @ 200 mm 4-leg ϕ10 @ 100 mm	- B450C B450C B450C -	- 12-ϕ28 (cover 40 mm) 4-leg ϕ12 @ 150 4-leg ϕ12 @ 100 -	Beam reinforcement continuous through joint	
NPS1i -MDI-	S355 J0 S355 J0 S355 J0 B450C	4-ϕ26 400 x 5 mm plate 2-ϕ20 diag. @ 400 mm 4-leg ϕ10 @ 100 mm	S355 J2 B450C B450C B450C -	400 x 400 x 8 mm 12-ϕ28 (cover 40 mm) 4-leg ϕ12 @ 150 - -	S355 J0 S355 J0 S355 J0	4-ϕ26 4-ϕ26 2-ϕ20 diag. @ 400 mm
NPS2Ai -MDI-	S355 J0 S355 J0 S355 J0 B450C	4-ϕ26 400 x 5 mm plate 2-ϕ20 diag. @ 400 mm -	S355 J2 B450C B450C B450C -	400 x 400 x 8 mm 12-ϕ28 (cover 40 mm) 4-leg ϕ12 @ 150 4-leg ϕ12 @ 100 -	B450C B450C -	3-ϕ30 3-ϕ30 -
NPS2Bi -MDI-	S355 J0 S355 J0 S355 J0 B450C	4-ϕ26 500 x 5 mm plate 2-ϕ20 diag. @ 400 mm 2-leg ϕ14 @ 100 mm	S355 J2 B450C B450C B450C -	400 x 400 x 8 mm 12-ϕ28 (cover 40 mm) 4-leg ϕ12 @ 150 4-leg ϕ12 @ 100 -	B450C B450C -	3-ϕ30 3-ϕ30 -
NPS4i -MDI-	S355 J0 S355 J0 S355 J0 B450C	4-ϕ26 500 x 5 mm plate 2-ϕ20 diag. @ 400 mm -	S355 J2 B450C B450C B450C S355 J2	400 x 400 x 8 mm 12-ϕ28 (cover 40 mm) 4-leg ϕ12 @ 150 4-leg ϕ12 @ 150 2-8 mm thick plates	B450C B450C -	3-ϕ30 3-ϕ30 -
REFe -MDE-	B450C B450C B450C B450C	8-ϕ18 (cover 40 mm) 8-ϕ18 (cover 40 mm) 4-leg ϕ10 @ 200 mm 4-leg ϕ10 @ 100 mm	- B450C B450C B450C -	- 12-ϕ28 (cover 40 mm) 4-leg ϕ12 @ 150 4-leg ϕ12 @ 100 -	Beam reinforcement continuous through joint	
NPS1e -MDE-	S355 J0 S355 J0 S355 J0 B450C	4-ϕ26 400 x 5 mm plate 2-ϕ20 diag. @ 400 mm 4-leg ϕ10 @ 100 mm	S355 J2 B450C B450C B450C -	400 x 400 x 8 mm 12-ϕ28 (cover 40 mm) 4-leg ϕ12 @ 150 - -	S355 J0 S355 J0 S355 J0	4-ϕ26 4-ϕ26 2-ϕ20 diag. @ 400 mm
NPS2Ae -MDE-	S355 J0 S355 J0 S355 J0 -	4-ϕ26 400 x 5 mm plate 2-ϕ20 diag. @ 400 mm -	S355 J2 B450C B450C B450C -	400 x 400 x 8 mm 12-ϕ28 (cover 40 mm) 4-leg ϕ12 @ 150 4-leg ϕ12 @ 100 -		3-ϕ30 3-ϕ30 -
NPS4E -MDE-	S355 J0 S355 J0 S355 J0 -	4-ϕ26 500 x 5 mm plate 2-ϕ20 diag. @ 400 mm -	S355 J2 B450C B450C B450C S355 J2	400 x 400 x 8 mm 12-ϕ28 (cover 40 mm) 4-leg ϕ12 @ 150 4-leg ϕ12 @ 150 2-8 mm thick plates	B450C B450C -	3-ϕ30 3-ϕ30 -

	Beam		Column		Continuity elements	
Specimen -Series-	**Steel type**	**Top long. bars Bot. long. bars Trans. bars Trans. bars end-region**	**Steel type**	**HSS Long. Bars Trans. bars Trans. bars panel zone Panel zone HSS**	**Steel type**	**Top long. Bars Bot long. bars Trans. bars**
NPS3i -HD-	S355 J0 S355 J0 S355 J0 B450C	4-ϕ24 500 x 5 mm plate 2-ϕ20 diag. @ 400 mm 2-leg ϕ14 @ 100 mm	S355 J2 B450C B450C B450C S355 J2	400 x 400 x 8 mm 12-ϕ28 (cover 40 mm) 4-leg ϕ12 @ 150 4-leg ϕ12 @ 150 -	S450 J0 S450 J0 -	2-ϕ36 2-ϕ36 -
NPS3e -HD-	S355 J0 S355 J0 S355 J0 B450C	4-ϕ24 500 x 5 mm plate 2-ϕ20 diag. @ 400 mm 2-leg ϕ14 @ 100 mm	S355 J2 B450C B450C B450C S355 J2	400 x 400 x 8 mm 12-ϕ28 (cover 40 mm) 4-leg ϕ12 @ 150 4-leg ϕ12 @ 150 -	S450 J0 S450 J0 -	2-ϕ36 2-ϕ36 -

> Table 3.4 provides a summary of the specimens' nominal strength, computed using the Eurocode formulation and assuming that the overall strength of the beam-column joint assemblies is limited by the flexural strength provided by the continuity elements or by the flexural strength of the NPS® beam (for specimens NPS3i and NPS3e). The results outlined in Table 3.4 show that the nominal strength of all specimens is reasonably close, with some of the NPS® specimens expected to achieve a (nominal) horizontal peak load about 10% higher than what was expected for the reference specimens. The nominal strength of the HD specimens appears to be somewhat higher than intended, given that they were designed for a seismic demand of approximately 70% of the reference specimen demand. This discrepancy is deemed acceptable at this stage. It should be noted that the strength values reported in Table 3.4 are estimates obtained using the Eurocode approach in combination with nominal material strength values and will be refined in later chapters.

Table 3.4: Specimens' Nominal Strength (Eurocode)

Test series	Specimen ID	M_{bn}^{+} [kN]	M_{bn}^{-} [kN]	F_{Hn}^{+} [kN]	F_{Hn}^{-} [kN]	$F_{Hn}^{+}/F_{Hn,ref}^{+}$	$F_{Hn}^{-}/F_{Hn,ref}^{-}$
MDI	REFi	278	278	179	179	1.00	1.00
	NPS1i	278	273	179	176	1.00	0.98
	NPS2Ai	306	298	198	192	1.10	1.07
	NPS2Bi	306	298	198	192	1.10	1.07
	NPS4i	306	298	198	192	1.10	1.07
MDE	REFe	278	278	90	90	1.00	1.00
	NPS1e	278	273	90	88	1.00	0.98
	NPS2Ae	306	298	99	96	1.10	1.07
	NPS4e	306	298	99	96	1.10	1.07
HD	NPS3i	242	236	156	152	0.87	0.85
	NPS3e	242	236	78	76	0.87	0.85

3.7 SPECIMEN FABRICATION AND MATERIAL TESTING [42] [43]

> All specimens, including all carpentry required for the realization of the experimental setup, were fabricated by Tecnostrutture srl in Noventa di Piave, Italy. Figure 3.10 shows some of the phases part of the fabrication process, alongside some of the main steel structural components.

(a) NPS® beam trusses

(b) NPS® column reinforcing cage

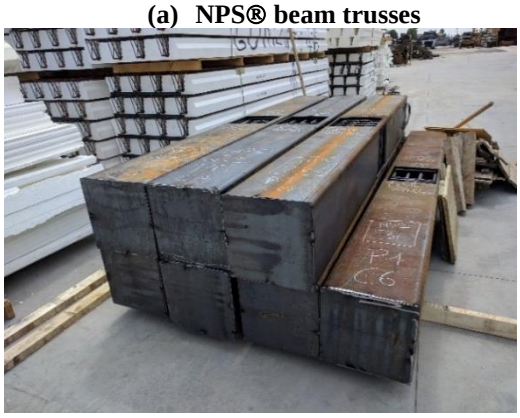

(c) NPS® columns (HSS and inernal bars)

(d) Specimen casting

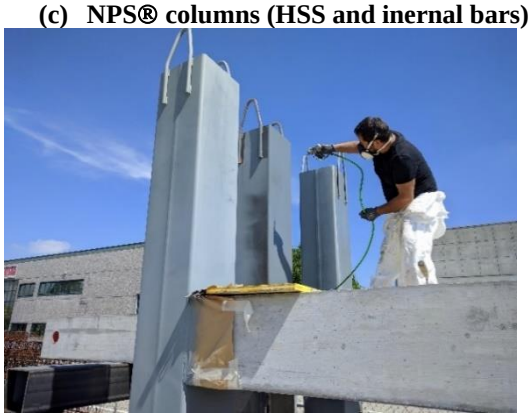

(e) Specimen polishing and painting

(f) Specimen transportation

Figure 3.10: Specimen Fabrication and Delivery

> Material testing was also performed by Tecnostrutture srl. The material test results are summarized in Table 3.5 and Table 3.6.

Table 3.5: Reinforcing Steel Properties

Steel type	f_y [MPa]	f_u [MPa]	f_u/f_y
ϕ20 - S355J0	384	532	1.39
ϕ24 - S355J0	418	567	1.36
ϕ26 - S355J0	371	517	1.39
ϕ36 – S450J0	474	659	1.39
HSS 400x400x8	383	535	1.40
5 mm thick plate	386	517	1.34
ϕ8 - B450C	470	577	1.23
ϕ10 - B450C	491	602	1.23
ϕ12 - B450C	495	611	1.23
ϕ14 - B450C	458	576	1.26
ϕ28 - B450C	519	635	1.22

Table 3.6: Concrete Properties

Sample	f'_c [MPa]
RckS0d8-1	44.7
RckS0d8-2	45.9
RckS0d8-3	44.8
Mean	45.2

3.8 TESTING AND ANALYSIS

3.8.1 Experimental Setup and Loading Protocol

The experimental program described in this report was conducted in the Shake Lab at Eucentre (see Figure 3.11), Italy, using the available 3D Strong wall-strong floor system (the "3D Reaction System"). This setup consists of two strong walls orthogonal to each other and is ideal to conduct large scale (including full-scale) pseudo-static and pseudo-dynamic tests on building prototypes or structural components.

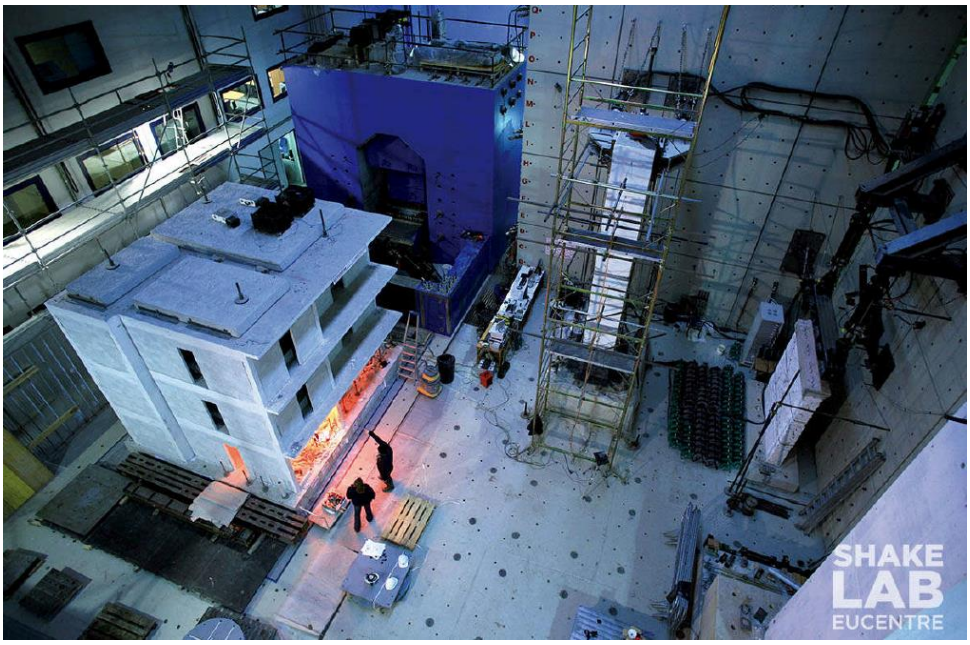

Figure 3.11: View of Eucentre Laboratory

The main characteristics of the Reaction System are reported in Table 3.7. All the available actuators are servo-controlled, connected to a series of flexible and rigid hoses, and fed by a series of pumps designed to achieve high pressure at high velocity (if necessary, accumulators are also available to achieve peak demands).

Table 3.7: Reaction System Characteristics

Strong floor dimensions	14.4 m x 9.6 m
Strong walls height	12 m
Maximum force applicable at 1 m	46120 kN
Maximum force applicable at 12 m	3840 kN
250 kN servo-controlled actuators available	5
500 kN servo-controlled actuators available	3
1000 kN servo-controlled actuators available	2
2500 kN servo-controlled actuators available	1

The experimental setup adopted in this program is schematically shown in Figure 3.12 and in the photographs in Figure 3.13. In the shown configuration the specimen is connected to the strong floor through two steel rods pinned to the extremity of each beam (Figure 3.12c) and through a cylindrical hinge located at the base of the column (Figure 3.12d). The top of the column is rigidly connected to two servo-controlled hydraulic actuators intended to simultaneously apply the desired loads (Figure 3.12b). All connections are 200mm from the edge of the respective member.

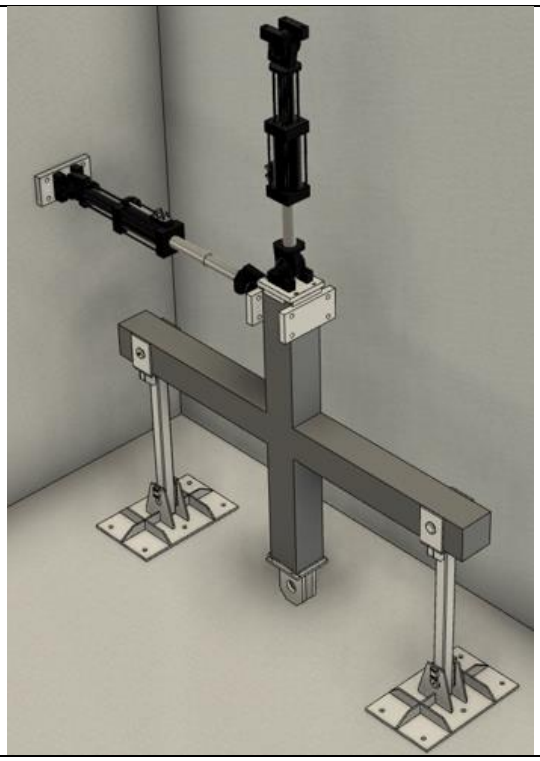

(a) Experimental setup overview

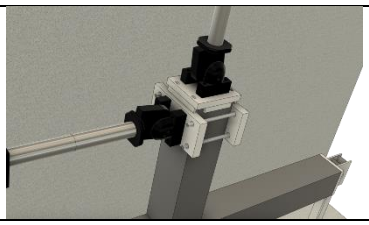

(b) Actuator-column connection detail

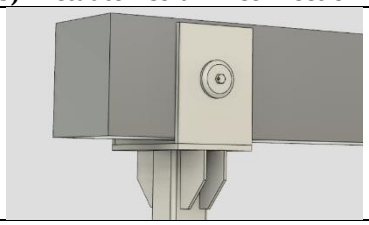

(c) Beam support connection detail

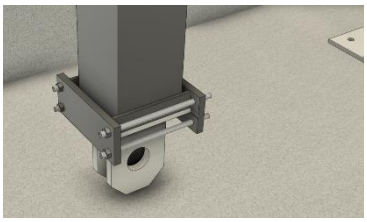

(d) Base of column detail

Figure 3.12: Schematic Representation of Experimental Setup

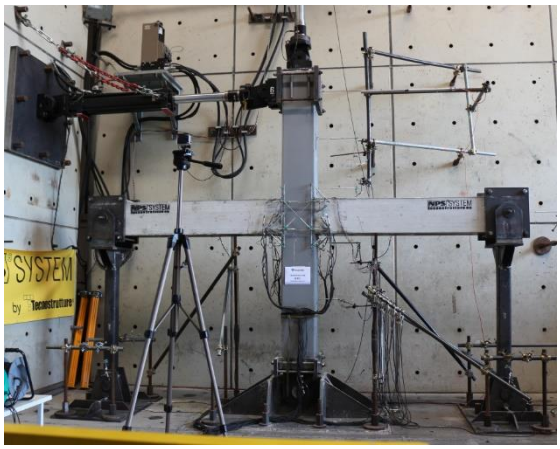

(a) Interior specimen ready to be tested

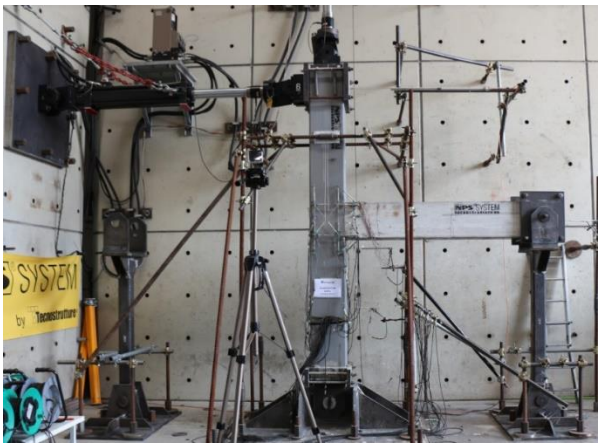

(b) Exterior specimen ready to be tested

Figure 3.13: Photographic View of Experimental Setup

> All specimens were tested under quasi-static reversed cyclic horizontal loads and constant vertical loads (applied at the top of the column), as shown in Figure 3.14. The loads were applied through two ±500 kN, ±500 mm stroke, servo-controlled actuators.

> The tests followed the loading protocol summarized in Table 3.8 and described in more detail below. The loading protocol involved three cycles at each selected drift level, followed by an increase in displacement amplitude, as can be seen in Figure 3.15.

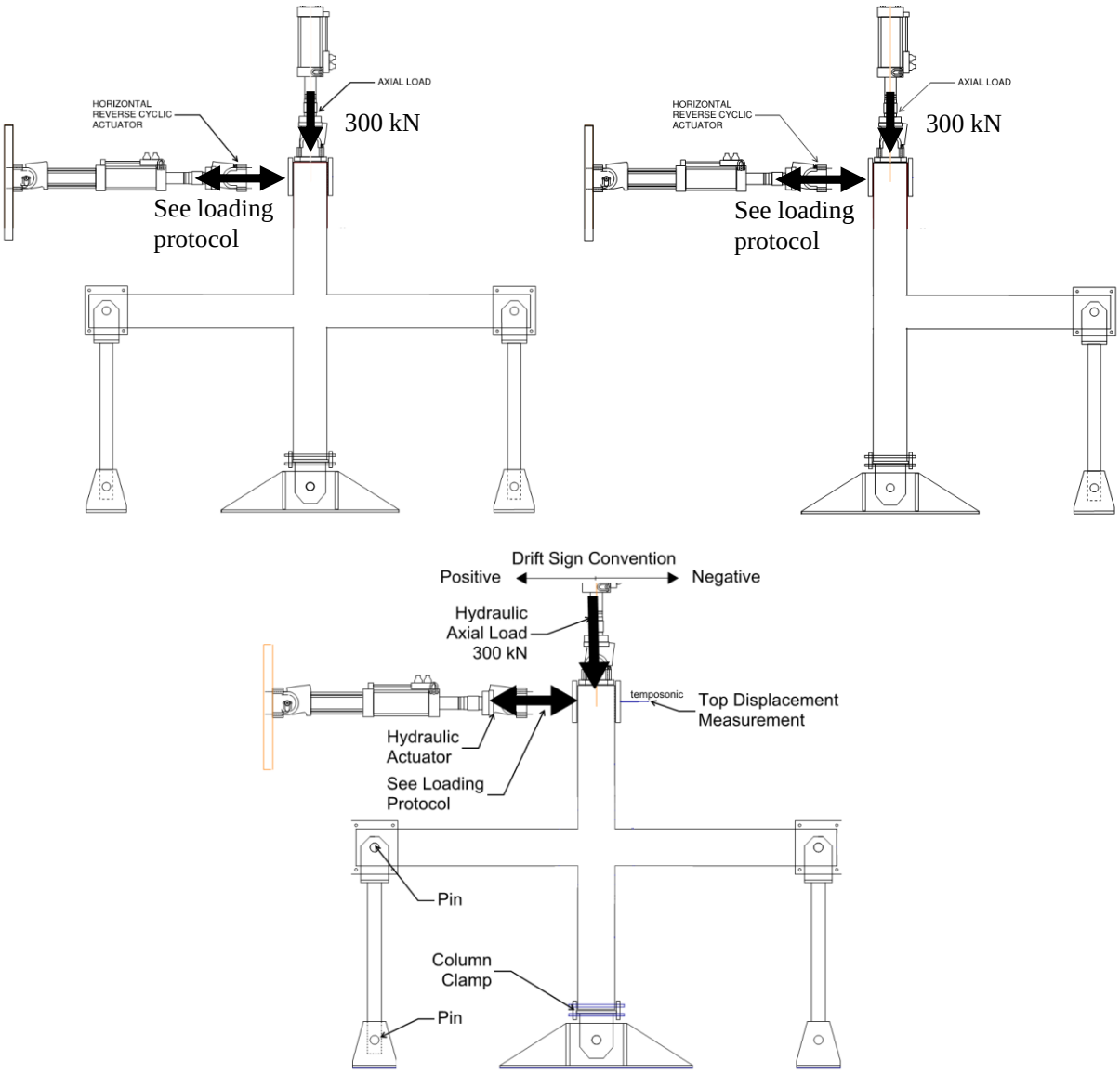

Figure 3.14: View of Loading Configuration

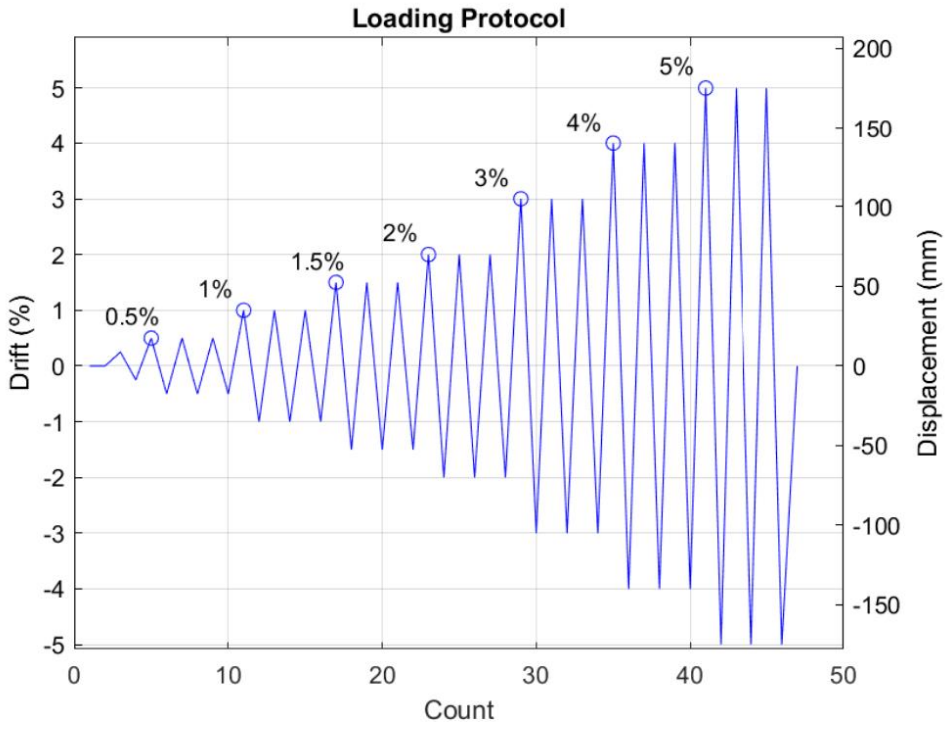

Figure 3.15: Loading Protocol

Table 3.8: Loading Protocol

Load stage #	Drift ratio [%]	Axial load [kN]	Horizontal displacement [mm]	Velocity [mm/s]	Number of cycles
1		300	-	1 kN/s	1
2	0.10	300	3.66	0.05	1
3	0.25	300	9.14	0.10	3
4	0.50	300	18.28	0.20	3
5	1.00	300	36.55	0.40	3
6	1.50	300	54.83	0.60	3
7	2.00	300	73.10	0.80	3
8	3.00	300	109.65	1.20	3
9	4.00	300	146.20	1.60	3
10	5.00	300	182.75	2.00	3

> The loading protocol reported in Table 3.8 can be summarized as follows:

1. Axial load application (compressive load of 300 kN), maintained constant throughout the test
2. Performance of one full cycle at horizontal displacement of 3.66mm (displacement control)
3. Performance of three full cycles at horizontal displacement of 9.14 mm (displacement control)
4. Performance of three full cycles at horizontal displacement of 18.28 mm (displacement control)
5. Performance of three full cycles at horizontal displacement of 36.55 mm (displacement control)

6. Performance of three full cycles at horizontal displacement of 54.83 mm (displacement control)
7. Performance of three full cycles at horizontal displacement of 73.10 mm (displacement control)
8. Performance of three full cycles at horizontal displacement of 109.65 mm (displacement control)
9. Performance of three full cycles at horizontal displacement of 146.20 mm (displacement control)
10. Performance of three full cycles at horizontal displacement of 182.75 mm (displacement control)

3.8.2 Instrumentation and Measurements

> Data acquisition for the tests was extensive with several GB of data stored to disks after each experiment. During each test global displacements, average surface strains, and local reinforcement strains were acquired continuously using a combination of linear potentiometers and strain gauges.

> Additionally, video and photographs were taken throughout all tests, capturing the more qualitative aspects of the experiments. Each source of data is described in the following sections.

3.8.3 Linear Potentiometers

> Primary real-time measurements of the global displacements and average strain state of all specimens were provided by up to 49 linear potentiometers (42 for exterior specimens) mounted on the front and back surfaces of the beam-column joints around the panel region (using concrete anchors) or arranged to monitor the horizontal displacements of the systems. More specifically:

- 3 potentiometers were mounted at the strong floor level to monitor potential displacements of the base supports
- 4 potentiometers were used to measure potential out-of-pane displacements
- 6 potentiometers were mounted at various heights along the height of the column (including one set up to directly monitor the horizontal displacement of the beam along the beam centerline)
- 12 potentiometers (6 on the front and 6 on the back) were dedicated to monitor the average displacements of the panel zone
- 24 potentiometers were arranged to provide data pertaining to the panel zone rotation, and the beam and column rotation near the interface region

> The potentiometer arrangement adopted for all specimens is shown in Figure 3.16, Figure 3.17, and Figure 3.18.

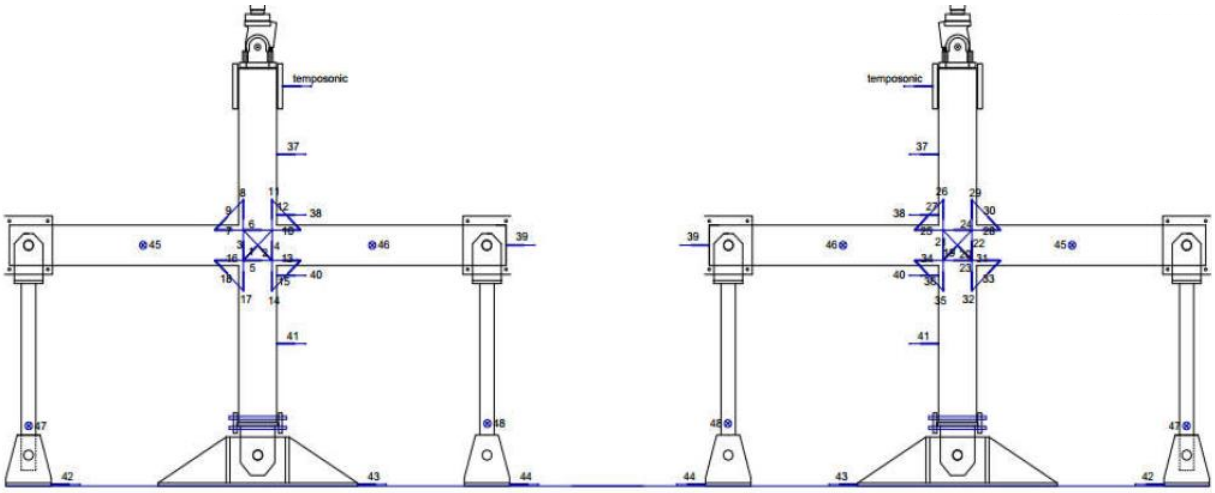

Figure 3.16: Surface Instrumentation/Potentiometer Arrangement for Interior Specimens Front (Left) - Back (Right)

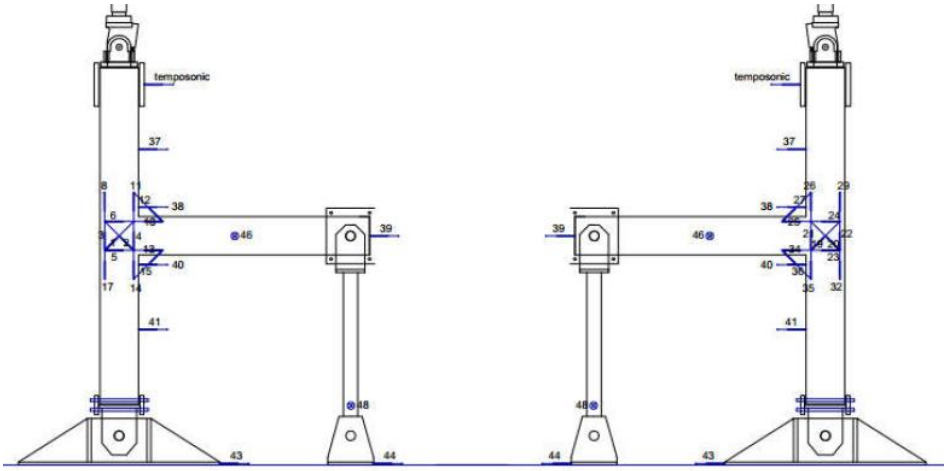

Figure 3.17: Surface Instrumentation/Potentiometer Arrangement for Exterior Specimens Front (Left) - Back (Right)

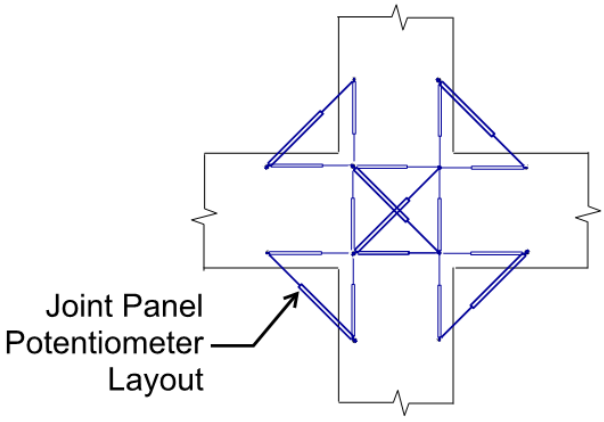

Figure 3.18: Typical Joint Panel Potentiometer Layout

3.8.4 Load Cells

> The actuators employed to generate the desired loading conditions were both outfitted with one load cell and one string potentiometer, allowing for continuous acquisition of the force and displacement. See Figure 3.14 for a visual view of the loading cells.

> The load cells also provided the primary means by which the applied forces, internal forces, and stress states were measured for this project. Since the specimens were statically determined systems, all main actions (i.e., internal shear and moments in beams and columns) could be computed from simple equilibrium considerations, knowing the applied force magnitudes and locations and the specimen geometry.

3.8.5 Strain Gauges

> Each specimen was instrumented with at least 10 strain gauges (6.25 mm gauge length) attached directly to selected reinforcing bars. The strain gauges were affixed to the bars after the welding had been completed and were protected by coatings of polyurethane and wax and covered with aluminum foil tape.

> The strain gauges were positioned as shown in Figure 3.19, as consistently as possible from one specimen to the next. The strain gauge locations were selected to allow monitoring of a wide range of reinforcing elements while maintaining the number of gauges employed reasonable. Elements of interest included the strain experienced by the continuity reinforcement, the joint shear reinforcement, the column longitudinal bars and some of the beam longitudinal and shear reinforcement.

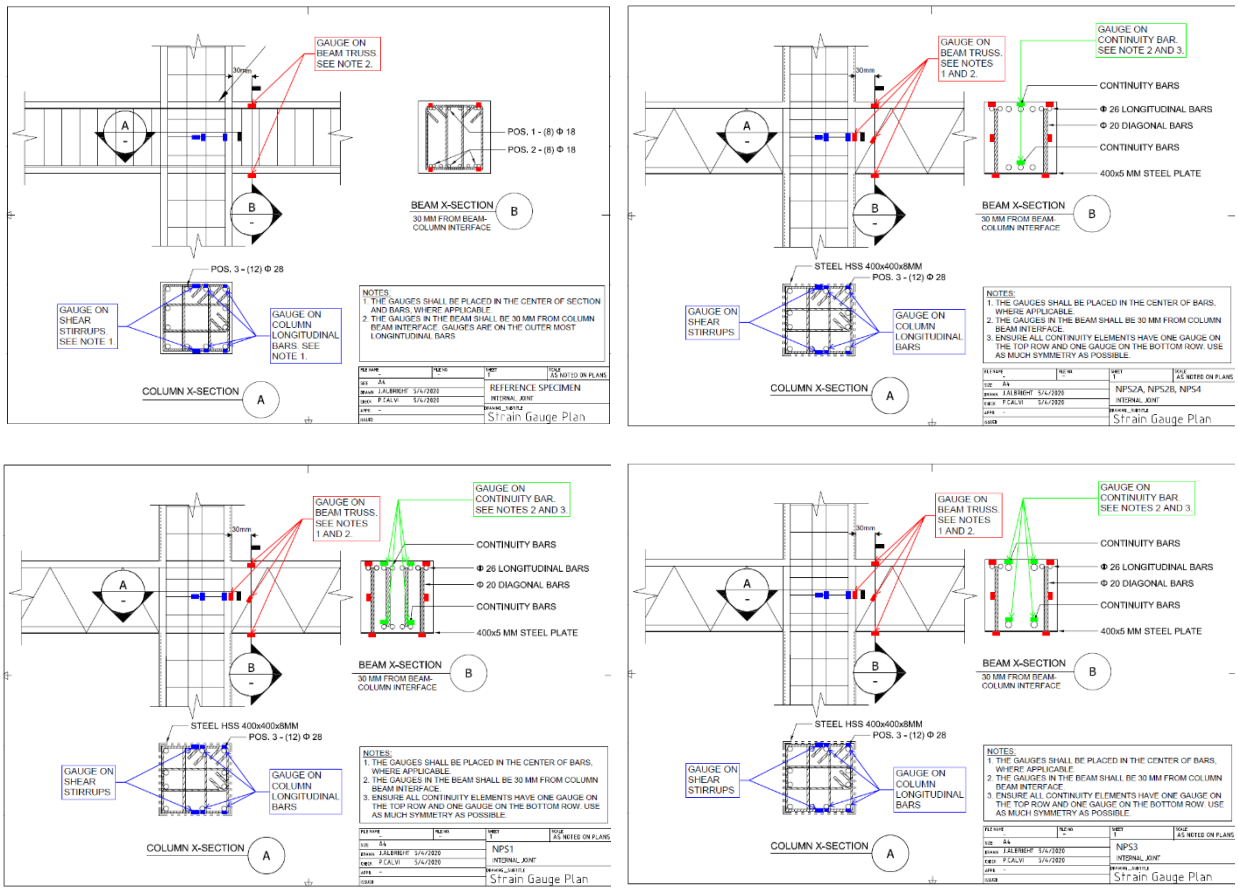

Figure 3.19: View of Strain Gauge Locations

Some photographs of strain gauges mounted on one of the NPS® beams and on the longitudinal reinforcing bars of one of the columns are provided in Figure 3.20.

(b) Strain gauges on NPS® beam bars

(a) Strain gauges on NPS® beam longitudinal bar

(c) Strain gauges on column longitudinal bars

Figure 3.20: Photographic View of Installed Strain Gauges

3.8.6 Crack Mapping and Crack Width Measurements

Crack widths were measured throughout the experiments at discrete "load stages," after the third cycle at a given load. Crack widths were measured by visual comparison with printed line-widths, to the nearest 0.05 mm. Widths were measured at several locations along each crack, typically in the panel region and at the beam ends, as well as at any other locations throughout the body of the specimens that presented signs of distress. The cracks were traced using permanent marker to make them more visible in the load stage photos.

3.8.7 Photos and Videos

A complete record of each of the tests exists in the form of still photos and videos. Video was recorded on the front face of each specimen. Still photos were taken of both faces during and between load stages. High-speed photos were also taken of the front face during loading by means of a remote trigger. Owing to the high frame it was possible in some instances to capture the propagation of failure via higher resolution photographs rather than through the videos.

CHAPTER 4 CALCULATIONS

> Chapter 4 explains in detail how each specimen was analyzed, from basic principles such as shear strain and shear stress, to more detailed desirable parameters such as stiffness and energy dissipation. This chapter does not focus on the differences or draw conclusions among the specimens, it is meant only as a technical reference to support later analytical chapters.

4.1 MOMENT AND SHEAR IN THE SYSTEM

> The joint region is arguably the most critical region of a moment resisting frame, when subjected to lateral seismic loading [17]. The internal forces of the column, assuming a homogenous section, are shown in Figure 4.1and adapted from Paulay [11]. The joint feels both horizontal and vertical shear forces which are typically much higher than the shear in the adjacent beams and columns [15]. Moment equations were obtained from global equilibrium, including second order effects, as seen in (Eq. 4-1) and (Eq. 4-2) for internal and external joint specimens, respectively.

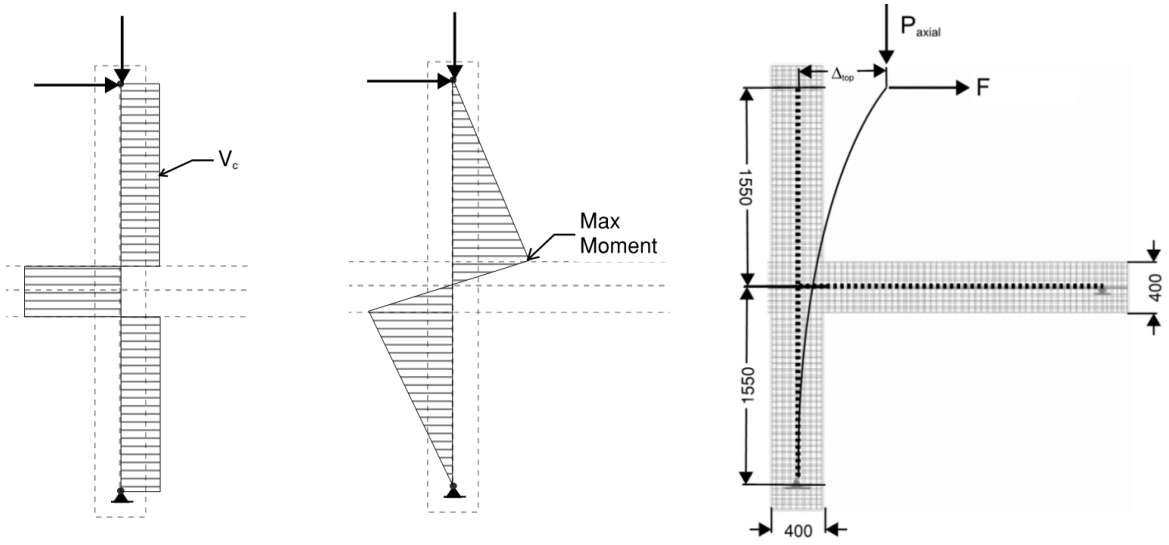

(a) Shear forces **(b) Bending Moments** **(c) P-Delta Effects**

Figure 4.1: Shear and Moment in Beam-Column Joints

> Since this system underwent large deformations, the consideration of second order effects was crucial to determining the correct moment demand on the system. Second order effects increased the moment in the

columns and beams to a non-trivial degree. A visual representation of simplified second-order, P-Δ effects, for an external specimen is illustrated in Figure 4.1. Internal specimens exhibited the same phenomenon. The forces in internal specimens were calculated (Eq. 4-1) while external specimens were calculated with (Eq. 4-2).

$$M_c = \left(\Delta_{top}\right) * P_{axial} + h_{column} * F = 2 * M_b$$
$$M_b = \left(\Delta_{top} - \Delta_{joint}\right) * P_{axial} + \frac{h_{column}}{2} * F$$
$$M_{b,int} = \left(\Delta_{top} - \Delta_{joint}\right) * 300kN + 1550mm * F \qquad \textbf{Eq. 4-1}$$

$$M_c = \left(\Delta_{top}\right) * P_{axial} + h_{column} * F = M_b$$
$$M_{b,ext} = \left(\Delta_{top}\right) * 300kN + 1550mm * F \qquad \textbf{Eq. 4-2}$$

> The moment in the joint undergoes a full reversal, from positive to negative. This large change in moment is concurrent with shear in the joint, as moments can also be represented by a force-couple. The high forces in the joint ultimately lead to shear failure, which is a brittle and undesirable response.

> In fact, the forces in the joint come about from flexure at the interface of the beams and columns, which can be seen in Figure 4.2a. These are transmitted as axial forces which transforms into a diagonal compression strut in the joint region and can be seen as the shaded region of Figure 4.2b.

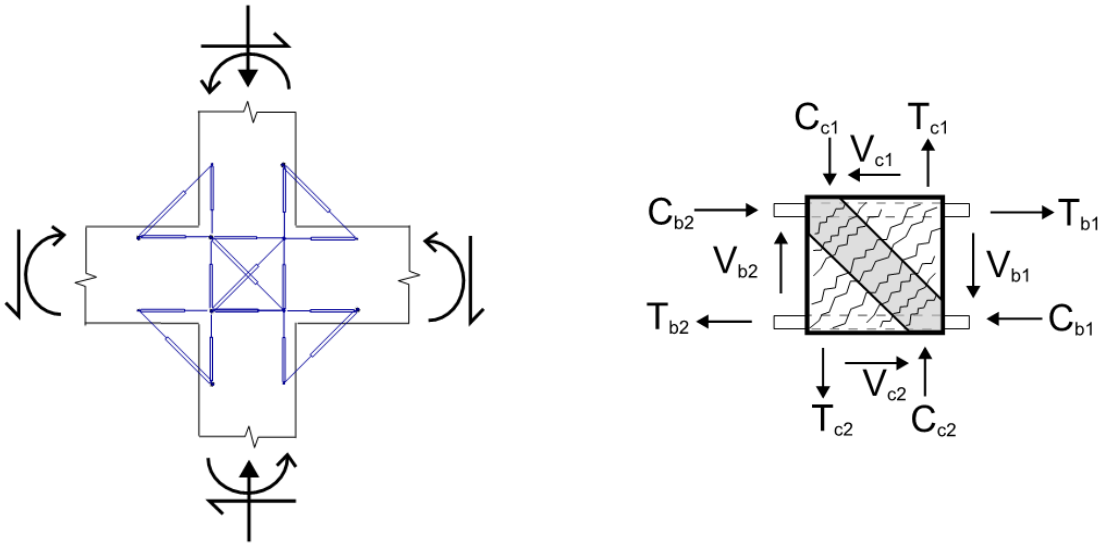

(a) Forces in system with potentiometer layout **(b) Forces in the joint with "continuity" rebar**

Figure 4.2: Force Transfer in the System (Image Adapted from ACI352 R-02 [45])

> The shear in the adjacent beams and columns is also directly transmitted into the joint region through bond. From equilibrium, the shear in the joint can be calculated with (Eq. 4-3) and (Eq. 4-4) for an internal and external joint specimen, respectively, where $j_d = 0.87*d_{eff} = 0.87*0.400$ m per Joh [45]:

$$V_{joint} = \frac{M_{br}+M_{bl}}{j_d} - V_{column} \qquad \textbf{Eq. 4-3}$$

$$V_{joint} = \frac{M_{br}}{j_d} - V_{column} \qquad \textbf{Eq. 4-4}$$

> Once the shear force in the joint is known, the average shear stress in the joint can be calculated by dividing the force by the joint area. A normalized shear stress can also be obtained by dividing the shear stress by the concrete strength as seen in (Eq. 4-5) [7].

$$\tau_{joint} = \frac{V_{joint}}{A_{joint}*f_c'} \qquad \textbf{Eq. 4-5}$$

> In addition to analyzing forces and stress, it is important to examine the system displacement and the joint strain field. Some potentiometers were able to provide useful direct displacement information pertaining to the overall specimen horizontal displacements. With some processing, potentiometer data can also be used to make reliable estimates of average joint strains that can be turned into shear displacements and/or used to make estimates of joint shear deformation and rigid body rotations. Isolating, for example, the joint displacement components schematically outlined in Figure 4.3.

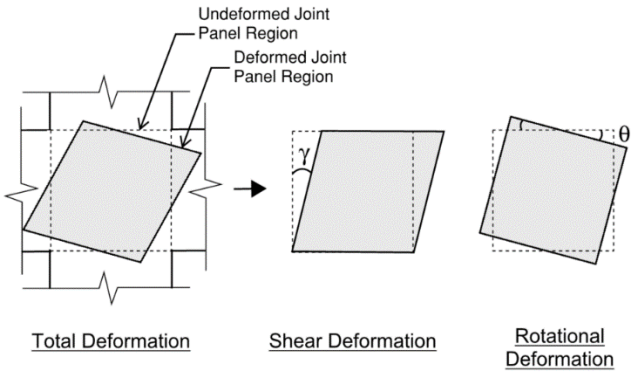

Figure 4.3: Simplified Representation of Joint-Region Deformations

> The knowledge of the strains in three different directions allows the full definition of the corresponding Mohr's circle, which in turn provides a complete definition of the strain state that the joint region undergoes. Evidently, the measurements taken over the course of the tests allow for the construction of more than one

circle of strains, depending on the trio of strains selected to perform the calculation There were four feasible triangles to use to calculate the shear strain as can be seen in Figure 4.4, on both the front and the back of the specimen. The overall shear strain was taken as the average of these eight estimates. Three examples of the rosette configuration used the strain calculation is shown in Figure 4.4.

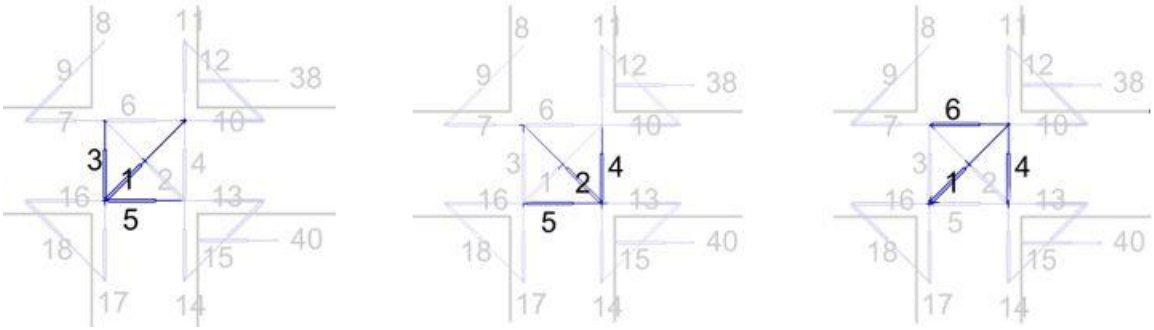

Figure 4.4: Example Rosette Configurations for Joint Shear Calculations

> Using the Mohr's circle first principles, and with the strains in the x- and y-direction known, the shear strain, γ_{xy}, may be calculated with (Eq. 4-6). Starting from the generic shear strain equation of:

$$\gamma_{xy} = \frac{\varepsilon_\theta - \varepsilon_x \cos^2\theta - \epsilon_y \sin^2\theta}{cos\theta sin\theta}$$

> Which can be simplified when theta is 45 degrees to:

$$\gamma_{xy} = 2(\varepsilon_{45} - \frac{\varepsilon_x + \varepsilon_y}{2})$$

> Replacing variables with some common terms results in (Eq. 4-6):

$$\gamma_{strain} = 2\left(\varepsilon_{p1} - x_0\right) \qquad \textbf{Eq. 4-6}$$

> Where x_0 is the center of the Mohr's circle calculated as $\frac{\varepsilon_x + \varepsilon_y}{2}$ and $\varepsilon_{p1}$is the principal tensile strain.

> Additionally, average potentiometer surface measurements can be used to make inferences regarding the overall strain status of the joint steel reinforcement. Within the panel zone, the x- and y-strains were calculated using the average strains obtained from the pair of gauges oriented in the pertinent direction. For instance (with reference Figure 4.4), the x-strain was obtained by averaging the potentiometer strain

readings from 5 and 6, and their corresponding pair on the back of the specimen (not shown). The same was done for vertical and diagonal strains of the panel region.

4.2 SUB-COMPONENTS OF DRIFT

> This section describes the specific analysis done to isolate subcomponents of the overall drift. The drift was divided into five distinct measurements, namely (i) column flexure, (ii) column fixed-end rotation, (iii) joint shear, (iv) beam fix-end rotation, and (v) beam flexure and remaining specimen shear. Note that all calculations were averaged between both the front and back potentiometers when possible. Figure 4.5 depicts the general setup for noteworthy parameters and the control node of the specimen for overall drift calculation.

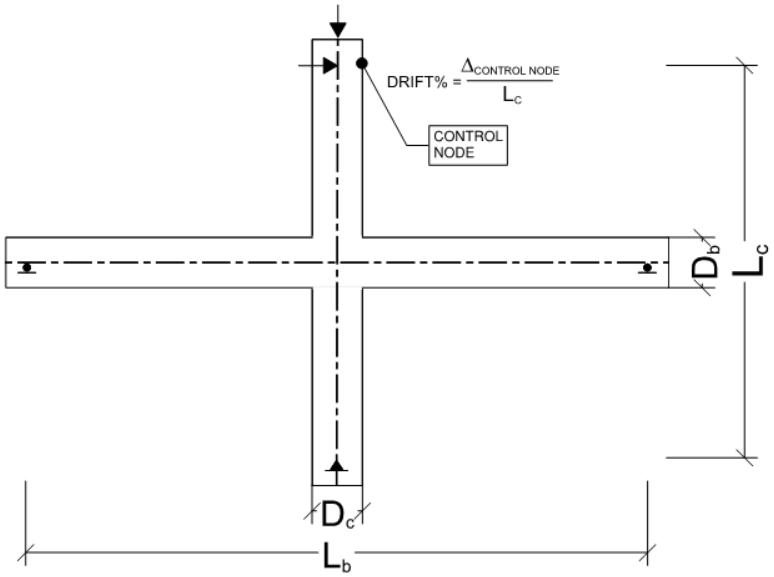

Figure 4.5: Simplified Specimen Setup

> Column rotation due to flexure was calculated from first principles, by (Eq. 4-7) or derived from Minimum Potential Energy [47]. The fact that this system was designed to be capacity protected, with strong columns and weak beams, further supports the idea that first principals will be an accurate representation of column flexure because the column will remain protected during nonlinear response.

$$\left(F * \frac{(L_c - D_b)^3}{12 * E_c I_c}\right) \qquad \textbf{Eq. 4-7}$$

> Parameters in (Eq. 4-7) are defined as follows: E_c is the measured modulus of elasticity of concrete, I_c is the transformed moment of inertia of the column, L_c is the total pinned length of the column, and D_b is the full height of the beam. Note that I_c was taken as 56% [47] of the total transformed moment of inertia for the REF specimen only meant to represent the cracked section properties. The NPS® specimens, however, used the full I_c since the columns were wrapped in steel and were assumed to contribute the full transformed moment of inertia capacity.

> The fixed-end rotation of both the columns and the beams was taken from potentiometers which spanned the interface between the joint and the member as can be seen in Figure 4.6.

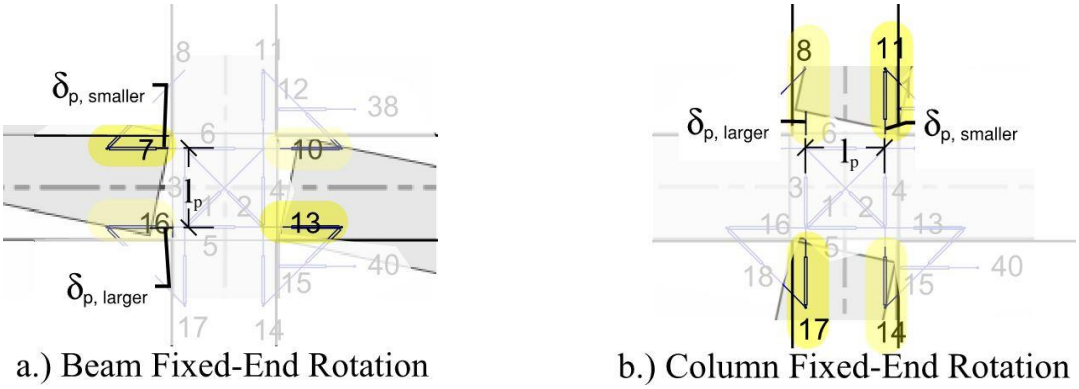

a.) Beam Fixed-End Rotation b.) Column Fixed-End Rotation

Figure 4.6: Fixed End Rotation

> This fixed end rotation, θ_{FE}, was calculated for each beam and column separately per (Eq. 4-8), then averaged between the top/bottom or left/right thetas respectively and the front/back to define one fixed-end rotation for the beam and one fixed end rotation for the column at each moment in time [21].

$$\theta_{FE} = \frac{\delta_{p,larger} - \delta_{p,smaller}}{l_p} \qquad \textbf{Eq. 4-8}$$

> The joint shear rotation is equivalent to the joint shear strain calculated earlier in this chapter.

> It was not possible to isolate the displacement component due to beam flexure from the available data. Therefore, the remainder of the drift of the specimen was considered an accurate representation for the beam flexure. Minor contributions from beam and column shear are assumed to be included in this remainder but are likely negligible [47, 48].

> The drift is a percentage, taken as the lateral top column movement over the height of the column. As a displacement based test (See CHAPTER 3) the total drift at any moment in time was measurable and precise. The rotations calculated above, when in radians, are equivalent to the drift at small rotations. This project stayed within an acceptably small angle rotation to take advantage of this equality (i.e., rotation as equal to drift). Each drift measurement was finally corrected for the distribution across the member lengths and can be seen summarized in Table 4.1 [21, 47, 49].

Table 4.1: Summary of Drift Sub-Component Equations

Sub-Component	Rotation (rad) From Potentiometer Data	Corrected Drift (%) Used in Analysis
Column Flexure	$\boldsymbol{\theta_{fl,c} = \left(F * \frac{(L_c - D_b)^3}{12 * E_c I_c}\right)}$	$\boldsymbol{\Delta_{fl,c} = \theta_{fl,c}\left(1 - \frac{D_b}{L_c}\right)}$
Column Fixed End	$\theta_{FE,c} = \frac{\delta_{y,larger} - \delta_{y,smaller}}{l_p}$	$\Delta_{FE,c} = \theta_{FE,c}\left(1 - \frac{D_b}{L_c}\right)$
Joint Shear	$\theta_{js} = 2 * \left(\varepsilon_{45} - \frac{1}{2}(\varepsilon_x + \varepsilon_y)\right)$	$\Delta_{js} = \theta_{js}\left(1 - \frac{D_b}{L_c} - \frac{D_c}{L_b}\right)$
Beam Fixed End	$\theta_{FE,b} = \frac{\delta_{x,larger} - \delta_{x,smaller}}{l_p}$	$\Delta_{FE,b} = \theta_{FE,b}\left(1 - \frac{D_c}{L_b}\right)$
Beam Flexure "Uncounted"	N/A	Remainder: $\Delta_{fl,b} = \Delta_{Total} - \Delta_{JointShear} - \Delta_{bFE} - \Delta_{cFE}$

4.3 STIFFNESS, ENERGY, AND DUCTILITY

> Useful metrics for determining the effectiveness of the systems include (i) stiffness degradation, (ii) energy dissipation, and (iii) ductility. These results are further discussed in CHAPTER 6 , but the technical methods of calculation are described here.

> The stiffness of the specimen can be calculated as the slope of the force-displacement curve, which has units of force per unit length. Two stiffness measurements were able to be calculated for each cycle of the F-d curve one on the top and bottom of the curve as can be seen in Figure 4.7. Relevant information regarding the stiffness degradation of the specimen can be obtained by considering the initial stiffness, K_i, and the residual stiffness, K_0. The initial stiffness is defined as the secant stiffness between an average of two secant lines between ±10% of the first cycle of the 0.5% drift hysteretic force-displacement graph, as can be seen in Figure 4.7 and calculated per (Eq. 4-9). K_0 is the residual stiffness at a specified drift (often the first cycle of the 3%, 4%, or 5% drift ratios for this experimental program) averaged between the top

and bottom secant lines through ±10% of the specified drift, as can be seen in Figure 4.7 and calculated with (Eq. 4-10). The residual secant stiffness per cycle, K_0, was computed per recommendations of ACI Committee 374 [42], summarized in in Figure 4.7.

> The initial stiffness, K_i, of each specimen. was taken as the slope of the force-displacement curve associated with the first cycle of the 0.5% drift ratio. Similarly, the residual stiffness, K_0, was calculated as the average of the secant lines between ±10% of the limiting drift ratio for the force displacement graph but was calculated for multiple drift ratios.

$$K_i = \Delta_{0.5\%,Cycle\ 1}/P_{0.5\%,Cycle1} \qquad \textbf{Eq. 4-9}$$

$$K_0 = \frac{1}{2}\left[\left(\frac{P_{+10\%} - P_{-10\%}}{\Delta_{+10\%} - \Delta_{-10\%}}\right)_{top\ of\ loop} + \left(\frac{P_{+10\%} - P_{-10\%}}{\Delta_{+10\%} - \Delta_{-10\%}}\right)_{bottom\ of\ loop}\right] \qquad \textbf{Eq. 4-10}$$

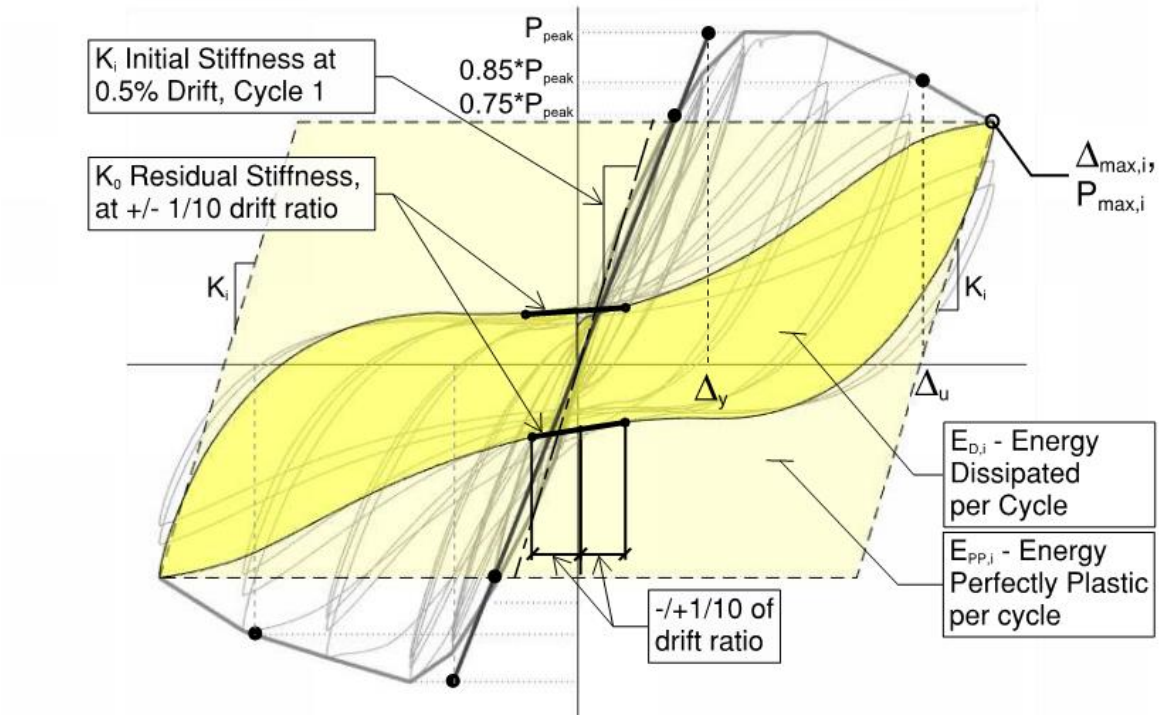

Figure 4.7: Specimen Performance Parameter Calculation

> The energy dissipation was calculated based on the area of the force-displacement graph, resulting in units of kN*mm, or Joules. The normalized energy dissipated per cycle $\bar{E}_i$, computed as per ACI and Parra Montisinios, is the energy under the hysteretic curve for a given drift ratio, divided by the elasto-perfectly

plastic area, as seen in Figure 4.7 and calculated per (Eq. 4-11) [42, 24]. The elasto-perfectly plastic border has a slope of K_i, described above, or zero. The energy dissipated per cycle was calculated a second way, as a normalized value of the maximum load and displacement per cycle, per (Eq. 4-12). This allowed for a secondary check on the relative energy dissipated per cycle, which tended to be necessary when severe pinching occurred and $E_{D,i}$ was exceedingly large compared to the calculated $E_{PP,i}$., resulting in unrealistic $\overline{E_i}$, per cycle.

$$\overline{E_i} = \frac{E_{D,i}}{E_{PP,i}} \qquad \textbf{Eq. 4-11}$$

$$E_{n,i} = \frac{E_{D,i}}{2\pi * P_{max,i} * \Delta_{max,i}} \qquad \textbf{Eq. 4-12}$$

> The yield displacement Δ_y is calculated from (Eq. 4-13), as recommended by Park [49] and utilizes a secant line through 75% of the peak strength of the specimen's backbone force-displacement curve, which can be seen in Figure 4.7. The ultimate displacement Δ_u, is taken as the displacement corresponding to 85% of the post-peak strength of the specimen's backbone force-displacement curve [50, 51]. The specimen ductility, μ, computed per (Eq. 4-14) is the ratio of the ultimate displacement, Δ_u, and the yield displacement, Δ_y.

$$\Delta_y = P_{peak} * \Delta_{.75P} / P_{.75} \qquad \textbf{Eq. 4-13}$$

$$\mu = \frac{\Delta_u}{\Delta_y}, \text{ where } \Delta_u = \Delta_{.85P} \qquad \textbf{Eq. 4-14}$$

> This concludes the explanation of the relevant calculations used for analysis of the performance parameters of interest.

CHAPTER 5 EXPERIMENTAL RESULTS

> CHAPTER 5 details the main results of the experimental program as quantitatively as possible. This chapter is intended to give an objective, overall summary of each experiment and relevant observations. Additional analytical methodology and further qualitative explanation on the data can be found in CHAPTER 6 .

> The results of this chapter are presented in terms of force-displacement response. Events such as beam cracking, joint cracking, and spalling were noted based on visual inspection of photographic and video evidence. Beam yielding and joint reinforcement yielding was also noted based on data from strain gauges where possible, and potentiometer data otherwise. The use of the potentiometer data resulted in surface strains, rather than direct steel strain readings, but could be linked to the average internal rebar strains.

5.1 MDI TEST SERIES

> The MDI Test Series includes specimens REFi, NPS1i, NPS2Ai, NPS2Bi and NPS4i. They represent an interior (cruciform beam-column joints) joint of a moderately ductile (MD) moment resisting frame (MRF). All the specimens were subjected to increasing horizontal reversed cyclic drift demand (3 loading cycles per drift level) and constant column axial load of 300 kN. All tests were terminated once the specimens reached a peak 5% drift ratio. The term “failure” is used somewhat loosely in this section to refer to the status of the specimens at 5% drift level, even though all specimens still had non-trivial residual strength at this point.

> Additional information regarding the experimental test setup, loading protocol, instrumentation, specimen details, and design considerations can be found in CHAPTER 3 .

> There were some commonalities among all MDI specimens. Namely, all MDI specimens reached their nominal strength, corresponding to the beam flexural yielding. They all experienced a pinched response and lateral stiffness degradation mostly attributed to bond-slip deterioration, alongside some extent of strength loss. All specimens exhibited initial cracking during the 0.25% load stage. Nearly all specimens

exhibited joint shear failure following beam yielding, with significant spalling of the joint region. It should be noted that while spalled concrete does impact the strength of the specimen, it was mainly due to intense diagonal cracking, so the time of initial spalling was relatively insignificant – merely indicating that cracking had become extensive and was not always concurrent with maximum drift levels. Also, concrete confined within stirrups did not spall, only external cover concrete spalled.

> The pinched response was expected because of the large diameter bars selected to provide moment continuity. Pinching effects can be typically reduced with smaller steel bars across the joint, and the use of deformed rather than plain bars. However, large diameter bars were selected in this program to collect evidence pertaining to the "worst case scenario". They were also of interest because they may provide a desirable solution to address constructability and reinforcement congestion issues in NPS® frame systems.

> All specimens, except for NPS4i, experienced a joint shear failure following beam yielding at the beam-column interface. This failure mode is typically referred to as "BJ" in the literature (bond-slip deterioration of the continuity bars was also evident). Given the higher level of protection of the joint region, specimen NPS4i failed in flexure at the beam-column interface (failure type identified as "BY"), with the joint panel zone still virtually undamaged at 5% drift ratio. Severe bond-slip issues were detected at the beam-column interface, and one may debate whether failure of NPS4i should be classified as "beam yielding followed by anchorage failure".

> Some of the key results are summarized in Table 5.1. Note that K_0 represents the residual secant lateral stiffness of the system (described in CHAPTER 4 with subscripts representing the either the first or the third loading cycle. The residual load represents the maximum load recorded on the first loading cycle at 5% drift in the positive direction.

> More details pertaining to the experimental response of each individual specimen are provided in the following sections.

Table 5.1: Summary of Test Results - MDI Test Series

Specimen ID	Peak Load+ (PL) [kN]	5%(Cycle 1) Residual Load+ (RL) [kN]	RL/PL	Strength Degradation		Stiffness Degradation		Failure mode
				3% Drift $P_{max,3}/P_{max,1}$	4% Drift $P_{max,3}/P_{max,1}$	3% Drift $K_{0,3}/K_{0,1}$	4% Drift $K_{0,3}/K_{0,1}$	
REFi	194.6	132.9	0.68	0.83	0.77	0.38	0.53	BJ
NPS1i	176.1	104.4	0.59	0.77	0.75	0.23	0.33	BJ
NPS2Ai	230.8	167.8	0.73	0.80	0.79	0.40	0.53	BJ
NPS2Bi	239.6	173.3	0.72	0.82	0.76	0.45	0.52	BJ
NPS4i	238.8	198.7	0.83	0.84	0.81	-0.05*	0.61	BY

*Due to severe pinching, negative residual stiffness calculated for 3% Drift Cycle 3

5.1.1 REFi Specimen

REFi was the baseline of performance for the remaining MDI specimens, as it was designed with standard Eurocode guidelines for a moderately ductile system and was a traditionally reinforced concrete beam-column joint. It was the first specimen tested in the experimental program. A view of the specimen at initial, 0%, and final, 5%, loading stages can be seen in Figure 5.1.

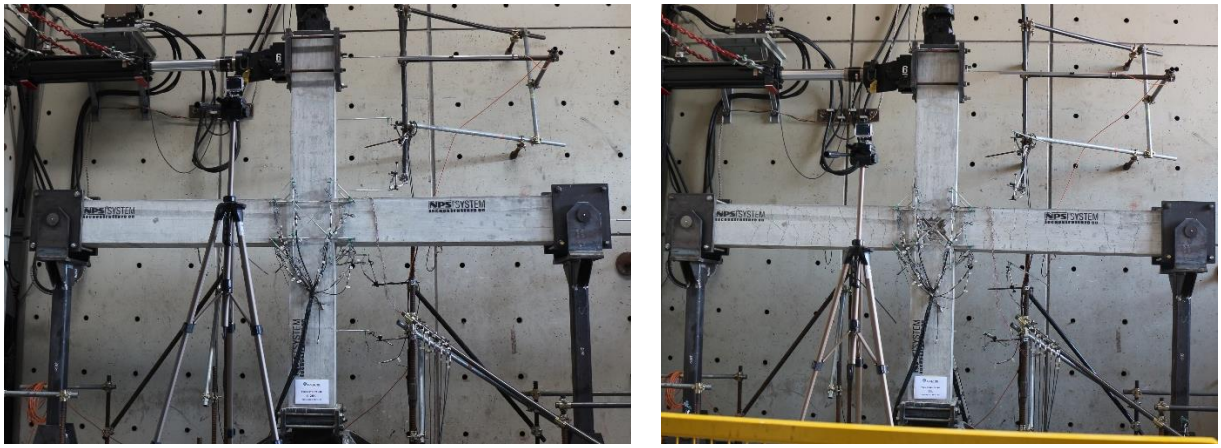

(a) Initial **(b) Final**

Figure 5.1: Reference Specimen Initial (Before Loading) and Final (After Loading) Conditions

The force-displacement response curve can be seen in Figure 5.2. This hysteretic loop is somewhat typical for a moderately ductile RC beam-column joint as it exhibits a good level of ductility. However, it is also characterized by evident pinching, most likely due to a combination of bond-slip and joint deterioration. The beam column assembly underwent the full loading protocol described in CHAPTER 3 up to 4% drift cycle, but only one full cycle of the peak 5% drift loading was completed.

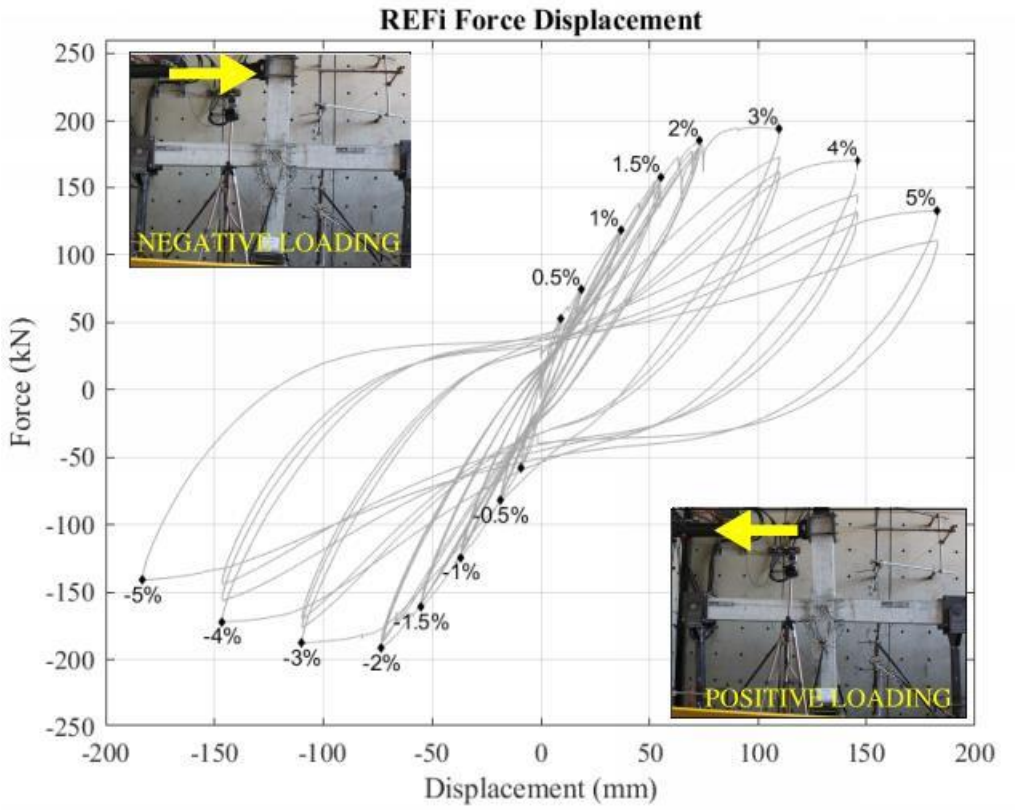

Figure 5.2: Force-Displacement Response of REFi Specimen

The specimen reached a positive peak strength of 195 kN during the first loading cycle of the 3% drift ratio, and a negative peak strength of -192 kN during the first loading cycle of the 2% drift ratio. Full yielding occurred near the end of the 2% loading, and fully during the 3% loading. Following this beam yielding, the specimen suffered evident and progressive loss of lateral stiffness, as can be seen in the reloading slope of the F-d graph in Figure 5.2. It is significant to note that the recorded residual strength at the 5% drift was 68% of the peak. This level of residual strength is non-trivial, considering that strength reductions due to second order effects alone may be expected to be significant (20%).

The specimen experienced full-depth cracking in the beam (flexural, at the beam-column interface) during the first 1.0% drift loading cycle. This was followed by diagonal cracking in the joint region detected during the first of the three 1.5% drift ratio cycle. First yielding of beam longitudinal reinforcement occurred at the 2% drift cycle. This is evidenced by the markedly non-linear response observed in Figure 5.2 and is supported by strain gauge readings, see Figure 5.3. Following the first 3% drift loadings cycle, joint

cracking became significant, and the average horizontal strain of the joint region computed from potentiometer readings suggested that full yielding of the joint shear reinforcement had occurred. Graphs of the strains determined in the system are shown for REFi, but are not noted for later subjects, merely the conclusions are noted, by which the reader can infer the methods of deduction which were used were similar to that used for the REFi specimen.

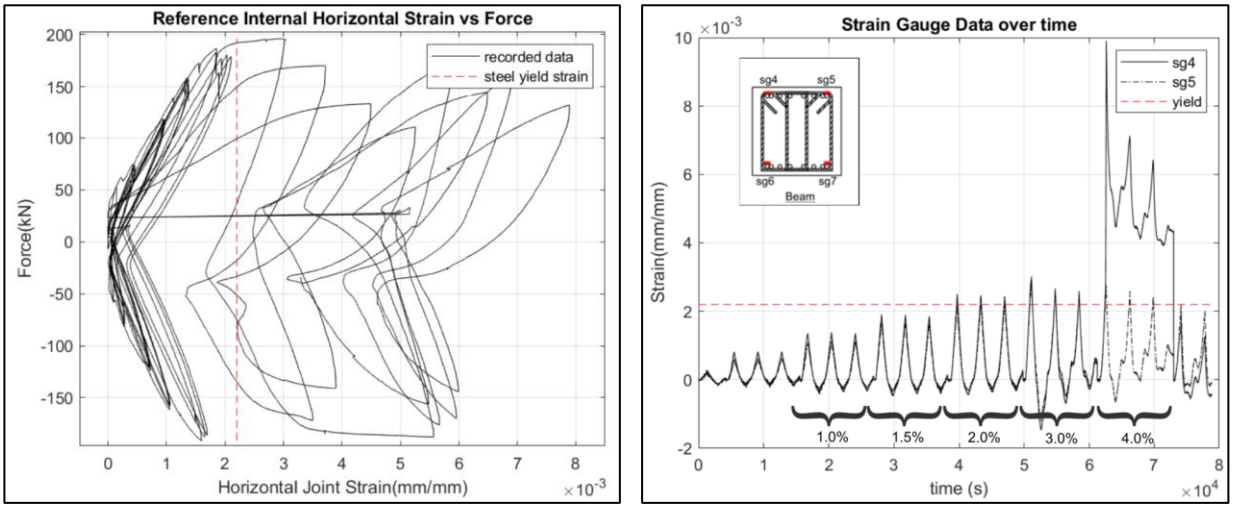

Figure 5.3: Internal Strain Data

Initial spalling occurred during the third cycle of the 3% loading, further degrading the capacity of the structure. Together with joint diagonal cracking the spalling became more critical as the drift demand increased (see Figure 5.4). As discussed earlier, joint damage resulted in a progressive loss of horizontal strength and stiffness. By the time the specimen was pushed to 5% drift ratio, the joint region was heavily damaged and the joint reinforcing bars were fully exposed (Figure 5.4). Because all damage was absorbed by the joint panel zone, the beams did not suffer any notable additional cracking following the 3% drift loading cycle. The columns remained essentially undamaged throughout the entirety of the test.

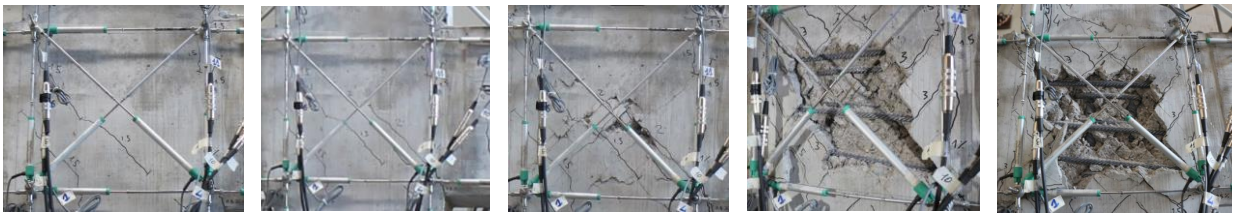

1.5% Drift **2.0% Drift** **3.0% Drift** **4.0% Drift** **5.0% Drift**

Figure 5.4: REFi – View of Joint Region at Various Drift Ratios

The subcomponents of drift, calculated per methods described in CHAPTER 4 , support the general conclusion that the main damage in the specimen occurred due to beam yielding followed by joint shear failure. During initial drift ratios, the majority of the drift was due to column rotation, however, as the force increased in the specimen, the beam and joint progressively took more damage and contributed more to the drift. See Figure 5.5 for a breakdown of the specimen subcomponents at each drift ratio. Only percentages higher than 10% are shown. As a brief reminder, the "uncounted" portion is assumed to be attributed to the beam flexure, and negligible shear in the systems beams and columns.

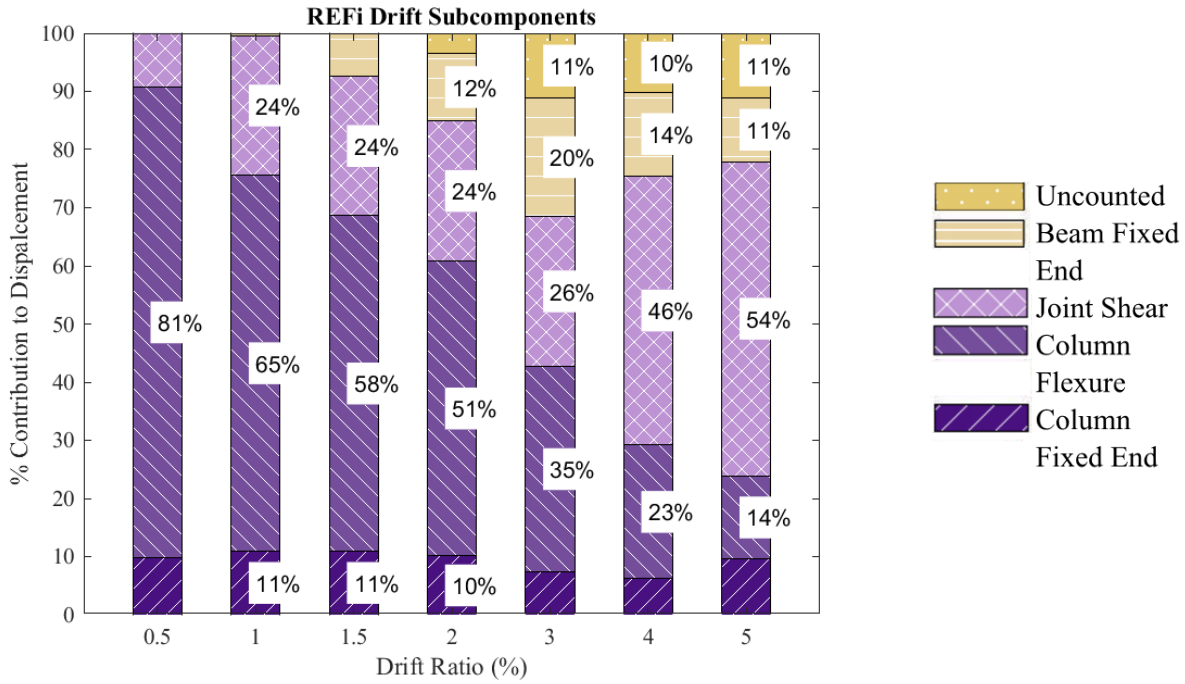

Figure 5.5: REFi Drift Subcomponents

5.1.2 NPS1i Specimen

NPS1 was the first specimen alteration on the basic NPS® System Design, and the second specimen tested overall. This specimen achieved moment continuity at the joint by means of two added trusses, like that used in each beam, with a steel plate as the bottom chord which doubled as formwork for the concrete. The beam plastic hinge regions were reinforced in shear with added stirrups, while no shear reinforcement (other than the continuity truss diagonal elements) was present in the joint region. A view of specimen NPS1i with the experimental setup is provided in Figure 5.6.

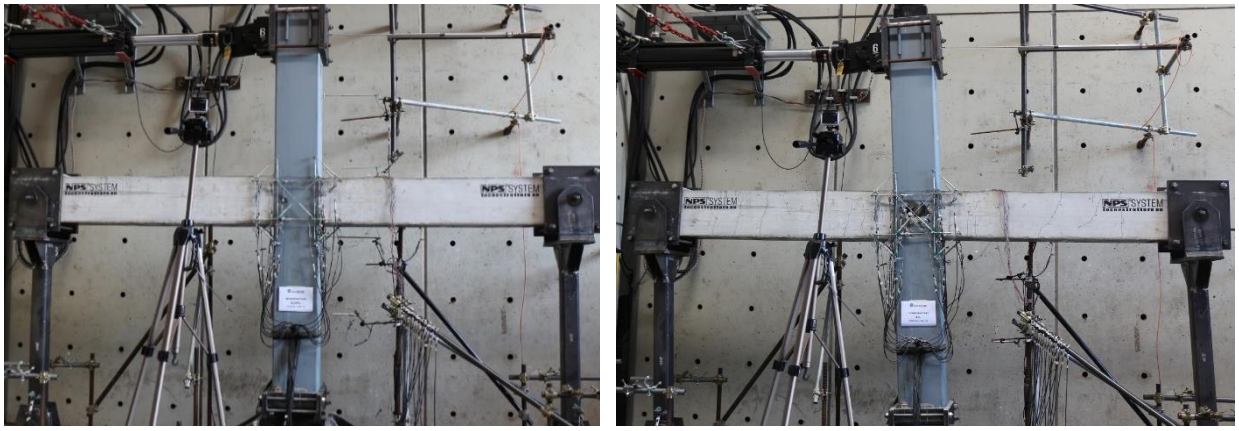

Figure 5.6: View of Specimen NPS1i Before (Left) and After (Right) Testing

The beam-column assembly underwent the full loading protocol described in CHAPTER 3 including three full cycles at peak drift ratio of 5%. The horizontal force-displacement response is outlined in Figure 5.7: Force-Displacement Response of Specimen NPS1i.

The specimen reached a positive peak strength of 176 kN and a negative peak strength of 166 kN. Both occurred during the first loading cycle to 1.5% drift ratio, in the pertinent loading direction. It is unclear if full flexural yielding was achieved at the beam-column interface, but it is reasonable to assume that first yielding occurred. The recorded peak loads are reasonably close (yet somewhat lower, particularly in the negative loading direction) to the expected yield strength. Strain gauge readings indicated some minor extent of yielding.

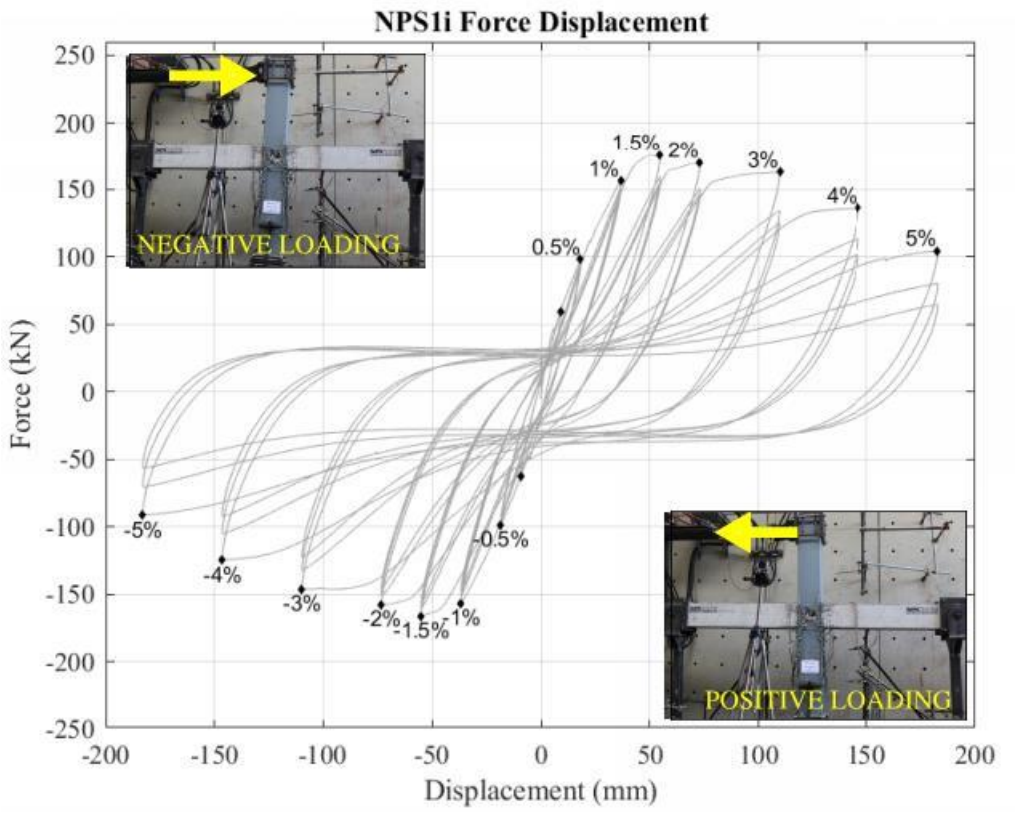

Figure 5.7: Force-Displacement Response of Specimen NPS1i

> The specimen started exhibiting a non-linear response during the first cycle of the 1.5% drift ratio. Past this point significant pinching and progressive degradation of lateral stiffness was observed. For instance, secant stiffness losses during each drift level of 3%, and 4% (quotient of secant stiffness values from cycles 1 and 3 of each drift, $K_{0,Drift\%,Cycle3}$ / $K_{0,Drift\%,Cycle1}$) consisted of 23%, and 33%, respectively. Non-trivial strength reduction was observed; the positive residual strength during the first cycle of the 5% drift ratio was 104 kN, which corresponded to 59% of peak.

> Flexural cracking in the beams and shear cracking in the joint region were observed during the early loading cycles. What was identified as first yielding of the beam longitudinal reinforcement occurred at 1.5% drift. During the following loading cycles, joint shear cracking progressed and became severe. Potentiometer readings suggested that yielding of the truss diagonal elements in the joint region had already fully yielded by the 1.5% cycle, presumably at around 1% drift ratio. There was not additional joint shear steel in this specimen, which could have helped delay the joint steel yielding, due to congestion issues.

> Concrete spalling in the joint panel zone began during the second cycle of the 3% drift loading and became considerable, as the drift demand increased (see Figure 5.8). Joint damage resulted in a progressive loss of horizontal strength and stiffness. By the time the specimen was pushed to 5% drift ratio, the joint region was heavily damaged (Figure 5.8). Nearly all the damage was absorbed by the joint panel zone, the beams did not suffer any notable additional cracking following the 1.5% drift loading cycle. The columns remained undamaged throughout the test.

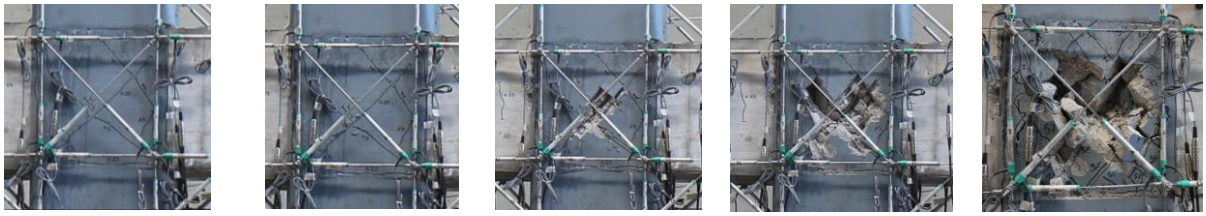

1.5% Drift **2.0% Drift** **3.0% Drift** **4.0% Drift** **5.0% Drift**

Figure 5.8: View of Joint Region at Various Drift Ratios

> The subcomponents of drift of NPS1i specimen can be seen in Figure 5.9[1] and demonstrate the progressive reduction of column action contributing to drift from more than 60% initially to less than 10% during the final loading stage. The column action is less than the REFi specimen, which exhibited 91% initially to 23% during the final load stage, likely due to the wrapped nature of the column. The shear in the joint remained somewhat constant until the 4% and 5% drift ratios where it increased significantly, and which can be visually compared with the damage seen in Figure 5.8. The beam contribution to drift steadily increased from initial loading stages until a peak of 59% contribution to total drift in the 3% drift loading. See Figure 5.9.

[1]Only percentages higher than 10% are shown; the "uncounted" portion is assumed to be attributed to the beam flexure plus negligible shear in the beams and columns. All contributions are taken from the first cycle of the pertinent drift loading ratio.

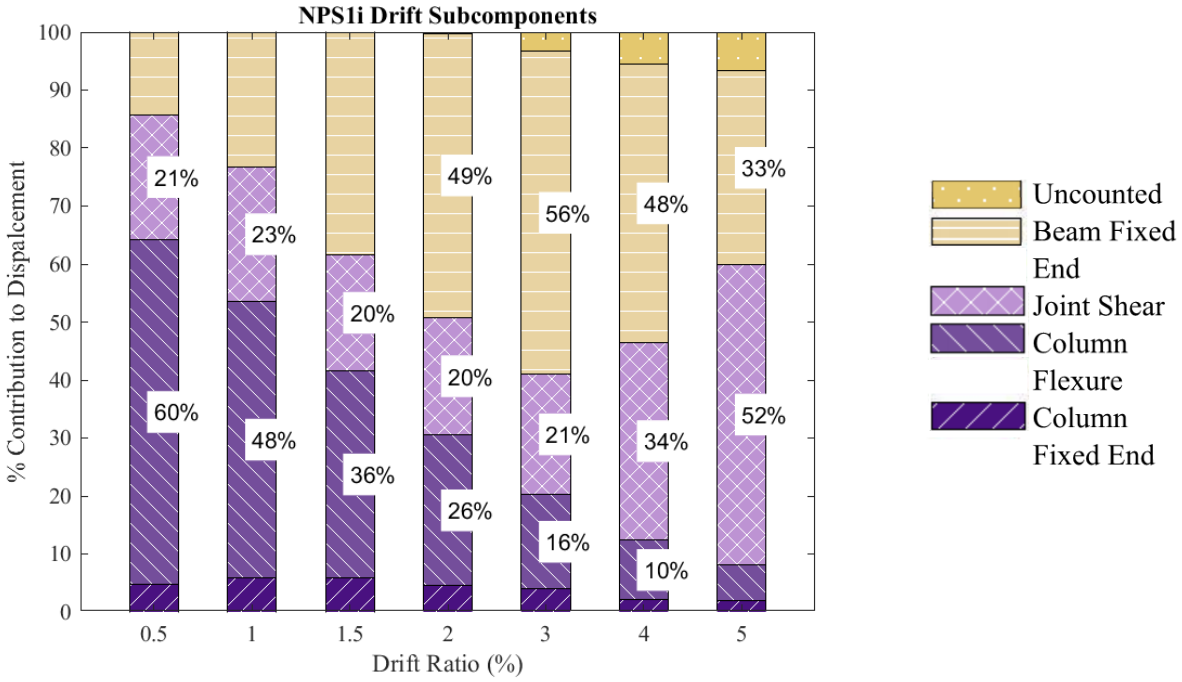

Figure 5.9: NPS1i Drift Subcomponents

5.1.3 NPS2Ai Specimen

NPS2Ai was based on the standard NPS® system configuration with the simplest continuity connection: traditional straight, deformed rebar spanning the joint region and extending beyond the critical regions of the beams. The beam plastic hinge regions were not reinforced in shear with added stirrups, while traditional shear reinforcement was present in the joint region. A view of specimen NPS2Ai with the experimental setup is provided in Figure 5.10.

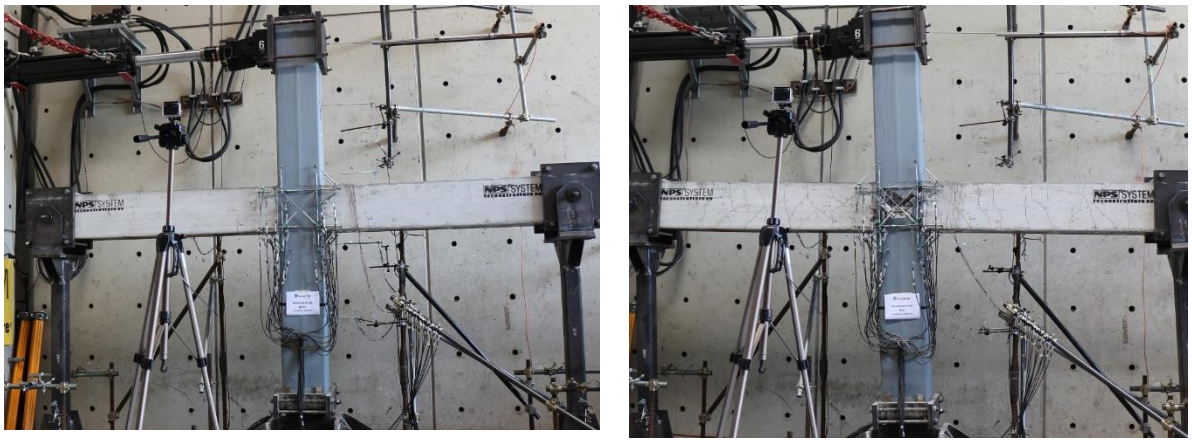

Figure 5.10: View of Specimen NPS2Ai Before (Left) and After (Right)

The specimen was subject to the full loading protocol described in CHAPTER 3 , including three full cycles at peak drift ratio of 5%. The horizontal force-displacement response is outlined in Figure 5.11. NPS2Ai reached a positive peak strength of 231 kN and a negative peak strength of 220 kN. Both occurred during the first loading cycle to 2.0% drift ratio, in the pertinent loading direction. The hysteretic response of NPS2Ai qualitatively resembles that of the specimen REFi and, more generally, the response of a moderately ductile RC beam-column joint. It is evident that the specimen possesses a good level of ductility, but is also characterized by pinching, likely due to a combination of bond-slip and joint deterioration.

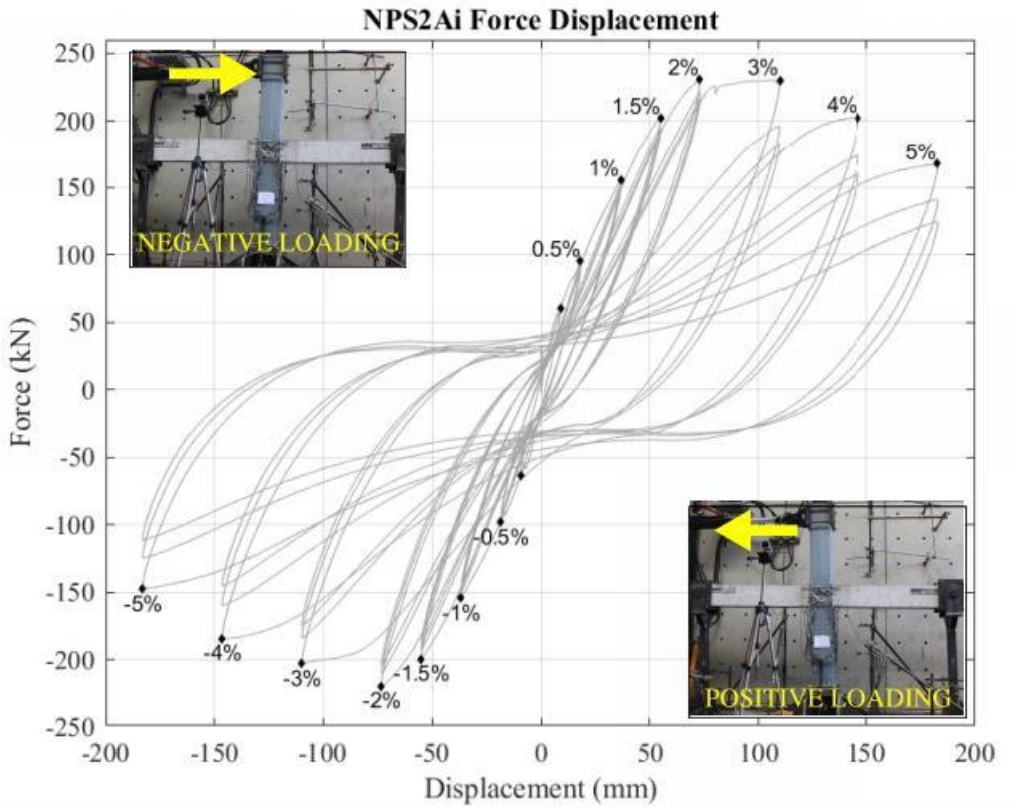

Figure 5.11: Force-Displacement Response of Specimen NPS2Ai

> Flexural yielding of the continuity reinforcement occurred at a drift ratio of 2% and peak load was sustained over the first 3% drift loading cycle. Following beam yielding, the specimen exhibited a non-linear response, suffering evident and progressive loss of lateral stiffness and strength. At drift ratios of 3% and 4% secant stiffness losses between the first and third cycles of the corresponding drift were 40%, and 53%. Some extent of strength reduction was also observed. The positive residual strength at 5% drift ratio (cycle 1) was 168 kN, which corresponds to about 73% of peak and is non-trivial.

> The beams exhibited initial vertical cracks prior to diagonal cracks forming in the joint region. The joint panel zone developed diagonal cracks at the 1% loading ratio. Joint cracking propagated on each subsequent loading cycle, until concrete spalling occurred at 3%. Potentiometer readings indicated that the shear reinforcement in the joint reached yielding during the 3%.

> Joint damage resulted in a progressive loss of horizontal strength and stiffness. By the time the specimen was pushed to 5% drift ratio, the joint region was heavily damaged and the joint reinforcing bars were fully

exposed (Figure 5.12). Damage was absorbed by the joint panel zone; the beams did not suffer any notable additional cracking following the 3.0% drift loading cycle. However, wide cracks were observed at the beam-column interface. The columns remained undamaged throughout the test.

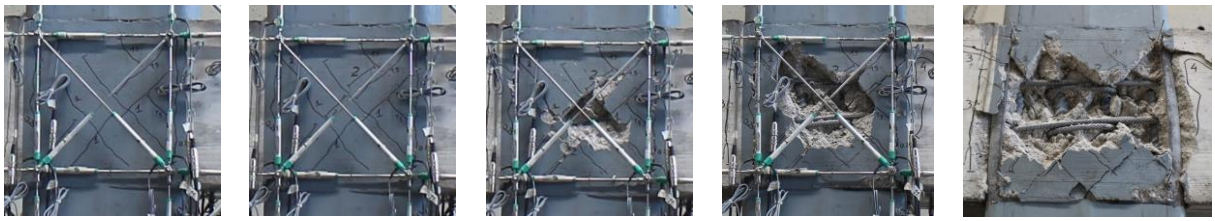

1.5% Drift 2.0% Drift 3.0% Drift 4.0% Drift 5.0% Drift

Figure 5.12: NPS2Ai – View of Joint Region at Various Drift Ratios

The subcomponents of drift of NPS2Ai specimen can be seen in Figure 5.13[2] and demonstrate the progressive reduction of column action contributing to drift, from more than 60% initially to less than 10% during the final loading stage. The beam action steadily increased, until the full yielding of the specimen during the 3% drift ratio. The shear in the joint remained, like NPS1i, somewhat constant until the 4% and 5% drift ratios.

[2]Only percentages higher than 10% are shown; the "uncounted" portion is assumed to be attributed to the beam flexure plus negligible shear in the beams and columns. All contributions are taken from the first cycle of the pertinent drift loading ratio.

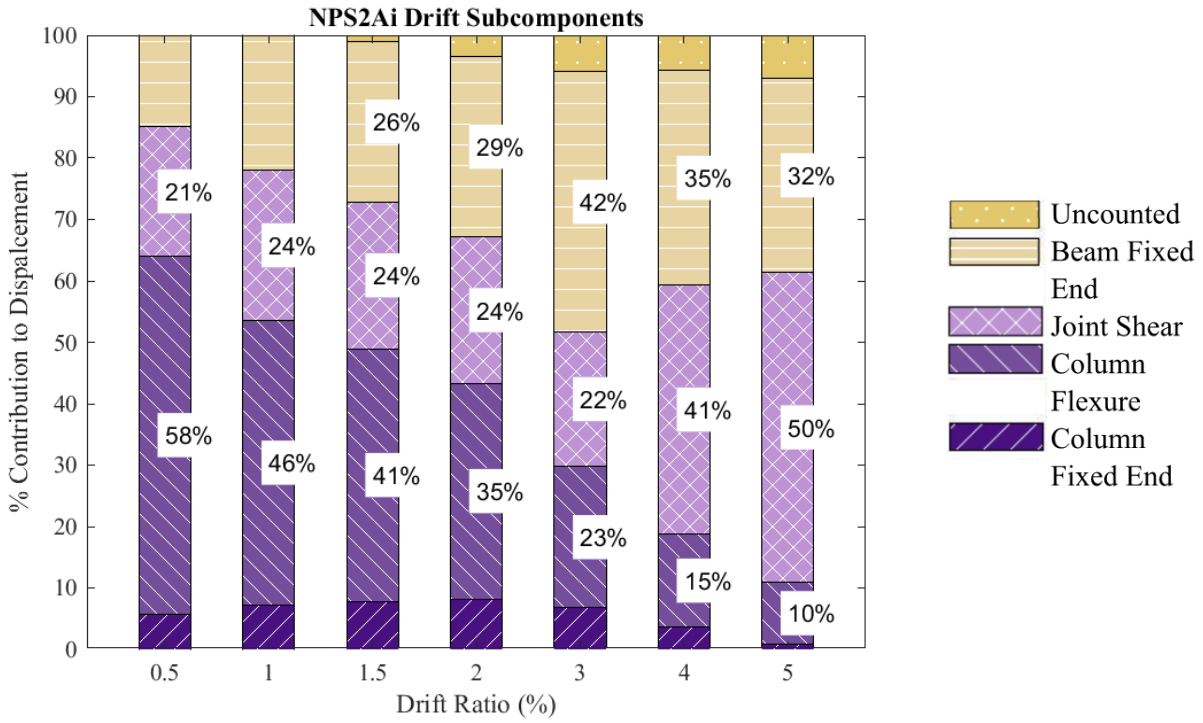

Figure 5.13: NPS2Ai Drift Subcomponents

5.1.4 NPS2Bi Specimen

This specimen was nominally identical to NPS2Ai, with moment continuity connection consisting of straight deformed bars spanning the joint region and extending beyond the critical regions of the beams and traditional shear reinforcement present in the joint region. However, unlike NPS2Ai, specimen NPS2Bi had additional shear stirrups in the plastic hinge/critical region of the beam. A view of specimen NPS2Bi with the experimental setup is provided in Figure 5.14.

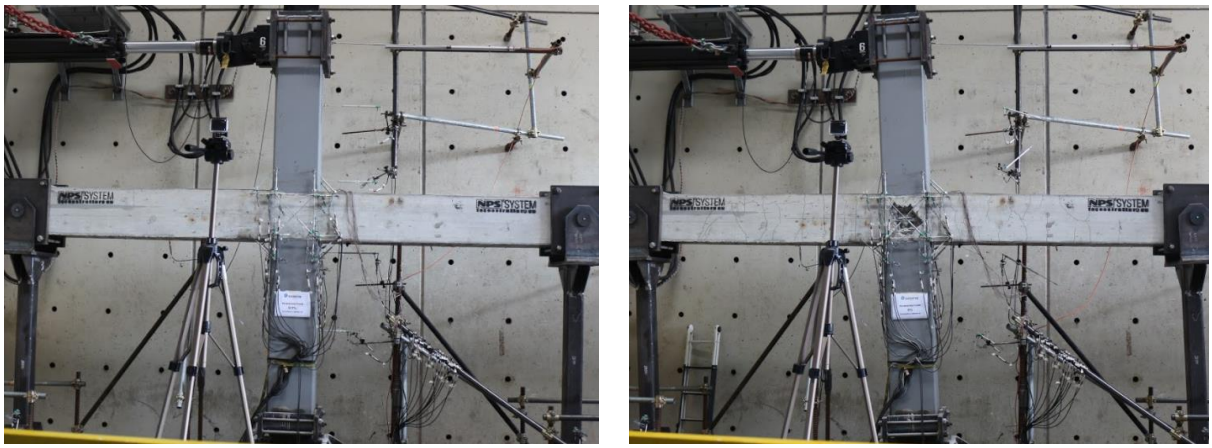

Figure 5.14: View of Specimen NPS2Bi Before (Left) and After (Right) Testing

The specimen was subject to the full loading protocol described in CHAPTER 3 , including three full cycles at peak drift ratio of 5%. The horizontal force-displacement response is outlined in Figure 5.15. NPS2Bi reached a positive peak strength of 240 kN during the first loading cycle to 3% drift ratio, and a negative peak strength of 226 kN at 2% drift ratio. Overall, the hysteretic response of NPS2Bi was qualitatively and quantitatively virtually identical to that of specimen NPS2Ai and discussed further in CHAPTER 6 .

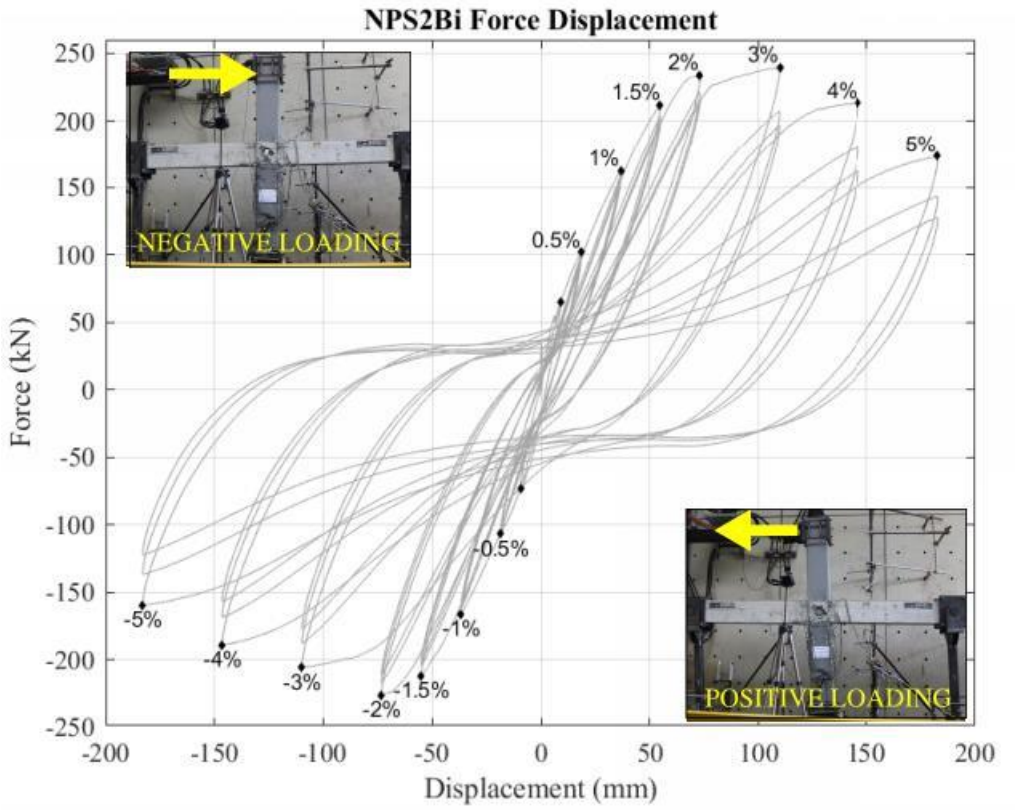

Figure 5.15: Force-Displacement Response of Specimen NPS2Bi

> Analogously to its companion moderately ductile NPS® specimens, after beam yielding occurred (around 2% drift ratio), NPS2Bi suffered progressive loss of lateral stiffness due to shear in the joint region. At drift ratios of 3% and 4% secant stiffness losses ($K_{0,Drift\%\ Cycle3}$/ $K_{0,Drift\%\ Cycle1}$) of about 45% and 52% occurred between loading cycles 1 and 3. Some extent of strength reduction was also observed. The positive residual strength at 5% drift ratio (cycle 1) was 173 kN, which corresponded to about 72% of peak.

> The resisting mechanisms and overall behavior observed for specimen NPS2Bi were like NPS2Ai. Full depth vertical beam cracks, diagonal cracks in the joint region, and full depth cracks along the beam column interface first developed in the specimen during the 0.5% loading cycle.

> Flexural yielding of the continuity reinforcement occurred at a drift ratio of 2% and peak load was sustained over the first 3% drift loading cycle (some minor extent of hardening in the response was observed between 2% and 3% drift). Following beam yielding, the specimen exhibited marked non-linear response, suffering progressive loss of strength and stiffness.

> Flexural cracking at the beam column interface corresponded with beam yielding at the 2% cycle. Joint cracking increased during the 2% drift loading level, propagating further on each subsequent cycle. Concrete spalling occurred at the 3% drift cycle, after significant joint diagonal cracking. Potentiometer readings indicated that, at this stage, the shear reinforcement in the joint reached full yielding.

> By the time the specimen was pushed to the 5% drift ratio, the joint region was heavily damaged and the joint reinforcing bars were fully exposed (Figure 5.16). All damage was absorbed by the joint panel zone, the beams did not suffer any notable additional cracking following the 3.0% drift loading cycle. However, wide cracks were observed at the beam-column interface, as noted above. The columns remained undamaged throughout the test.

1.5% Drift **2.0% Drift** **3.0% Drift** **4.0% Drift** **5.0% Drift**

Figure 5.16: NPS2Bi – View of Joint Region at Various Drift Ratios

> The subcomponents of drift of NPS2Bi specimen can be seen in Figure 5.17[3]. It is evident that the progressive reduction of column action contributing to drift, from more than 60% initially, to 10% during the final loading stage. The beam action steadily increased, until the full yielding of the specimen during the 3% drift ratio, at which point the shear in the joint started to dominate. The shear in the joint remained, like NPS1i, somewhat constant until the 4% and 5% drift ratios, post beam yielding where it increased rapidly.

[3]Only percentages higher than 10% are shown; the "uncounted" portion is assumed to be attributed to the beam flexure plus negligible shear in the beams and columns. All contributions are taken from the first cycle of the pertinent drift loading ratio.

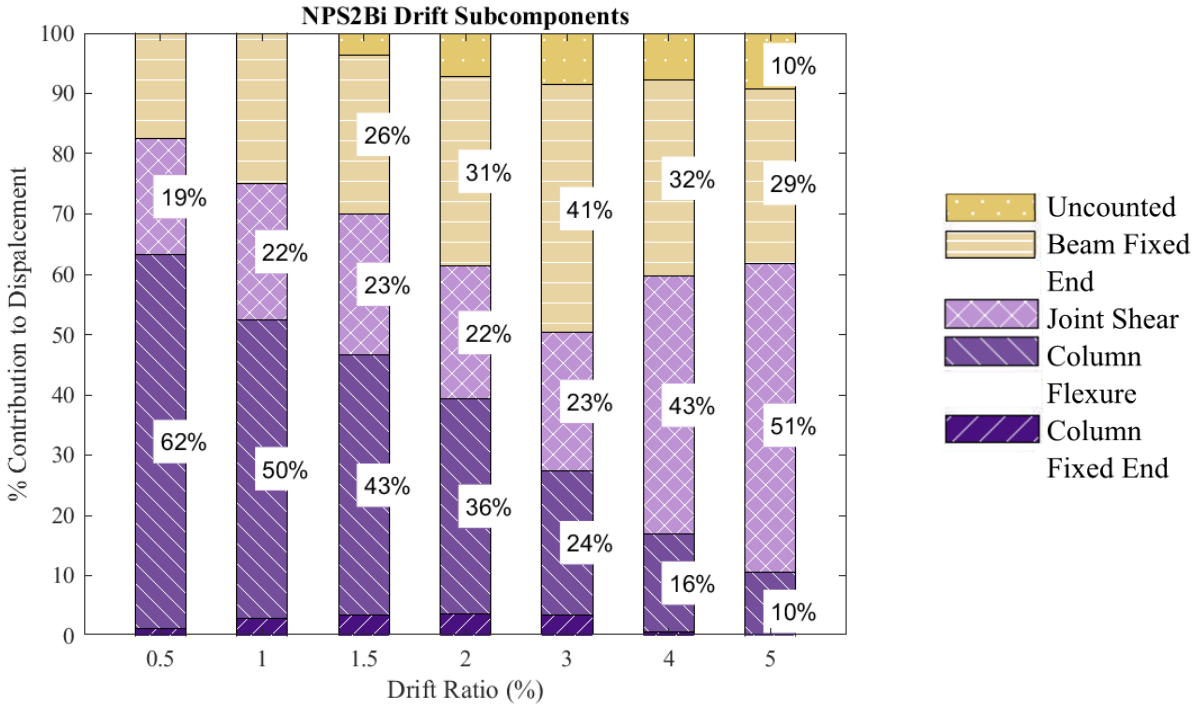

Figure 5.17: NPS2Bi Drift Subcomponents

5.1.5 NPS4i Specimen

As previously discussed, this specimen was nearly the same as NPS2Ai, and the final specimen tested in the MDI Test Series, achieving moment continuity with straight deformed bars, without additional beam shear reinforcement in the critical region. The differences include (i) 150 mm shear stirrup spacing in the joint region instead of 100 mm and (ii) a steel encased joint region. A view of specimen NPS4i with the experimental setup is provided in Figure 5.18.

Figure 5.18: View of Specimen NPS4i Before (Left) and After (Right) Testing

The specimen was subject to the full loading protocol described in CHAPTER 3 , including three full cycles at peak drift ratio of 5%. The horizontal force-displacement response is outlined in Figure 5.19. NPS4i reached a positive peak strength of 239 kN during the first loading cycle to 3% drift ratio, and a negative peak strength of 234 kN at 2% drift ratio. The hysteretic response is in Figure 5.19 is analogous to that of specimens NPS2Ai and NPS2Bi, but NPS4i suffered a lower extent of strength degradation as the displacement demand increased and had an overall more ductile response. However, marked pinching caused by bond-slip deterioration was still observed, beyond what might be considered acceptable levels. This is discussed in detail in CHAPTER 6

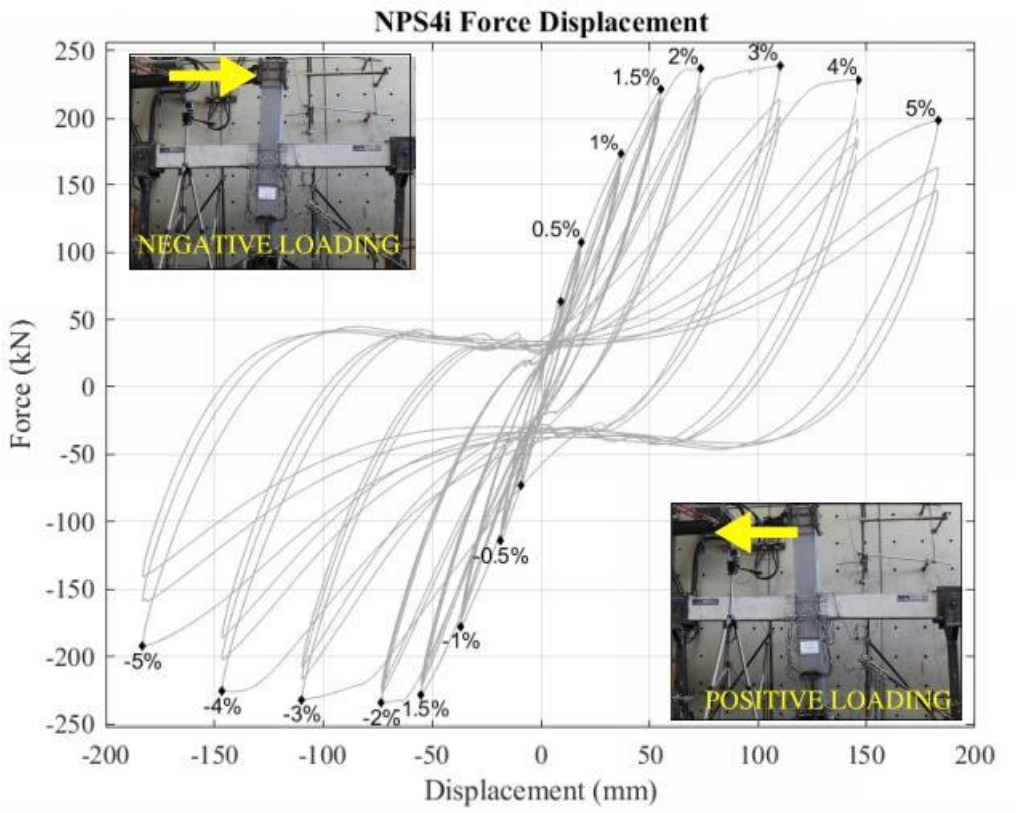

Figure 5.19: Force-Displacement Response of Specimen NPS4i

> Analogously to its companion specimens, NPS2Ai and NPS2Bi, after beam yielding occurred (around 2% drift ratio), NPS4i suffered progressive loss of lateral stiffness. At drift ratios of 3% and 4% secant stiffness losses ($K_{0,Drift\%\ Cycle3}$/ $K_{0,Drift\%\ Cycle1}$) of about -5% and 61% occurred between loading cycles 1 and 3. However, minor strength losses were detected. The positive residual strength at 5% drift ratio (cycle 1) was 199 kN, which corresponds to about 83% of peak. This is remarkable, suggesting that this strength reduction can be almost entirely attributed to second order (P-Δ) effects.

> Despite the evident similarities between the force-displacement response of specimen NPS4i, NPS2Ai and NPS2Bi, the overall behavior observed for specimen NPS4i was different from that of its companion specimens. Namely, due to the increased stiffness provided at the critical joint region, the specimen did not exhibit the same characteristics of many of the other specimens, including joint diagonal cracking or spalling in the joint region. The specimen failed at the interface of the beam column joint which was interpreted as yielding in the beam (BY) with no shear deterioration of the joint.

> Full depth flexural beam cracks and full depth cracks along the beam column interface first developed in the specimen during the 0.5% loading cycle. Flexural yielding of the continuity reinforcement occurred at a drift ratio of 2% and peak load was sustained (with negligible reduction) over the 4% drift loading cycle. Following beam yielding, the specimen exhibited marked non-linear response, suffering progressive loss of lateral stiffness due to bond-slip deterioration of the continuity bars. No joint damage was detected due to the presence of the steel HSS. Thus, rather than diagonal cracks and concrete spalling in the joint region, the only extent of damage that was observed as the displacement demand on the system increased, was of a flexural nature. A major vertical crack formed early in the test at the beam-column interface that became wider with subsequent loading cycles. As the displacement demand increased between the 4% and 5% drift ratios, evidence of concrete crushing and buckling of the beam bottom chord could be seen (see Figure 5.20). This is typical of interior beam-column joint systems with large bond demands and adequately protected joint region. The steel HSS was cut out and the joint was inspected after completing the test, showing no sign of damage (Figure 5.20). The columns remained undamaged throughout the test.

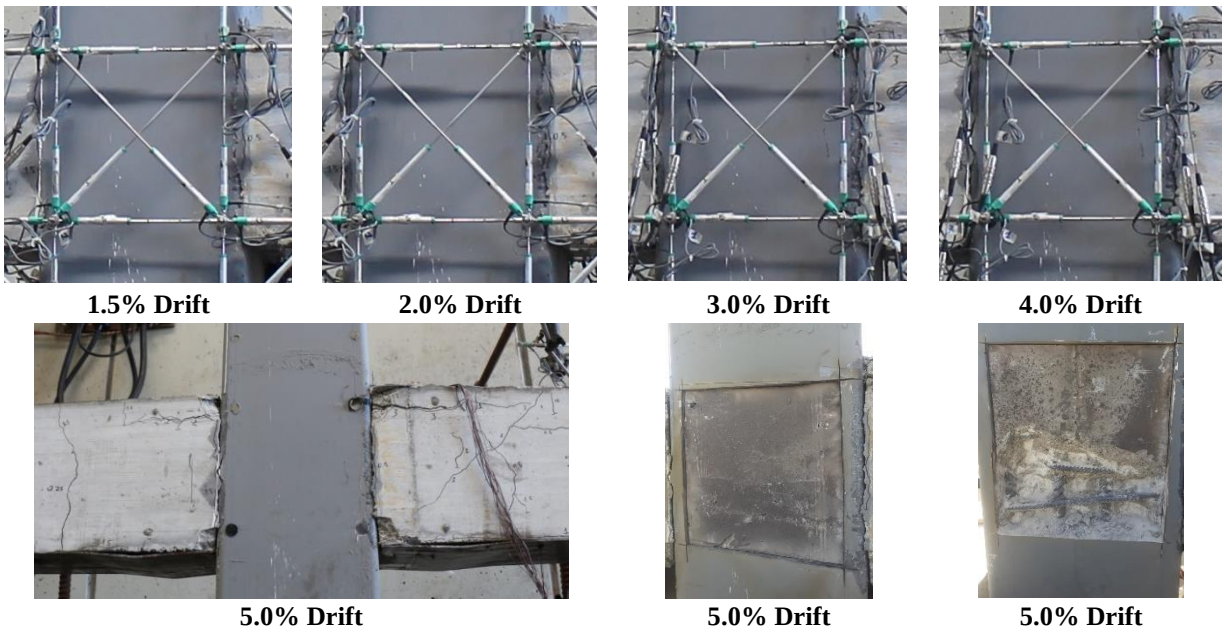

1.5% Drift **2.0% Drift** **3.0% Drift** **4.0% Drift**

5.0% Drift **5.0% Drift** **5.0% Drift**

Figure 5.20: NPS4i - View of Joint Region at Various Drift Ratios

The subcomponents of drift of NPS4i specimen can be seen in Figure 5.21[4]. Note that there was an error in data collection, and unfortunately the 4% loading stage was unable to be adequately recorded by the potentiometers. It is evident that the progressive reduction of column action contributing to drift, from more than 60% initially, to 13% during the final loading stage. The beam action steadily increased for the duration of the test. The shear in the joint started, and then remained, at less than 10%, which is unsurprising and supports the previously noted joint protection mechanism.

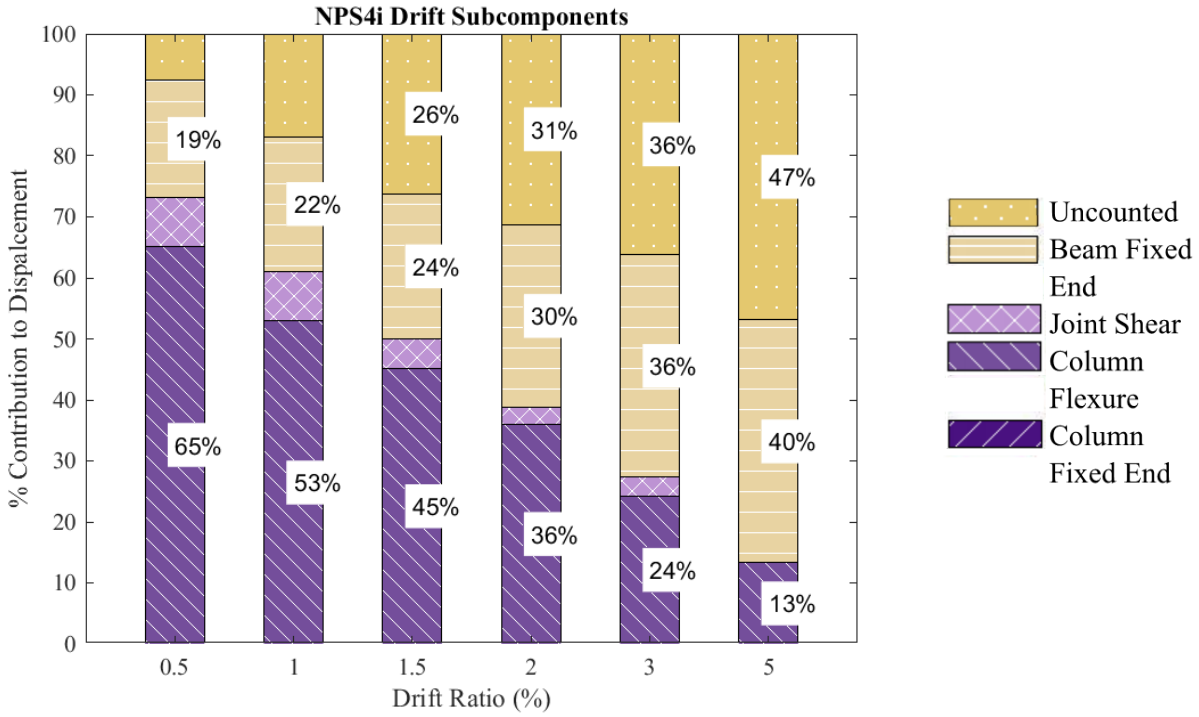

Figure 5.21: NPS4i Drift Subcomponents

[4]Only percentages higher than 10% are shown; the "uncounted" portion is assumed to be attributed to the beam flexure plus negligible shear in the beams and columns. All contributions are taken from the first cycle of the pertinent drift loading ratio. 4% data was unable to be collected.

5.2 MDE TEST SERIES

> The moderately ductile external (MDE) Test Series included five (5) specimens, REFe, NPS1e, NPS2Ae, and NPS4e. NPS2Be was not included, as the internal specimen was intended to further reinforce the assumption that additional shear in the beam critical region would not be necessary for the NPS® System, which was evidenced in the results. All specimens were intended to represent exterior beam-column joints of a moderately ductile moment resisting frame (MRF). As discussed in CHAPTER 3 , the external specimens were subjected to the same loading protocol as the internal specimens: increasing reversed cyclic drift demand (3 loading cycles per drift level) and constant axial load of 300 kN. See CHAPTER 3 for additional details regarding the design, layout, testing protocol, and instrumentation of these specimens.

> Specimen REFe suffered an unexpected failure at the base of the column due to undesired out-of-plane loads induced by the test setup. This issue was corrected for all other specimens by including additional bracing. Thus, testing of REFe had to be stopped at a drift level of 3% (failure classified as OP, "out-of-plane"), however the data up until the point of failure is considered reliable, as it aligned with expected trends. All other tests were terminated once the specimens reached a peak 5% drift ratio (without necessarily completing 3 full cycles). The term "failure" is used somewhat loosely in this section to refer to the status of the specimens at 5% drift level, even though all specimens had non-trivial residual strength at this point.

> There were commonalities among the responses of all MDE specimens. All beam-column assemblies reached their nominal strength, corresponding to beam flexural yielding. Most of the specimens also showed a ductile response characterized by highly dissipative wide hysteretic loops and experienced a failure mode classified as "beam yielding" (BY). This was an expected response mechanism, as the force in the joint region was less than an internal specimen, as discussed in CHAPTER 3 The response of specimen NPS1e was somewhat unique, in that beam yielding was followed by significant bond-slip deterioration at the beam-column interface, resulting in a ductile yet markedly pinched response. Its failure mode was classified as "beam yielding with anchorage issues" (BY-A).

> Some of the key experimental results are summarized in Table 5.2. Note that K_0 represents the residual secant lateral stiffness of the system (described in CHAPTER 4 with subscripts representing the either the first or the third loading cycle. The peak load and residual loads are noted for the negative loading directions. More details pertaining to the experimental response of each individual specimen are provided in the following sections.

Table 5.2: Summary of Test Results - MDE Test Series

Specimen ID	Peak Load- (PL) [kN]	5%(Cycle 1) Residual Load- (RL) [kN]	RL/ PL	Strength Degradation		Stiffness Degradation		Failure mode
				3% Drift $P_{max,3}/P_{max,1}$	4% Drift $P_{max,3}/P_{max,1}$	3% Drift $K_{0,3}/K_{0,1}$	4% Drift $K_{0,3}/K_{0,1}$	
REFe	103	NA	NA	NA	NA	NA	NA	OP
NPS1e	86	55	0.64	0.82	0.87	0.17	-0.21*	BY-A
NPS2Ae	114	76	0.67	0.92	0.93	0.89	0.74	BY
NPS4e	116	65	0.56	0.88	0.96	0.89	0.73	BY

*Due to severe pinching, negative residual stiffness calculated for 4% Drift Cycle 3

5.2.1 REFe Specimen

> The reference specimen was the same as the internal specimen, sans one beam, and it was the first specimen of the MDE series tested. This specimen was intended to serve as a reference as a traditionally reinforced concrete moderately ductile beam-column joint. For additional design considerations and details see CHAPTER 3 . The moment continuity of this specimen was achieved with hooked deformed rebar. To account for the loss of available development length, the continuity bars were hooked vertically into the column.

> A view of the specimen is provided in Figure 5.22, in the form of two photographs taken before initiation and upon completion of the experiment.

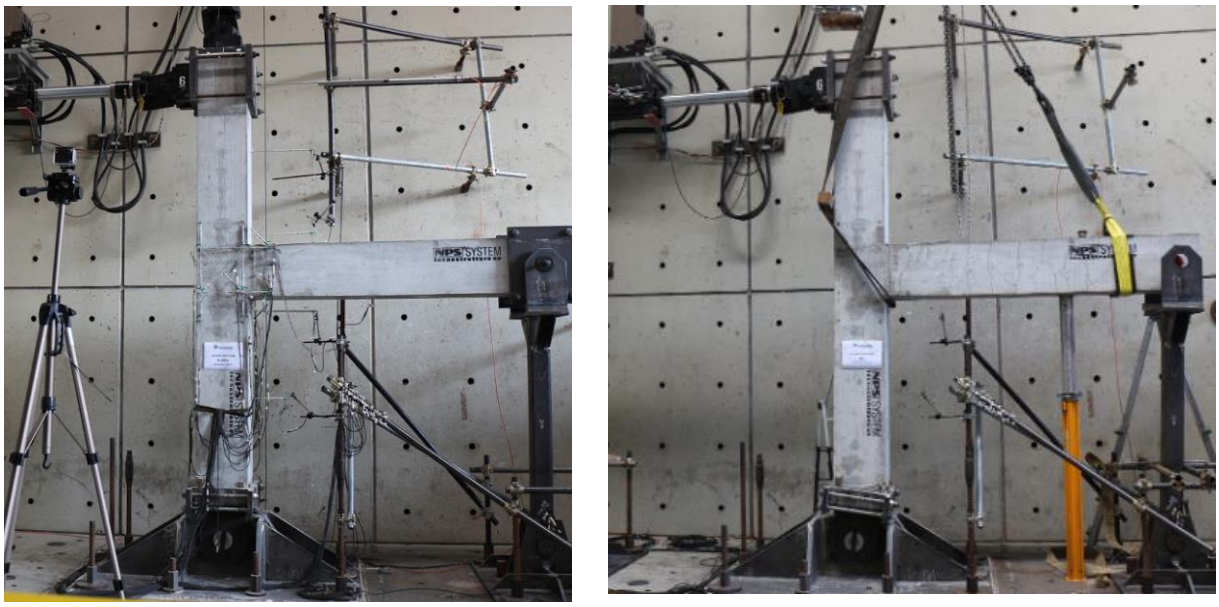

Figure 5.22: View of Specimen REFe Before (Left) and After (Right) Testing

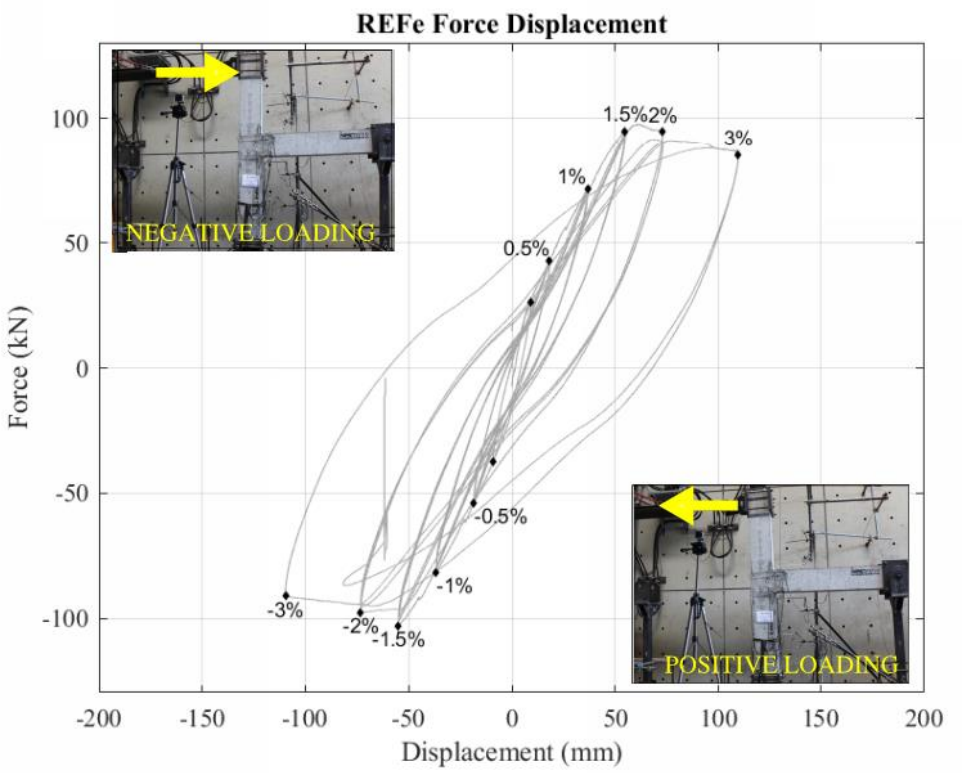

Figure 5.23: Force-Displacement Response of Specimen REFe

The horizontal force-displacement response of specimen REFe is outlined in Figure 5.23. The maximum displacement reached during the test was 109.65 mm, which corresponds to a drift ratio of 3%.

> During the second cycle of the 3% loading the specimen broke at the base of the column, and testing could not be completed to the full loading protocol described in CHAPTER 3 The specimen suffered an unexpected failure at the base of the column (see Figure 5.24) due to undesired out-of-plane loads induced by the test setup.

Figure 5.24: Base of the Column After Out-of-Plane Failure Occurred

> Even though specimen REFe did not fail in-plane as intended, the data collected during the test was still valid, particularly while the out-of-plane displacements were small. The early behavior was entirely in-plane, and only the last loop of the hysteresis showed significant evidence of the impending torsional failure.

> REFe reached a positive peak strength of 95 kN and a negative peak strength of 103 kN. Both occurred during the first loading cycle of the 1.5% drift ratio, in the pertinent loading direction.

> The force-displacement data collected to 3% drift ratio show a ductile response and a reasonably fat hysteretic loop which results in high energy dissipation capacity. Extrapolating based on the available data, it is reasonable to assume that the system would have developed a complete flexural mechanism in the form of a plastic hinge at the beam end, without suffering substantial joint damage or bond deterioration effects. No damage in the panel zone was observed at the 3% drift, which can be seen in Figure 5.25.

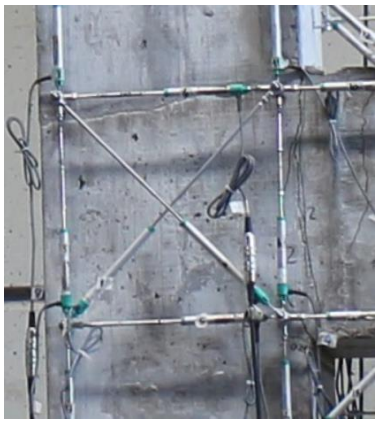

Figure 5.25: REFe Panel Zone at 3%

> Full depth vertical cracks did form in the beam during the 0.5% loading cycle and continued to expand and propagate on following cycles, as shown in Figure 5.26. Beam yielding occurred at 1.5% drift ratio and peak load was sustained with negligible strength loss up to 3% drift. No damage other than spread flexural cracks in the beams were observed at failure.

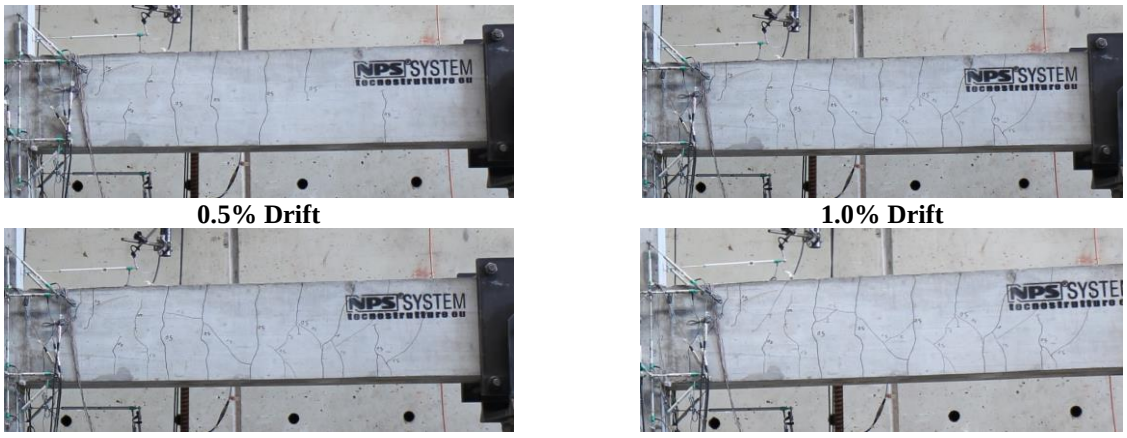

0.5% Drift **1.0% Drift**

1.5% Drift **2.0% Drift**

Figure 5.26: REFe - Beam Cracking Propagation

The subcomponents of drift of the REFe specimen can be seen in Figure 5.27[5]. It should be noted that data from this experiment may differ from the standard, due to the out of plane failure. With that in mind, the results do seem to support the visual evidence of joint protection, with beam flexural cracking at the beam-column interface – indicated by the beam fixed-end subcomponent – increasing during 2% and 3% loading ratios.

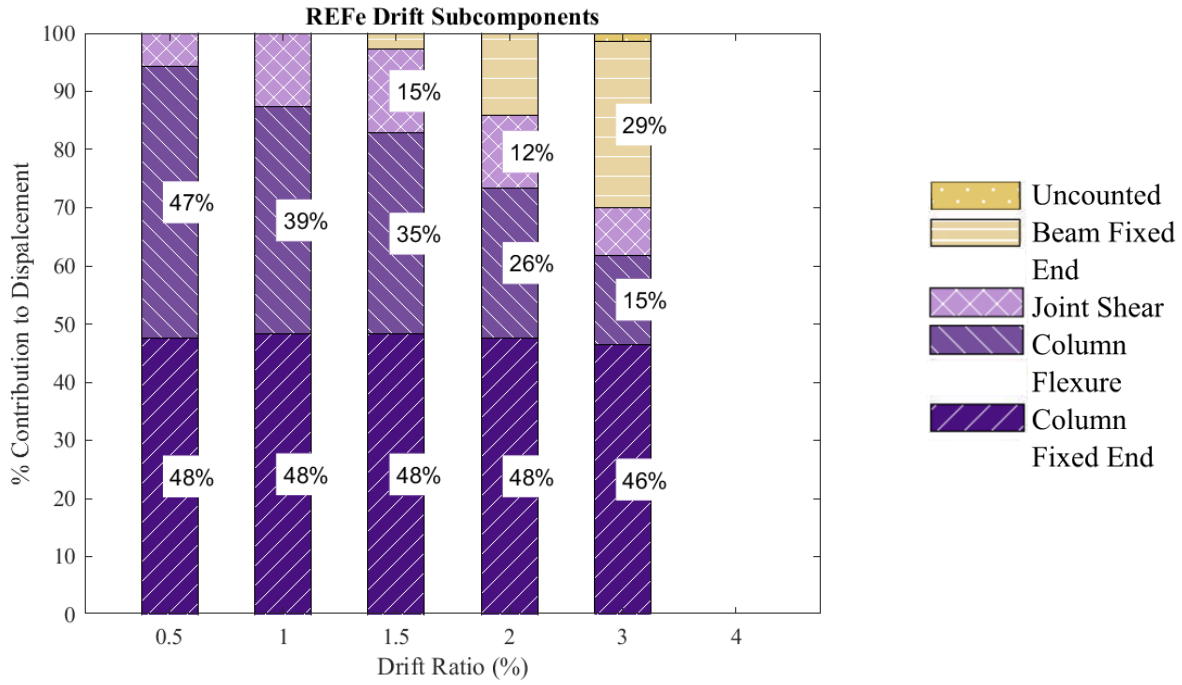

Figure 5.27: REFe Drift Subcomponents

[5]Only percentages higher than 10% are shown; the "uncounted" portion is assumed to be attributed to the beam flexure plus negligible shear in the beams and columns. All contributions are taken from the first cycle of the pertinent drift loading ratio.

5.2.2 NPS1e Specimen

> Additional bracing was included in the experimental setup to prevent out of plane issues after the undesired torsional failure in the REFe specimen. Specimen NPS1e achieved moment continuity at the joint by means of two added trusses, identical to its internal counterpart. To ensure adequate anchorage of the continuity truss elements, additional rebar at the corners of the continuity truss were added to provide anchorage in the joint region. Recall this specimen had a lower reinforcement ratio in the joint region due to space concerns (i.e., no shear reinforcement other than the continuity truss diagonal elements was present in the joint region). The beam plastic hinge region was reinforced in shear with added stirrups, and windows were cut into the HSS column to replicate future beam placement. A view of specimen NPS1e with the experimental setup is provided in Figure 5.28.

Figure 5.28: View of Specimen REFe Before (Left) and After (Right) Testing

> The horizontal force-displacement response of specimen NPS1e is outlined in Figure 5.29. The specimen reached a positive peak strength of 76 kN and a negative peak strength of 86 kN. Both occurred during the first loading cycle to 1.0% drift ratio, in the pertinent loading direction. The specimen started exhibiting marked non-linear response just past the 1.0% drift ratio mark, which is when yielding in the longitudinal bars of the continuity trusses was detected from strain gauge readings.

> Overall, the observed response showed good ductility, but the hysteretic response was affected by significant pinching attributed to poor bond between the continuity truss smooth bars and the surrounding concrete that evidently resulted in progressive bond-slip deterioration. Some extent of capacity reduction was also observed, with the negative residual strength at 5% drift ratio (cycle 1) at 55 kN, which corresponds to about 64% of peak.

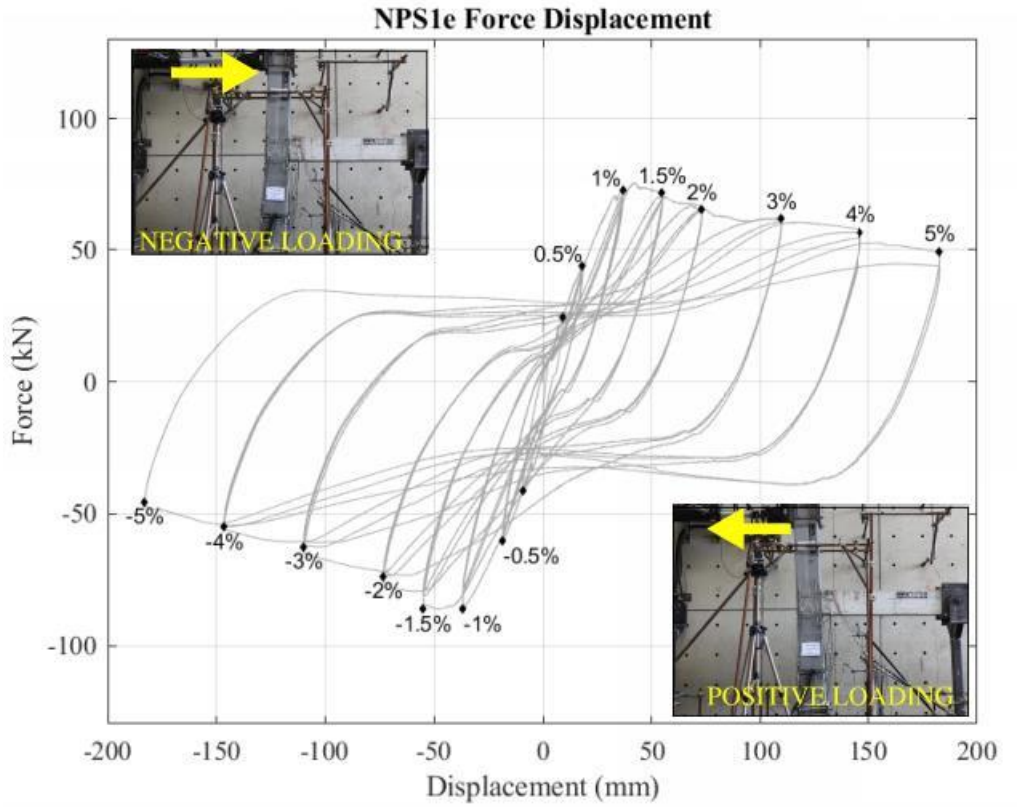

Figure 5.29: Force-Displacement Response of Specimen NPS1e

> Beam flexural cracks first appeared during the early stages of the test (drift ratio of 0.25% to 0.50%). Diagonal cracking of the joint occurred during the first cycle of the 2% drift loading. Joint cracking appeared to be well-controlled throughout the test and did not result in any noticeable joint deterioration or spalling. In contrast, a major crack formed at the beam-column interface that progressively widened (displaying evident local debonding) as the magnitude of the imposed displacements increased, particularly after beam yielding (the crack is visible in Figure 5.30). This “flexural” mechanism governed the response of the specimen, protecting all other elements from suffering any serious damage. Figure 5.30 shows that

beam cracking at 2% drift was essentially identical to the crack pattern detected at 5% drift ratio. Analogous conclusions can be drawn pertaining to the joint at 5% as 2%, as can be seen in Figure 5.31.

> This failure mechanism for specimen NPS1e was subsequently classified as “beam yielding with anchorage issues” (BY-A).

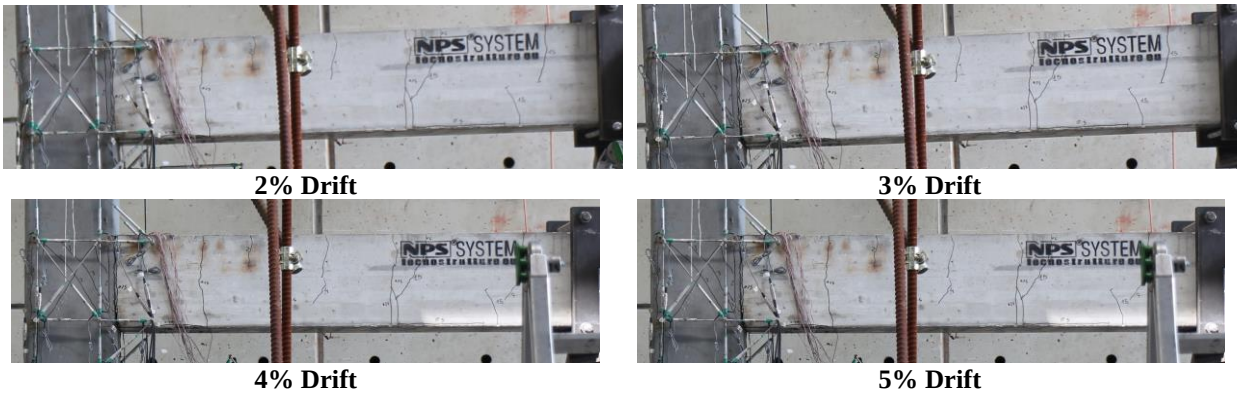

2% Drift **3% Drift**

4% Drift **5% Drift**

Figure 5.30: NPS1e – Beam Cracking Propagation

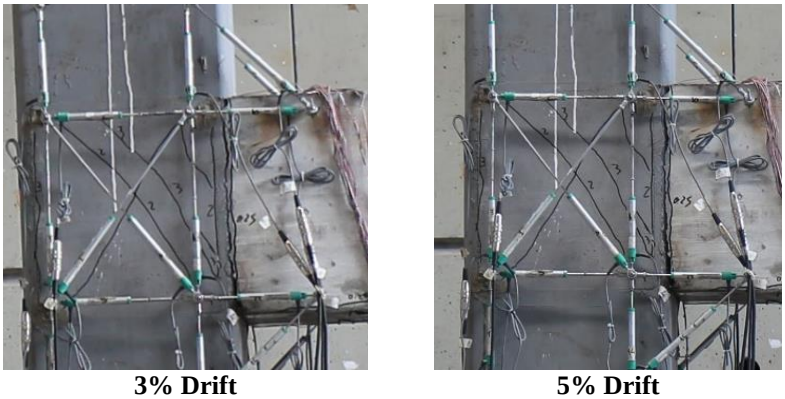

3% Drift **5% Drift**

Figure 5.31: NPS1e - View of Joint Region and Main Flexural Crack

> The subcomponents of drift of the NPS1e specimen can be seen in Figure 5.32[6]. The column flexure was substantially less for external specimens, relative to internal, as expected. Not only are external specimens subjected to lower beam flexural demands, but the internal shear and flexural steel was not altered for the

[6]Only percentages higher than 10% are shown; the “uncounted” portion is assumed to be attributed to the beam flexure plus negligible shear in the beams and columns. All contributions are taken from the first cycle of the pertinent drift loading ratio.

exterior specimens, resulting in stronger column and joint regions relative to anticipated loads, which may be described as “over designed”. As evidenced in the drift subcomponents in Figure 5.32 the joint shear was a minor contributor, with less than 10% of the overall contribution to drift for the entirety of the test. In contrast, the beam action, due to both the flexure and fixed end, contribute to more than half of the overall displacement during all drift levels.

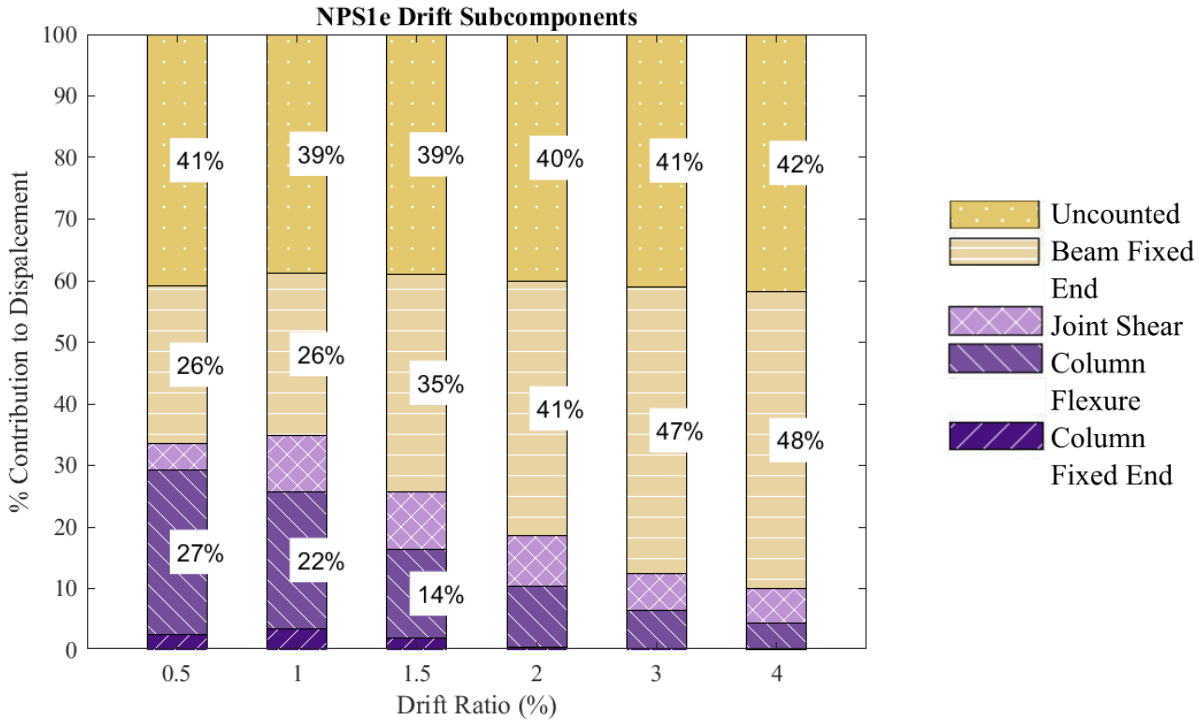

Figure 5.32: NPS1e Drift Subcomponents

5.2.3 NPS2Ae Specimen

NPS2Ae is the same as NPS2Ai specimen sans one beam, like all the other external specimens. The moment continuity connection consisted of hooked (only on joint side) deformed bars extending beyond the critical regions of the beam. The beam plastic hinge region was not reinforced in shear with added stirrups, while traditional shear reinforcement was present in the joint region. This joint reinforcement ratio is the same as REFe. There were also two "windows" in the HSS column to represent two phantom beams. A view of specimen NPS2Ae with the experimental setup is provided in Figure 5.33.

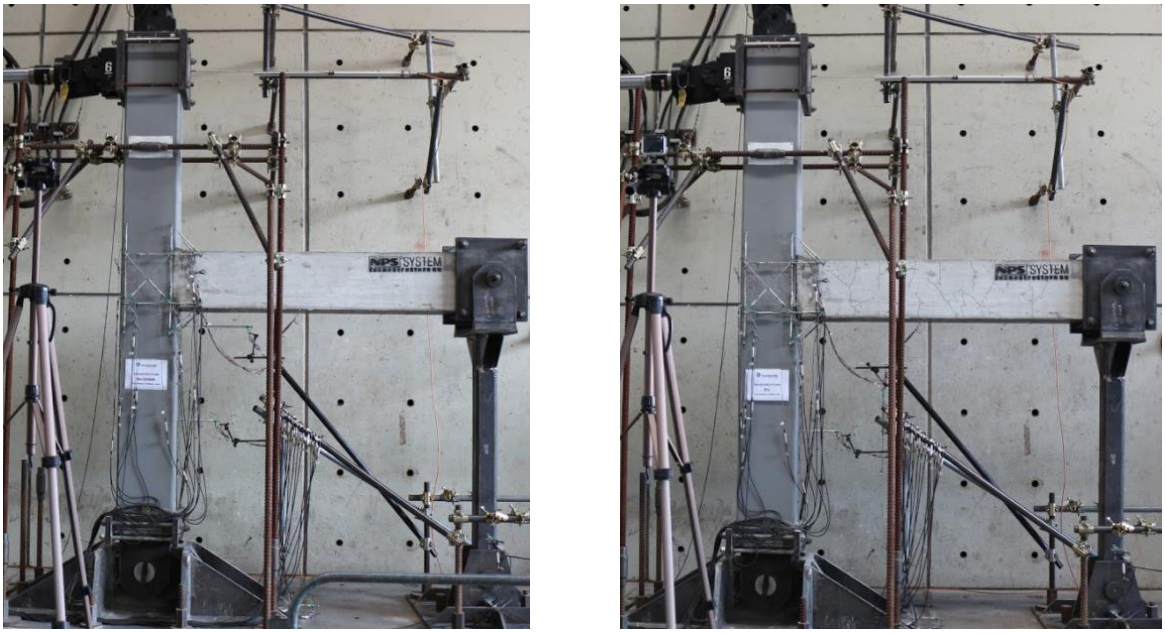

Figure 5.33: View of Specimen NPS2Ae Before (Left) and After (Right) Testing

The horizontal force-displacement response of specimen NPS2Ae is outlined in Figure 5.34. The specimen reached a positive peak strength of 105 kN and a negative peak strength of 114 kN. Both occurred at about 1.5% drift ratio, in the pertinent loading direction. The specimen started exhibiting marked non-linear response around 1.0% drift, during the first loading cycle to 1.5% drift. This is when yielding in the beam continuity bars was detected from strain gauge readings.

The observed response showed good ductility, with a reasonably fat hysteretic response capable of providing high energy dissipation. Minimal secant stiffness degradation is observed between consecutive loading cycles at a target drift level. Some extent of capacity reduction (largely attributable to second order

effects) was also observed, with the negative residual strength at 5% drift ratio (cycle 1) equal to 76 kN, which corresponds to about 67% of peak.

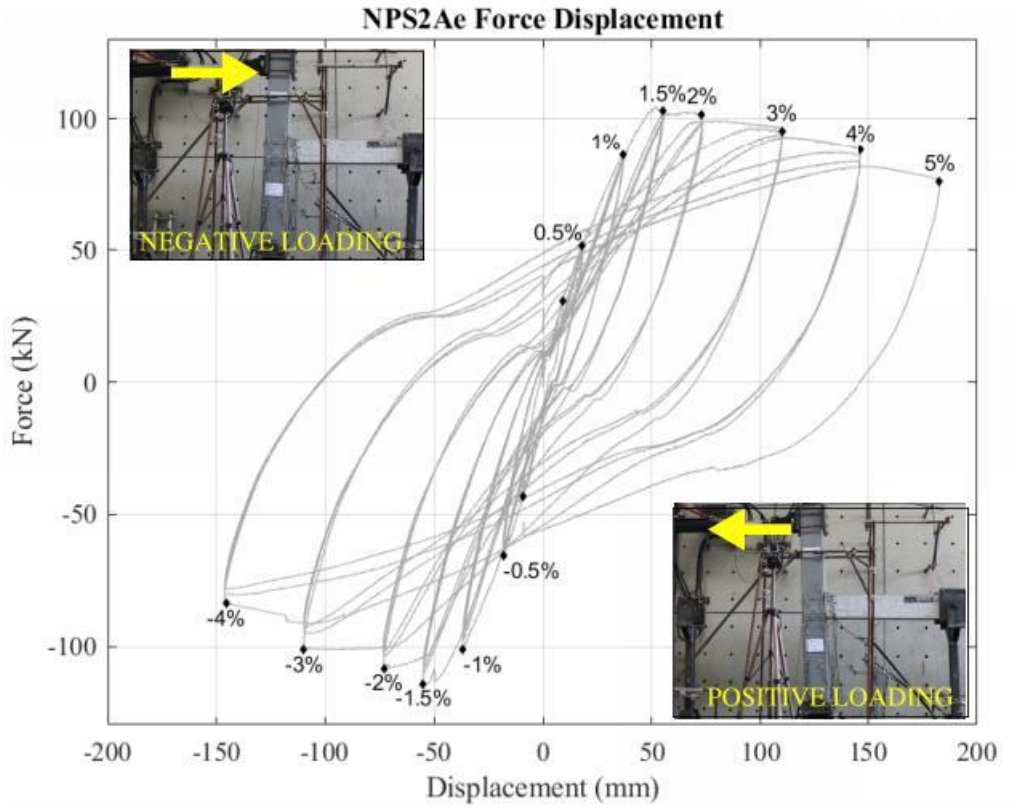

Figure 5.34: Force-Displacement Response of Specimen NPS2Ae

Beam flexural cracks first appeared during the early stages of the experiment (drift ratio of 0.25% to 0.50%). Beam cracking propagated throughout the test, in the form of additional (minor) flexural cracks and (very minor) shear-flexural cracks, spread quite uniformly along the beam length. First diagonal cracking of the joint occurred during the first cycle of the 3% drift loading. Joint cracking was limited and well-controlled and did not result in any noticeable joint deterioration. In contrast, a major flexural crack formed at the beam-column interface that progressively widened as the magnitude of the imposed displacements increased, particularly after beam yielding (the crack is visible in Figure 5.35). The continuity bars appeared to be well-anchored within the joint core, thus full beam yielding could develop effectively. This flexural mechanism governed the response of the specimen, protecting all other elements from suffering any serious extent of damage. Figure 5.35 shows beam cracking progression from 2% to 5%

drift level, while the joint crack pattern is visible in Figure 5.36 for two drift levels. Because of the type of response observed, the failure mechanism for specimen NPS2Ae was classified as “beam yielding” (BY).

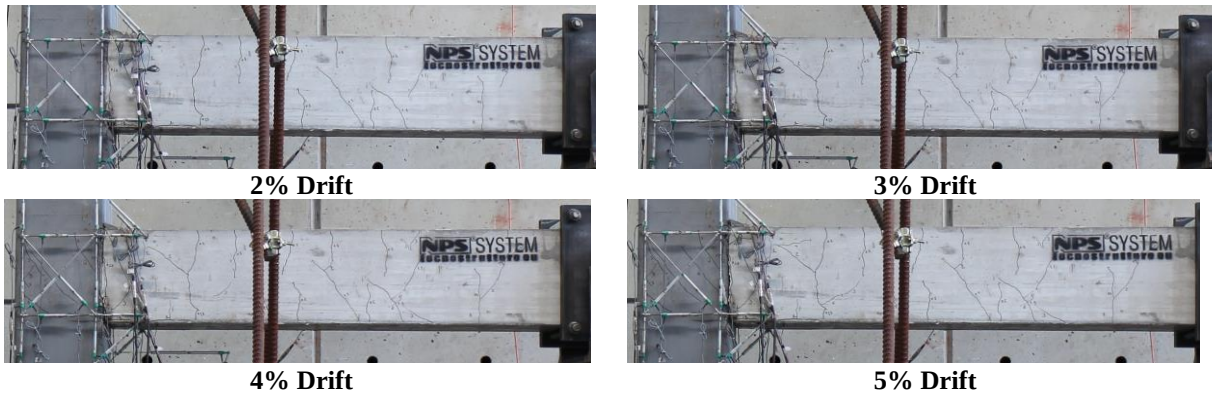

2% Drift **3% Drift**

4% Drift **5% Drift**

Figure 5.35: NPS2Ae - Beam Cracking Propagation

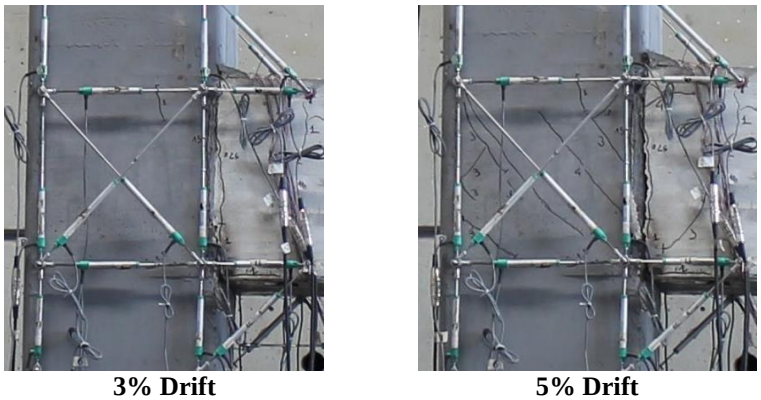

3% Drift **5% Drift**

Figure 5.36: NPS2Ae – View of Joint Region and Main Flexural Crack

> The subcomponents of drift of the NPS2Ae specimen can be seen in Figure 5.37[7]. The column flexure was initially 35% and steadily decreased. The joint shear remained constant or decreased. The beam flexure and fixed end contributions, however, increased progressively and always remaining above 50% of the total drift. This is similar to the NPS1e result.

[7]Only percentages higher than 10% are shown; the “uncounted” portion is assumed to be attributed to the beam flexure plus negligible shear in the beams and columns. All contributions are taken from the first cycle of the pertinent drift loading ratio.

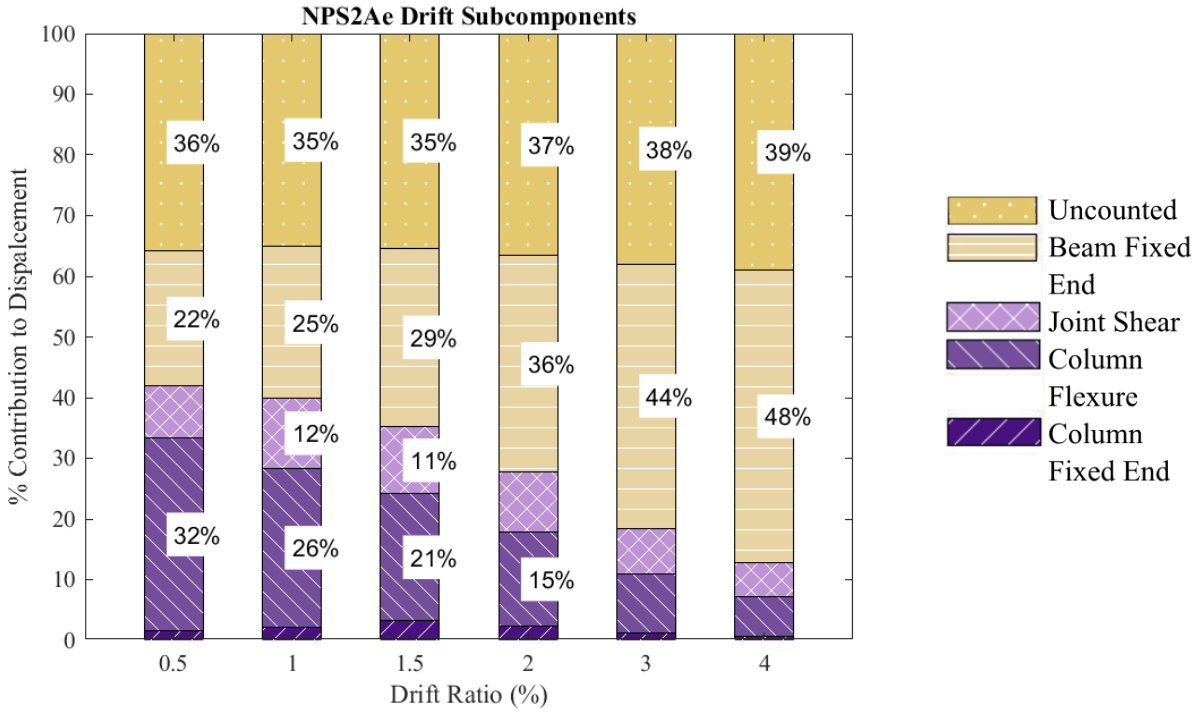

Figure 5.37: NPS2Ae Drift Subcomponents

5.2.4 NPS4e Specimen

For the most part, this specimen was nominally identical to NPS2Ae, with moment continuity connection consisting of hooked (joint side) deformed bars extending beyond the critical region of the beam and no added shear reinforcement in the beam plastic hinge region. However, the joint region of specimen NPS4e had a lower amount of internal shear reinforcement (i.e., stirrups spaced at 150 mm instead of 100 mm), and the steel HSS tube of the column did not have a section cut out i.e., there were no "windows" in the HSS on the side not connected to the beams. A view of specimen NPS4e with the experimental setup is provided in Figure 5.38

Figure 5.38: View of Specimen NPS4e Before (Left) and After (Right) Testing

The horizontal force-displacement response of specimen NPS4e is outlined in Figure 5.39. The specimen reached a positive peak strength of 94 kN and a negative peak strength of 116 kN, which occurred at drift ratios of about 1.2% and 1.5%, respectively. The specimen started exhibiting marked non-linear response around 1.0% drift. This is when yielding in the beam continuity bars was first detected from strain gauge readings.

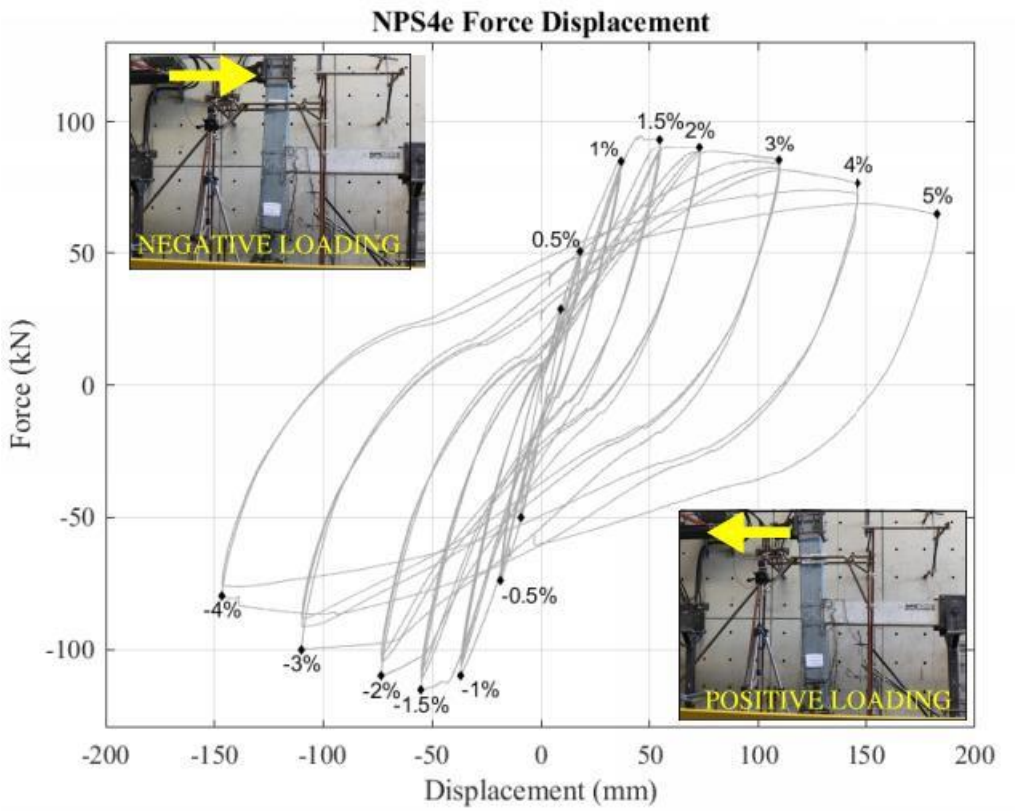

Figure 5.39: Force-Displacement Response of Specimen NPS4e

> The observed response showed good ductility, with a reasonably fat hysteretic response capable of providing high energy dissipation. Minimal secant stiffness degradation is observed between consecutive loading cycles at a target drift level. Some extent of capacity reduction (largely attributable to second order effects) is also observed, with negative residual strength at 5% drift ratio (cycle 1) equal to 65 kN, which corresponds to about 56% of peak.

> The overall response of specimen NPS4e was virtually identical to that of NPS2Ae. Beam flexural cracks first appeared during the early stages of the experiment (drift ratio of 0.25% to 0.50%). Beam cracking propagated throughout the test, in the form of additional minor flexural and shear-flexural cracks, spread quite uniformly along the beam length, as shown in Figure 5.40. No damage was detected (i.e., no damage occurred) in the joint region due to the presence of the steel HSS. In contrast, a major flexural crack formed at the beam-column interface that progressively widened as the magnitude of the imposed displacements increased, particularly after beam yielding (the crack widening progression is visible in Figure 5.41). The

continuity bars appeared to be well-anchored within the joint core, thus full beam yielding could develop effectively. Some evidence of flexural concrete crushing and buckling of the beam bottom chord was detected (see Figure 5.41), as the displacement demand increased. This flexural mechanism governed the response of the specimen, protecting all other elements from suffering any serious extent of damage. Figure 5.40 shows beam cracking progression from 2% to 5% drift level, while Figure 5.41 zooms in on the evolution of the main crack. Because of the type of response observed, the failure mechanism for specimen NPS2Ae was classified as “beam yielding” (BY).

Figure 5.40: NPS4e - Beam Cracking Propagation

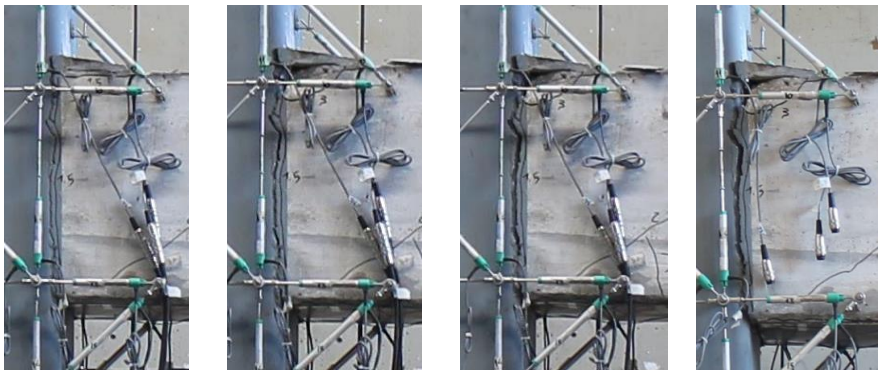

Figure 5.41: NPS4e - View of Joint Region and Main Flexural Crack

The subcomponents of drift of the NPS4e specimen can be seen in Figure 5.42[8]. The column flexure was initially 35% and steadily decreased. The joint shear was almost non-existing throughout the entirety of the test. The beam flexure and beam fixed end contributions remained at or above 50% of the total drift, similar to the other NPSe specimens.

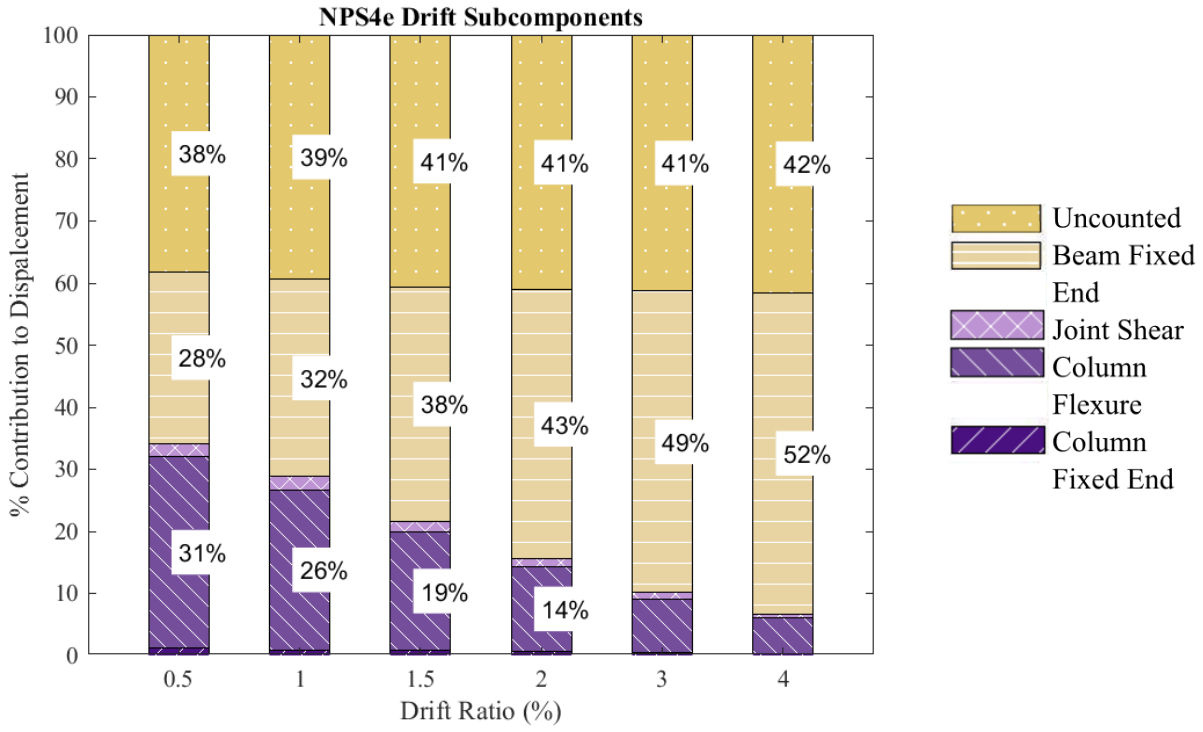

Figure 5.42: NPS4e Drift Subcomponents

[8]Only percentages higher than 10% are shown; the "uncounted" portion is assumed to be attributed to the beam flexure plus negligible shear in the beams and columns. All contributions are taken from the first cycle of the pertinent drift loading ratio.

5.3 HD TEST SERIES

> The HD Test Series includes pilot specimens NPS3i and NPS3e. As discussed in CHAPTER 3 all specimens were subjected to increasing reversed cyclic drift demand (3 loading cycles per drift level) and constant axial load of 300 kN. The two specimens tested in this series represented a preliminary explorative effort into the possibility of exploiting concepts of plastic hinge relocation. This was done in the attempt of finding viable solutions to protect the integrity of the joint region, without the need of providing large amounts of shear reinforcement. Providing large amounts of joint shear reinforcement is often difficult in NPS® beam-column joints because of reinforcement congestion and constructability concerns.

> Specimen NPS3i was subject to the full loading protocol described in CHAPTER 3 while testing of specimen NPS3e was stopped at 4% drift due to excessive damage to the specimen. Again, the term "failure" is used somewhat loosely in this section to refer to the status of the specimens at the highest drift level reached, even though all specimens still had non-trivial residual strength at this point.

> Both specimens reached their yield strength, corresponding to beam yielding in the plastic hinge region. Both specimens were also effective at relocating the plastic hinge in the beam, protecting the joint from experiencing any extent of damage.

> Several behavior issues also emerged during the experiments, in part conceptual, in part solvable with more attention to detail. One major issue that was identified had to do with the anchorage of the continuity bars and of the NPS® beam. On this account, the failure mode of both systems was classified as beam yielding with anchorage issues (BY-A).

> Some of the key experimental results are summarized in Table 5.3. Note that K_0 represents the residual secant lateral stiffness of the system (described in CHAPTER 4 with subscripts representing the either the first or the third loading cycle. More details pertaining to the experimental response of each individual specimen are provided in the following sections.

Table 5.3: Summary of Test Results - HD Test Series

Specimen ID	Peak Load (PL) [kN]	5%(Cycle 1) Residual Load (RL) [kN]	RL/PL	Strength Degradation		Stiffness Degradation		Failure mode
				3% Drift $P_{max,3}/P_{max,1}$	4% Drift $P_{max,3}/P_{max,1}$	3% Drift $K_{0,3}/K_{0,1}$	4% Drift $K_{0,3}/K_{0,1}$	
NPS3i	152	73	0.48	0.79	0.73	0.39	-0.48*	BY-A
NPS3e	68	48*	0.70	0.91	NA	-6.37*	NA	BY-A

Severe Pinching

5.3.1 NPS3i Specimen

For the most part, this specimen was nominally identical to other NPS#i specimens (i.e., NPS1i to NPS2Bi) discussed in earlier sections. However, a notably different continuity solution was adopted for NPS3i that involved smooth hoop bars that extended 550 mm into the beams. Additional shear reinforcement in the beam-end regions was also present over a length of 850 mm, and the joint core was reinforced with 4 leg-14 mm diameter shear reinforcement, spaced at 100 mm. A view of specimen NPS3i with the experimental setup is provided in Figure 5.43

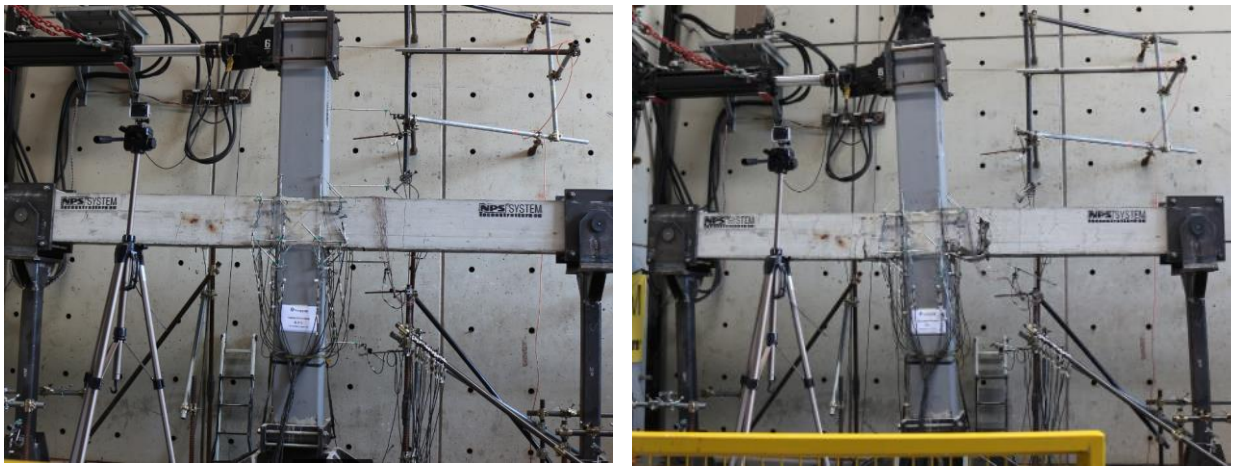

Figure 5.43: View of Specimen NPS3i Before (Left) and After (Right) Testing

The horizontal force-displacement response of specimen NPS3i is outlined in Figure 5.44. The specimen reached a positive peak strength of 152 kN and a negative peak strength of 150 kN. Both occurred during the first loading cycle to 3.0% drift ratio, in the pertinent loading direction.

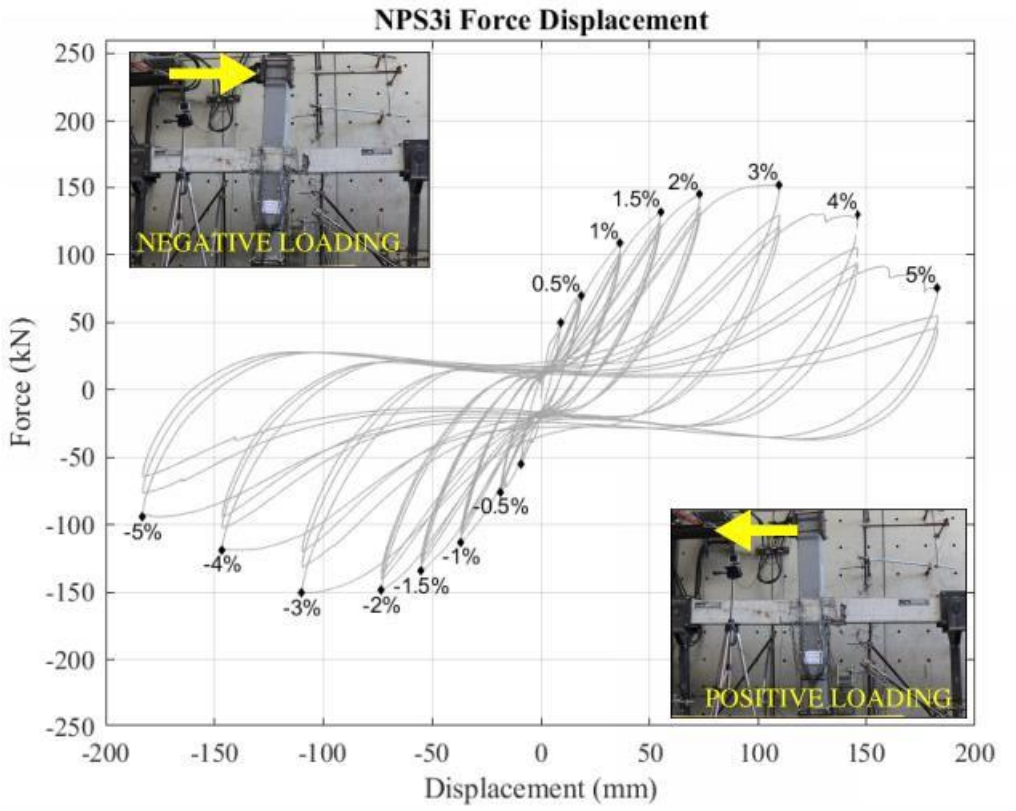

Figure 5.44: Force-Displacement Response of Specimen NPS3i

> The specimen exhibited somewhat soft and non-linear response from early loading stages. The non-linear response became more marked at a drift ratio of 2% in Figure 5.44, which is when beam yielding occurred in the intended plastic hinge region.

> Post-yielding, the specimen response exhibited significant pinching and progressive degradation of lateral stiffness. For instance, secant stiffness losses of about 21% and 27% occurred between loading cycles 1 and 3, at drift levels 3% and 4%, respectively. Non-trivial strength reduction was also observed. The positive residual strength at 5% drift ratio (cycle 1) was 73 kN, which corresponds to about 48% of peak. Note that this is significantly smaller than all other internal specimens.

> The behavior of the specimen was markedly different from that of all the other internal specimens discussed thus far. Throughout the test, damage occurred almost exclusively in the beams (particularly in the beam-end regions), with all other structural components (i.e., joint region and columns) virtually undamaged.

> Flexural cracks in the beam formed early, and cracking became progressively more extensive in the beam region designed to form a flexural plastic hinge mechanism (about 500 mm from the beam-column interface). Beam damage appeared extensive prior to yielding. For instance, in addition to extensive concrete cracking, the bottom chords of the beam trusses exhibited buckling during the 1.5% loading cycle, due to the high rotation demand on the beam. This is visible in Figure 5.45.

> At 3% drift, evidence of flexure-induce concrete crushing appeared and non-trivial spalling began to occur, first in the plastic hinge region near the bottom of the beam, and later more extensively, during subsequent loading cycles. Buckling of the beam bottom chords also became severe (see Figure 5.45), and the specimen went on to progressively lose strength and stiffness.

> A flexural failure occurred in the beam, at the intended location, with the joint region and the column fully intact. Nevertheless, the specimen was evidently affected by several issues, that jeopardized the efficiency of the system and that need to be addressed before the continuity solution presented herein can be adopted. For instance, the bond and more generally the anchorage of the continuity hoops, and the anchorage of the NPS® beam to the joint, represented two of the main concerns. The severe pinching observed in the response can be largely attributed to anchorage problems.

> Overall, for simplicity and despite the numerous undesirable phenomena observed over the course of the experiment, the failure mechanism for specimen NPS3i was classified as “beam yielding with anchorage issues” (BY-A).

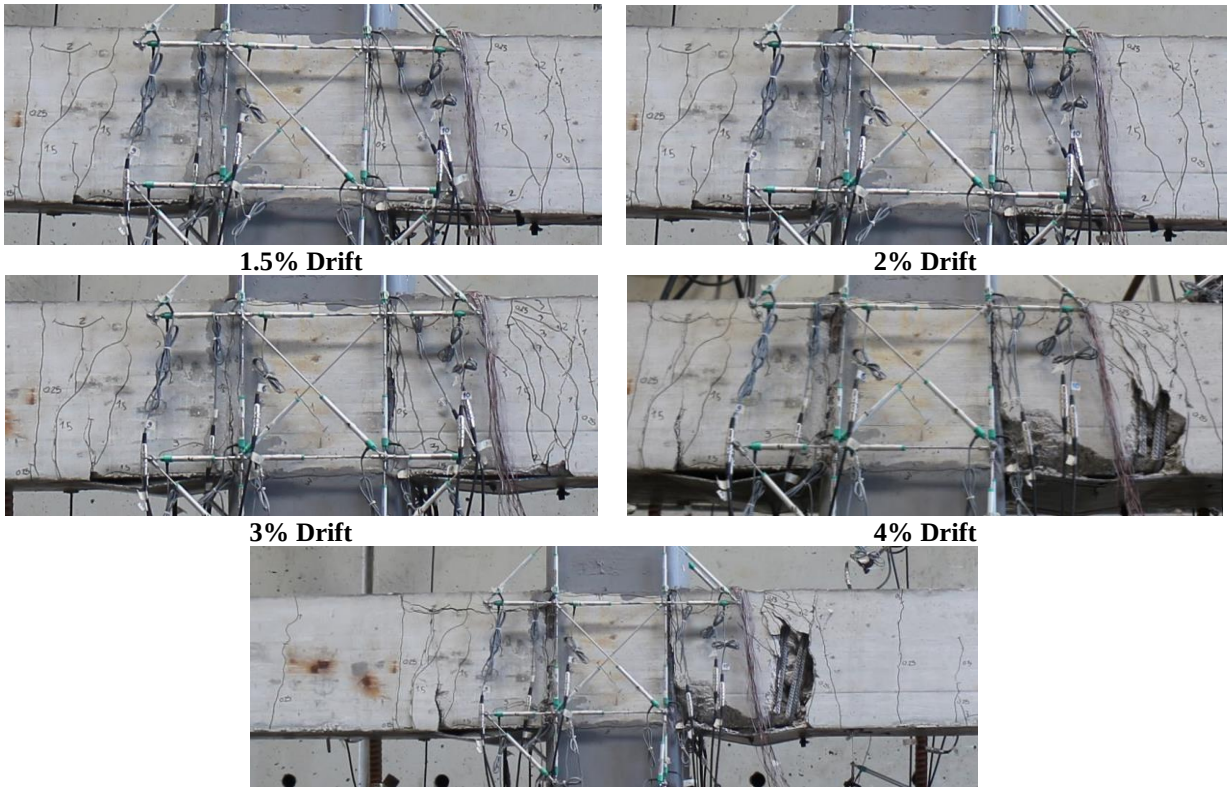

Figure 5.45: NPS3i - Beam-end and Joint Region Damage Propagation

The subcomponents of drift of the NPS3i specimen can be seen in Figure 5.46[9]. The subcomponents show the majority of the drift was due to the beam action occurring. The beam fixed end damage remained relatively constant throughout the experiment, around 40% of the total drift. The flexure in the beam was contrastingly increasing steadily, finally resulting in 53% of the overall drift. The combined column and joint action decreased consistently.

[9]Only percentages higher than 10% are shown; the "uncounted" portion is assumed to be attributed to the beam flexure plus negligible shear in the beams and columns. All contributions are taken from the first cycle of the pertinent drift loading ratio.

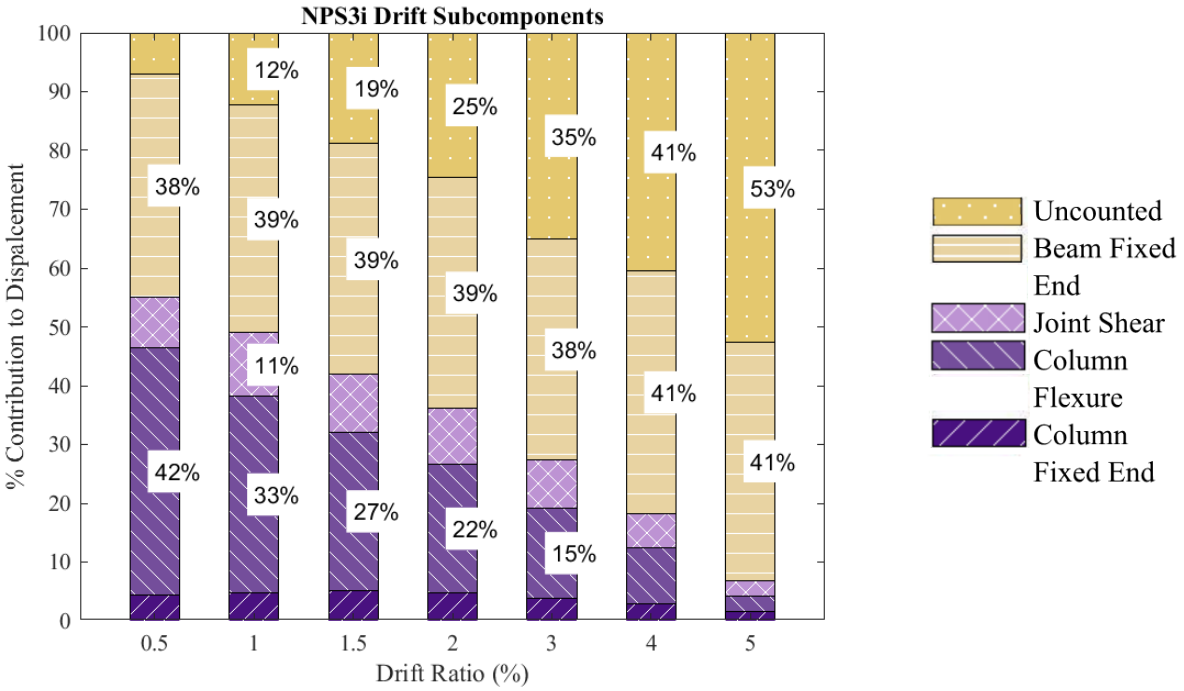

Figure 5.46: NPS3i Drift Subcomponents

5.3.2 NPS3e Specimen

For the most part, this specimen was nominally identical to other NPS#e specimens (i.e., NPS1e and NPS2Ae) discussed in earlier sections. However, moment continuity at the joint was achieved using smooth hoop bars that were anchored within the joint core and extended about 550 mm into the beam. Additional shear reinforcement in the beam-end regions and in the joint core was also present, as described for specimen NPS3i. A view of specimen NPS3e with the experimental setup is provided in Figure 5.47.

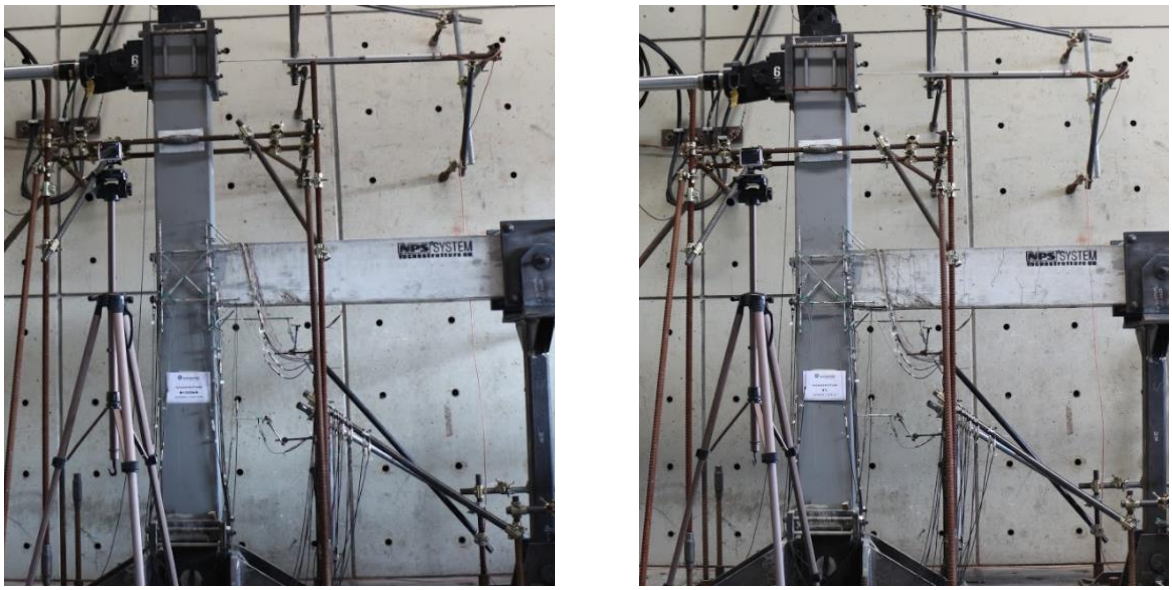

Figure 5.47: View of Specimen NPS3e Before (Left) and After (Right) Testing

> The horizontal force-displacement response of specimen NPS3e is outlined in Figure 5.48. The specimen reached a positive peak strength of 69 kN and a negative peak strength of 49 kN, which occurred at drift ratios of 2% and 1.5%, respectively.

> Analogously to NPS3i, the specimen exhibited somewhat soft and non-linear response from early loading stages. The non-linear response became more marked at a drift ratio of 3% on the positive side and 2% on the negative side. This is consistent with beam yielding, which was estimated to have occurred somewhere between 2% and 3% drift.

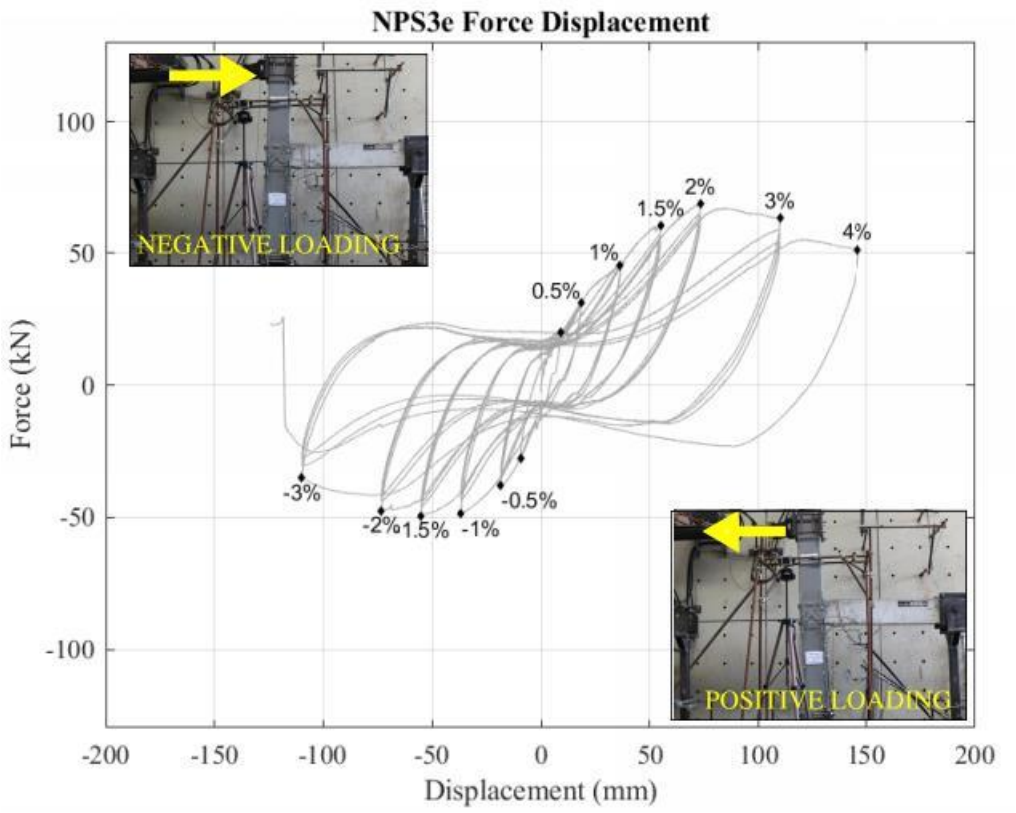

Figure 5.48: Force-Displacement Response of Specimen NPS3e

> The damage to the specimen progressed quickly and it was so severe that testing was stopped at a drift level of 4%. Post-yielding, the specimen response exhibited significant pinching and progressive degradation of lateral stiffness. A secant stiffness loss of about 19% occurred between loading cycles 1 and 3, at 3% drift level. Non-trivial strength reduction was also observed. The positive residual strength at 4% drift ratio (cycle 1) was 73 kN, which corresponds to about 48% of peak (no loading cycles at 5% drift were completed).

> The behavior of the specimen was qualitatively like that of NPS3i. Throughout the test, damage occurred almost exclusively in the beam (particularly in the designated plastic hinge region), with all other structural components (i.e., joint region and columns) virtually undamaged.

> Flexural cracks in the beam formed early, and cracking became progressively more extensive in the beam region designed to form a flexural plastic hinge mechanism (see Figure 5.49). Buckling of the bottom chord of the beam truss occurred during the 1.5% loading cycle.

> The beam reached full flexural yielding at 3% drift, while flexural failure occurred at 4% drift, with the complete opening of a major vertical crack in the beam, at the cross section where the continuity bars were anchored mechanically (see Figure 5.49).

> The failure mechanism was again classified as BY-A. It should be noted that the same behavior issues identified for specimen NPS3i affected specimen NPS3e. Those need to be addressed before the continuity solution presented herein can be adopted for future use.

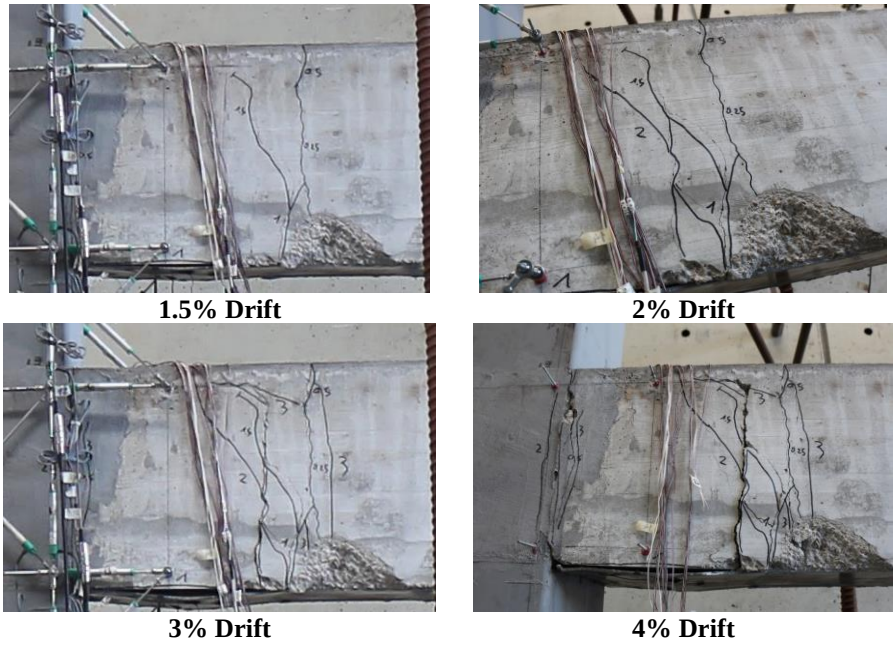

1.5% Drift **2% Drift**

3% Drift **4% Drift**

Figure 5.49: NPS3e - Beam-end Region Damage Propagation

> The subcomponents of drift of the NPS3e specimen can be seen in Figure 5.50[10]. Contrarily to the internal specimen, the column flexure did not contribute more than 20% at any point; nearly all the drift was

[10]Only percentages higher than 10% are shown; the "uncounted" portion is assumed to be attributed to the beam flexure plus negligible shear in the beams and columns. All contributions are taken from the first cycle of the pertinent drift loading ratio. 3% data for this specimen was unusable.

comprised of beam action from the beginning. The beam's contribution to drift remained at or above 79% for the entirety of the test. It should be noted that 3% data was corrupted and unable to be used.

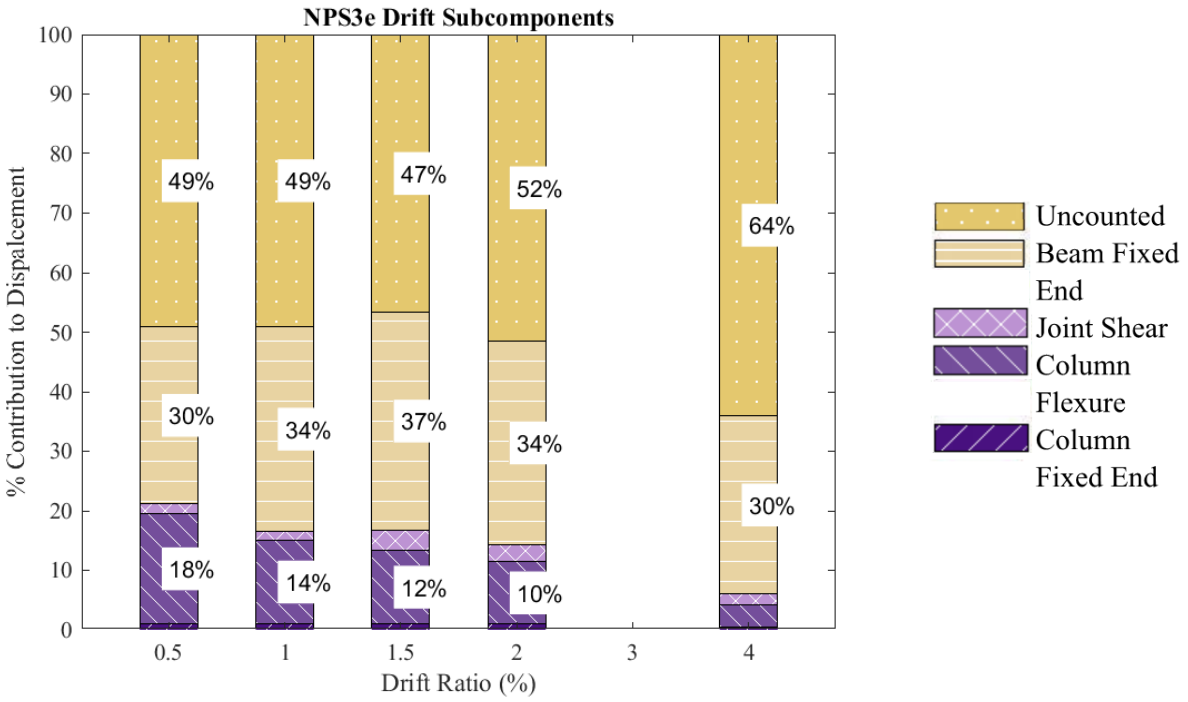

Figure 5.50: NPS3e Drift Subcomponents

5.3.3 HD Experimental Analysis

> This section will provide a brief discussion on the performance of the HD specimens, however since this was an exploratory investigation into the ability to create a highly ductile system by way of relocated flexural plastic beam hinges, future study should be done to draw more complete conclusions.

> Peak and residual strength results obtained from the HD Test Series are summarized in Table 5.4. Note that NPS3e did not complete any cycles at the 5% drift ratio.

Table 5.4: Summary of Test Results - HD Test Series

Specimen ID	F_{peak}^{+} F_{peak}^{-} [kN]	$F_{5\%}^{+}$ $F_{5\%}^{-}$ [kN]	F_n^{+} F_n^{-} [kN]	$F_{5\%}^{+}/F_{peak}^{+}$ $F_{5\%}^{-}/F_{peak}^{-}$	F_{peak}^{+}/F_n^{+} F_{peak}^{-}/F_n^{-}	Failure mode
NPS3i	152.2	91.4	156.0	0.60	0.99	BY-A
	-150.6	-94.2	-152.0	0.63	0.97	
NPS3e	68.7	NA	78	NA	0.89	BY-A
	-49.4	NA	-76	NA	0.62	

> NPS3 did not reach its nominal capacity, particularly in the external specimen, due to reduced bond strength between the plain steel conitnuity elemnt and the bottom plate buckling. Both internal and external specimens exhibited plate buckling and full yielding during the same cycles. The pate buckled duirng the 1.5% cycle, however overall yielding of the specimens was observed during the 3% load ratio.

> Severe pinching was exhibited during the loading protocol, resulting in a negative residual stiffness values. See CHAPTER 4 for technical details of the stiffness calculation. The pinching is indictivie of the smooth bars, as well as the increased bar diameter. These elements resulted in a poor bond connection between the steel rebar and the surrouning concrete. The bars "slip" out of their lanes and the requisite distance required to push them through this slipped distance extends the displacement of the specimen without providing resistance so the force stays constant. Once the bar has been pushed thorugh this slipped distance, the bar enters its bonded region and is able to provide resistance. This is seen in the graph near zero displacement where the loop pinches and the stiffness approaches zero.

> The overall HD specimen response is summarized in Table 5.5.

Table 5.5: HD Performance Assessment Results

Specimen	Failure Mode	Performance evaluation, first cycle at 3% drift				Performance Evaluation, first cycle at 4% drift				Δ_y^{+} Δ_y^{-} (mm)	μ^{+} μ^{+-}
		P_0/P_{peak}	K_0/K_i	E_n	$\bar{E}$	P_0/P_{peak}	K_0/K_i	E_n	$\bar{E}$		
NPS3i	BY	1	0.14	0.16	0.39	0.82	0.03	0.17	0.36	54.3 -48.7	2.31 2.69
NPS3e	BY-A	0.86	.01	0.31	0.64	0.75	0**	NA	NA	38.8 -23.0	2.97 3.18

****Bounded by zero.**

> The stiffness degradation is severe for the NPS3 specimens due to the pinching phenomenon noted earlier. The strength degradation in the external specimen is 25% between the 3% and 4% drift loadings.

> A summary of the main conclusions for these specimens per the results obtained in this experimental program are noted below.

> HD Test Series

- Plastic hinge relocation is possible and can be achieved through proper reinforcement detailing.
- Plastic hinge relocation can be effective at protecting the joint core from severe damage.
- While the specimens were able to achieve near peak strength and formed a plastic hinge thereby failing in flexure at the design-intended location, there are several conceptual issues that need to be addressed before the continuity solution adopted in this program can be adopted. This is beyond the scope of this project and will not be discussed further.

5.4 EXPERIMENTAL RESULTS SUMMARY

> Summaries, separated by MDI, MDE, and HD specimens are noted below.

MDI Test Series:

- All specimens tested reached nominal strength and, in all cases, flexural yielding occurred at the beam-column interface.
- All NPS® specimens exhibited a level of ductility that is consistent with that of a traditional moderately ductile RC beam-column joint.
- All specimens exhibited a markedly pinched response, mostly attributable to bond-slip issues affecting the beam longitudinal bars.
- Except for specimen NPS4i, all specimens experienced a joint shear failure following beam yielding at the beam-column interface.
- Specimen NPS4i experienced a beam yielding failure at the beam-column interface, with the joint region fully undamaged. The performance of NPS4i indicates that higher protection of the joint region may provide benefits in terms of overall system ductility. However, the response was still affected by severe pinching.
- Adding shear stirrups in the beam end region does not seem to provide any benefit in capacity designed NPS® beam-column joints.

MDE Test Series:

- Specimen REFe suffered premature out-of-pane failure caused by the experimental setup. This issue was addressed by adding a bracing system, but data pertaining to the reference specimen is limited.
- All specimens tested reached nominal strength and, in all cases, flexural yielding occurred at the beam-column interface.
- All specimens experienced a beam yielding failure, with the joint region remaining virtually undamaged or only lightly cracked.

- Specimens NPS2Ae and NPS4e showed good ductility, minimal pinching, and high energy dissipation capacity.
- Specimen NPS1e exhibited significant bond-slip deterioration at the beam-column interface, resulting in a ductile yet markedly pinched response. This affects the energy dissipation capacity of the system in a negative way.

HD Test Series:

- Plastic hinge relocation can be achieved through proper reinforcement detailing and can be effective at protecting under-reinforced joint cores from severe damage.
- While the specimens tested reached the desired strength, formed a plastic hinge, and failed in flexure at the intended location, there are several conceptual issues that need to be addressed before the solution tested in this program can be adopted. This is beyond the scope of this project and will not be discussed further but may be addressed as part of future research if the solution is of interest.

CHAPTER 6 EXPERIMENTAL ANALYSIS

> This chapter focuses on assessing the effects of the variables studied, and on assessing the seismic performance of the specimens tested in a more general sense. This chapter is separated into two main sub-sections (for internal and external specimens separately) organized as follows:

- Performance of the NPS® System regarding the variables of interested considered:
    - The influence of the moment continuity solution adopted
    - The influence of joint core shear reinforcement and confinement
    - The influence of additional stirrups in the beam end regions
- Performance of the NPS® System regarding typically accepted criteria informing the performance under earthquake loading, namely:
    - Strength degradation
    - Stiffness degradation
    - Energy Dissipation
    - Ductility
    - Characteristics of the hysteretic response
    - Visual damage and other damage progression

> At the end of this chapter all specimens are classified in the context of the "ACI Moment Criteria Acceptance for Moment Resisting Frames" [45], which is the only guideline found in the literature for achieving an acceptable system for use in seismic regions. The performance of the NPS® systems is further evaluated through a direct performance comparison to the reference, or traditional, RC beam-column joint systems.

> Finally, there is a short discussion on the results of the HD specimens. However, it is not appropriate to draw conclusions against the other specimens within the program because they were not designed to the same level of ductility, and therefore their performance behavior is not expected to be the same.

6.1 MDI (INTERNAL) EFFECTS OF STUDIED DESIGN VARIABLES

> Peak and residual strength results obtained from the MDI Test Series are summarized in Table 6.1. Specimens NPS2Ai, NPS2Bi and NPS4i displayed similar strengths (peak loads within 4% of one another) which were, on average, 17% stronger than the reference specimen, REFi, the traditionally reinforced concrete specimen. In contrast, NPS1i reached a peak load of 176 kN, which corresponds to 90% of the peak load recorded for REFi.

> These strengths are reflective of the nominal strengths of the respective systems. All specimens were designed for identical seismic demand, and careful consideration was given during the design phase to ensure that all systems had similar capacities. However, inherent differences in the structural solutions adopted (particularly pertaining to the moment continuity elements across the joints) and, to a lesser extent, in variation in the material properties, inevitably led to specimens characterized by unequal ability to resist lateral loads (somewhat significant in some cases, e.g. NPS4i was 35% stronger than NPS1i).

> Specimen peak strength should not be taken as a measure of performance in an absolute sense, since the nominal strengths designed were similar, but not exactly equivalent. However, it holds as an important parameter that has nontrivial response implications and must be considered in the context of performance evaluations. For instance, a stronger beam-column connection - all other parameters being equal -induces higher demand on the panel joint region, potentially causing more severe damage. However, when all other parameters are not equal, i.e. the continuity connection utilizes fewer large diameter bars instead of more small diameter bars, the system could be more prone to bond-slip deterioration phenomena. In such cases, a stronger beam-column assembly may exhibit overall poorer performance than a weaker companion.

> Table 6.1 also lists residual strengths, taken as the peak loads recorded on the positive and negative side, during the first loading cycle at 5% drift. Values ranging from 55% (NPS1i) to 83% (NPS4i) of peak strengths can be observed. Specimens REFi, NPS2Ai and NPS2Bi show similar levels of residual capacity, around 70% of peak on average.

> It is interesting to note that the strength of all specimens is predicted accurately using the Eurocode approach, with average test-to-predicted strength ratio of 0.99 and COV of only 2.3%. System strength predictions were based on the estimated flexural strength of the beams, assuming elasto-plastic steel response and without considering second order effects.

Table 6.1: Summary of Test Results – MDI Test Series

Specimen ID	F_{peak}^+ F_{peak}^- [kN]	$F_{5\%}^+$ $F_{5\%}^-$ [kN]	F_n^+ F_n^- [kN]	$F_{5\%}^+/F_{peak}^+$ $F_{5\%}^-/F_{peak}^-$	F_{peak}^+/F_n^+ F_{peak}^-/F_n^-	Failure mode
REFi	195.0	133.0	199.0	0.68	0.98	BJ
	-191.5	-141.0	-199.0	0.74	0.96	
NPS1i	176.1	104.4	172.0	0.59	1.02	BJ
	-166.2	-91.5	-165.9	0.55	1.00	
NPS2Ai	230.8	167.9	236.5	0.73	0.98	BJ
	-219.7	-147.6	-231.0	0.67	0.95	
NPS2Bi	239.6	173.4	236.5	0.72	1.01	BJ
	-226.5	-159.6	-231.0	0.70	0.98	
NPS4i	238.8	198.7	236.5	0.83	1.01	BY(a)
	-234.3	-192.5	-231.0	0.82	1.01	
				Mean	0.99	
				COV [%]	2.3	

> The backbone force-displacement response of all MDI specimens is shown in Figure 6.1: MDI Backbone Force-Displacement . While this representation omits information pertaining to loading-reloading, cyclic stiffness degradation etc., it provides a concise summary of the experimental data collected.

> Notable observations that can be made based the displayed data include the following:

- The NPS® beam-column joints exhibit higher cracked stiffness than the RC specimen (REFi)
- Except for NPS1i (which manifests signs of yielding around 1.2%-1.3% drift), all specimens reach flexural yielding at drift ratios between 1.5% and 2%
- NPS1i peaks at a load of 176 kN, which is about 90% of the resistance displayed by specimen REFi, while NPS2Ai, NPS2Bi and NPS4i reach 231 kN, 240 kN and 239 kN, respectively (20% higher than REFi, on average)

- NPS4i shows a superior ability to sustain loads at large displacements, while all other specimens show similar extents of strength degradation
- The enveloped response of specimens NPS2Ai and NPS2Bi is virtually identical

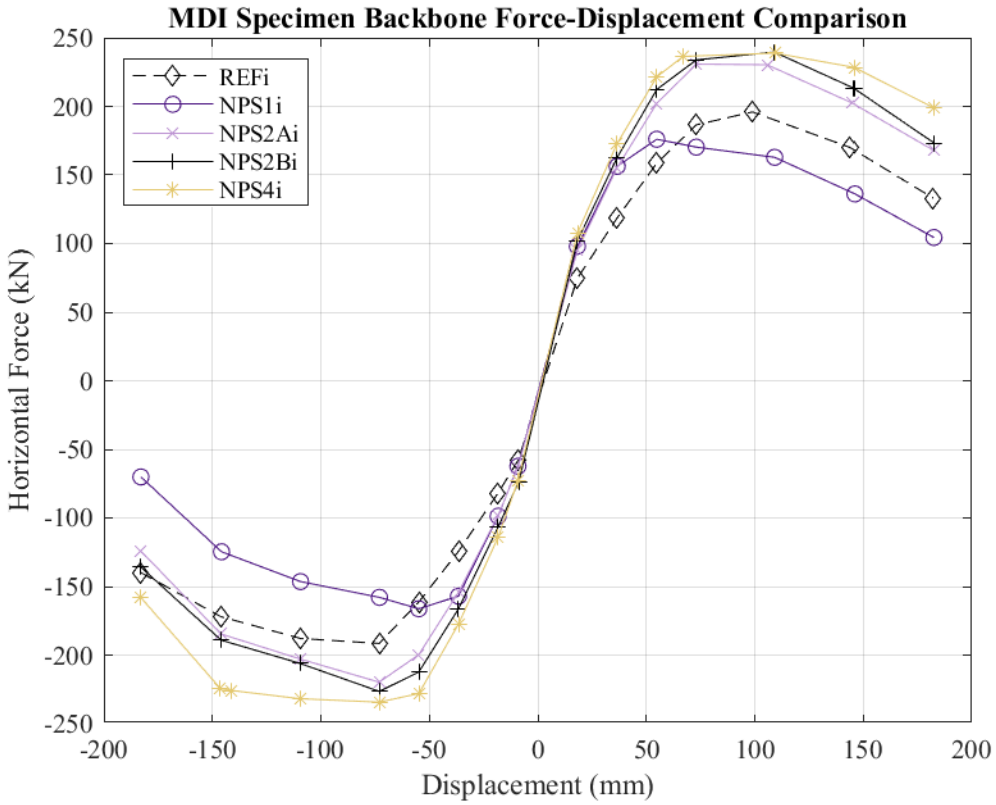

Figure 6.1: MDI Backbone Force-Displacement Comparison

> For ease of comparison, the subcomponents of the MDI specimens at critical drift ratios are shown in Figure 6.2 (note that NPS4i 4% data was corrupted and unable to be used).

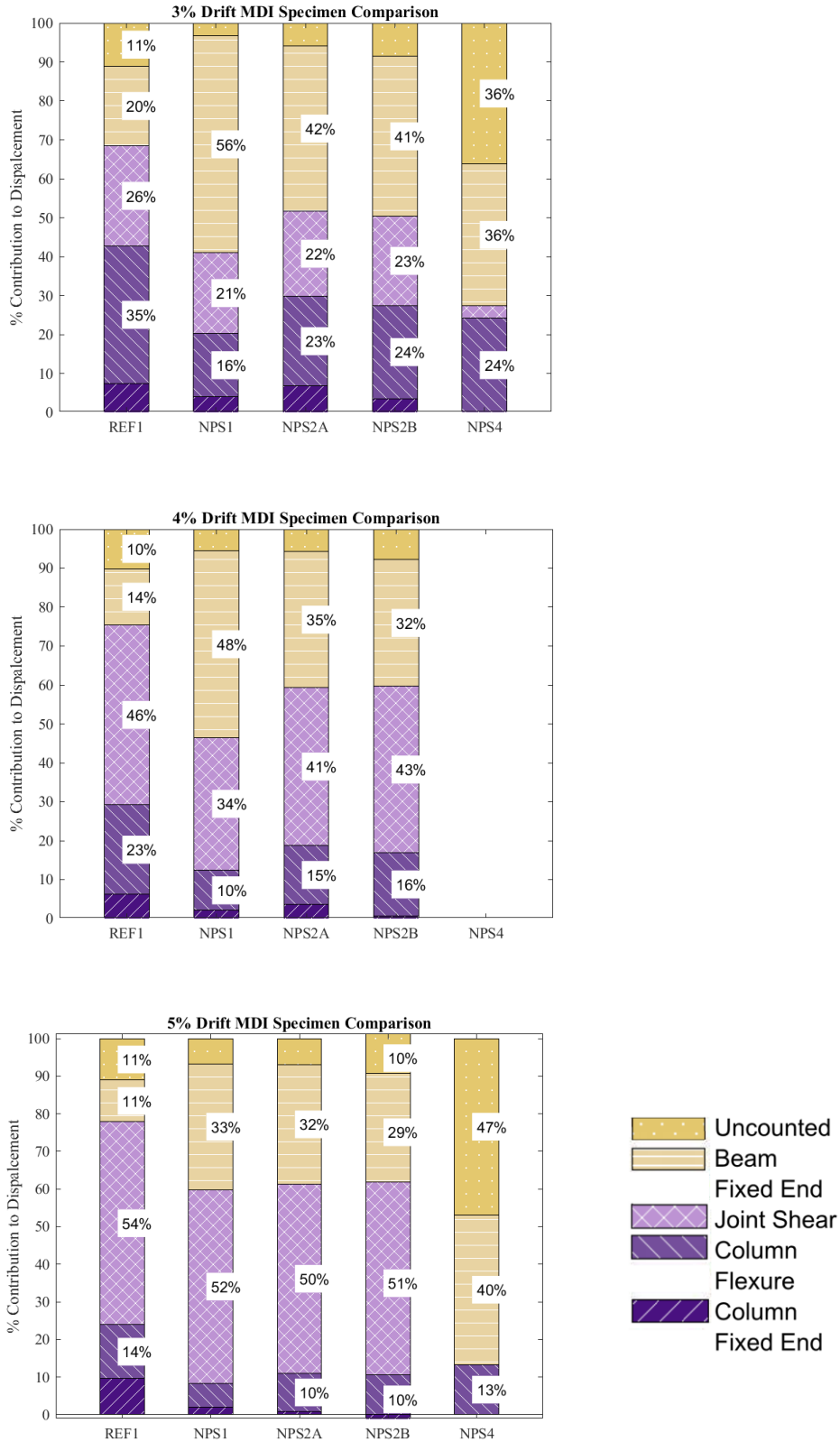

Figure 6.2: MDI Drift Subcomponent Comparison

Figure 6.3 compares the final damage state of the joint region of the five MDI specimens tested. Note that REFi was subject to one full cycle at 5%, while all other specimens completed three cycles at that drift level. Specimens REFi, NPS1i, NPS2Ai, and NPS2Bi exhibited the same failure mode that involved beam continuity reinforcement yielding followed by progressive joint deterioration. Similar extent of damage can be observed for the four joints that include extensive diagonal cracking, concrete spalling, and fully exposed reinforcing bars. The joint region of specimen NPS4i benefitted from higher protection thanks to the intact steel HSS surrounding part of the joint core. This resulted in a different failure mode of the system that involved flexural beam yielding, with the formation of a major vertical crack at the beam-column interface and evidence of local crushing.

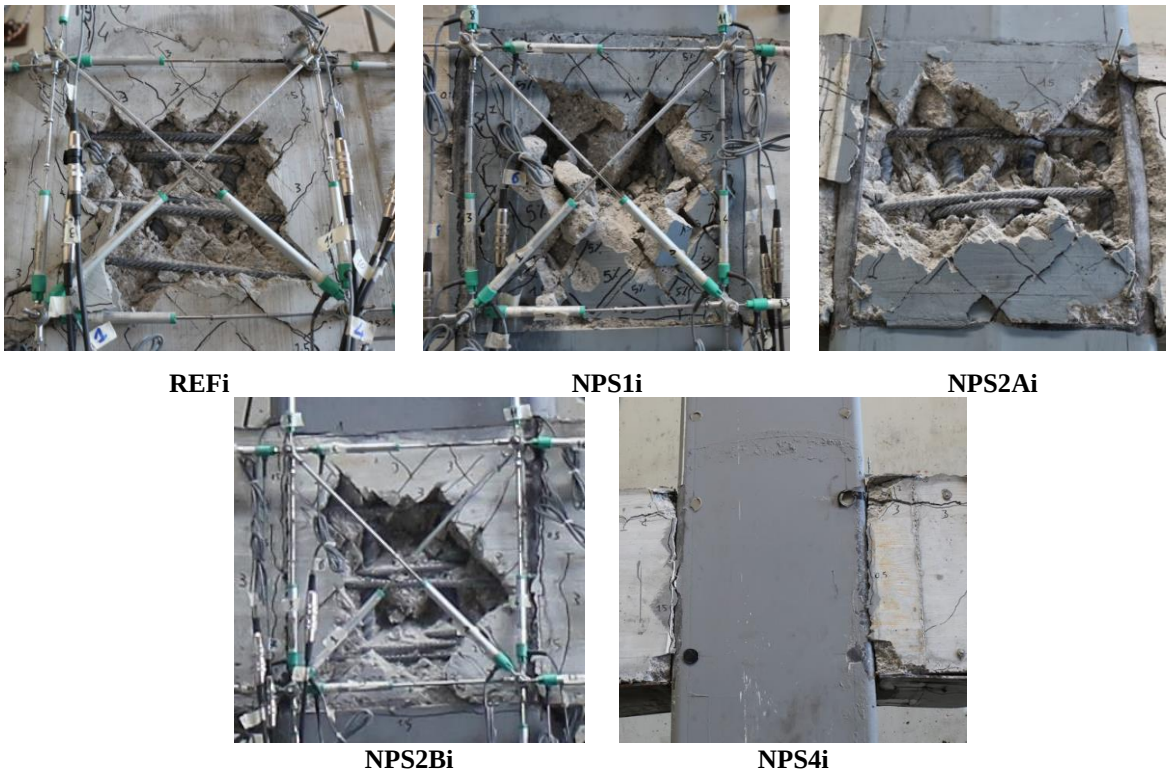

REFi **NPS1i** **NPS2Ai**

NPS2Bi **NPS4i**

Figure 6.3: View of Joint Region of MDI Specimens at Failure

6.1.1 NPSi - Effect of Different Continuity Solutions

In this experimental program the moment continuity solutions adopted were either traditional deformed steel bars or a truss structure made of plain steel, like the NPS® beam system. This section describes the influence of these variables on the NPS® performance, through the inspection of the NPS1i specimen and

the NPS2Bi specimen. These specimens were nominally identical, except for the different continuity solutions proposed. These two systems were nominally identical, including additional shear steel in the beam end region, but NPS1i had plain steel continuity trusses crossing the joint to provide moment continuity, while NPS2Bi had straight deformed continuity bars. For more information on the specimen setups or individual specimen results, see CHAPTER 3 and CHAPTER 4 .

> The force-displacement response of both specimens is shown in Figure 6.4. Both sustained the full loading protocol, including three loading cycles at 5% drift. Both systems also reached flexural beam yielding as per design objective, developing their full nominal strength. As briefly discussed earlier, while the two specimens were designed for the same seismic demand, by the time the design was complete, their nominal strengths differed by about 35%. Thus, NPS1i displayed an experimental peak strength of 176 kN, while NPS2Bi reached a peak load of 240 kN. Evidently, this outcome alone does not provide meaningful insight into the performance of the system. The peak loads were experienced in the positive loading direction; however the residual strength is noted as the average between the positive and negative loading directions strength degradations.

> It is important to note that NPS2Bi showed a superior ability to sustain the applied peak as the displacement demand increased. That is to say that at drift ratios of 3%, 4% and 5% respectively, NPS2Bi exhibited a residual strength ratio (defined as the ratio between the $P_{max,i}/P_{peak}$ and the maximum resistance in the same loading direction, see Chapter 4) of 100%, 89%, and 72%. At the same drift levels, NPS1i had a residual strength ratios of 93%, 77%, and 59%, respectively.

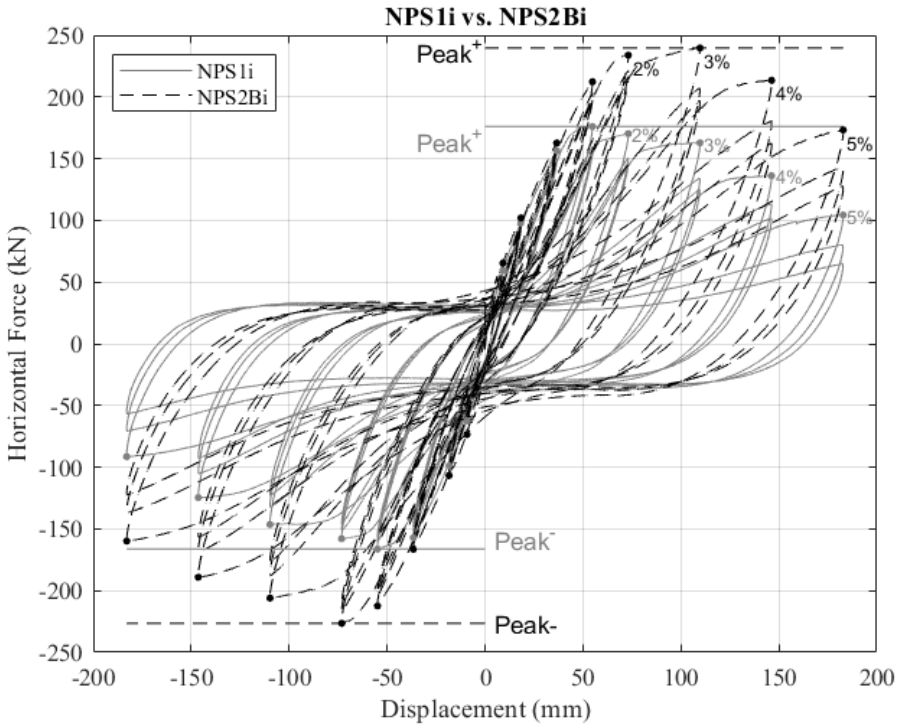

Figure 6.4: Force-Displacement Response of Specimens NPS1i and NPS2Bi

> It can be seen in Figure 6.4 that the two systems exhibited a similar "pre-yielding" behavior. For example, initial stiffness values of 4.8 kN/mm and 6.0 kN/mm were computed for NPS1i and NPS2Bi, respectively. These stiffness estimates were obtained with techniques described in CHAPTER 5 .

> Beam yielding was detected between 1.0% and 1.5% for NPS1i and between 1.5% and 2.0% for NPS2Bi. The higher yield drift characterizing specimen NPS2Bi is consistent with the yield strain properties of the continuity elements ($\varepsilon_{y,truss} = 1.85 \times 10^{-3}$ and $\varepsilon_{y,bar} = 2.6 \times 10^{-3}$) The ductility of these specimens was 3.3 and 2.7 for NPS1i and NPS2Bi respectively, in the positive direction.

> However, the data outlined in Figure 6.4 shows that, after beam yielding occurred, both specimens suffered progressive loss of lateral stiffness, which can be seen as the K_0 residual secant stiffness (see CHAPTER 4 for a detailed discussion on calculation). NPS2Bi showed superior performance in that it experienced lower extents of stiffness degradation. For instance, at drift ratios of 3%, and 4%, NPS2Bi experienced stiffness losses of about 55% and 48%, between loading cycles 1 and 3 ($K_{0,3\%\ Cycle3}/K_{0,3\%\ Cycle1}$

and $K_{0,4\%\ Cycle3}/K_{0,4\%\ Cycle1}$) of each respective drift ratio. Considering the same drift range and same cycle comparisons, stiffness losses of 77% and 67% per drift ratio were computed for NPS1i.

> It is clear visually in Figure 6.4 that NPS1i experienced more stiffness degradation than NPS2Bi, which resulted in lower calculated residual stiffness values. This phenomenon in the force displacement response is known as “pinching. Pinching is the progressive reduction of the re-loading stiffness, which causes reduction of the area under the hysteretic curve) in the force displacement response. It can be seen in Figure 6.4 that while both specimens exhibited non-trivially pinched response, specimen NPS1i was affected somewhat more severely.

> The two specimens discussed in this section suffered a joint failure following beam yielding. The damage sequence observed during the tests involved some minor beam cracking followed by severe joint deterioration. While the same failure mode was observed for both specimens, joint deterioration appeared to progress more rapidly and to be more severe for NPS1i. This is of particular concern, because the joint region of specimen NPS1i was subjected to significantly lower demand, which was a result of the beam cross section being 35% weaker than for NPS2Bi. This suggests that the joint core reinforcement configuration for a system with continuity provided by added trusses (i.e., placement of traditional shear reinforcement is not possible) may represent a criticality of this type of solution. It is evident that joint shear reinforcement, present in the core of specimen NPS2Bi, played a positive role, and allowed the system to absorb a significantly higher demand.

> Figure 6.5 provides a view of one of the beams and the joint panel zone at failure (i.e., 5% drift ratio) for both specimens tested. In both cases, the beam exhibits minor cracking, while the joint region is severely damaged having experienced extensive diagonal cracking, yielding (of the truss diagonals or of the shear reinforcement) and concrete spalling/crushing throughout the tests.

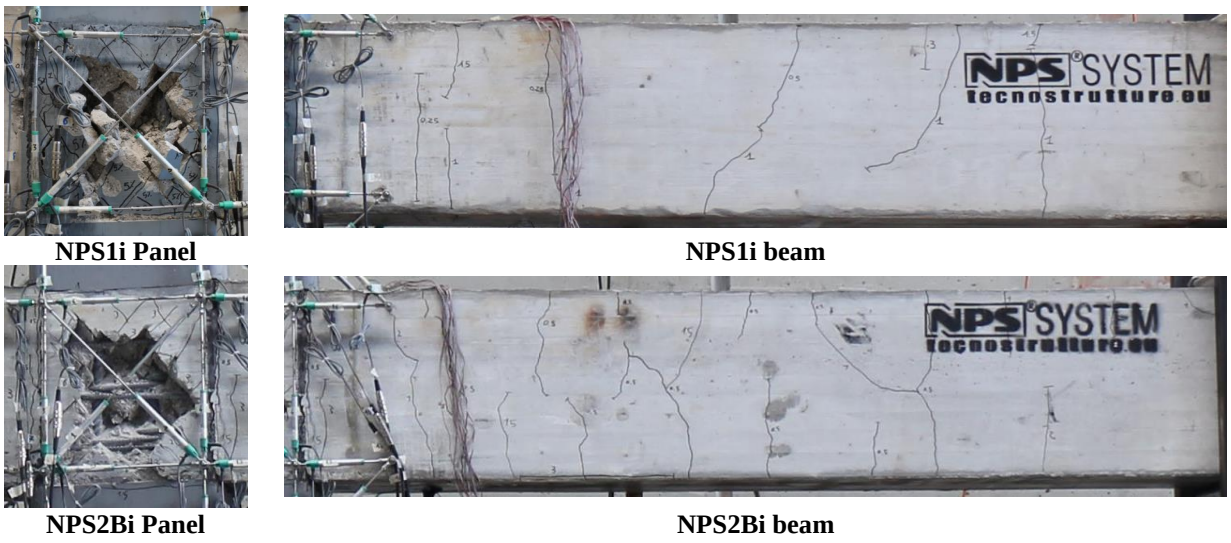

NPS1i Panel **NPS1i beam**

NPS2Bi Panel **NPS2Bi beam**

Figure 6.5: View of Beam and Joint Region of Specimens NPS1i and NPS2Bi at Failure

6.1.2 NPSi - Influence of Joint Shear Reinforcement and Confinement

> Another investigation in this experimental program was the potential effects of confinement from the column HSS on the integrity of the joint region, while reducing the amount of shear reinforcement within the joint core. To study these aspects, the response of specimens NPS2Ai and NPS4i is analyzed. These two systems were nominally identical, except for the joint core conditions. For one, the HSS column of NPS4i was kept "continuous" on the two sides of the joint not connected to beams, and secondly the internal shear reinforcement was reduced to 4-leg stirrups spaced at 150 mm. For NPS2Ai, "windows" were cut out in the HSS on the two sides of the joint with no connected beams and the joint core was reinforced with 4-leg stirrups spaced at 100 mm, like the other NPS® specimens (where applicable).

> The force-displacement response of the two specimens is shown in Figure 6.6. Both sustained the full loading protocol, including three loading cycles at 5% drift. Both systems also reached flexural beam yielding as per design objective, developing their full nominal strength. Specimen NPS2Ai reached a peak load of 231 kN, while NPS4i was 3% stronger, showing a maximum resistance of 240 kN. These were both reached during positive loading. Similar trends were exhibited in the negative loading direction, so the overall strength degradation reported is an average of the positive and negative loading directions.

> It can be seen in Figure 6.6 that the two systems exhibited qualitatively similar behavior. The specimens exhibited similar abilities to maintain loads during multiple cycles of the same drift load (i.e., $P_{max,Drift\% Cycle3}/P_{max, Drift\% Cycle1}$). For NPS4i the strength maintained per drift cycle for 3%, 4%, and 5% loading was 84%, 81%, and 73%, respectively. For the same drift ratios, NPS2Ai retained strength of 80%, 79%, and 74%. However, NPS4i exhibited a slightly superior ability to maintain peak strength over multiple drift ratios. For instance, the residual strength relative to the peak strength ($P_{max,Drift\% Cycle1}/P_{peak}$) of NPS4i between the 3%, 4%, and 5% loading cycles was 100%, 96%, and 83%. In contrast, NPS2Ai sustained 100%, 88%, and 73% under the same criteria.

> NPS4i also displayed a more severely pinched response, to the point that the re-loading stiffness (K_0) assumed negative values, at times. The performance seen in Figure 6.6 shows that, after beam yielding occurred, both specimens suffered progressive loss of lateral stiffness. The 3% and 4% drift loads, between

the third and first cycles ($K_{0,\ 3\%\ Cycle3}$/ $K_{0,\ 3\%\ Cycle1}$), saw a stiffness degradation of -5% and 61% for NPS4i and 40% and 53% for NPS2Ai. NPS4i has a deceptively large stiffness retention in the 4% drift, because the first cycle of this drift is merely 0.29 kN/mm, while the third cycle is even less at 0.18 kN/mm. these numbers in are around 60% smaller than NPS2Ai's residual stiffness (i.e., 4% Cycle 1: 0.52 kN/mm, 4% Cycle 3: 0.28 kN/mm) for the same drift and cycle in the testing procedure. This supports the evidence that severe pinching is occurring in NPS4i.

> The ductility of the systems was calculated as 2.62 and 3.42 for NPS2Ai and NPS4i in the positive loading direction; it was calculated as 2.60 and 3.33 in the negative loading directions.

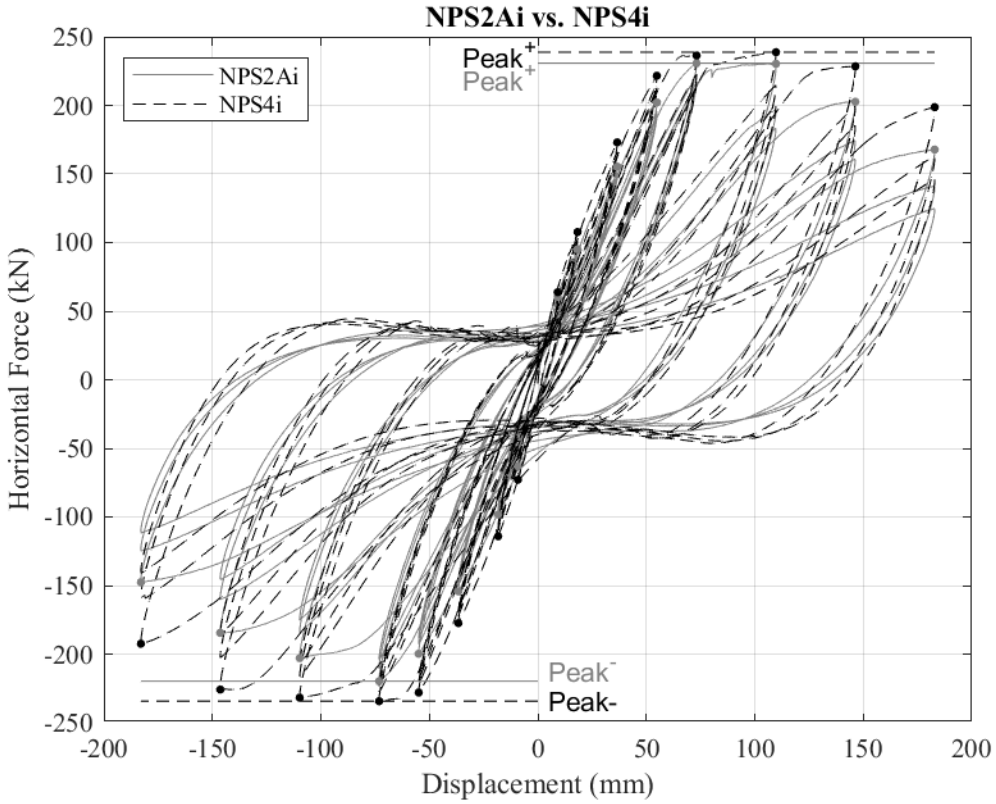

Figure 6.6: Force-Displacement Response of Specimens NPS2Ai and NPS4i

> Despite the overall similar force-displacement response shown in Figure 6.6, specimens NPS2Ai and NPS4i experienced substantially different type and extent of damage. NPS2Ai suffered a joint failure following flexural yielding at the beam column interface. Damage extended into the joint region, which

suffered severe deterioration, in the form of extensive diagonal cracking, stirrup yielding and concrete spalling/crushing.

> In contrast, the joint region of NPS4i was entirely undamaged, effectively protected by the intact column HSS. No joint cracking, stirrup yielding, or any other sign of distress was detected after cutting out the HSS at the end of the experiment. The failure of specimen NPS4i was classified as beam yielding accompanied by nontrivial bond-slip deterioration of the continuity bars around the beam-column interface region (identified as the main source of the severe pinching effects observed in the force-displacement response). Evidence of flexure-induced concrete crushing and buckling of the beam bottom chord was also detected. This is typical of interior beam-column joint systems with large bond demands and adequately protected joint region. Figure 6.7 provides a view of one of the beams and the joint panel zone at failure (i.e., 5% drift ratio) for both specimens tested.

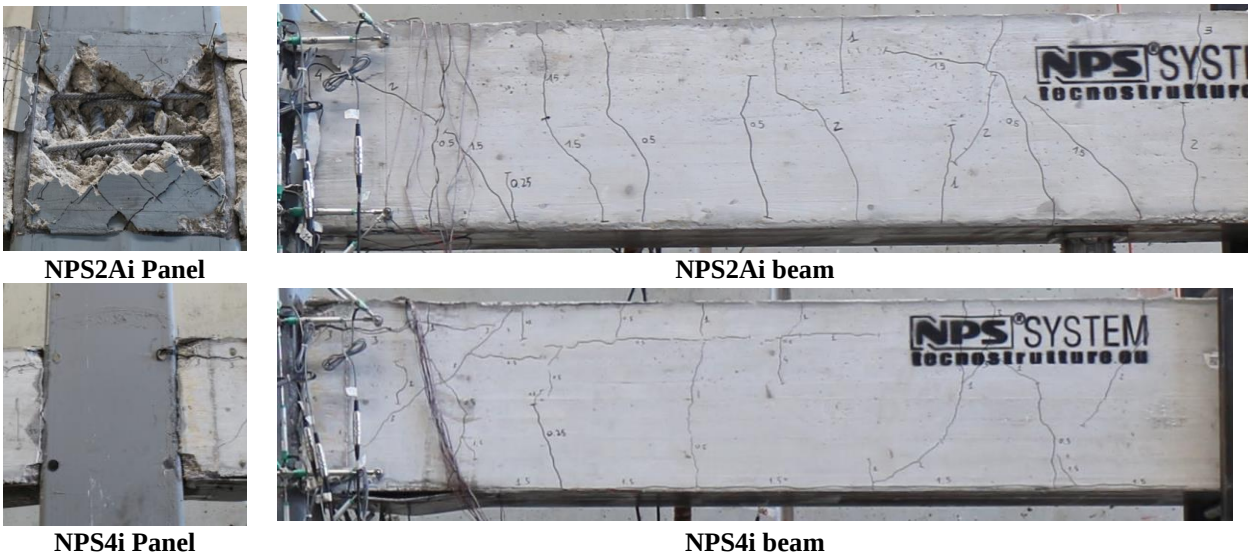

Figure 6.7: View of Beam and Joint Region of Specimens NPS2Ai and NPS4i at Failure

> Despite the impressive protection of the joint region, the overall response was not much different from NPS2Ai. In fact, while the ductility of NPS4i higher than NPS2Ai, the stiffness degradation and effects of bond slippage (observed via pinching) was more evident. This could potentially lead to an undesirable

failure mechanism in larger drifts, despite the higher ductility. Therefore, it is important to consider the responses wholistically and not rely on one parameter to be the sole judge of capacity for the specimen.

6.1.3 NPSi - Influence of Additional Beam Stirrups

> The presence/absence of added shear reinforcement in the beam-end regions represents the third variable of interest in this experimental program. To study the effects that added stirrups have on the NPS® system performance, the response of specimens NPS2Ai and NPS2Bi was analyzed. These two systems were nominally identical, except for the shear reinforcement configuration of the beam ends. NPS2Ai did not have any added stirrups, while NPS2Bi had 2 leg-14 mm diameter stirrups spaced at 100 mm at the beam ends, spanning a length of 650 mm in total.

> The force-displacement response of the two specimens is shown in Figure 6.8. Both sustained the full loading protocol, including three loading cycles at 5% drift. Both systems also reached flexural beam yielding as per design objective, developing their full nominal strength. They displayed nearly identical strength. NPS2Ai reached a peak load of 231 kN, while NPS2Bi was 3% stronger, showing a maximum strength of 240 kN.

> Virtually identical performance was also observed in terms of residual strength. For instance, at drift ratios or 3%, 4%, and 5% NPS2Bi exhibited a residual strength ratio (RSR) of 100%, 89% and 72%. At the same drift levels, NPS2Ai had a RSR of 100%, 88%, and 73% respectively.

> It can be seen in Figure 6.8 that the two systems exhibited extremely similar behavior, including essentially equal extents of pinching. Beam yielding was detected between 1.5% and 2.0% drift for both specimens. The ductility of the systems, as defined in CHAPTER 4 , are 2.71 and 2.62 for NPS2Bi and NPS2Ai respectively in the positive direction, and 2.74 and 2.60 in the negative loading direction.

> The data shown in Figure 6.8 shows that, after beam yielding occurred, both specimens suffered progressive loss of lateral stiffness. The specimens experienced nearly identical extents of stiffness degradation. For instance, at drift ratios of 3% and 4%, NPS2Bi experienced residual stiffness losses ($K_{0,3\%}$

$_{Cycle3}/K_{0,3\%\ Cycle1}$ and $K_{0,4\%\ Cycle3}/K_{0,4\%\ Cycle1}$) of 45% and 52%, between loading cycles 1 and 3. Considering the same range, stiffness losses of 40% and 53% were computed for NPS2Ai.

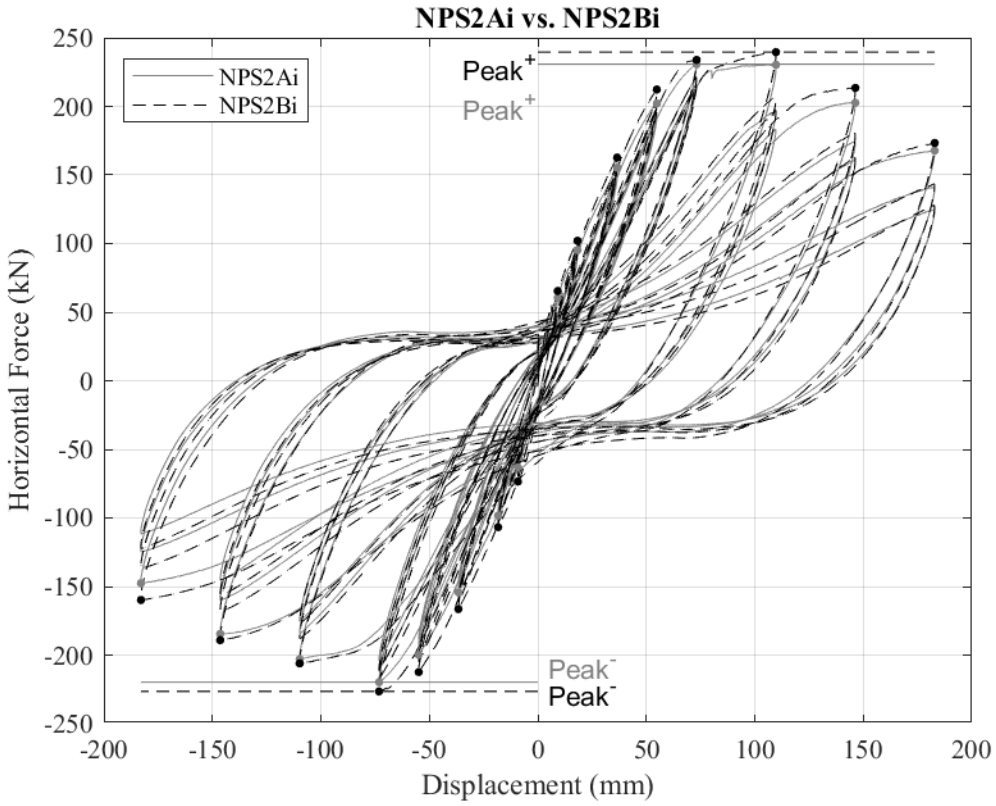

Figure 6.8: Force-Displacement Response of Specimens NPS2Ai and NPS2Bi

> Specimens NPS2Ai and NPS2Bi suffered a joint failure following flexural yielding at the beam column interface. The damage sequence observed during both tests involved some minor beam cracking followed by severe joint deterioration, with no notable response differences to report.

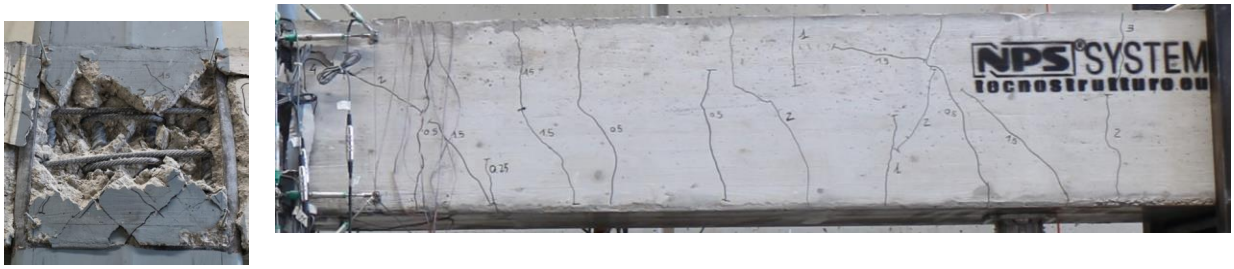

NPS2Ai Panel **NPS2Ai beam**

NPS2Bi Panel **NPS2Bi beam**

> Figure 6.9 provides a view of one of the beams and the joint panel zone at failure (i.e., 5% drift ratio) for both specimens tested. In both cases, the beam exhibits minor extent of cracking, while the joint region is severely damaged having experienced extensive diagonal cracking, yielding (of the truss diagonals or of the shear reinforcement) and concrete spalling, throughout the tests.

NPS2Ai Panel **NPS2Ai beam**

NPS2Bi Panel **NPS2Bi beam**

Figure 6.9: View of Beam and Joint Region of Specimens NPS2Ai and NPS2Bi at Failure

6.2 MDI RESPONSE CLASSIFICATION

> The outcome of the analysis described in the previous section is summarized in Table 6.2, for drift ratios of 3% and 4%. The performance results show good levels of compatibility between the different NPS® specimens and between the NPS® specimens and the reference RC specimens.

Table 6.2: MDI Performance Assessment Results

Specimen	Failure Mode	Performance evaluation, first cycle at 3% drift				Performance Evaluation, first cycle at 4% drift				Δ_y^+ Δ_y^- (mm)	μ^+ μ^{+-}
		P_0/P_{peak}	K_0/K_i	E_n	$\bar{E}$	P_0/P_{peak}	K_0/K_i	E_n	$\bar{E}$		
REFi	BJ	0.99	0.33	0.06	0.42	0.89	0.13	0.12	0.40	66.0 -61.5	2.23 2.55
NPS1i	BJ	0.90	0.13	0.19	0.42	0.76	0.03	0.20	0.40	38.6 -35.3	3.30 3.34
NPS2Ai	BJ	0.96	0.25	0.15	0.41	0.86	0.10	0.16	0.36	58.0 -54.4	2.62 2.60
NPS2Bi	BJ	0.95	0.21	0.15	0.40	0.86	0.10	0.16	0.37	57.1 -50.7	2.71 2.74
NPS4i	BY(a)	0.99	0.22	0.15	0.39	0.96	0.05	0.15	0.32	51.8 -48.1	3.42 3.33

6.2.1 MDI Stiffness and Strength Degradation

> The stiffness degradation is shown in Figure 6.10 for the first cycle of each subsequent drift as it relates to the initial stiffness (see CHAPTER 4 for details on calculation procedures). The stiffness degradation for the NPS1i specimen was swifter than the other MD specimens. The trend in Figure 6.10 appears to indicate the general stiffness degradation of the NPS® specimens occurred at a faster rate than the REFi specimen initially, but at higher drift ratios (i.e., greater than 4%) the reference specimen's stiffness degradation was faster than the NPSi specimens. Overall, the REFi specimen exhibited a less ductile response than the other specimens.

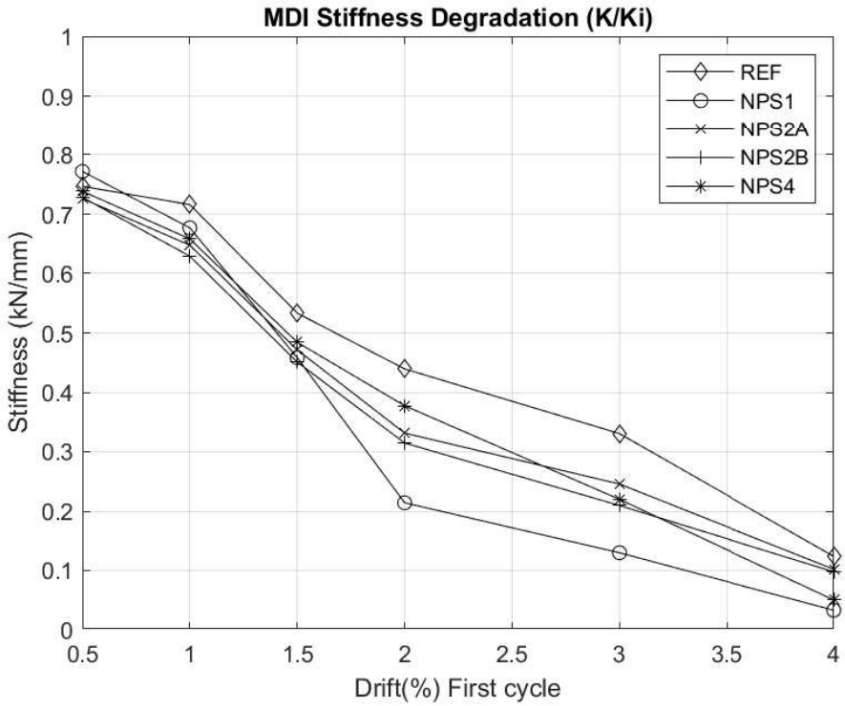

Figure 6.10: MDI Stiffness Degradation

The peak strength of the specimens was reached typically during the 3% loading cycle, after which or during the specimens yielded. The maximum peak strength reached during each cycle was normalized by the overall peak strength ($P_{max,i}/P_{peak}$) in the same loading direction (positive or negative), and the final reported result in Table 6.2 is the average of both respective directions of strength degradation. The strength degradation of NPS1i was the most pronounced, resulting in a peak strength ratio of 0.76 for the first cycle of the post yield drift ratio (4%), while NPS4i retained the most strength under that same condition with a ratio of 0.96. NPS2Ai, NPS2Bi, and the REFi maintained similar levels of post peak strength, with ratios of 0.86, 0.86, and 0.89, respectively.

6.2.2 MDI Energy Dissipation

The energy dissipation was calculated as the area within the hysteretic force-displacement loop, normalized by the perfectly elasto-plastic rhombus area for the corresponding cycle (See CHAPTER 4 , [45]). The energy dissipation tended to increase with each subsequent drift level, and the energy dissipated per the first cycle of each drift ratio is shown in Figure 6.11. NPS1i dissipated more energy with each cycle

than all other internal MD specimens. This is consistent with the above section on stiffness and strength degradation – as the NPS1i specimen broke down in strength and stiffness, the energy dissipation was greater as more of the specimen yielded to accommodate the cyclic loading. NPS2Ai and NPS2Bi follow a very similar trend and appear to be the second highest energy dissipating structures, followed by NPS4i, and finally REFi.

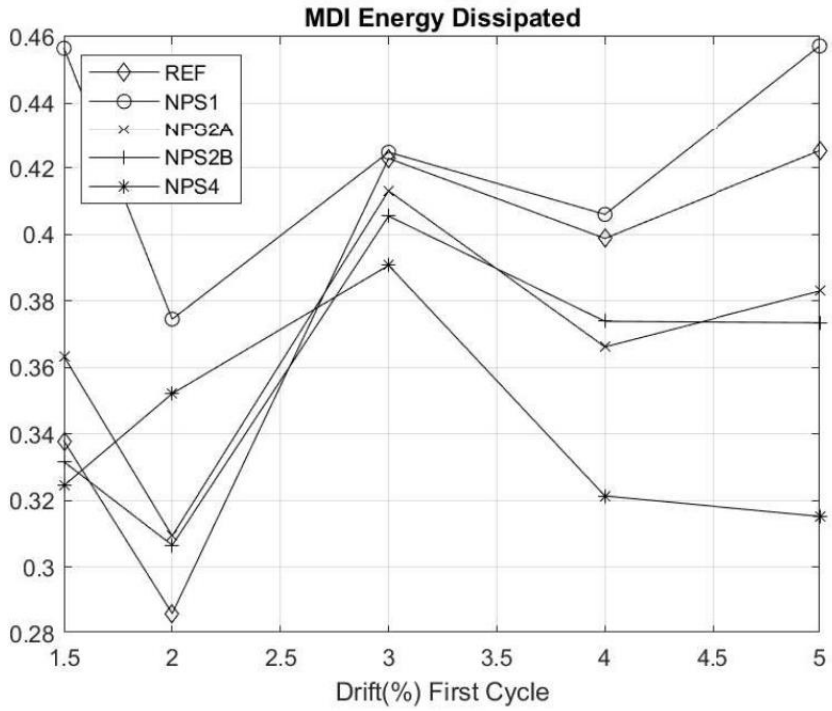

Figure 6.11: MDI Energy Dissipation

6.2.3 MDI Ductility

The specimens had ductility ratios ranging from 2.23 to 3.42. NPS1i and NPS4i were the most ductile specimens with approximate ductility of 3.30. These were also the two specimens with the worst bond-slip. REFi showed the lowest calculated ductility of 2.23, while NPS2Ai and its variation NPS2Bi were around 2.60. The variation in the positive and negative loading was small, generally less than 2% difference for the NPSi, and 12% difference for REFi. It is interesting to note that NPS1i specimen yielded at the smallest displacement within the MD specimen group, ergo the first one to yield.

6.2.4 MDI ACI Comparison

> A variety of procedures may be formulated that can be used to evaluate the performance of beam-column joints based on the hysteretic force-displacement response obtained experimentally. In general, multiple performance parameters need to be identified, computed, and checked against empirically established thresholds. The objective of these performance assessment methodologies is to ensure that the beam-column joint part of a moment resisting frame can sustain multiple earthquake-induced loadings cycles at large displacements, without suffering excessive strength and stiffness losses. They must also possess adequate ductility and energy dissipation capacity. With that in mind, the specimens in this experimental program were evaluated against specific acceptance criterion per the ACI code [42].

> For instance, the ACI acceptance criteria prescribes that the performance of a beam-column joint part of a special moment resisting frame (response factor R = 8.5) must be assessed as a function of the following three parameters: (i) the ratio between the peak force recorded during the third loading cycle at a selected limiting drift and the maximum strength of the system in the same loading direction; (ii) the residual secant stiffness, calculated between ±1/10 of the limiting drift ratio; and (iii) the ratio between the energy dissipated in the limiting drift cycle and the idealized elastoplastic energy of that drift ratio. These parameters are intended to provide insight into the system response with respect to strength degradation, stiffness deterioration and energy dissipation characteristics. See CHAPTER 4 for a graphic and further details. Specifically, the acceptance criteria can be summarized by:

- Strength degradation at the peak displacement of the limiting drift cycle shall not exceed 25% of the maximum load resistance in the same loading direction (note the values are averaged between the positive and negative loading strength ratios).
- Residual secant stiffness between ±1/10 of the limiting drift ratio shall not be less than 5% of the initial stiffness obtained from the first cycle.
- Energy dissipated in the limiting drift cycle shall not be less than 12.5% of the idealized elastoplastic energy of that drift ratio.

> In other words:

- $\frac{P_{peak}}{P_{max}} \geq 0.75$
- $\frac{K_o}{K_i} \geq 0.05$
- $\frac{E_D}{E_{PP}} \geq 0.125$

> The limiting drift ratio recommended in the ACI code is 3.5%. However, the loading protocol adopted in the experimental program did not include the specific loading cycle of 3.5%. Thus, two limiting drift levels were selected for which to perform the calculations, namely 3% and 4%. It should be noted that more recently, ACI 374.2R-13 [48] reported that a minimum of two cycles at each drift ratio is enough to consider the damage associated with the number of cycles at a given drift ratio. Evidently, if subjected to only two loading cycles per drift level, all specimens tested in this program would have achieved higher ratings.

> The results of the analysis are summarized in Table 6.3. At a limiting drift ratio of 3%, all specimens meet the ACI acceptance criteria. This is remarkable and provides further evidence that the NPS® beam-column joints tested achieved high performance, despite the large diameter bars adopted to provide moment continuity at the joint. Additionally, at a 4% limiting drift ratio all specimens, except for NPS1i meet the ACI acceptance criteria. All considered, the results are extremely positive and provide additional evidence in support of the NPS® beam-column joints.

Table 6.3: MDI ACI Acceptance Criteria

Specimen	Performance evaluation, first cycle at 3% drift			Performance Evaluation, first cycle at 4% drift			First Cycle 4% Acceptable per ACI Criteria?		
	P_0/P_{peak}	K_0/K_i	$\bar{E}$	P_0/P_{peak}	K_0/K_i	$\bar{E}$	$P_0/P_{peak}>0.75$	$K_0/K_i>0.05$	$\bar{E} > 0.125$
REFi	0.99	0.33	0.42	0.89	0.13	0.40	Yes	Yes	Yes
NPS1i	0.90	0.13	0.42	0.76	0.03	0.40	Yes	No	Yes
NPS2Ai	0.96	0.25	0.41	0.86	0.10	0.36	Yes	Yes	Yes
NPS2Bi	0.95	0.21	0.40	0.86	0.10	0.37	Yes	Yes	Yes
NPS4i	0.99	0.22	0.39	0.96	0.05	0.32	Yes	Yes	Yes

> To add a comment, there are inherent differences between REF and NPS® specimens that can affect the performance and that are not explicitly weighted in when computing these performance criteria. For example, some of the NPSi specimens were about 20% stronger than REFi. This results in higher demand on the joint which can result in greater deterioration and/or more severe bond-slip related phenomena, ultimately affecting energy dissipation and stiffness degradation. Evidently, this does not represent an inherent limitation of the NPS® systems which could have easily been designed to be somewhat weaker than the reference specimen, reducing the demand on the joint with a series of favorable implications.

> The outcome of the performance evaluation conducted at 4% drift is overall in line with what would be observed at drift ratio of 3.5%. The only notable changes are due to a low residual stiffness score, resulting in an unacceptable performance of NPS1i. This is attributed to the severely pinched response that this specimen exhibited at large displacements, correlated with poor bond of the integrative truss solution. NPS2Ai and NPS2Bi exhibit nearly identical performance, and overall comparable performance to the reference specimen, REFi.

6.2.5 MDI Comparison Between NPS® and Ref

> A preliminary performance assessment of the interior NPS® beam-column joints was conducted by comparing the response of specimens REFi and NPS2Ai. REFi represents a traditional, Eurocode compliant, moderately ductile beam-column joint. NPS2Ai is chosen as a representative NPS® "baseline" specimen. It features standard NPS® column and beams, no added stirrups in the beam end region, cut out "windows" in the steel HSS in the joint region (on the two sides lacking beams), traditional shear reinforcement in the joint core (equal in ratio to the reference specimen) and moment continuity provided by straight deformed bars crossing the joint and extending beyond the critical region of the beams.

> The force-displacement response of both specimens is shown in Figure 6.12. NPS2Ai sustained the full loading protocol, including three loading cycles at 5% drift, while REFi completed only one full cycle at peak drift of 5%. Both systems also reached flexural beam yielding as per design objective, developing their full nominal strength. As briefly discussed earlier, while the two specimens were designed for the

same seismic demand, by the time the design was complete, their nominal strengths differed by about 18%. Thus, NPS2Ai displayed an experimental peak strength of about 231 kN, while REFi reached an approximate peak load of 196 kN.

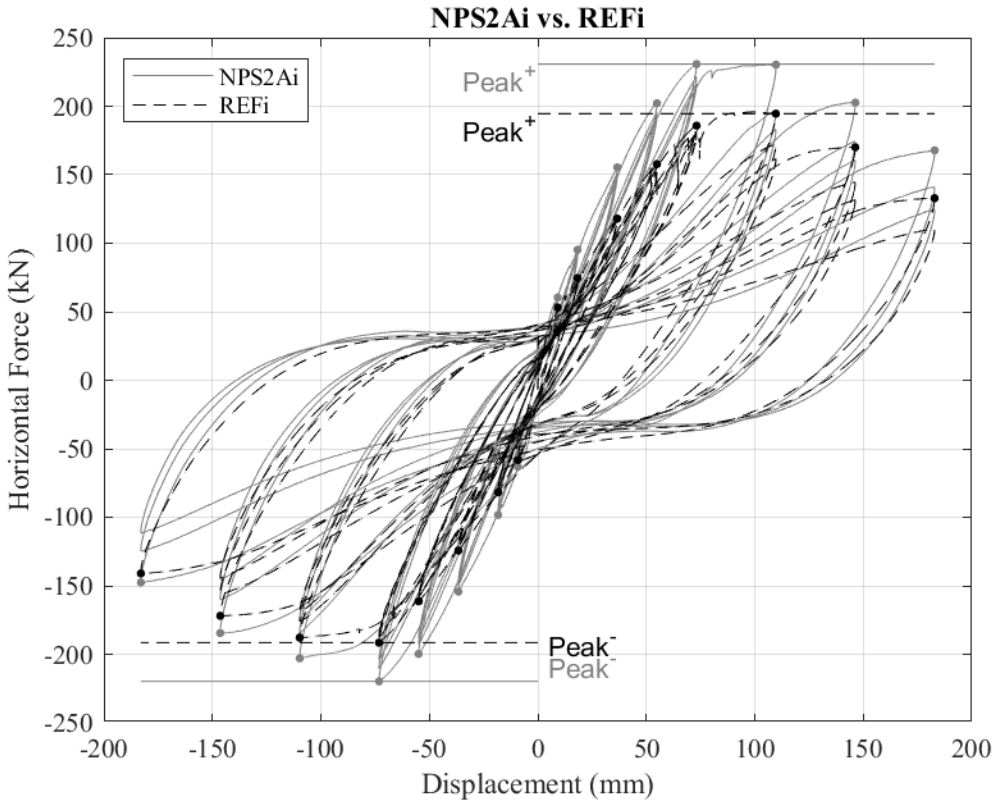

Figure 6.12: Force-Displacement Response of Specimens NPS2Ai and REFi

> It can be seen in Figure 6.12 that, pre-yielding, REFi was characterized by a softer response than its NPS® companion. Initial stiffness values (computed as K_i per discussion in CHAPTER 4) of 4.6 kN/mm and 5.1 kN/mm were computed for REFi and NPS2Ai, respectively. The curves in Figure 6.12 show that, after beam yielding occurred, both specimens suffered progressive loss of lateral stiffness. In this regard, the specimens experienced nearly identical extents of stiffness degradation. For instance, at drift ratios of 3% and 4%, REFi experienced secant stiffness losses ($K_{0,\text{Drift\% Cycle3}}/K_{0,\text{Drift\% Cycle1}}$) of about 38% and 53%, between loading cycles 1 and 3. Considering the same range, stiffness losses of 40% and 53% were computed for NPS2Ai. The response of the two specimens also shows comparable extent of pinching. This

is consistent with the stiffness degradation found per the ACI method, of the stiffness at a relevant cycle with the overall initial stiffness of the specimen. Per Table 6.3, at drift ratios of 3% and 4%, REFi exhibited a 33% and 13% reduction in overall stiffness ($K_{0,Drift\%\ Cycle1}/K_i$) while NPS2Ai exhibited 25% and 10% reduction from the initial stiffness.

Both REFi and NPS2Ai suffered a joint failure following beam yielding between 1.0% and 1.5%, somewhat typical for moderately ductile cruciform joints. The damage sequence observed during the tests involved some extent of beam cracking followed by severe joint deterioration. The same failure mode was observed for both specimens, with no notable response differences to report. The joint region of specimen NPS2Ai did not deteriorate any faster nor displayed more severe/extensive damage than REFi, despite being subjected to higher demand coming from the stronger (by about 18%) beam.

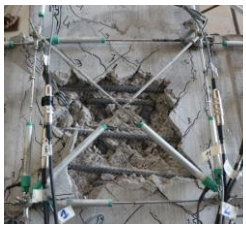

REFi Panel

REFi beam

NPS2Ai Panel

NPS2Ai beam

Figure 6.13 provides a view of one of the beams and the joint panel zone at failure (i.e., 5% drift ratio) for both specimens tested. In both cases, the beam exhibits minor extent of cracking, while the joint region is severely damaged having experienced extensive diagonal cracking, yielding of transverse reinforcement and concrete spalling, throughout the tests.

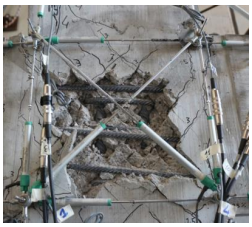

REFi Panel

REFi beam

NPS2Ai Panel

NPS2Ai beam

Figure 6.13: View of Beam and Joint Region of Specimens NPS2Ai and REFi at Failure

> Despite their different strengths, the specimens exhibited nearly identical performance in terms of residual strength Table 6.3 shows that the residual strengths ($P_{max,i}/P_{peak}$) at the 4% drift load ratio of REFi and NPS2Ai is 0.87 and 0.88, respectively.

> Expanding the comparison of all NPS® interior specimens with the reference specimen shows that, for the most part, the results show good levels of compatibility with the performance of REFi. However, some interesting aspects are worth discussing in some detail. NPS1i had the lowest overall performance, (per Section 6.2 discussion) thus far. The residual stiffness-to-initial stiffness ratio appears remarkably low compared to the other parameters, which is coherent with the force-displacement response of this specimen, characterized by significant pinching and stiffness degradation.

> Specimens NPS2Ai and NPS2Bi behaved similarly, with NPS2Bi performing slightly better across the board and particularly in terms of residual stiffness. This confirms that the response of these two specimens was virtually identical, as discussed earlier and suggests that the specimens are equivalent.

> Perhaps the most unexpected outcome reported in Table 6.3, is the stiffness degradation of specimen NPS4i with a K0,4% Cycle1/Ki of 0.05, which, while still a “passing score” per ACI guidelines, is lower than both NPS2Ai and NPS2Bi. This is mostly due to the severely pinched nature of the force-displacement response observed for this specimen.

> Bond-slip deterioration at the beam-column interface characterized the response of all interior specimens, including that of the reference specimen REFi. However, the NPS® specimens were subject to greater demand and were overall more severely affected by this phenomenon that, performance-wise, induced different extents of stiffness and energy dissipation reduction. Again, it should be noted that this is not an inherent limitation of the NPS® system. In fact, a conscious decision was made in design to push the typical design limits and adopt continuity reinforcement made of large diameter bars, increasing the vulnerability of the system to bond-slip phenomena. Despite this, the performance of specimens such as NPS2Ai and NPS2Bi was nearly identical to that of REFi, which is remarkable and indicates that capacity protected NPS® beam-column joints crossed by large diameter bars can exhibit comparable performance to Eurocode compliant moderately ductile RC joints. It is also reasonable to believe that superior to "moderately ductile" performance can be met if smaller diameter continuity bars are used or, more generally, if better bond of those bars is achieved.

6.2.6 MDI Shear Stress vs. Shear Strain

> Overall, it is interesting to consider the backbone curves for the shear stress vs. shear strain graphs. This is often noted in the literature, as many models have been developed to directly correlate the shear strength of the joint to the shear strain in the joint region (see CHAPTER 2). Figure 6.14 is similar to the overall backbone curves show at the beginning of this chapter of the force displacement responses of all the MDI specimens, and follows a similar pattern for overall behavior. NPS4i, obviously with no degradation to the joint region, exhibits little to no change in shear strain. The other specimens, correspondingly to their force displacement graphs, show similar behaviors, with the NPS1i specimen exhibiting the lowest shear stress, and NPS2Ai, NPS2Bi, and NPS4i exhibiting similar levels of behavior. They experience slightly higher shear stress than the reference specimen, which sees higher shear stress in turn than the NPS1i specimen.

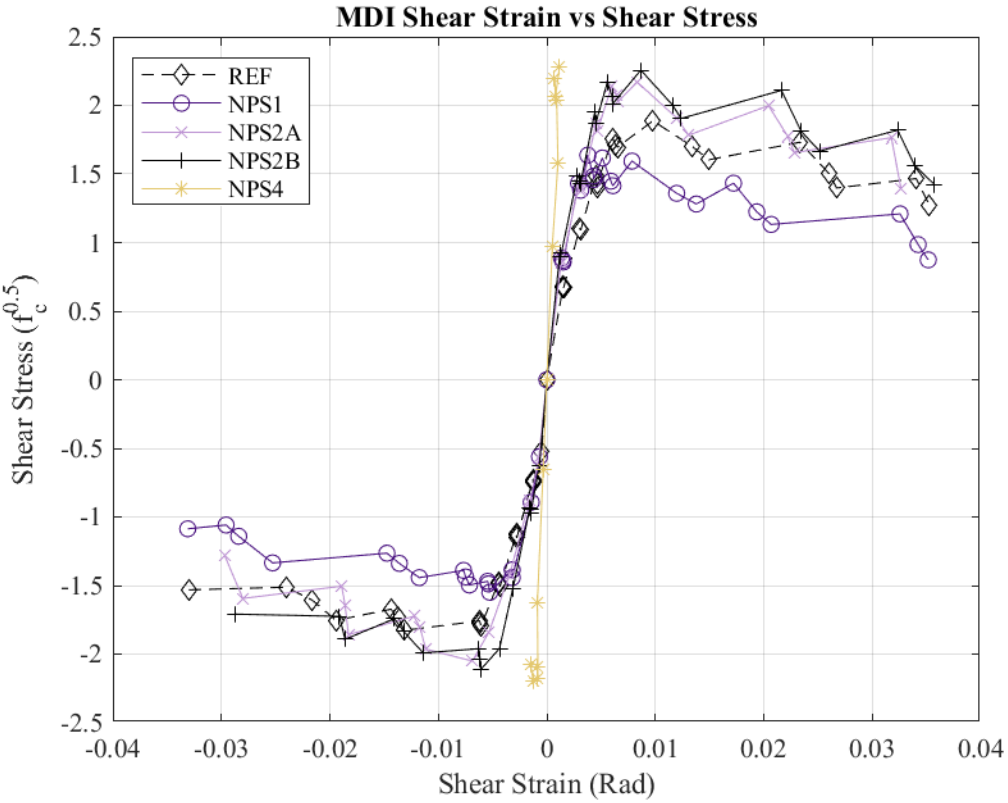

Figure 6.14: MDI Shear Strain vs. Shear Stress

6.3 MDE (EXTERNAL) EFFECTS OF STUDIED DESIGN VARIABLES

> Peak and residual strength results obtained from the MDE Test Series are summarized in Table 6.4. The specimens showed somewhat non-symmetrical responses, displaying higher resistance in the negative loading direction in all cases. Specimens NPS2Ae and NPS4e exhibited identical negative strength (about 115 kN), while NPS2A was approximately 10% stronger under positive loading than NPS4e. The strength of the reference specimen REFe was slightly lower, with peak load recorded in the negative loading direction of 102.8 kN. NPS1i had lower resistance, with maximum loads of 72.4 kN and 86.3 kN in the positive and negative direction, respectively. Averaging the two loading directions, this corresponds to about 80% of the strength displayed by REFe.

> As discussed for MDI Test Series, these strengths are reflective of the nominal strength of the various systems, which was reached during testing in all cases. Opposite to the internal specimens, the external specimens reached peak strengths during the negative loading cycle, instead of the positive loading. Reported residual strength losses are reported in terms of the average strength degradation between positive and negative loading. As for the interior joint specimens, all exterior joints were designed for identical seismic demand, and careful consideration was given during the design phase to ensure that all systems had similar capacity. However, inherent differences in the structural solutions adopted, inevitably led to specimens characterized by unequal ability to resist lateral loads.

> Table 6.4 also lists residual strengths, taken as the peak loads recorded on positive and negative side, during the first loading cycle to 5% drift. Values ranging from 59% (NPS1e) to 76% (NPS4e) of peak strengths can be observed. It should be noted that it was not possible to record the residual strength at 5% drift for some of the specimens. REFe failed prematurely due to unintended out-of-plane loads, while testing of specimens NPS2Ae and NPS4e was interrupted after completing the first half-cycle at 5% in the positive loading direction, because the instrumentation started to pick up some undesired out-of-plane movements.

> Overall, the strength of all specimens is predicted accurately using the Eurocode approach, with average test-to-predicted strength ratio of 0.95 and COV of 9%. However, the positive strength of the specimens

was somewhat lower than expected, and some unconservative strength predictions can be seen in Table 6.4. System strength predictions were based on the estimated flexural strength of the beam, assuming elasto-plastic steel response and without considering second order effects. Note that more refined strength predictions can be obtained using more sophisticated tools and modeling assumptions, if desirable.

Table 6.4: Summary of Test Results – MDE Test Series

Specimen ID	F_{peak}^{+} F_{peak}^{-} [kN]	$F_{5\%}^{+}$ $F_{5\%}^{-}$ [kN]	F_{n}^{+} F_{n}^{-} [kN]	$F_{5\%}^{+}/F_{peak}^{+}$ $F_{5\%}^{-}/F_{peak}^{-}$	F_{peak}^{+}/F_{n}^{+} F_{peak}^{-}/F_{n}^{-}	Failure mode
REFe	95.0	NA	99.5	NA	0.95	OP
	-102.8	NA	-99.5	NA	1.03	
NPS1e	72.4	49.2	86.0	0.68	0.84	BY
	-86.3	-54.4	-83.0	0.63	1.04	
NPS2Ae	102.9	76.0	118.3	0.74	0.87	BY
	-114.1	-58.2	-115.5	0.51	0.99	
NPS4e	93.5	64.7	118.3	0.69	0.79	BY
	-115.3	-60.6	-115.5	0.53	1.00	
				Mean	0.94	
				COV [%]	9.00	

> The envelope force-displacement response of all MDE specimens is outlined in Figure 6.15: While this representation omits information pertaining to loading-reloading, cyclic stiffness degradation etc., it provides a concise summary of the experimental data collected.

> Notable observations that can be made based the displayed data include the following:

- NPS2Ae and NPS4e exhibit higher cracked stiffness that the RC specimen, but not to the extent observed earlier for MDI specimens. In contrast, up to yielding, NPS1e displays a response that is similar to that of REFe.
- All specimens reach flexural yielding at drift ratios between 1.0% and 1.5%.
- All specimens show similar extents of strength degradation at large displacements.
- NPS2Ae and NPS4e show similar strength and overall response. Though somewhat stiffer and stronger, their response is comparable to that of REFe (limited to the available data, up to 3% drift).

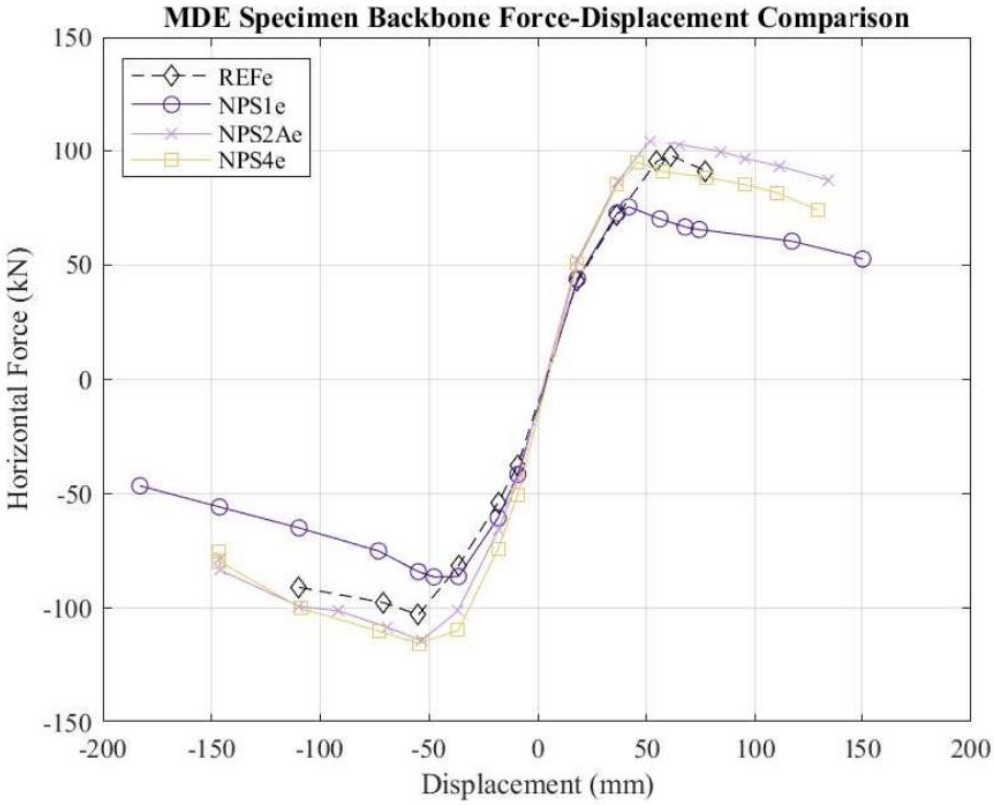

Figure 6.15: MDE Backbone Force-Displacement Comparison

> For ease of comparison the sub-components of the MDE specimens at critical drift ratios is shown below. Note that due to the out of plane failure of REFe, there is no data for the 4% and 5% loading cycles. Recall that the reference specimen did not complete 4% or 5% drift ratio.

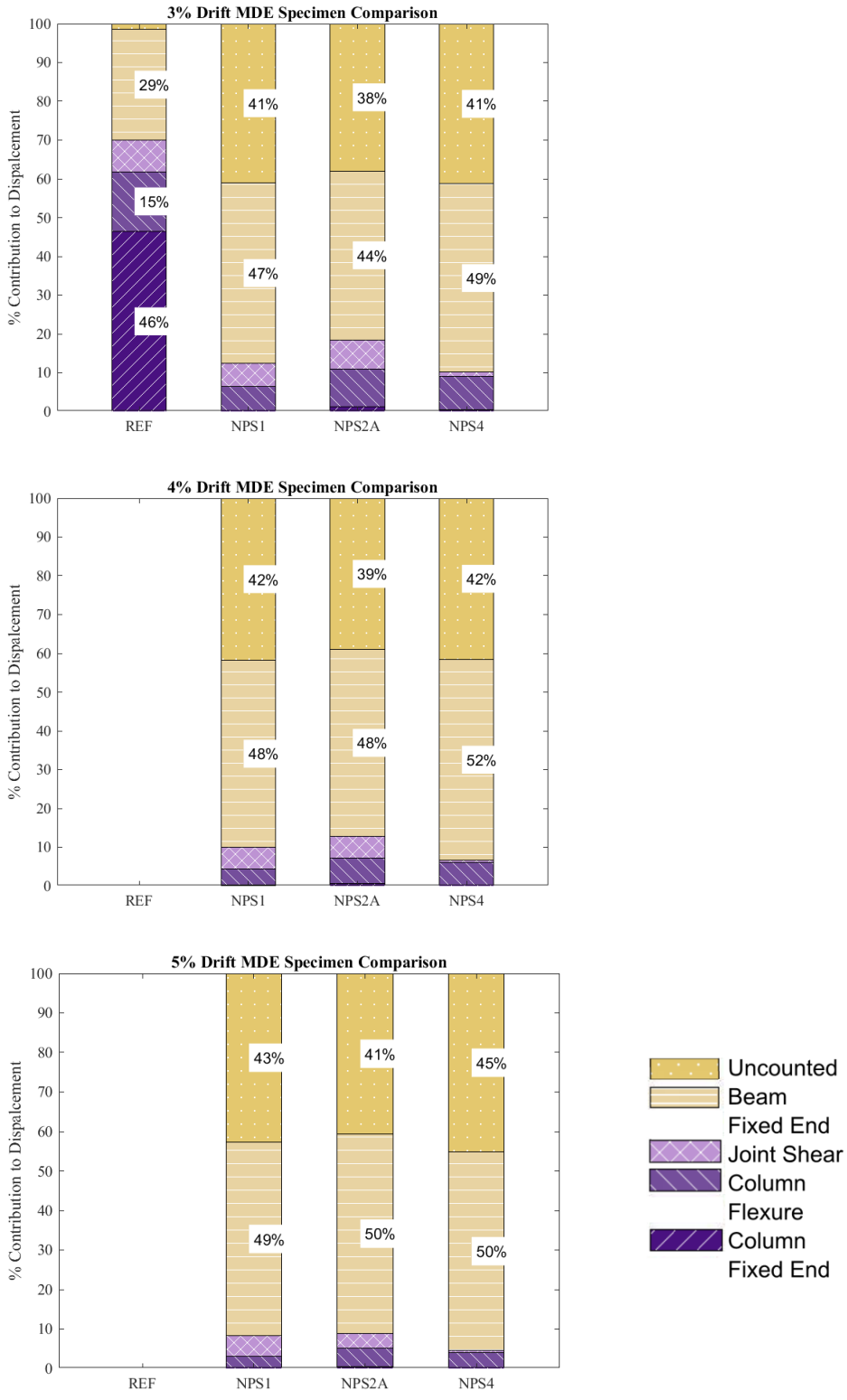

Figure 6.16: MDE Drift Subcomponent Comparison

> Figure 6.17: View of Joint Region of MDE Specimens at Failure compares the final damage state of the failure region of the four MDE specimens tested. Note that the base of the column is shown for REFe, because that is where premature out-of-plane failure occurred during the second loading cycle to 3% drift. All other specimens exhibited the same flexural failure mode that involved beam continuity reinforcement yielding. In all cases, the joint region exhibited minor to no (NPS4e) diagonal cracking. Instead, a major vertical crack formed at the beam-column interface that worked as an effective localized "plastic hinge".

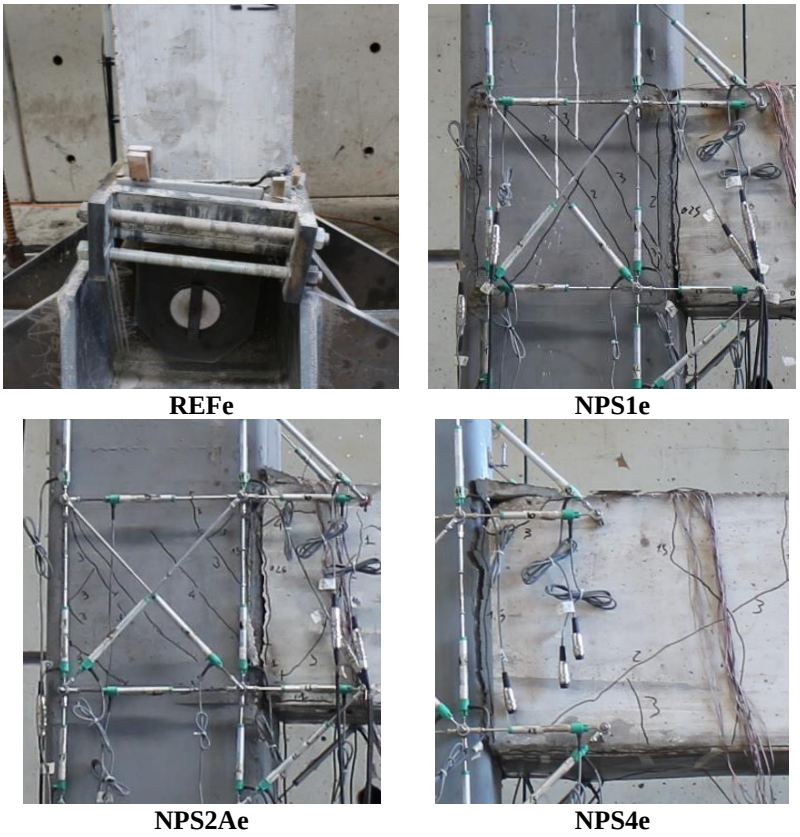

Figure 6.17: View of Joint Region of MDE Specimens at Failure

6.3.1 NPSe - Effect of Different Continuity Solutions

> The effect of moment continuity on the performance of exterior NPS® beam-column joints was evaluated comparing the response of specimens NPS1e (continuity through added trusses) and NPS2Ae (continuity through added hooked bars). Details on these systems can be found in CHAPTER 3 Note that unlike NPS1e, NPS2Ae had no added shear reinforcement in the beam region. However, the presence of ductility stirrups in the beam "critical length" was shown earlier to have no effect on the specimen response.

> The tests were interrupted before completing the full loading protocol because of concerns with undesired out-of-plane phenomena. NPS1e completed 1.5 cycles at 5% drift, while testing of NPS2Ae was stopped after one half loading cycle at 5% drift ratio.

> The force-displacement response of both specimens is shown in Figure 6.18. The two systems exhibited a markedly different overall response, with NPS1e affected by nontrivial pinching and NPS2Ae displaying fat, highly dissipative hysteretic response. Both systems also reached flexural beam yielding as per design objective. However, the response was markedly non-symmetrical and the strength on the positive loading cycle was somewhat lower than expected. Peak resistance values (recorded on the negative loading cycle) were 86.3 kN and114.1 kN for NPS1e and NPS2Ae, respectively.

> NPS2Ae showed a superior ability to sustain the applied peak as the displacement demand increased. For instance, at drift ratios or 3% and 4% between cycles 3 and 1 ($P_{max,3\%Cycle3}/P_{max,3\%Cycle1}$) NPS2Ae exhibited RSR of 92% and 94%. At the same drift levels, NPS1e had RSR of 83% and 89%, respectively.

> Beam yielding was detected around 1.0% and for NPS1e and around 1.5% for NPS2Ae. Based on the yield drift and on the overall response, and adopting the definition introduced earlier, levels of ductility between 2.5 and 3.2 were calculated in the positive loading direction for NPS1e and NPS2Ae respectively; a ductility of 2.2 and 3.0 were calculated in the negative loading direction.

> Specimen NPS2Ae exhibited somewhat stiffer "pre-yielding" response. Initial stiffness, K_i, values of 2.50 kN/mm and 2.94 kN/mm were computed for NPS1e and NPS2Ae, respectively (See procedure outlined in CHAPTER 4).

> The data outlined in Figure 6.18 show that, after beam yielding occurred, both specimens suffered minor loss of lateral stiffness within loading cycles. For instance, at drift ratios of 3% and 4%, NPS2Ae experienced residual stiffness losses ($K_{0,Drift\%Cycle3}/K_{0,Drift\%Cycle1}$) of about 89% and 74% were observed between loading cycles 3 and 1 of the respectively drift ratios. Considering the same range, stiffness losses of 17% and -21%, were observed for NPS1e (note that a negative stiffness was observed in the third cycle of the 4% drift of NPS1e).

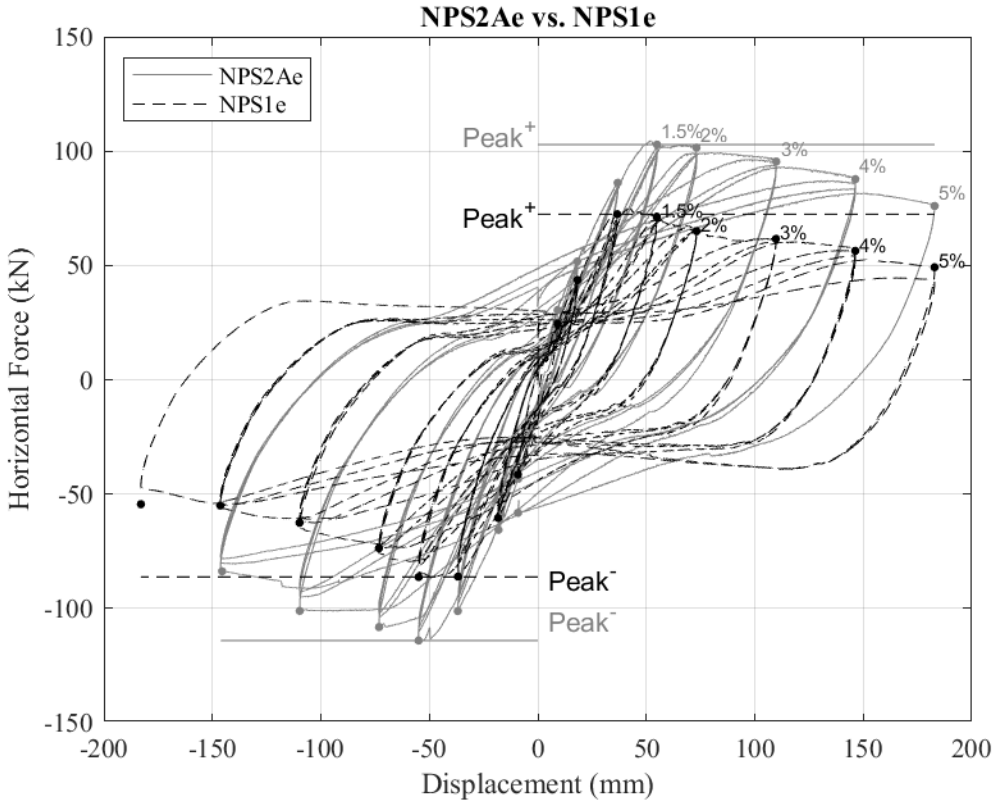

Figure 6.18: Force-Displacement Response of Specimens NPS1e and NPS2Ae

> The two specimens discussed in this section suffered a flexural beam failure. The damage sequence observed during the tests involved some minor beam cracking followed by minor diagonal joint cracking. A flexural plastic hinge developed in the form of a single major crack at beam-column interface, protecting the integrity of all other components. The shear reinforcement present in the joint core was enough to preserve its integrity.

> The main difference in the response was that the continuity truss elements of specimen NPS1e (despite being mechanically anchored within the joint core) were affected by bond-slip deterioration at the beam-column interface, while the continuity bars of specimen NPS2A appeared to be effectively anchored and to rely on good level of bond. This is consistent with the mechanical characteristics of the longitudinal bars of the continuity trusses, which consisted of smooth steel reinforcement. Once more, this indicates that achieving moment continuity across the joint by means of smooth steel elements does not represent an effective solution.

> The failure of specimen NPS2Ae was classified as traditional beam yielding, while NPS1e classified as beam yielding accompanied by nontrivial bond-slip deterioration/anchorage issues (identified as the main source of the pinching effects observed in the force-displacement response). Minor evidence of flexure-induced concrete crushing was also detected at the beam-end. Figure 6.19 provides a view of one of the beams and the joint panel zone at failure (i.e., 5% drift ratio) for both specimens tested.

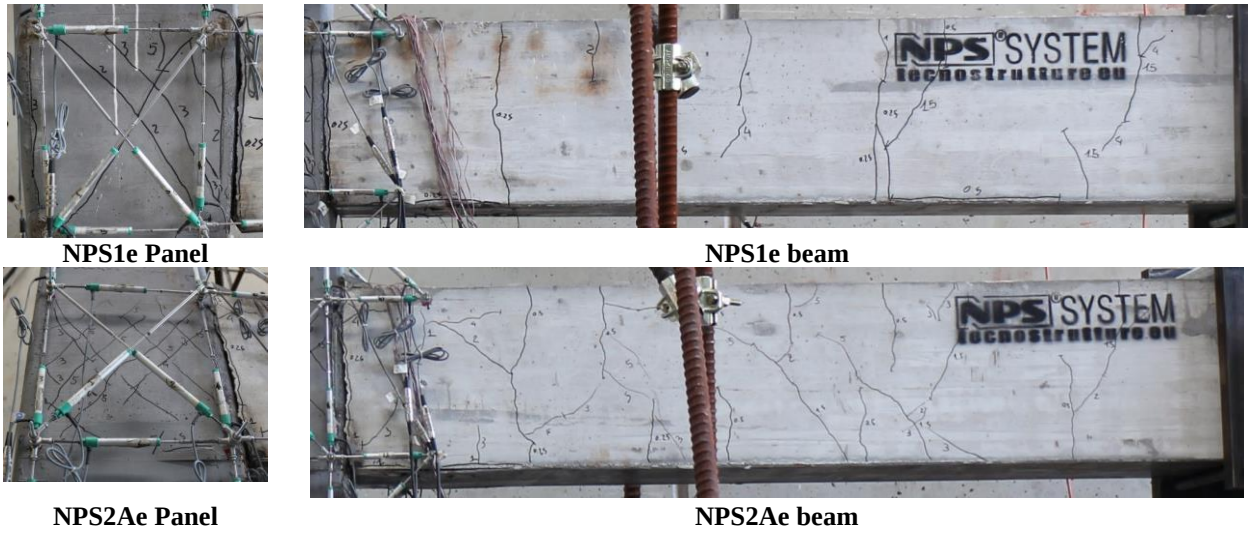

Figure 6.19: View of Beam and Joint Region of Specimens NPS1e and NPS2Ae at Failure

6.3.2 NPSe - Influence of Joint Shear Reinforcement and Confinement

> Potential beneficial effects of the column HSS on the integrity of the joint region, with reduced amount of shear reinforcement within the join core, were examined by analyzing the response of specimens NPS2Ae and NPS4e. The tests were interrupted before completing the full loading protocol because of concerns with undesired out-of-plane phenomena. Both specimens completed one-half loading cycle at 5% drift ratio.

> The force-displacement response is shown in Figure 6.20. Because NPS2e did not experience any joint issue, enhancing the strength of the joint panel via steel HSS did not produce any notable performance improvement. The response of NPS2e and NPS4e was virtually identical, with NPS2Ae (no HSS around joint core) behaving negligibly better. Both systems reached flexural beam yielding as per the design objective. However, the response was non-symmetrical and the strength on the positive loading cycle was somewhat lower than expected. Peak resistance values (recorded on the negative loading cycle) were 114 kN and115 kN for NPS2Ae and NPS4e, respectively.

> NPS2Ae showed slightly superior ability to sustain the applied peak as the displacement demand increased. For instance, at drift ratios or 3% and 4% between cycles 3 and 1, NPS2Ae exhibited residual strength ratio (RSR, $P_{max,Drift\%Cycle3}$/ $P_{max,Drift\%Cycle1}$) of 96% and 94%. At the same drift levels, NPS4e had RSR of 97% and 85%, respectively.

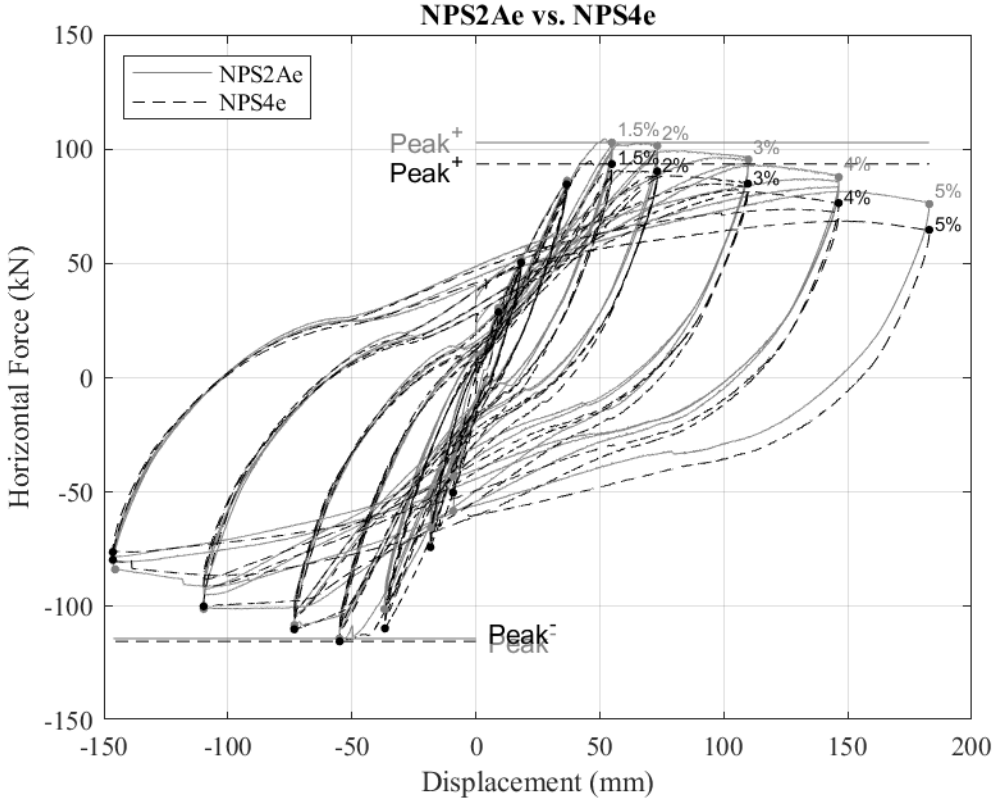

Figure 6.20: Force-Displacement Response of Specimens NPS2Ae and NPS4e

> Beam yielding was detected between 1.5% and 2.0% drift. Based on the yield drift and on the overall response, the ductility of both systems was calculated as 3.22 for NPS2Ae in the positive loading, and 2.97 for NPS4e; negative loading yielded ductility values of 3.01 and 3.24 for NPS2Ae and NPS4e, respectively.

> The specimens exhibited essentially identical "pre-yielding" response. Initial stiffness values of 2.94 kN/mm and 3.15 kN/mm were computed for NPS2Ae and NPS4e, respectively.

> The specimens exhibited essentially identical "post-yielding" responses as well. The data outlined in Figure 6.20 shows that, after beam yielding occurred, both specimens suffered similar extents of loss of lateral stiffness within loading cycles ($K_{0,Drift\%Cycle3}/K_{0,Drift\%Cycle1}$). For instance, at drift ratios of 3% and 4% between cycles 3 and 1, NPS2Ae experienced secant residual stiffness losses of about 89% and 74% Considering the same range, stiffness losses of 89% and 73% were computed for NPS4e – nearly identical.

> Specimens NPS2Ae and NPS4e experienced flexural beam failure. The damage sequence observed during the tests involved some minor beam cracking followed by minor diagonal joint cracking (only in

NPS2Ae). Minor evidence of flexure-induced concrete crushing was also detected at the beam-end. A flexural plastic hinge developed in the form of a single major crack at the beam-column interface, effectively protecting the integrity of all other components. The shear reinforcement present in the joint core of NPS2Ae was enough to preserve its integrity, thus the steel HSS around the joint core of NPS4e did not produce any appreciable benefits, other than preventing the joint from cracking.

> Figure 6.21 provides a view of one of the beams and the joint panel zone at failure (i.e., 5% drift ratio) for both specimens tested.

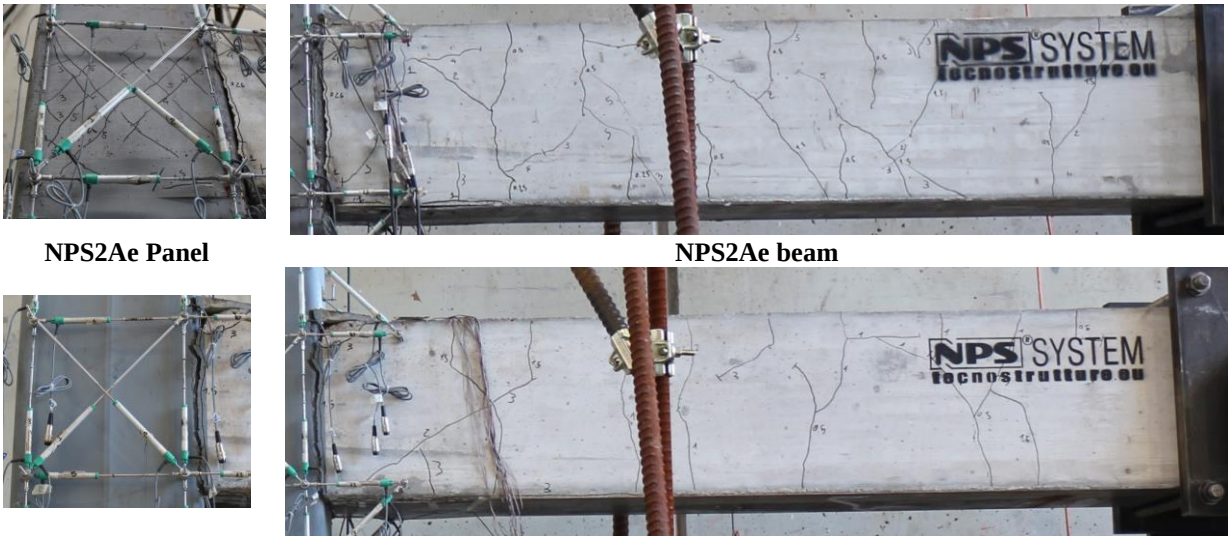

NPS2Ae Panel **NPS2Ae beam**

NPS4e Panel **NPS4e beam**

Figure 6.21: View of Beam and Joint Region of Specimens NPS2Ae and NPS4e at Failure

6.4 MDE RESPONSE CLASSIFICATION

The outcome of the analysis described in the previous section is summarized in Table 6.5, for drift ratios of 3% and 4%. While the highest peak resistance was recorded in the negative direction for the external specimens, the strength degradation analysis is averaged between the positive and negative loading directions. The performance results show good levels of compatibility between the different NPS® specimens and between the NPS® specimens and the reference RC specimen.

Table 6.5: MDE Performance Assessment Results

Specimen	Failure Mode	Performance evaluation, first cycle at 3% drift				Performance Evaluation, first cycle at 4% drift				Δ_y^+ Δ_y^- (mm)	μ^+ μ^{+-}
		P_0/P_{peak}	K_0/K_i	E_n	$\bar{E}$	P_0/P_{peak}	K_0/K_i	E_n	$\bar{E}$		
REFe	BY-O	0.91	0.31	0.29	0.43	NA	NA	NA	NA	50.6 -44.9	2.32* 2.80*
NPS1e	BY	0.85	0.17	0.34	0.40	0.75	0.06	0.36	0.51	35.0 -28.4	2.46 2.19
NPS2Ae	BY	0.91	0.24	0.25	0.34	0.79	0.19	0.31	0.45	43.2 -38.1	3.22 3.01
NPS4e	BY	0.89	0.22	0.28	0.35	0.75	0.16	0.36	0.49	38.8 -32.9	2.97 3.24

*Linearly extrapolated from data.

6.4.1 MDE Stiffness and Strength Degradation

The stiffness degradation for the NPS1e specimen was swifter than the other specimens. This resulted in a slightly less ductile response than the other specimens. The trend in Figure 6.22 appears to indicate the general stiffness degradation of the NPS® specimens occurred at a faster rate than the Reference specimens. Figure 6.22 shows the first cycle of each of the drift level normalized by the initial stiffness of the specimen, as described in CHAPTER 4 .

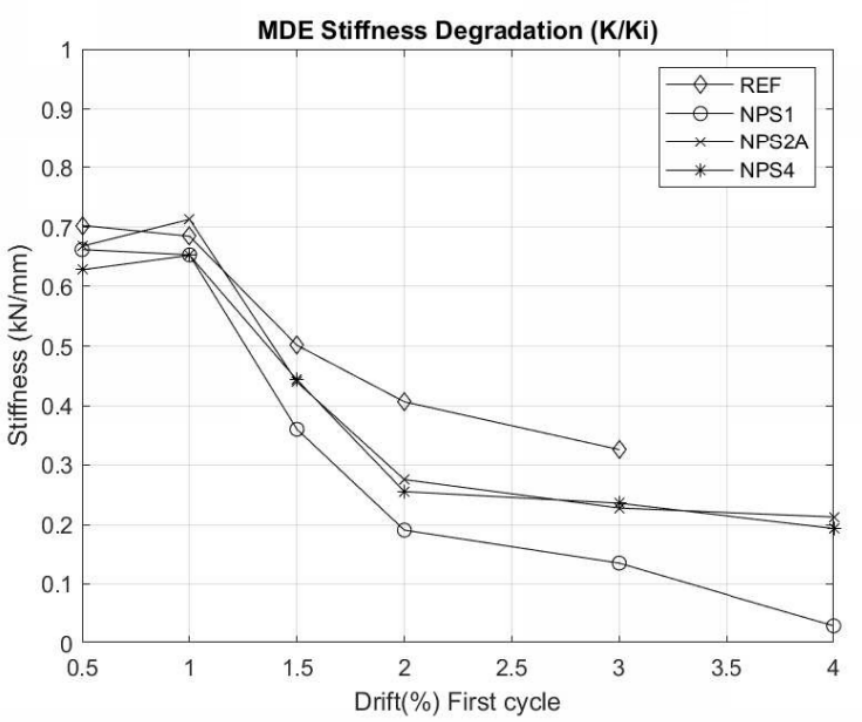

Figure 6.22: MDE Stiffness Degradation

> It is not obvious, since Table 6.5 does not include the 2% loading cycle, but the peak strength for each specimen was typically reached during the 2% cycle, (except for NPS1e which peaked during the 1.5% loading cycle) after which or during the specimens yielded. All of the external specimens failed in beam yielding (BY).The first cycle of each loading cycle was normalized by the peak strength overall for the specimen. The strength degradation of NPS1e was the most pronounced, resulting in a residual strength ratio (RSR: $P_{max,Drift\%Cycle1}/P_{peak}$) of 85% and 75% for the drift ratios of 3% and 4%. Contrastingly, NPS2Ae resulted in RSRs of 91% and 79% for the same range. NPS4e exhibited ratios of 89% and 75%.

6.4.2 MDE Energy Dissipation

> The energy dissipation was calculated as the area within the hysteretic force-displacement loop, normalized by the maximum load and displacement for the corresponding cycle, as discussed by Parra-Montesinos [24].

> The energy dissipation generally increased with each subsequent drift level, beyond 2%. The first cycle of each subsequent drift level was used to calculate the values shown in Figure 6.22. NPS1e dissipated more energy with each cycle than NPS2Ae or NPS4e.

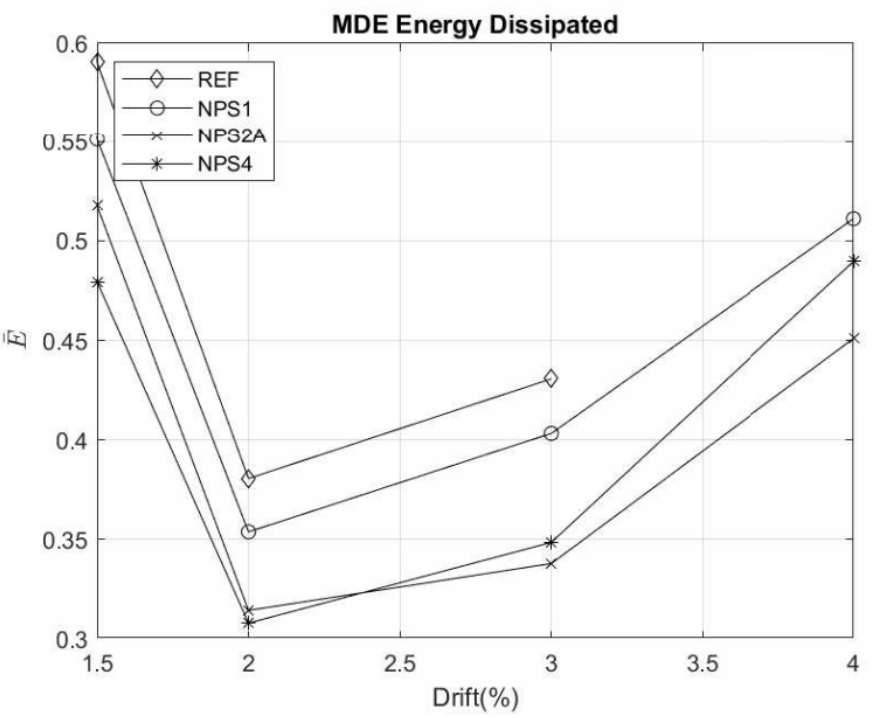

Figure 6.23: MDE Energy Dissipation

6.4.3 MDE Ductility

The specimens had ductility ratios ranging from 2.19 to 3.24. NPS1e was the least ductile of the external specimens, with calculated ductility ratios of 2.5 and 2.2 for the positive and negative loading directions, respectively. NPS2Ae and NPS4e had similar levels of ductility, at or above 3.0, in both the positive and negative directions, with REFe falling somewhere in between these most and least ductile specimens. As already noted in this section, the external specimens typically exhibited less symmetry than the internal specimen; this is an expected outcome when there is one beam with different nominal strengths in the positive and negative directions (i.e., the external specimens). This is reflected in the ductility calculations, which have more variation between each specimen's positive and negative loading direction than the internal specimens. It is important to note that for both the internal and external specimens the NPS1 model yielded at the smallest displacement within the bunch.

6.4.4 MDE ACI Comparison

> For a thorough discussion of the ACI procedure, motivation for its use, and important caveats as it relates to this specific project procedure, see Section 6.2.4. Due to failure out of plane, REFe did not reach 4% drift, so a direct comparison to a traditional reinforced concrete exterior beam-column joint is impossible.

> The results pertaining to the performance evaluation conducted at 3% and 4% drift are summarized in Table 6.6. It is interesting to note that if the negative loading direction only were to be assessed for the strength degradation, the specimens would not "pass"; however, since the stiffness degradation values were averaged between the positive and negative loading directions, the overall score is "passing". It is likely that during the limiting drift ratio of 3.5% required by the ACI code (but not directly replicated during this experiment) all NPSe specimens likely would have high enough strength retention in both the positive and negative loading directions independently.

Table 6.6: MDE ACI Acceptance Criteria

Specimen	Performance evaluation, first cycle at 3% drift			Performance Evaluation, first cycle at 4% drift			First Cycle 4% Acceptable per ACI Criteria?		
	P_0/P_{peak}	K_0/K_i	$\bar{E}$	P_0/P_{peak}	K_0/K_i	$\bar{E}$	$P_0/P_{peak} \geq 0.75$	$K_0/K_i \geq 0.05$	$\bar{E} \geq 0.125$
REFe	0.91	0.31	0.43	N/A	N/A	N/A	N/A	N/A	N/A
NPS1e	0.85	0.17	0.40	0.75	0.06	0.51	Yes	Yes	Yes
NPS2Ae	0.91	0.24	0.34	0.79	0.19	0.45	Yes	Yes	Yes
NPS4e	0.89	0.22	0.35	0.75	0.16	0.49	Yes	Yes	Yes

6.4.5 MDE Comparison Between NPS® and Ref

> Preliminary performance of exterior NPS® beam-column joints was conducted by comparing the response of specimens REFe and NPS2Ae. REFe represented a traditional, Eurocode compliant, moderately ductile exterior beam-column joint. NPS2Ae was chosen as a representative exterior NPS® "baseline" specimen.

> The force-displacement response of both specimens is shown in Figure 6.24. The maximum demand sustained by NPS2Ae consisted of one-half cycle at 5% drift, while REFe only completed one full cycle at peak drift of 3% because it suffered a premature out-of-plane failure.

> The force-displacement response is shown in Figure 6.24. The available data (only up to 3% drift), show that the response of NPS2e and REFe was virtually identical, with NPS2Ae being initially slightly stiffer and somewhat stronger in the positive loading direction. Both systems reached flexural beam yielding as per design objective, developing their full nominal strength. NPS1e showed peak strength of 103 kN and was about 10% weaker than NPS2Ae, which peaked at 114.5 kN, both in the negative loading direction. The available data show that the specimens exhibited nearly identical performance in terms of residual strength. At drift ratio of 3% REFe had 8% strength degradation while NPS2Ae had 11%.

> Beam yielding was detected between 1.0% and 1.5%, while initial stiffness values of 2.6 kN/mm and 2.9 kN/mm were computed for REFe and NPS2Ae, respectively. No information pertaining to stiffness losses at 3% and 4% drift could be collected for REFe.

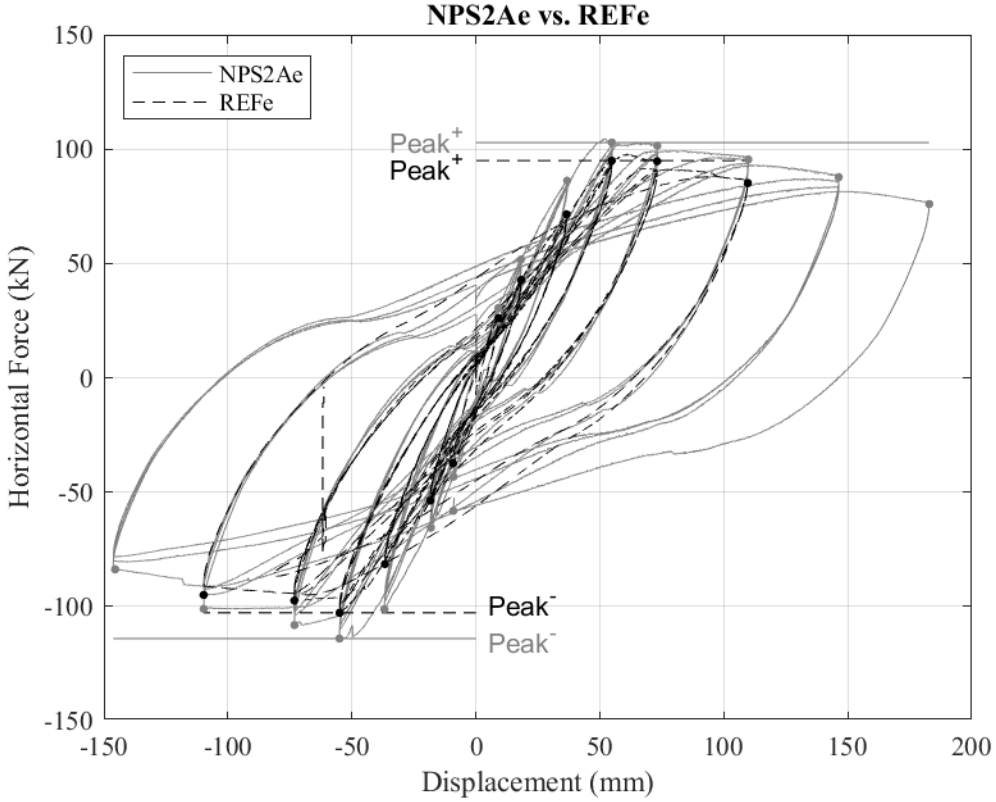

Figure 6.24: Force-Displacement Response of Specimens NPS2Ae and REFe

Specimen NPS2Ae experienced flexural beam failure, while REFe failed out-of-plane (induced by the experimental setup) at a drift of 3%, following beam yielding. It is believed that REFe would have experienced similar response to NPS2Ae, had it not suffered a premature twist-induced collapse at the base of the column. Up to 3% drift, the response of the two specimens was essentially identical, and visible damage involved only beam flexural cracking.

6.5 MD PERFORMANCE SUMMARY

> This chapter presented a detailed analysis of the results of the experimental program from the angle of assessing and contextualizing the performance of the NPS® beam-column joints tested. Some of the main observations that can made based on the analysis of the experimental results are briefly reported below.

> Effects of Studied Design Variables:

- MDI Test Series:
    - Systems whereby moment continuity across the joint is achieved by means of straight deformed bars that extend beyond the beam "critical length" display better performance than systems with continuity trusses.
    - Integrative shear reinforcement (i.e., ductility stirrups) at the beam-ends does not provide any benefit or performance enhancement, in capacity designed NPS® systems with NPS® beams adequately sized to resist the maximum shear demand.
    - If maintained continuous on the sides of the joint core not connected to beams, the steel HSS is highly effective at protecting the integrity of a 2D joint but does not offer significant strength or stiffness enhancement.
- MDE Test Series:
    - Specimen NPS2Ae showed superior performance with respect to NPS1e, confirming that deformed bars represent a better continuity solution than integrative trusses.
    - Specimens with no ductility stirrups within the beam critical length did not exhibit any structural issues, confirming that integrative shear reinforcement is not required in the beams of capacity designed NPS® systems.

> Joint Performance Assessment:

- MDI Test Series:
    - Consistently with the points made above, NPS1i (with moment continuity trusses) exhibited poor performance and did not meet ACI acceptance criteria at limiting drift ratio of 3%.
    - Specimens NPS2Ai and NPS2Bi (with continuity deformed bars) exhibited virtually identical performance. They both met ACI acceptance criteria at limiting drift ratio of 3% and their overall performance was showed to be equivalent to that of the reference specimen REFi.
    - While still meeting ACI acceptance criteria at 3% drift, specimen NPS4i showed overall lower performance than REFi, based on the metrics adopted. The main issue was the excessive bond demand on the continuity bars, which resulted in bond-slip deterioration. This problem can be easily mitigated by using smaller diameter bars, theoretically.
- MDE Test Series:
    - All NPSe specimens showed overall good performance, meeting ACI acceptance criteria at 3% drift and 4% drift.
    - The two systems with continuity bars exhibited higher performance than their companion specimen with beam-column connection achieved through integrative trusses.

CHAPTER 7 CONCLUSIONS

> Chapter 7 summarizes the results of this experimental program with conclusive statements. This chapter also provides overall conclusions and recommendations for future research.

7.1 MD SPECIMENS

> The following conclusions can be drawn for the moderately ductile internal and external specimens:

7.1.1 With Respect to the Design Variables Studied

> Based on the evidence collected, it is believed that integrative trusses should not be selected as moment continuity solutions in NPS® beam-column joints. They exhibit poor performance compared with systems connected with deformed steel bars, while also presenting practical limitations. For instance, they cannot be easily implemented in 3D beam-column joints and they make it virtually impossible to provide an adequate level of reinforcement within the joint core. This is concerning, particularly for interior joints. Furthermore, because the truss longitudinal elements consist of smooth steel bars, they are prone to bond-slip deterioration issues.

> The response of beams in capacity-designed NPS® beam-column joints is not influenced by the presence/absence of integrative shear reinforcement (i.e., ductility stirrups) in the beam end regions. If adequately designed, the NPS® beam truss alone can resist the full shear action while most of the displacement demand is absorbed in the form of localized rotation at the beam-column interface (over-reinforced joint cores) or as a combination of localized rotation at the beam-column interface and shear deformation of the joint panel zone (under-reinforced joint cores). Either way, the rotation demand in the beam is sufficiently low that it can be comfortably absorbed by the composite NPS® beam.

> Shear reinforcement within the joint core is necessary to ensure that flexural plastic mechanisms can effectively develop at the beam-column interface. The amount of necessary joint reinforcement depends on the “ductility class” that is targeted in design. Using the column HSS as a substitute for traditional stirrups represent a highly effective way of achieving full protection of the joint panel zone. It proved particularly

effective with respect to the response of the planar interior joints tested in this program, for which a clear failure mode shift was observed.

7.1.2 With Respect to the NPS® Joint Performance

- All systems reached their targeted design strength, displaying a good level of ductility. For the most part, interior joints exhibited joint failure following beam yielding at the beam-column interface, while exterior joints did not show signs of distress in the joint and experienced beam yield failure. In both cases, the demand on the system was controlled by the yield strength provided by the continuity elements at the beam-column interface.
- All interior joints were characterized by a markedly pinched force-displacement response, due to bond-slip deterioration caused by the severe bond demand on the continuity bars. Despite the level of pinching observed, all systems that used continuity bars displayed sufficiently high levels of strength, ductility, stiffness, and energy dissipation. This is seen as a positive and promising outcome, particularly considering that large continuity bars with a joint depth-to-bar diameter ratio of 13 was purposely selected in this program. For context, the ACI code sets a lower bound for this ratio at 20, for RC special moment resisting frame. Evidently, bond-slip deterioration phenomena can be mitigated via smaller diameter continuity bars.
- All exterior beam-column joints that used continuity deformed bars exhibited excellent performance with no deterioration of the joint panel zone and trivial bond-slip degradation. Their force-displacement response was characterized by fat hysteretic loops denoting high levels of energy dissipation and ductility.
- All specimens, except NPS1i, met ACI acceptance criteria set forth for special moment resisting frames at (R = 8.5) at limiting drift of 4% [42]. Overall, the experimental data show that their performance can be considered equivalent to that of the RC control specimens.

7.1.3 With Respect to Design Implications

- The results of this experimental program demonstrated that NPS® beam-column joints can be successfully designed to achieve the same performance of moderately ductile (by Eurocode definition) RC

systems. This supports the notion that a behavior factor of up to 3.9 can be considered in design to estimate the seismic demand.

> The capacity design approach adopted in this study worked well, leading to the design of a series of full-scale NPS® specimens that behaved as intended, without displaying undesired mechanisms in beams and columns. This design approach is thus recommended moving forward.

> To address practical/constructability issues, the use of large diameter continuity bars is often required. The specimens tested in this program were characterized by a joint depth-to-bar diameter ratio of 13 and exhibited good performance. For the time being, this value may be used as a reference, knowing that higher ratios would lead to better performance, all else being equal.

7.2 HD SPECIMENS

> The following conclusions can be drawn for the internal and external specimens designed in high ductility class:

- Plastic hinge relocation is possible and can be achieved through proper reinforcement detailing.
- Plastic hinge relocation can be effective at protecting the joint core from severe damage.
- While the specimens were able to achieve near peak strength and formed a plastic hinge thereby failing in flexure at the design-intended location, there are several conceptual issues that need to be addressed before the continuity solution adopted in this program can be adopted. This is beyond the scope of this project.

7.3 FUTURE WORK

> While this program was able to draw useful conclusions, future study of the NPS® is warranted for increased safety, understanding and optimization. Some suggestions the author has for potential future work are noted below.

> Through the NPS3 specimens, which were designed to be part of the highly ductile class of joints, it was shown that the relocation of the plastic hinge region can ultimately be successful and reduce damage in the

joint panel. Additionally, the experimental results pertaining to the exterior beam-column joint specimens suggest that the NPS® system can be designed to match the performance of RC systems in high ductility class. Bond-slip deterioration, which was the main issue detected for interior specimens, can be mitigated, to a substantial extent, by simply reducing the diameter of the continuity bars and/or utilizing deformed bars rather than plain for the continuity element. Note that if the NPS® system is conceived as a high ductility class system, higher behavior factor can be used in design. This reduces the flexural demand on the beams and, in turn, the bond demand on the continuity bars and the shear demand on the joint panel zone. Future experimental programming to advance the NPS® system design to be classified as highly ductile might be worth pursuing.

> Additionally, an interesting configuration that was not addressed in this paper, but would be practical to study, is a knee joint. Knee joints occur at a structure's roof level. They differ from the specimens tested in this program because they lack an upper column and consequently a column axial load. This would be interesting to consider, as they are undeniably present in any complete building with this NPS® System. The lack of an axial load (See CHAPTER 2 for note of inconclusively of this variable) might provide less confinement for the concrete in the joint, or it might reduce the shear demands in the region. The lateral load would need to be applied at a unique location, as obviously there would be no top column to apply the load in a similar fashion to the specimens in this experimental program. Further consideration should be given to the testing setup, but would be a useful experiment, nonetheless.

> Another valuable and somewhat simple experiment that could be performed (which, if this project had abundant scope and budget would have been), is to replicate the external reference specimen with out-of-plane bracing. Recall that the external specimen failed out of plane, prior to failure, and so was unable to act as complete comparison for the NPS® external specimens.

> The final suggestion this paper will make for future work to be considered is the implementation of the REF and NPS2A specimens as fully 3D specimens. Currently, the specimens were all two-dimensional, with representative "windows" cut out of the column steel HSS tube to mimic the real world condition of

additional beams out of plane. Including the two additional beams would provide additional confinement to the joint core and reduce spalling, resulting in better bond between the concrete and the continuity elements. In a complete system, the adjacent slab would increase the confinement level of the joint as well. This likely would not have a large impact on the external specimens, where the joint regions remained virtually undamaged, with nearly all specimens failing in beam-yielding. Nonetheless, it is reasonable to assume that a 3D specimen could reach better performance levels for strength and ductility than its 2D counterpart.

REFERENCES

[1] I. Wiest, J. Colaco, R. Furlong, G. L.G., R. Leon and L. Wyllie, Composite Construction Design for Buildings, McGraw-Hill Professional, 1996.

[2] P. Calvi, "Earthquake-resistant construction system composed of steel-concrete coposite beams, columns and beam-to-column joints: Special Considerations for Beam-Column Joints and Plastic Hinge Regions," Technical Report submitted to TECNOSTRUTTURE, 2019.

[3] R. P. P. D. A. Costa, "Component-based reinforced concrete beam-column joint model," *Structural Concrete: Journal of the FIB,* vol. 18, no. 1, pp. 164-176, 2017.

[4] A. Belleri, E. Brunesi, R. Nascimbene, M. Pagani and P. Riva, "Seismic Performance of Precast Industrial Facilities Following Major Earthquake in the Italian Territory," *Journal of Performance of Constructed Facilities,* vol. 29, no. 5, p. 04014135, 2015.

[5] F. J. Vecchio and M. P. Collins, "The Modified Compression Field Theory for Reinforced Concrete Elements Subjected to Shear," *ACI Structural Engineering Journal,* pp. 219-231, 1986.

[6] J.-Y. Lee, J.-Y. Kim and G.-J. Oh, "Strength Deterioration of Reinforced Cocnrete Beam-Column Joints Subjected to Cyclic Loading," *Engineering Structures,* vol. 31, pp. 2070-2085, 2009.

[7] M. Shin and J. M. LaFave, "Modeling of Cyclic Joint Shear Deformation Contributions in RC Beam Column Connections to Overall Frame Behavior," *Structural Engineering and Mechanics,* vol. 18, no. 5, pp. 645-669, 2004.

[8] L. N. Lowes, N. Mitra and A. Altoontash, "A beam-column joint model for simulating the earthquake response of reinforced concrete frames (2003)," Pacific Earthquake Engineering Research Center, Berkeley, University of California, 2003.

[9] S. Hwang and H.-J. Lee, "Analtyical Model for predicting shear strengths of exterior reinforced concrete beam-columnjoints for seismic resistance," *ACI Structural Journal,* vol. 96, no. 5, pp. 846-857, 1999.

[10] J. Schlaich, K. Schäfer and M. and Jennewein, "Toward a Consistent Design of Structural Concrete," *Journal of the Prestressed Concrete Institute,* vol. 32, no. 3, pp. 74-150, 1987.

[11] T. Paulay, R. Park and M. Priestley, "Reinforced concrete beam-column joints under seismic actions," *J. ACI,* vol. 75, no. 11, pp. 585-593, 1978.

[12] T. Paulay, "Equilibrium Criteria for Reinforced Concrete Beam-Colum Joints," *ACI Structural Journal,* vol. 86, no. 1-6, pp. 635-643, 1989.

[13] R. Leon, "Shear strength and hysteretic behavior of interior beam-column joints," *ACI Structural Journal,* vol. 87, no. 1, pp. 3-11, 1990.

[14] S. Attaalla, "Seismic shear capacity of beam-column joints in multi-storey reinforced concrete frame buildings," Ph.D. dissertation, Civil Engineering Department, University of Southern California, Los Angeles, California, 1997.

[15] G.-L. Wang, J.-G. Dai and J. Teng, "Shear strength model for RC beam-column joints under seismic loading," *Engineering Structures,* vol. 40, pp. 350-360, 2012.

[16] H. Y. Choi and J. Y. Lee, "Strength Evaluation of Reinforced Concrete Beam-Column Joints," in *15th World Conference on Earthquake Engineering*, Lisbon, Portugal, 2012.

[17] J. Kim and J. M. LaFave, "Joint Shear Behavior of Reinforced Concrete Beam-Column Connections subjected to Seismic Lateral Loading," NSEL Report Series - Report No. NSEL-020, Urbana-Champaign, University of Illinois, 2009.

[18] K. Kitayama, S. Otani and H. Aoyama, "Development of design criteria for RC interior beam-column joints (SP-123)," American Concrete Institute , Detroit, 1991.

[19] H. Shiohara and K. F., "Comprehensive series of tests on seismic performance of reinforced concrete beam-column joints.," in *Preceedings of the 3rd international conference on advances in experimental structural engineering*, San Francisco, California, 2009.

[20] H.-J. Hwang, T.-S. Eom and H.-G. Park, "Shear Strength Degradation Model for Performance-Based Design of Interior Beam-Column Joints," *ACI structural journal,* vol. 114, no. 5, p. 1143, 2017.

[21] D. Gombosuren and T. Maki, "Prediction of Joint Shear Deformation Index of RC Beam-Column Joints," *MDPI Buildings,* vol. 10, no. 176, p. 10100176, 2020.

[22] L. J., "Experimental study on seismic performance of rectangular concrete filled steel tubular column to steel beam connections," Master Thesis: Fuzhou University, Fuzhou, Fujian, 2004.

[23] Q. K. C. C. Nie JG, "Seismic behavior of connections composted of CFSSTCs and steel-concrete composite beams-experimental study," *J Construct Steel Res,* 2008.

[24] D. P. G. S. Parra-Montesinos G.J., "Development of connections between hybrid steel truss FRC beams and RC columns for precast earthquake resistant framed construction," *Engineering Structures,* vol. 27, no. 13, pp. 1931-1941, 2005.

[25] L. X. W. J. Parra-Montesinos G.J., "Towards Deformation Based Capacity Design of RCS beam-column connections," *Engineering Structures,* vol. 25, no. 5, pp. 681-690, 2003.

[26] T. M. Sheikh, G. G. Deierlein, J. A. Yura and J. O. Jirsa, "Beam-column moment connections for composite frames: Part 1," *Journal of Structural Engineering (ASCE),* vol. 115, no. 11, pp. 2858-2876, 1989.

[27] H. Ma, J. Dong, Y. Liu and D. Yang, "Cyclic loading tests and shear strength of composite joints with steel-reinforced recycled concrete columns and steel beams," *Enineering Structures,* vol. 199, p. 109605, 2019.

[28] R. S. L. Herrera, "Seismic Performance Evaluation of Steel Moment Resisting Frames with Cocnrete Filled Tube Columns," in *Conference: International Workshop on Steel and Concrete Composite construction*, TaiPei, Taiwan, 2003.

[29] ACI Inovation Task Group 1 and Collaborators, "Acceptance Criteria for moment frames based on structural testing," Report ACI ITG/T1.1-99, Farmington Hills, MI, 1999.

[30] J. Ricles, S. Peng and L. Lu, "Seismic Behavior of Composite Concrete Fileld Steel Tube Column-Wide Flange Beam Moment Connections," *Journal of Structural Engineering*, vol. 130, no. 2, pp. 223-232, 2004.

[31] C. Cosgun, A. M. Turk, A. Mangir, T. Cosgun and G. Kiymaz, "Experimental behavior and failure of beam-column joints with plain bars, low-strength concrete and different anchorage details," *Engineering Failure Analysis*, vol. 109, pp. 1350-6307, 2020.

[32] C. &. M. Fernandes and H. C. A. Jose & Varum, "Cyclic Behavior of Substandard Reinforced Concrete Beam-Column Joints with Plain Bars," *ACI Structural Journal*, vol. 110, no. 1, pp. 137-148, 2013.

[33] R. Eligehausen, E. Popov and V. Bertero, "Local bond stress-slip relationships of deformed bars under generalized excitations: experimental results and analytical model," 1983.

[34] P. Soroushian, K. Obasaki and S. Marikunte, "Analytical Modeling of Bonded Bars under Cyclic Loads," *Journal of Structural Engineering*, vol. 117, no. 1, pp. 48-60, 1991.

[35] S. Park and K. M. Mosalam, "Experimental and Analytical Studies on Reinforced Concrete Buildings with Seismically Vulnerable Beam-Column Joints," Pacific Earthquake Engineering Research Center, Berkeley, 2012.

[36] ACI Committee 318, Building code requirements for structural concrete (ACI 318-19) and commentary., Farmington Hills, MI: American Concrete Institute.

[37] Standards Association of New Zealand, The design of concrete structures, NZS 3101:1995, New Zealand Standards Authority, New Zealand, 2006.

[38] EN 1998-1:2013, "Eurocode 8: Design of structures for earthquake resistance - Part 1: General rules, seismic actions and rules for buildings".

[39] S. Uma and S. K. Jain, "Seismic design of beam0column joints in RC moment resisting frames - review of codes," *Structural engineering and mechanics*, vol. 23, no. 5, pp. 579-597, 2006.

[40] K. Parate and R. Kumar, "Shear strength criteria for design of RC beam-column joints in building codes," *Bulletin of Earthquake Engineering*, pp. 1407-1493, 2019.

[41] P. Calvi, "Earthquake-resistant construction system composed of steel-concrete composite beams, columns and beam-to-column joints: Design Recommendations," Technical Report submitted to TECNOSTRUTTURE, 2019.

[42] P. Calvi, "Earthquake-resistant construction system composed of steel-concrete composite beams, columns and beam-to-column joints: Explanatory Notes on Design Recommendations," Technical Report submitted to TECNOSTRUTTURE, 2020.

[43] EN 10025-1:2006, Hot rolled products of structural steels - Part 1: general technical delivery conditions.

[44] EN 10080:2005, Steel for the reinforcement of concrete - Weldable reinforcing steel - General.

[45] ACI Committee 374, Acceptance criteria for moment frames based on structural testing and commentary (ACI 374.1-05)., Farmington Hills, MI: American Concrete Institute, 2005.

[46] O. Joh, Y. Goto and T. Shibata, "Influence of Transferse Joint and Beam Reinforcement and Relocation of Plastic HInge Region on Beam Column Joint Stiffness Deterioration," *ACI Struct. J.*, vol. 123, pp. 187-224, 1991.

[47] M. S. Ashtiani, R. P. Dhakal and A. N. Scott, "Seismic Performance of High-Strength Self-Compacting Concrete in Reinforced Concrete Beam-Column Joints," *ASCE Journal of Structural Engineering,* vol. 140, no. 5, p. 04014002, 2014.

[48] B. Li and Q. Kai, "Seismic Behavior of Reinforced Concrete Interior Beam-Wide Column Joints Repaired Using FRP," *ASCE Journal of Composites for Construction,* vol. 15, no. 3, pp. 327-338, 2011.

[49] R. Park, "Ductility Evaluation from laboratory and Analytical Testing," in *Proceedings of Ninth World Conference on Earthquake Engineering, Vol VIII*, Tokyo-Kyoto, Japan, 1988.

[50] W. Liu and J. Jia, "Experimental Study on the Seismic Behavior of Steel-Reinforced Ultra-High-Strength Concrete Frame Joints with Cyclic Loads," *Advances in Structural Engineering,* vol. 21, no. 2, pp. 270-286, 2018.

[51] J. Wang, L. Cheng and Y. Yang, "Experimental Study of Seismic Behavior of High-strength RC Columns Strengthened with CFRP Under Cyclic Loading," *Journal of Structural Engineering,* vol. 145, no. 2, 2019.

[52] ACI Committee 374, Guide for testing reinforced concrete structural elements under slowly applied simulated seismic loads, ACI 374.2R-13, 2013.

[53] J. W. Park, D. Kim, S. G. Yoon and J. Y. Lee, "Shear Deterioration of Reinforced Concrete Beam-Column Joints," in *Proceedings of the fifteenth world conference on earthquake engineering*, Lisbon, Portugal, 2012.

[54] ASCE Task Committee on Design Criteria for Composite Structues in Steel and Concrete, "Design of joints between steel beams and reinforced concrete columns," *ASCE Journal of Structural Engineering,* vol. 120, no. 8, pp. 2330-2357, 1994.

[55] S. Peng, "Seismic resistant connections for concrete filled tube column to -WF beam moment resisting frames," Ph.D. dissertation, Bethlehem (Pa) Lehigh University, 2001.

[56] W. Y. P. e. a. Kam, "Seismic performance of reinforced concrete buildings in the 22 February Christchurch (Lyttelton) earthquake," *Bulletin of the New Zealand Society for Earthquake Engineering,* vol. 44, no. 10, pp. 239-278, 2011.

[57] P. Cheung, T. Paulay and R. Park, "Behaviour of beam-column joints in seismically loaded RC frames," *The Structural Engineer,* vol. 71, no. 8, pp. 129-138, 1993.

[58] N. Hanson and H. Connor, "Seismic Resistance of Reinforced Concrete beam-column joints," *Journal of the Structural Division, ASCE,* vol. 93, no. 5, pp. 533-560, 1967.

[59] M. Ehsani and J. Wight, "Exterior reinforced concrete beam-to-column connections subjected to earthquake-type loading," *ACI Structural Journal,* vol. 82, no. 43, pp. 492-499, 1985.

[60] A. Albright, A. Argentoni and P. Calvi, "Experimental behavior of interior and exterior steel-concrete composite NPS beam-column joints," *Engineering Structures,* vol. 251, no. 113589, 2022.